Deutsches Biomasseforschungszentrum
gemeinnützige GmbH

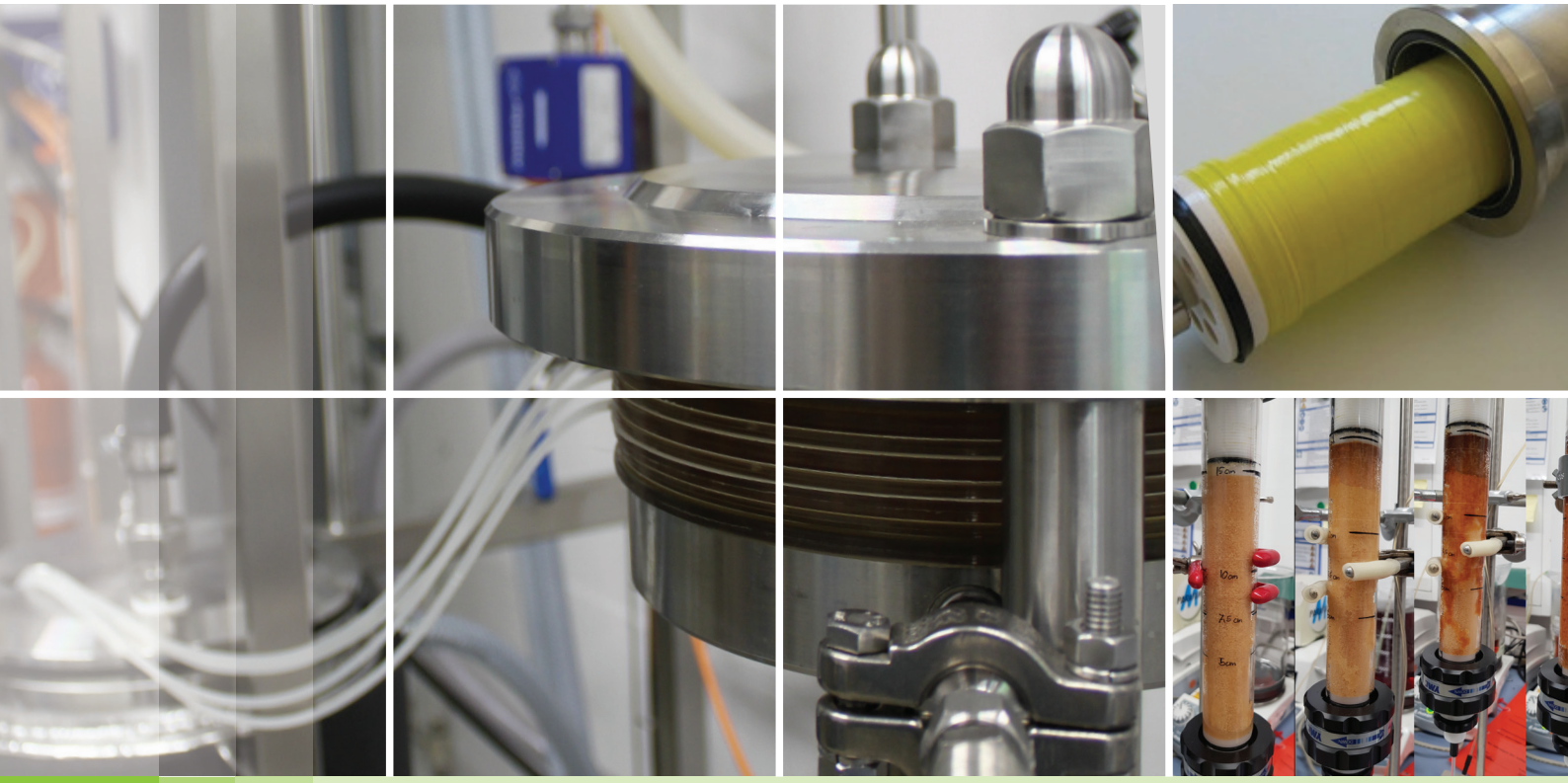

DBFZ REPORT NR. 48

Adsorption and Membrane Filtration for the Separation and Valorization of Hemicellulose from Organosolv Beechwood Hydrolyzates

Doctoral thesis

Roy Nitzsche

IMPRINT

Publisher:
DBFZ Deutsches Biomasseforschungszentrum
gemeinnützige GmbH
Torgauer Straße 116
04347 Leipzig
Phone: +49 (0)341 2434-112
info@dbfz.de

Funding:
DBFZ Deutsches Biomasseforschungszentrum gemeinnützige GmbH, Leipzig, an enterprise of the German Government with funding from the Federal Ministry of Food and Agriculture pursuant to a resolution by the German Bundestag.

With support from

Federal Ministry
of Food
and Agriculture

by decision of the
German Bundestag

General Management:
Prof. Dr. mont. Michael Nelles
(Scientific Managing Director)
Dr. Christoph Krukenkamp
(Administrative Managing Director)

DBFZ Report Nr. 48
Adsorption and Membrane Filtration for the Separation and Valorization of Hemicellulose from Organosolv Beechwood Hydrolyzates – Doctoral thesis Roy Nitzsche
Leipzig: DBFZ, 2023
ISSN: 2197-4632 (Online)
ISBN: 978-3-946629-96-2
DOI: 10.48480/z2mn-2r87

Author:
Roy Nitzsche

Pictures:
If not indicated on the image: DBFZ, Stefanie Bader (Map)

Date of Publication:
23/08/2023

DIRECTIONS

By train: Arrival Leipzig main station; streetcar line 3/3E (direction Taucha/Sommerfeld) to stop Bautzner Straße; cross the street, leave the parking lot on the right and use the main entrance of the DBFZ (house 1, Torgauer Str. 116). Please register at the reception

By car: on the A 14 motorway. Exit at Leipzig Nord-Ost; follow signs for Taucha; then follow signs for Leipzig; then follow signs for Zentrum, Innenstadt. Turn off left after the “bft” filling station (see “By train” for further directions).

By tram: line 3/3 E towards Taucha/Sommerfeld; Bautzner Strasse stop (see “By train” for further directions)

The German National Library lists these publications in the German National Bibliography; detailed bibliographic data are available on the Internet at the address www.dnb.de.

Adsorption and Membrane Filtration for the Separation and Valorization of Hemicellulose from Organosolv Beechwood Hydrolyzates

vorgelegt von

Dipl.-Ing.

Roy Nitzsche

ORCID: 0000-0001-8922-8420

an der Fakultät III – Prozesswissenschaften

der Technischen Universität Berlin

zur Erlangung des akademischen Grades

Doktor der Ingenieurwissenschaften

- Dr.-Ing. -

genehmigte Dissertation

Promotionsausschuss:

Vorsitzender: Prof. Dr.-Ing. habil. Jens-Uwe Repke (TU Berlin)

Gutachter 1: Prof. Dr.-Ing. Matthias Kraume (TU Berlin)

Gutachter 2: Prof. Dr. mont. Michael Nelles (Univ. Rostock)

Tag der wissenschaftlichen Aussprache: 09. Juni 2023

Berlin 2023

Acknowledgement

The present work was carried out at the DBFZ Deutsches Biomasseforschungszentrum gemeinnützige GmbH in the Department Biorefineries in the Working Group Separation Technologies and Process Design. I want to thank the following people for their professional, personal, and private support. Without you, this thesis would not have been possible.

- Arne Gröngröft, my supervisor at the DBFZ, for his patient guidance, enthusiastic encouragement, and constructive criticism during this research work. His support was essential realizing this study.
- Professor Matthias Kraume, my supervisor at the Technical University of Berlin, for his interest in this topic, his scientific advice, as well as for his constructive and fruitful comments on the publications.
- Professor Michael Nelles, who agreed to review and evaluate my thesis as external referee.
- Dr. Franziska Müller-Langer, Head of Department Biorefineries, for giving me the opportunity to do my research at the DBFZ and for always having an open door for any kind of issues.
- All members of the Working Group Separation Technologies and Process Design for a pleasant and creative working atmosphere. Especially to the technician Marcel Fritzsch for his support in operating the experimental equipment and preparing samples for analysis.
- All members of the Analytical Laboratory, especially Dr. Jana Mühlenberg and Jessica Pester, for conducting numerous analyses and enduring my impatience.
- All co-authors of the publications for their content contribution, help, and the constructive working environment.
- Dr. Maik Budzinski, Dr. Johannes Boog, and Hans Schott for our regular Skat tables. The time together has always helped me to clear my head, reset my focus and finally finish this work.

Finally, I owe my deepest gratitude to my wife and kids. Thank you, Karin, for all the support and sympathy and for sharing both the great and the uncomfortable moments during this study. Thank you, Paula and Peter, for being a joyful part of my life. This work is for the three of you!

Abstract

The sustainable use and conversion of biomass for the production of energy, fuels, and chemicals can help to counteract the declining availability of fossil resources and increasing climate change. In biorefineries, woody raw materials are fractionated into their three main constituent's cellulose, hemicellulose, and lignin. The dissolved hemicellulose and its degradation products usually end up in the wood hydrolyzate. Due to relatively low concentrations and inhomogeneous composition of this process stream, it is usually not recovered. However, if the hemicellulose and its derived sugars can be separated and purified, they could be used to produce high-value-added products and raise up the competitiveness and sustainability of existing and future biorefineries. Within the scope of this work, the separation and valorization of hemicellulose from beechwood hydrolyzates by adsorption and membrane filtration were experimentally investigated and techno-economically assessed.

At first, an adsorption process was developed to separate residual lignin from hemicellulose out of beechwood hydrolyzate. Four polymeric resins and one zeolite were compared in batch experiments, and competitive adsorption isotherms were modeled. The most efficient resin SP700 was studied in more detail in column tests. The adsorption of lignin and hemicellulose from beechwood hydrolyzate could be fitted best to the extended Freundlich isotherm. In a continuous adsorption process, 80 % of lignin was removed with 99.5 % hemicellulose recovery. Adsorbed lignin could be efficiently desorbed with a 50 wt.% ethanol solution.

Membrane filtration was developed, on the one hand, for the recovery and concentration of hemicellulose from beechwood hydrolyzate by ultrafiltration, and on the other hand, for the separation of xylose from hydrothermally pretreated beechwood hydrolyzate by nanofiltration. The ultrafiltration was optimized in terms of high permeate flux and hemicellulose retention as well as low lignin retention as a function of transmembrane pressure, temperature, and pH. In addition, the effect of a prior adsorption step on ultrafiltration of beechwood hydrolyzate was studied. For the process design the statistical approach of response surface methodology and Pareto optimization was used. Optimum process parameters using the polymeric membrane UA60 were found to be a transmembrane pressure of 0.98 MPa, a temperature of 55 °C, and a pH of 2.5, resulting in a permeate flux of 49 L/(m²h), hemicellulose retention of 85 %, and lignin retention of 41 %. Adsorption previous to ultrafiltration enhanced the permeate flux by 174 % and reduced the hemicellulose and lignin retention by 12 and 54 %, respectively. Hence, higher losses of hemicellulose, but simultaneously a purer concentrate and a higher throughput. For nanofiltration, the influence of hydrothermal pretreatment of beechwood hydrolyzate on the separation of xylose from fermentation inhibitors as well as the overall process performance was investigated. At first, a hydrothermal process was developed, to convert the remaining oligomeric hemicellulose into xylose. Then, the nanofiltration process using untreated and hydrothermally pretreated beechwood hydrolyzate was assessed by a performance and fouling analysis. The average permeate flux increased by up to 33 % during filtration of the pretreated solution. It was found that this is due to reduced concentration polarization and membrane fouling as a result of macromolecular sugar degradation. Thus, due to higher xylose concertation and lower inhibitor retentions a cleaner retentate stream could be obtained. To

design an energetically favorable process appropriate parameters were identified. Using the polymeric membrane Alfa Laval NF, a volume reduction of 80 % was achieved with an average permeate flux of 22.5 L/(m²h) and retentions for xylose, furans, and acetic acid of 95, 31, and 4 %, respectively.

The experimental findings were used to assess two industrial scale purification cascades. Purification cascade 1 consists of adsorption and ultrafiltration and aimed a purified hemicellulose stream. Purification cascade 2 consists of hydrothermal treatment and nanofiltration, with the aim to achieve a purified xylose stream. Both purification cascades were simulated in Aspen Plus® to calculate mass and energy balances and conduct a techno-economic assessment. In purification cascade 1, 80 % of the lignin was removed by adsorption, and 7.6 t/h of a purified hemicellulose solution with a concentration of 200 g/L was obtained using ultrafiltration. In purification cascade 2, almost the entire oligomeric hemicellulose was hydrothermally converted to xylose and purified by nanofiltration to 8.9 t/h of a xylose solution with a concentration of 200 g/L. The energy efficiency of the cascades was 24 and 56 %, respectively. Furthermore, the estimation of specific production costs showed that hemicellulose could be recovered from beechwood hydrolyzate at 135.1 EUR/t and xylose at 71.4 EUR/t.

Kurzfassung

Die nachhaltige Nutzung und Konversion von Biomasse für die Erzeugung von Energie, Kraftstoffen und Chemikalien kann dazu beitragen, der abnehmenden Verfügbarkeit fossiler Ressourcen und einem zunehmenden Klimawandel entgegenzuwirken. In Bioraffinerien werden die holzigen Rohstoffe in ihre drei Hauptbestandteile Zellulose, Hemizellulose und Lignin aufgespalten. Die gelöste Hemizellulose und ihre Abbauprodukte verbleiben üblicherweise in dem Holzhydrolysat. Aufgrund der relativ geringen Konzentrationen und inhomogenen Zusammensetzung findet dieser Prozessstrom für gewöhnlich keine relevante Verwertung. Wenn jedoch die Hemizellulose und die daraus zu gewinnenden Zucker abgetrennt werden können, könnten diese zur Herstellung von Produkten mit hohem Mehrwert verwendet werden und die Wirtschaftlichkeit sowie Nachhaltigkeit bestehender und zukünftiger Bioraffinerien erhöhen. In der vorliegenden Arbeit wurde die Abtrennung und Verwertung von Hemizellulose aus Buchenholzhydrolysaten mittels Adsorption und Membranfiltration experimentell untersucht und techno-ökonomisch bewertet.

Zuerst wurde ein Adsorptionsverfahren entwickelt, welches die Abtrennung von verbleibendem Lignin aus Buchenholzhydrolysat ermöglicht. Dazu wurden vier polymere Harze und ein Zeolith in Batch-Experimenten verglichen und kompetitive Adsorptionsisothermen modelliert. Das effizienteste Harz SP700 wurde in Kolonnentests genauer untersucht. Die Adsorption von Lignin und Hemizellulose aus Buchenholzhydrolysat konnte am besten mit der Extended Freundlich-Isotherme beschrieben werden. In einem kontinuierlichen Adsorptionsprozess wurden 80 % des Lignins entfernt und 99,5 % der Hemicellulose zurückgewonnen. Adsorbiertes Lignin konnte mit einer 50 Ma.-% Ethanollösung effizient desorbiert werden.

Membranfiltration wurde zum einen für die Rückgewinnung und Aufkonzentrierung von Hemizellulose aus Buchenholzhydrolysat mittels Ultrafiltration und zum anderen für die Abtrennung von Xylose aus hydrothermal vorbehandeltem Buchenholzhydrolysat mittels Nanofiltration entwickelt. Die Ultrafiltration wurde hinsichtlich eines hohen Permeatfluxes und Hemizelluloseretention sowie einer niedrige Ligninretention in Abhängigkeit von Transmembrandurck, Temperatur und pH-Wert optimiert. Darüber hinaus wurde der Effekt eines vorherigen Adsorptionsschrittes auf die Ultrafiltration von Buchenholzhydrolysat untersucht. Für die Prozessentwicklung wurde der statistische Ansatz der Wirkungsflächenmethode und Pareto-Optimierung angewandt. Als optimale Prozessparameter und unter der Verwendung der Polymermembran UA60 wurden ein Transmembrandurck von 0,98 MPa, eine Temperatur von 55 °C und ein pH-Wert von 2,5 ermittelt, was zu einem Permeatflux von 49 L/(m²h), einer Hemicelluloseretention von 85 % und einer Ligninretention von 41 % führte. Eine Adsorption vor der Ultrafiltration erhöhte den Permeatflux um 174 % und verringerte die Hemicellulose- und Ligninretention um 12 bzw. 54 %. Das heißt, höhere Hemizelluloseverluste, aber gleichzeitig ein reineres Konzentrat und höherer Volumendurchsatz. Für die Nanofiltration wurde der Einfluss der hydrothermalen Vorbehandlung von Buchenholzhydrolysat auf die Abtrennung von Xylose von Fermentationsinhibitoren sowie auf die Gesamtprozessleistung untersucht. Zu Beginn wurde ein hydrothermales Verfahren entwickelt, um verbleibende oligomere Hemizellulose in Xylose

umzuwandeln. Anschließend wurde der Nanofiltrationsprozess unter Verwendung von unbehandeltem und hydrothermal vorbehandeltem Buchenholzhydrolysat mittels einer Leistungs- und Foulinganalyse bewertet. Der durchschnittliche Permeatflux stieg bei der Filtration der vorbehandelten Lösung um bis zu 33 %. Es konnte festgestellt werden, dass dies auf geringere Konzentrationspolarisation und Membranfouling infolge des Abbaus makromolekularer Zucker zurückzuführen ist. Aufgrund der höheren Xylosekonzentration und der geringeren Inhibitorretention konnte so ein reinerer Retentatstrom erzielt werden. Um ein energetisch günstiges Verfahren zu entwickeln, wurden geeignete Prozessparameter ermittelt. Unter Verwendung der Polymermembran Alfa Laval NF wurde eine Volumenreduktion von 80 % bei einem durchschnittlichen Permeatflux von 22,5 L/(m²h) und Retentionen für Xylose, Furane und Essigsäure von 95, 31 bzw. 4 % erzielt.

Basieren auf den experimentellen Ergebnissen wurden zwei Aufreinigungskaskaden im industriellen Maßstab simuliert und bewertet. Aufreinigungskaskade 1 besteht aus Adsorption und Ultrafiltration und zielt auf einen aufgereinigten Hemizellulosestrom ab. Aufreinigungskaskade 2 besteht aus einem hydrothermalen Prozess und Nanofiltration mit dem Ziel, einen gereinigten Xylosestrom zu erhalten. Beide Aufreinigungskaskaden wurden mittels Aspen Plus® simuliert, um Massen- und Energiebilanzen zu berechnen und eine techno-ökonomische Bewertung durchzuführen. In Aufreinigungskaskade 1 wurden 80 % des Lignins durch Adsorption entfernt und 7,6 t/h einer aufgereinigten Hemizelluloselösung mit einer Konzentration von 200 g/L mittels Ultrafiltration gewonnen. In Aufreinigungskaskade 2 wurde nahezu die gesamte oligomere Hemizellulose hydrothermal zu Xylose abgebaut und durch Nanofiltration zu 8,9 t/h einer Xyloselösung mit einer Konzentration von 200 g/L aufgereinigt. Die Energieeffizienz der Kaskaden beträgt 24 bzw. 56 %. Darüber hinaus ergab die Berechnung der spezifischen Produktionskosten, dass Hemizellulose aus Buchenholzhydrolysat zu 135,1 EUR/t und Xylose zu 71,4 EUR/t hergestellt werden kann.

List of Publications

This cumulative thesis is based on the following publications, which are listed in chronological order according to their date of publication/submission. The publications are referred to in the text by the Roman numerals I-V.

I. **Roy Nitzsche**, Arne Gröngröft, Matthias Kraume: Separation of lignin from beech wood hydrolysate using polymeric resins and zeolites – Determination and application of adsorption isotherms. Separation and Purification Technology 209 (2019), 491-502. DOI: https://doi.org/10.1016/j.seppur.2018.07.077

   Roy Nitzsche, Arne Gröngröft, Matthias Kraume: Corrigendum to 'Separation of lignin from beech wood hydrolysate using polymeric resins and zeolites – determination and application of adsorption isotherms' Corrigendum in Journal 'Separation and Purification Technology 209 (2019) 491–502'. Separation and Purification Technology 219 (2019), 303-306. DOI: https://doi.org/10.1016/j.seppur.2019.02.011

II. **Roy Nitzsche**, Arne Gröngröft, Ilona Goj, Matthias Kraume: Ultrafiltration of beech wood hydrolysate for concentrating hemicellulose sugars and removal of lignin – Parameter estimation using statistical methods and multiobjective optimization. Industrial and Engineering Chemistry Research 59 (2020), 7875-7887. DOI: https://doi.org/10.1021/acs.iecr.0c00487

III. **Roy Nitzsche**, Jakob Köchermann, Arne Gröngröft, Matthias Kraume: Nanofiltration of organosolv hemicellulose hydrolyzate: Influence of hydrothermal pretreatment and membrane characteristics on filtration performance and fouling. Industrial and Engineering Chemistry Research 60 (2021), 916-930. DOI: https://doi.org/10.1021/acs.iecr.0c03256

IV. **Roy Nitzsche**, Arne Gröngröft, Jakob Köchermann, Kathleen Meisel, Hendrik Etzold, Marlen Verges, Moritz Leschinsky, Julian Bachmann, Bodo Saake, Sandra Torkler, Katja Patzsch, Björn Rößiger, Daniela Pufky-Heinrich, Gerd Unkelbach: Platform and fine chemicals from woody biomass: Demonstration and assessment of a novel biorefinery. Biomass Conversion and Biorefinery 11 (2020), 2369-2385. DOI: https://doi.org/10.1007/s13399-020-00769-z

V. **Roy Nitzsche**, Hendrik Etzold, Marlen Verges, Arne Gröngröft, Matthias Kraume: Demonstration and assessment of purification cascades for the separation and valorization of hemicellulose from organosolv beech wood hydrolysates. Membranes 12 (2022), 82. DOI: https://doi.org/10.3390/membranes12010082

Contributions of the main Author

I. The author planned and carried out the experimental work. The author evaluated and interpreted the results together with the co-writers. The author and technicians of the

Department Biorefineries at the DBFZ conducted the chemical analysis. The author wrote the article.

II. The author planned and carried out the experimental work. The author evaluated and interpreted the results together with the co-writers. The author and technicians of the Department Biorefineries at the DBFZ conducted the chemical analysis. The author wrote the article.

III. The author planned and carried out the experimental work together with Jakob Köchermann. The author evaluated and interpreted the results together with the co-writers. The technicians of the Department Biorefineries at the DBFZ conducted the chemical analysis. The author wrote the article together with Jakob Köchermann.

IV. The author planned the study together with Arne Gröngröft, Jakob Köchermann, Kathleen Meisel, and Hendrik Etzold, and planned and carried out part of the experimental work. Further experimental work was carried out by Marlen Verges, Moritz Leschinsky, Julian Bachmann, Bodo Saake, Sandra Torkler, Katja Patzsch, Björn Rößiger, and Daniela Pufky-Heinrich. The author evaluated and interpreted the results together with the co-writers. The author, together with Kathleen Meisel and Hendrik Etzold, carried out the process assessment. The author wrote the article together with the co-writers.

V. The author planned and carried out the experimental work together with Marlen Verges. The author evaluated and interpreted the results together with the co-writers. The technicians of the Department Biorefineries at the DBFZ and of the Fraunhofer Center for Chemical-Biotechnological Processes conducted the chemical analysis. The author carried out the process assessment together with Hendrik Etzold. The author wrote the article together with Hendrik Etzold and Marlen Verges.

Other related Publications

Jakob Hildebrandt, Maik Budzinski, **Roy Nitzsche**, Andreas Weber, Andreas Krombholz, Daniela Thrän, Alberto Bezama: Assessing the technical and environmental performance of wood-based fiber laminates with lignin based phenolic resin systems. Resources, Conservation and Recycling 141 (2019), 455–464. DOI: https://doi.org/10.1016/j.resconrec.2018.10.029

Maik Budzinski, Otávio Cavalett, **Roy Nitzsche**, Anders Hammer Strømman: Assessment of lignocellulosic biorefineries in Germany using a hybrid LCA multi-objective optimization model. Journal of Industrial Ecology 23 (2019), 1172-1185. DOI: 10.1111/jiec.12857

Maria Braune, Bomin Yuan, Heike Sträuber, Stewart Charles McDowall, **Roy Nitzsche**, Arne Gröngröft: A Downstream Processing Cascade for Separation of Caproic and Caprylic Acid from Maize Silage-Based Fermentation Broth. Frontiers in Bioengineering and Biotechnology 9 (2021), 725578. DOI: 10.3389/fbioe.2021.725578

Stewart Charles McDowall, Maria Braune, **Roy Nitzsche**: Recovery of bio-based medium-chain fatty acids with membrane filtration. Separation and Purification Technology 286 (2022), 120430. DOI: https://doi.org/10.1016/j.seppur.2021.120430

Contents

List of Figures

List of Tables

Nomenclature

Abbreviations

5-HMF	5-Hydroxymethylfurfural
ANOVA	Analysis of variance
APR	Aqueous Phase Reforming
A:S	Adsorbent-to-solution
BV	Bed volume
BWH	Beechwood hydrolyzate
CBP	Chemical-Biotechnological Processes
CCD	Central composite design
CEPCI	Chemical engineering plant cost index
CFV	Cross-flow velocity
CHP	Combined heat and power plant
CP	Compromise point
CW	Cool water
Da	Daltons
DAD	Diode array detector
DIW	De-ionized water
DP	Degree of polymerization
EE	Electricity
FCI	Fixed-capital investments
FID	Flame-ionization detector
GC	Gas chromatography
HPBWH	Hydrothermally pretreated beechwood hydrolyzate
HPLC	High performance liquid chromatography
HPS	High pressure steam
HTC	Hydrothermal carbonization
HTL	Hydrothermal liquefaction
LPS	Low pressure steam
MF	Microfiltration

MS	Model solution
MW	Molecular weight
MWCO	Molecular weight cut-off
NF	Nanofiltration
NTP	Number of theoretical plates
odw	Oven-dry weight
PA	Polyacrylate
PCD	ProcessNet Chemieanlagen-Index Deutschland
PO	Pareto optimization
PS-DVB	Polystyrene-divinylbenzene
PWF	Pure water flux
pH	pH value
RID	Refractive index detector
RO	Reverse osmosis
RSM	Response surface methodology
SCWG	Supercritical Water Gasification
SL	Spent liquor
TMP	Transmembrane pressure
UF	Ultrafiltration
UP	Utopia point
WBB	Wood-based biorefinery
WL	Wash liquor

Symbols

A	m²	Surface area
A_{280}	-	Absorbance value at 280 nm
A_m	m²	Membrane surface area
A_p	m²	Pore surface
a_{RP}	$(L/mmol)^{\beta}$	Parameter in (competitive) Redlich-Peterson model
a_s	m²	Specific pore surface
b_0	-	Constant coefficient

b_i	-	Linear coefficient
b_{ii}	-	Quadratic coefficient
b_{ij}	-	Interaction coefficient
C_0	g/L	Initial concentration
C_{eq}	g/L	Equilibrium concentration
C_f	g/L	Concentration in the feed
C_i	g/L	Concentration of component *i*
C_j	g/L	Concentration of component *j*
$C_{lignin,0}^{ads}$	g/L	Initial lignin concentration during adsorption
$C_{lignin,0}^{ads}$	g/L	Initial lignin concentration during adsorption
$C_{lignin,eq}^{des}$	g/L	Equilibrium lignin concentration during desorption
C_m	g/L	Concentration at the membrane
C_p	g/L	Concentration in the permeate
C_t	g/L	Concentration at time *t*
D_i	m²/s	Diffusion coefficient
d_h	m	Hydraulic diameter
$\dot{E}$	W	Energy flow
F	C/mol	Faraday's constant
J	L/(m²h)	Permeate flux
J_{conv}	L/(m²h)	Convective permeate flux
J_{diff}	L/(m²h)	Diffusive permeate flux
J_ψ	L/(m²h)	Permeate flux due to electric charge
K_F	(mg/g)/(mg/L)$^{1/n}$	Parameter in (extended) Freundlich model
K_L	L/g	Langmuir constant
K_{RP}	L/g	Parameter in (competitive) Redlich-Peterson model
k	-	Kozeny constant
L_i	-	Mobility coefficient of component *i*
LHV	kWh/kg	Lower heating value
l	m	Length of the cuvette
$MPSD$	%	Marquardt's percent standard deviation
m	kg	Mass

$\dot{m}$	kg/h	Mass flow
m_f	kg	Mass of the feed
m_p	kg	Mass of the permeate
N	-	Number of data points
N	-	Number of experimental runs
n	-	Parameter in Freundlich model
n	-	Independent variables
n	-	Number of decision variables in Pareto optimization
n_c	-	Center/replica point
$\dot{n}_i$	mol/m³h	Molar permeate flux
$n_{L,j}$	-	Interaction term in modified Langmuir model
n_p	-	Number of pores
$n_{RP,j}$	-	Interaction term in competitive Redlich-Peterson model
P	-	Degree of freedom of isotherm equation
PWF_a	L/(m²h)	Pure water flux after the experiment/filtration
PWF_b	L/(m²h)	Pure water flux before the experiment/filtration
PWF_r	%	Pure water flux reduction
p	MPa	Pressure
p_f	MPa	Feed side pressure
p_i^0	MPa	Reference pressure
p_r	MPa	Retentate side pressure
Δp	MPa	Transmembrane pressure
Δp_f	MPa	Frictional pressure drop
Q_0	mg/g	Parameter in (extended) Langmuir model
Q_0	mg/g	Adsorption capacity of one adsorbate when present alone
Q_{mix}	mg/g	Adsorption capacity of one adsorbate in mixture
q_e	mg/g	Equilibrium adsorption capacity
q_e^{cal}	mg/g	Calculated equilibrium adsorption capacity
q_e^{exp}	mg/g	Experimentally determined equilibrium adsorption capacity
R	J/(mol K)	Universal gas constant
R^2	-	Coefficient of determination

$R_{a/p}$	m^{-1}	Adsorption/pore blocking resistance
R_{cm}	m^{-1}	Resistance of cleaned membrane
R_{cp}	m^{-1}	Concentration polarization resistance
R_f	m^{-1}	Fouling resistance
$R_{g/c}$	m^{-1}	Gel/cake layer resistance
R_L	-	Separation factor
R_m	m^{-1}	Membrane resistance
R_{obs} or R	%	Observed retention
R_q	nm	Root mean square roughness
R_{tot}	m^{-1}	Total resistance
R_{true}	%	True retention
Re	-	Reynolds number
r	-	Inequality constrain in Pareto optimization
s	-	Equality constrain in Pareto optimization
T	K	Temperature
t	s	Time
$\dot{V}$	m^3/h	Volume flow
V_0	L	Volume of adsorbate solution
V_{BWH3}	L	volume of BWH 3 in contact with the adsorbent
$V_{desorbent}$	L	Volume of the desorbent in contact with the adsorbent
V_p	L	Volume of the permeate
V_{tot}	m^3	Total volume
VR	%	Volume reduction
X	-	Coded value of the factor
X	-	Feasible design space in Pareto optimization
x	-	Vector of decision variables in Pareto optimization
$x_{i,m}$	mol/mol	Molar fraction of component *i* dissolved in the membrane
x_{lb}	-	Lower bound constraint vector in Pareto optimization
x_{ub}	-	Upper bound constraint vector in Pareto optimization
x, y, z	-	Parameter in extended Freundlich model
Y	-	Predicted response

Y	%	Yield
Z_i	-	Ion valence
Δz	m	Membrane thickness
α	L/(g m)	Absorptivity factor
$\alpha_{i/j}$	-	Separation factor of component *i* to component *j*
β_{RP}	-	Parameter in (competitive) Redlich-Peterson model
γ_i	-	Activity coefficient
ε	-	Membrane porosity
η	kg/(m s)	Dynamic viscosity
η	%	Efficiency
$\mu_{el,i}$	J/mol	Electrochemical potential
μ_i	J/mol	Chemical potential of component i
μ_i^0	J/mol	Chemical potential at reference pressure p_i^0
$\Delta\pi_p$	MPa	Osmotic pressure difference
υ_i	m³/mol	Molar volume
φ	V	Electrical potential

1. Introduction

1.1 Background

The strong global dependence on fossil resources results from the intensive use and consumption of petroleum and natural gas based derivatives [1]. With the risks of diminishing reserves and growing climate change, a progressive shift from fossil-based chemistry to bio-based chemistry is necessary to ensure the long-term supply of chemicals, fuels, and materials. Due to their ubiquitous availability, wood and other lignocellulosic residues have the potential to become a valuable renewable resource. The use of integrative and multifunctional biorefineries in which such lignocellulosic raw materials can be fractionated into its three main constituents cellulose, hemicellulose, and lignin, is seen as a path with great prospects in future bioeconomies [2].

In present wood-based biorefineries (WBBs), pulping of the biomass is mostly realized by the kraft process with the main focus on the valorization of the cellulose [3]. The cellulose from the kraft process is usually further processed into chemical pulp with an annual global output of 135 Mt, for which 300 Mt of wood are required [3, 4]. As a by-product of the pulping process, a liquid stream remains, which, in addition to the pulping chemicals, contains approx. 80 % of the hemicellulose and 90 % of the lignin from the initially used wood [5]. Although the heating value of the hemicellulose is relatively low with 14 MJ/kg, whereas the corresponding value for lignin is 25 MJ/kg, this process stream is combusted to provide electricity and heat to the process and for external use [6–8]. Hence, the hemicellulose and lignin fractions are lost for material use. However, for the overall efficiency of WBBs it is important that hemicellulose and lignin can be recovered. Enhanced pulping processes, which make it possible to separate each biomass fraction, can lead to plant concepts with diversified product portfolios and new products.

Among the different pulping processes, especially the organosolv process, i.e., pulping with ethanol-water, is considered appropriate for the valorization of all wood components [9]. Furthermore, it benefits from relatively mild process conditions and easy-to-recover solvents. The released solid cellulose fibers can be used to produce pulp, which is processed into boards, fibers, and paper or can be hydrolyzed into sugars [3]. Pure, solid lignin can directly be used as a substitute in binding agents and fillings or depolymerized into smaller molecules [10]. Hemicellulose and its degradation products monomeric sugars, furans and carboxylic acids end up in the so-called wood hydrolyzate [11]. Due to relatively low concentrations, inhomogeneous composition, and the presence of plenty of impurities, the components in wood hydrolyzates are most challenging to recover for further use [12]. However, suppose the hemicellulose and its derived sugars are separated from the wood hydrolyzates. In that case, they could be used to produce high-value-added products and raise the competitiveness and sustainability of WBBs. As a promising feedstock for organosolv pulping, beechwood (*Fagus sylvatica*) was identified, accounting for 15 % of total forestland and 17 % of total wood

reserves in Germany. It is the third most common tree species and has an unused potential of 1.3 Mt of dry matter per year [13].

Hemicellulose is the second most abundant polysaccharide on earth and receiving increasing attention as a base polymer for bio-based chemistry [14, 15]. Promising products are biopolymers and bioplastics for their use as coatings [16], barrier materials in packaging films [17], xylo-oligosaccharides, e.g., in food and medical applications [18, 19], hydrogels [20], and paper additives [16, 21]. Hemicellulose can also be a starting material for monomeric sugars [22], which are currently considered the largest platform in terms of volume for the production of bio-based chemicals [23]. There is a growing interest in chemical sugar derivatives such as xylitol [24], furfural [25], levulinic acid [26], ethanol, and others [23].

To utilize the hemicellulose and its derived sugars for bio-based products, they have to be separated from other components in the wood hydrolyzate, concentrated, and depending on the wanted product, fractionated according to their molecular weight. Separation and purification processes account for the major production and operating costs in WBBs. It is, therefore, crucial to use separation technologies that are highly selective, efficient, and at the same time robust enough to deal with dissolved components (e.g., lignin) which may negatively affect the separation. Furthermore, separation and purification in WBBs is usually not achieved by standalone technologies but require a series of successive stages using cascade configurations [27]. However, several methods for recovering and purifying hemicellulose and other sugars from wood hydrolyzates have been investigated. Techniques commonly used include precipitation, coagulation, extraction, filtration, centrifugation, and evaporation [28-35]. These techniques exhibit various disadvantages, such as adding chemicals, high energy requirements, phase changes, and relatively high costs. Methods that could overcome these disadvantages are adsorption and membrane filtration processes. Adsorption is highly efficient and selective regarding the fractionation of complex systems [36], and membrane filtration can remove water and other solutes without adding chemicals and phase changes.

During the adsorption process, dissolved molecules are selectively bound to the solid surface of adsorbent material. The attractive forces between the adsorbent surface and the adsorbate molecules can be of physical and chemical nature. In physical adsorption (physisorption), the attractive force is relatively weak and is governed by van der Waals' and electrostatic forces. It is generally a reversible process, and most of industrial adsorption processes are based on physisorption [27]. In chemical adsorption (chemisorption), the attractive force is governed by chemical bonding and tends to be irreversible [37]. The development of an adsorption process depends crucially on the adsorption equilibrium and breakthrough curves [38]. Moreover, the regeneration or desorption of the loaded adsorbent material is a critical part of the adsorption process, as the separation must be completed over a long term.

Membrane filtration, whereas ultrafiltration (UF) and nanofiltration (NF) are most relevant for the separation and concentration of dissolved macromolecules and monomers [39, 40] in WBBs, is a pressure-driven process. The mass transport in UF is due to a convective flux through pores caused by a pressure difference across the membrane [6]. In NF, the mass transport is characterized by a convective flux and, in addition, by a diffusive flux due to differences in the (electro-)chemical potential on the retentate and the permeate side [41]. The

fractionation is mainly influenced by the membrane pore size and material as well as process parameters. However, fouling can cause severe performance reductions in membrane filtration, especially for NF membranes [42]. Therefore, the identification and reduction of those fouling mechanisms are crucial for the utilization of membrane processes in WBBs.

1.2 Aim of this Thesis

As a consequence of the above, this thesis aimed to develop and assess separation processes and cascades for the recovery and valorization of hemicellulose and its derived sugars from process streams in WBBs. Liquid phase adsorption and membrane filtration, particularly UF and NF, were used in these processes. In addition, a hydrothermal process for the pretreatment of the process streams was investigated. The process streams used came from the organosolv pulping of beechwood and are referred to as beechwood hydrolyzates (BWHs). Hence, the work also covered the utilization of completely new process streams from a novel WBB concept [43]. For achieving the aim, four general research parts were defined:

I. Separation and recovery of lignin from BWH by adsorption (Publications I and V),
II. UF of BWH for concentrating hemicellulose and removal of lignin (Publications II and V),
III. NF of hydrothermally treated BWH for concentrating hemicellulose derived xylose and removal of fermentation inhibitors (Publications III and V), and
IV. Demonstration and assessment of purification cascades for the separation and valorization of hemicellulose and derived xylose from BWH (Publications IV and V)

Adsorption studies were carried out with the aim of (i) separating and recovering lignin from BWH for further processing and (ii) minimizing hemicellulose losses. For this purpose, various adsorbent materials (polymeric resins and zeolites) were screened, and equilibrium studies, including the modeling of single- and multi-component adsorption isotherms, were conducted. This was done, on the one hand, with model solutions (MSs) to reduce complexity and to work with well-defined compositions, and, on the other hand, with authentic BWH. In addition, deviations between the isotherm models obtained from MSs and BWH were statistically evaluated. For the development of a continuous adsorption process in a fixed bed column, the effect of flow rate and dynamic lignin adsorption capacity was determined, and for the recovery of lignin desorption studies were carried out.

UF studies aimed at (i) the optimization of the process parameters transmembrane pressure (TMP), temperature, and pH value (pH) in terms of maximum permeate flux and hemicellulose retention, as well as minimal lignin retention and (ii) determine the influence of a previous adsorption step on the UF. Statistical design of experiments was applied to develop a mathematical correlation between the process parameters and the responses permeate flux, hemicellulose retention, and lignin retention. This enabled to assess the effect of each parameter on the responses and their interactions. In addition, various UF membranes, which differ in their polymeric materials and molecular weight cut-offs (MWCOs), were tested. Based on the results, the approach of Pareto optimization was used to identify optimized process conditions.

The influence of a previous adsorption step on UF was studied by comparing permeate fluxes and solute retentions of untreated and pretreated BWH at optimized process conditions.

In the NF studies, it was the aim to identify (i) the influence of hydrothermal pretreatment of BWH on the separation of xylose from fermentation inhibitors (e.g., furanic components and carboxylic acids) and (ii) appropriate process parameters and membrane materials. For this purpose, a newly designed hydrothermal process was developed, which enables the conversion of oligomeric hemicellulose in the BWH to xylose without the formation of chemical successors. Using a MS, BWH, and hydrothermally pretreated BWH, a performance (permeate flux, solute retentions, and selectivity) and fouling (resistance-in-series model) analysis was completed. In this context, various NF membranes, which differed in their polymeric materials and MWCOs, were also tested. Finally, to achieve an energetically favorable NF process with high xylose recovery rates, a parameter screening regarding TMP and temperature was carried out.

A technical and economic assessment of the developed separation processes is essential concerning a transfer of the processes to a commercial scale as well as for further scientific investigations. Based on the first three research parts, two potential purification cascades for the separation and valorization of hemicellulose and derived xylose from BWH were designed (Figure 1). Flowsheet simulation using Aspen Plus® was chosen for the calculation of mass and energy balances as well as sizing of the equipment. Specific production costs were calculated using a simplified approach based on VDI Guideline 6025 [44]. To compare the two purification cascades with each other, the same plant dimension and initial concentration of BWH were defined.

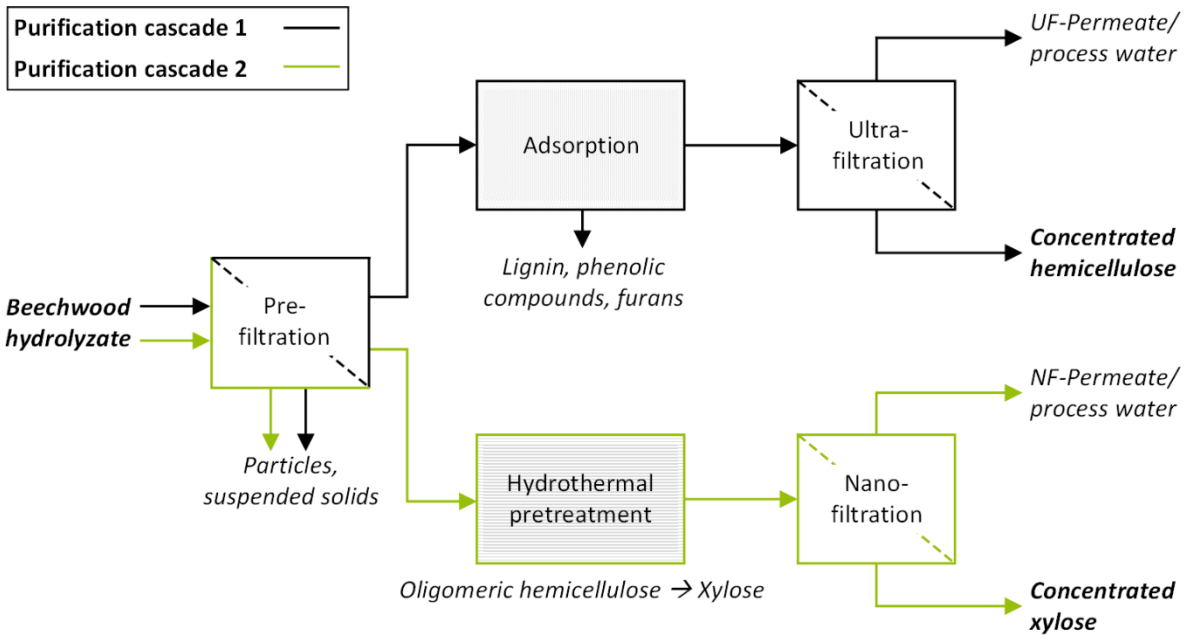

Figure 1: Purification cascade 1 (black line) and 2 (green line) for the separation and valorization of hemicellulose and derived sugars from organosolv beechwood hydrolyzate.

Thus, this thesis aimed to expand the application of adsorption and membrane filtration for the separation and valorization of hemicellulose from real biomass substrates in a large scale.

1.3 Outline of this Thesis

In order to take account of the described aim, the thesis is divided into the following key sections (Figure 2).

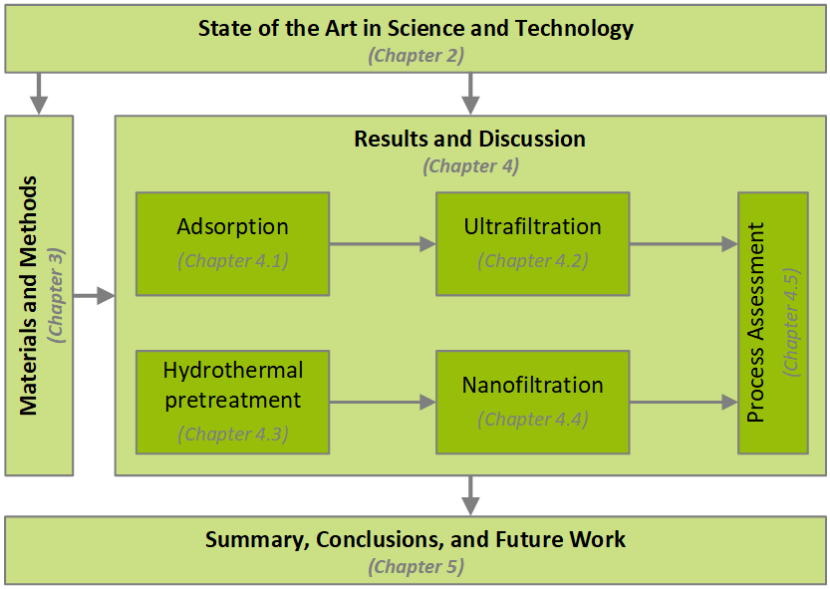

Figure 2: Structural outline of this thesis

Chapter 2 presents the state of the art in science and technology. First, the origin of wood hydrolyzates and their main components hemicellulose and lignin, as well as their chemical structure and molecular properties relevant for the separation by adsorption and membrane filtration are discussed. Then the hydrothermal pretreatment of hemicellulose is briefly presented. Next, methods that have already been used for the separation and valorization of hemicellulose and derived sugars from biomass streams are examined in more detail. Finally, fundamental aspects of the separation processes adsorption, UF, and NF are described.

The materials and methods used for the adsorption, ultrafiltration, hydrothermal pretreatment, and nanofiltration experiments are provided in **chapter 3**. In addition, the approach for the comparative technical and economic process assessment is described.

In **chapter 4,** the results obtained during the process development and assessment are presented and discussed. The separation and recovery of lignin by adsorption are divided in adsorbent screening, isotherm modeling, determination of the effect of flow rate and dynamic lignin adsorption capacity, and desorption studies. For the UF of BWH, for concentrating hemicellulose and removal of lignin, membrane screening, the influence of process parameters determined by response surface methodology, multiobjective optimization, and the effect of adsorption on UF are presented. Results of the hydrothermal pretreatment are discussed. Presentation of NF results for concentrating hemicellulose derived xylose and removal of inhibitory components is divided into membrane screening, performance and fouling analysis, and influence of process parameters. The process assessment of the two developed purification cascades results from mass and energy balances, and specific production costs are provided.

Finally, **chapter 5** draws conclusions concerning the aim and research parts elucidated at the beginning of the thesis. In addition, suggestions for future research are presented.

2. State of the Art in Science and Technology

In this section, the state of the art in science and technology regarding the dissolution of wood and resulting wood hydrolyzate streams, as well as characteristics of the solvable components hemicellulose and lignin are presented. Furthermore, the hydrothermal pretreatment of dissolved hemicellulose is briefly discussed. The major focus is on recovery methods of hemicellulose from wood hydrolyzates, especially on the separation processes adsorption and membrane filtration.

2.1 Dissolution of Wood and Hydrolyzate Streams

Cell walls of woody biomass mainly consist of cellulose fibers within a matrix of hemicellulose and lignin (Figure 3), which are closely connected via covalent and non-covalent linkages. Ester and ether bonds cross-link lignin with cellulose and hemicellulose and hydrogen bonds are present between the cellulose and hemicellulose molecules [45]. To a lesser extent, low molecular weight substances (e.g., wood extractives and inorganic compounds) can also be found in the structure [3]. The proportion and chemical composition of hemicellulose and lignin differ in hardwoods and softwoods, while cellulose is a relatively uniform component of all wood species [3]. For dissolving woody biomass or rather for the breakdown of these linkages, called pulping, strong alkaline or acid solutions and/or elevated temperatures and pressures are necessary. The composition of resulting hydrolyzate streams mainly depends on the pulping conditions and the wood specie used.

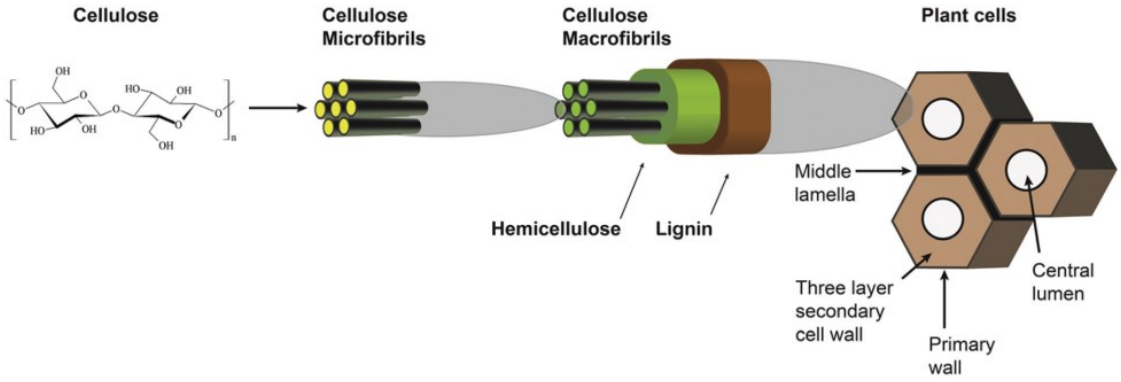

Figure 3: Schematic illustration of the lignocellulose structure [46]

2.1.1 Pulping Processes

Pulping processes are required to make the best possible use of the individual components from the bio-polymer composite. They can be divided into physical, physico-chemical, chemical, and biological processes, as well as combinations of these treatments. An overview of pulping processes sorted according to the basic principles is presented in Figure 4, and their functionality, as well as advantages and disadvantages, are described in detail in the literature [46–52].

The pulping processes differ significantly in terms of energy requirements and efficiency. While the energy requirements for physical processes are high, enzymatic processes are characterized by a long process time. In both cases, the fractionation of wood in its three main components is incomplete. Only the use of chemical pulping enables to separate the individual wood fractions with high purity [53].

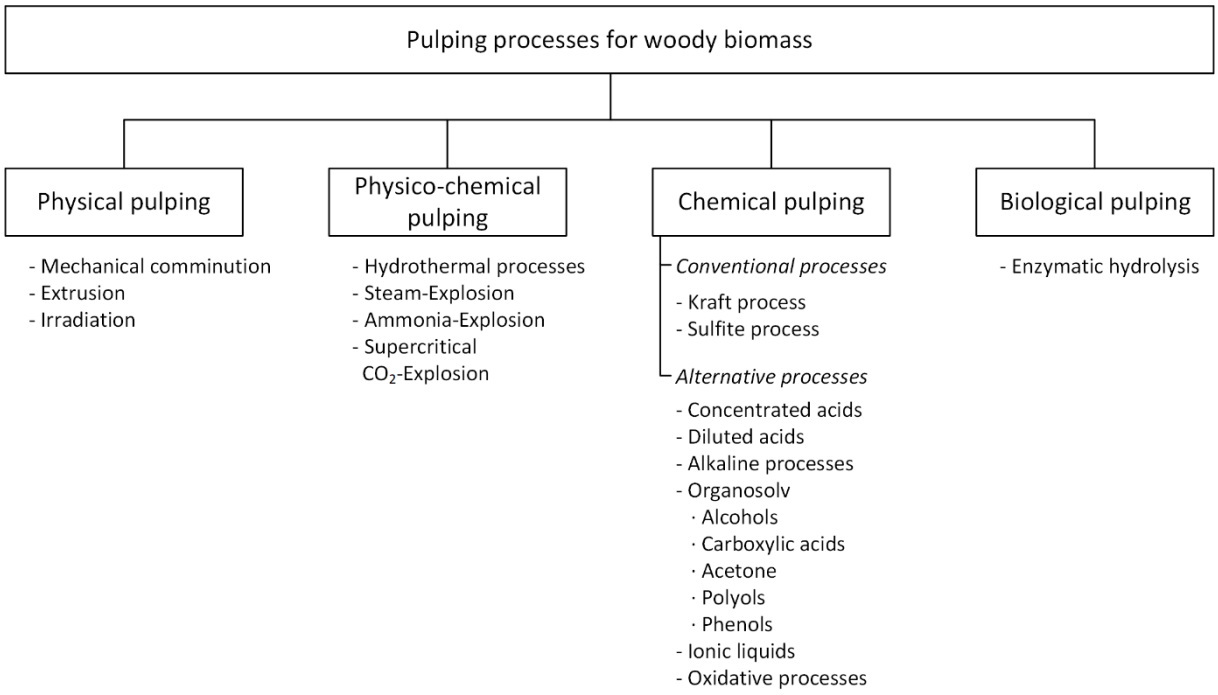

Figure 4: Overview of pulping processes for woody biomass (based on [48] and [53])

The main commercial chemical pulping techniques are the alkaline kraft process and the acid sulfite process. Both pulping processes are characterized by the residual lignin content, the carbohydrate yield, and final fiber composition. The kraft process tends to be better for treating hardwoods and the sulfite process for treating softwoods [3]. However, as mentioned above, kraft pulping has developed as the principal cooking process. Within kraft pulping, the wood is chipped and cooked with the active chemical agent's hydroxide and hydrosulfide anions, whereby hydrosulfide is largely responsible for accelerating the delignification. The cooking takes place at about 160–180 °C and 0.7–1.1 MPa [54]. The high alkalinity and the elevated temperature and pressure cause a considerable cleavage of the ether bonds in the phenolic units of lignin and the dissolution of hemicellulose. The insoluble cellulose fibers are further processed to chemical pulp via bleaching, and the cooking chemicals, as well as the remaining biomass components hemicellulose and lignin, end up in the black liquor. This hydrolyzate stream is typically concentrated and burned to provide heat and electrical energy for the process itself as well as to recover the cooking chemicals. Researchers have become increasingly interested in the material use of black liquor or extracting its valuable products [55–61]. However, during the kraft process, lignin is structurally changed so that material added value is made more complex and, due to the undesirable peeling reaction, hemicellulose and other carbohydrates are also broken down [62]. In addition, the lignin has a high degree of condensation and sulfur content. Nevertheless, a commercial method, the so-called LignoBoost process, has been developed to recover lignin, which can be used as a solid fuel [63]. The high

sulfur content of the lignin is still problematic and there are environmental concerns for the use of this kind of lignin. Despite all efforts, the hemicellulose remains unused regarding its material value.

The focus of enhanced pulping processes in WBB concepts must be on the complete use of each wood component and the generation of high-value-added products. In addition, the pulping process has to be a clean technology with easy to recover cooking chemicals. Organosolv pulping using organic solvents (e.g., alcohols, organic acids, acetone, polyols, and phenols) as cooking chemicals, first studied and described in 1931 by Kleinert et al. [64], has emerged as one of the most promising processes regarding this requirements. Using organic solvents that can be obtained from renewable sources, such as ethanol, acetic acid, or glycerol, makes its application for the sustainable production of fuels and chemicals even more attractive. Ethanol, as a low-cost, renewable solvent and comparatively easy to recover, is the most commonly used solvent for pulping by organosolv treatment [46]. The pulping process is conducted under pressure at temperatures significantly below the solvent's boiling point and with or without the addition of a catalyst. Acid-catalyzed (e.g., sulfuric acid [65]) organosolv pulping generally performs better than a non-catalyzed process [53]. The cellulose fibers are an enhanced feedstock for enzymatic saccharification and subsequent fermentation [46]. Organosolv pulping produces lignin that is relatively pure, low in sulfur, and less condensed than that produced by the kraft and LignoBoost process [66, 67]. Hence, higher-value products can be produced from the lignin. The hemicellulose and its degradation products monomeric sugars, furans, carboxylic acids, as well as remaining lignin and its degradation products, end up in the wood hydrolyzate. The separation of the hemicellulose and its derived sugar components from this kind of wood hydrolyzate is the subject of this thesis.

2.1.2 Hemicellulose

Hemicellulose is the second most abundant plant renewable material and includes all non-cellulosic carbohydrates of the lignocellulosic biomass. Thus, hemicellulose is an amorphous polysaccharide consisting of several sugar units that are mostly branched and have lower molecular weights (MW) than cellulose. Consequently, it is more hydrophilic and has a higher solubility in most solvents, including water. The degree of polymerization (DP) is 50–200, which corresponds to a MW of approx. 7500–36,000 g/mol. The sugar units of the hemicellulose can be subdivided into different types such as pentoses (e.g., xylose and arabinose units), hexoses (e.g., glucose and mannose units), hexuronic acids (e.g., glucuronic and galacturonic acid), and deoxy-hexoses (e.g., rhamnose units). If the main chain of the polysaccharides is composed of only one type of sugar unit, it is called homopolysaccharides, e.g., xylan. If the main chain of the polysaccharides is composed of two or more types of sugar units, it is called heteropolysaccharides, e.g., glucomannan. Some sugar units only act as side groups of the main chain (backbone), for example, 4-*O*-methylglucuronic acid and galactose [3, 45, 46].

In dependence on the wood specie, the average content of hemicellulose is 20–35 % of the dry solids. In hardwoods, the primary type of hemicellulose is xylan (glucuronoxylan), formed from a xylose backbone appended with 4-*O*-methylglucuronic units (Figure 5 (a)). Approx. 60 % of the xylose units of hardwoods can also carry an acetyl group attached either to the C-2 or C-3 position [3, 68]. Only a small amount of the hemicellulose in hardwoods consist of glucomannan. The major hemicellulose in softwoods are glucomannan (galactoglucomannan). Its backbone consists of *β*-D-glucopyranose and *β*-D-mannopyranose units linked together via 1,4-linkages (Figure 5 (b)). The hydroxyl groups at C-2 and C-3 in the chain are substituted by *O*-acetyl groups [45]. The amount of xylan in softwoods is about half of that of glucomannan [69].

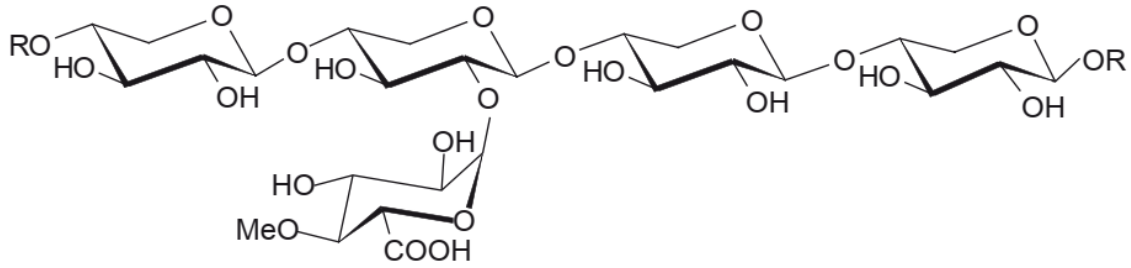

a) Xylan

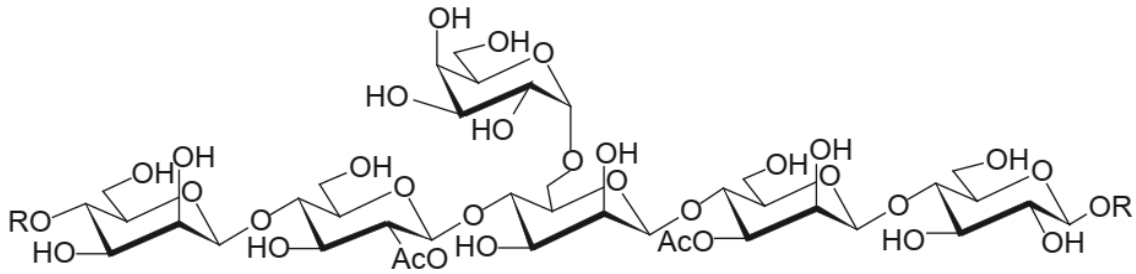

b) Glucomannan

Figure 5: Molecular structure of (a) xylan and (b) glucomannan

During organosolv pulping, the hemicellulose is dissolved and broken down by acid-catalyzed hydrolytic splitting of glycosidic linkages to water-soluble hemicellulose oligomers and their derived monosaccharides. By further elimination of water, the monosaccharides react to furans. In the case of pentoses, mainly furfural is formed, and hexoses are mainly converted to 5-hydroxymethylfurfural (5-HMF). The furans are intermediates for the formation of carboxylic acids, such as levulinic, acetic, and formic acid [3, 53]. The hemicellulose degradation products and intermediates are dissolved in the hydrolyzate stream. In this thesis, wood hydrolyzates from the organosolv pulping of beechwood were used as input material. Hence, the dissolved constituents in the BWHs are basically oligomeric hemicellulose and its derived pentoses, mainly xylose, and their follow-up products. The major components in the BWHs, including their physico-chemical properties, are listed in Table 1, and typical concentrations of these components can be found in Table 3.

Table 1: Major hemicellulose degradation products and intermediates in organosolv beechwood hydrolyzates and their physico-chemical properties

Component	Molecular formula	Molecular structure	Molecular weight [g/mol]	pK_a [-]	Diffusion coefficient [10^{-6} cm²/s]	Stokes diameter [nm]
Oligomeric hemicellulose	-	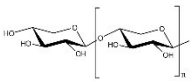	300-10,000[a,b]	12-13[c,d]	-	48-160[e]
Glucose	$C_6H_{12}O_6$	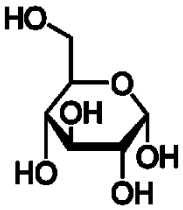	180.16	12.28[f]	6.76[g]	0.73[d]
Xylose	$C_5H_{10}O_5$	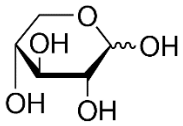	150.13	12.15[f]	7.69[g]	0.64[d]
Arabinose	$C_5H_{10}O_5$	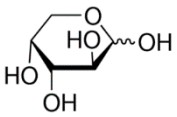	150.13	12.34[f]	7.73[g]	0.64[d]
5-HMF	$C_6H_6O_3$	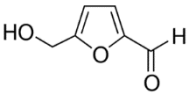	126.11	-	10.6[h]	0.46[d]
Furfural	$C_5H_4O_2$	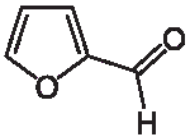	96.08	-	11.2[i]	0.44[d]
Acetic acid	$C_2H_4O_2$	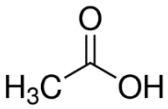	60.05	4.76[f]	11.9[i]	0.41[d]
Formic acid	CH_2O_2	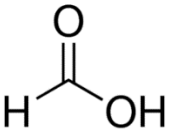	46.03	3.75[f]	15.2[i]	0.32[d]

[a][70]; [b][71]; [c][72]; [d][73]; [e][74]; [f][75]; [g][76]; [h][77]; [i][78]

2.1.3 Lignin

Lignin is an abundant and complex aromatic biopolymer that accounts for 20–40 % of the dry solids in wood and is responsible for liquid transport and mechanical strength in the plant [3]. The three-dimensional macromolecular structure of lignin is formed by the polymerization of the phenolic precursors sinapyl alcohol, guaiacyl alcohol, and p-coumaryl alcohol (Figure 6). These monolignols have similar structures but differ in the number of methoxy groups. During the polymerization, the monolignol units are connected in a random order resulting in a non-

linear, highly cross-linked amorphous network [54]. The proportions of the three structural units in the lignin macromolecule differ depending on the lignocellulose species. Whereas softwood lignin mainly consists of guaiacyl units, hardwood lignin also contains 50 % syringyl units, and all three units contribute to the macromolecular structure of agricultural plants [45].

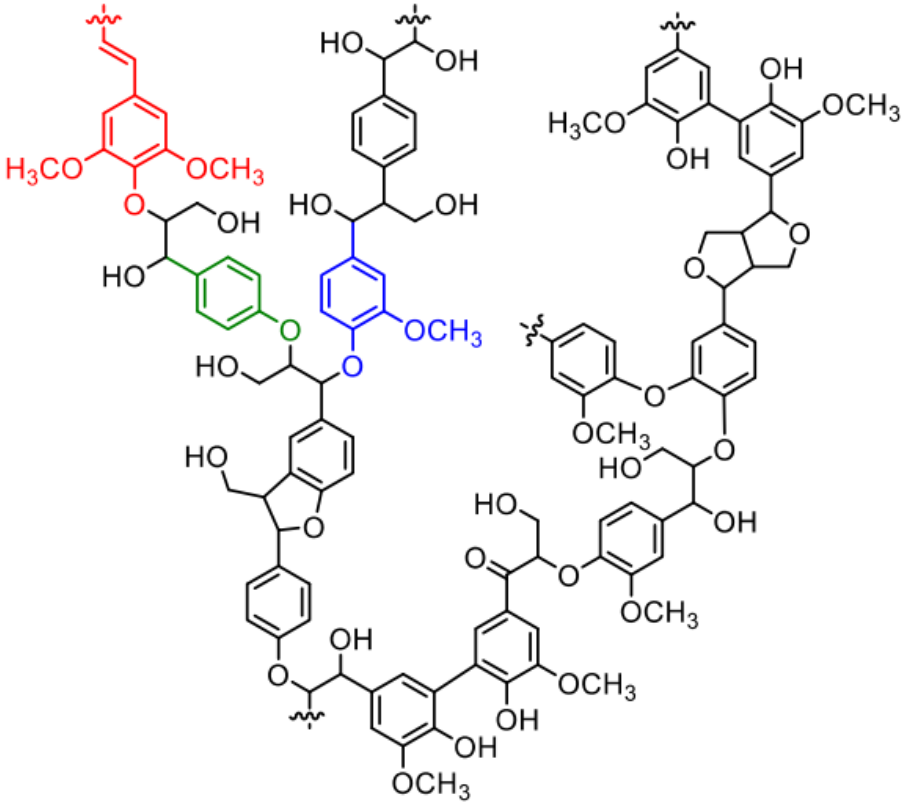

Figure 6: Schematic macromolecular structure of lignin with the major monolignol units colored as sinapyl alcohol in red, guaiacyl alcohol in blue, and p-coumaryl alcohol in green [79]

Ether bonds, mainly *β*-*O*-4-bonds and carbon-carbon bonds, are the dominating linkages within the lignin network [80]. In addition, lignin forms covalent bonds and cross-links to the carbohydrate components, mainly with the hemicellulose and to some extent with the cellulose, in the lignocellulose complex [46]. These lignin-carbohydrate complexes make the fractionation of the individual lignocellulose components complicated. However, as presented in Section 2.1.1, these linkages can be cleaved by several pulping processes. Therefore, depending on the wood species and the pulping process used, the structure and functional groups of lignin change compared to its native form [3].

The homolytic cleavage of the *β*-*O*-4-bonds is considered the dominant reaction of the lignin during organosolv pulping and is catalyzed by acids [81]. This creates free phenolic OH groups, which have a significant contribution to the reactivity of the lignin fragments. Cleavage of the carbon-carbon bonds during the pulping process was not observed. At the same time as the lignin degradation reactions, condensation reactions with carbohydrate derivatives can occur, forming humic substances [3]. However, remaining lignin fragments dissolved in organosolv BWH have hydrophobic and antioxidant properties [53], a MW from 500 to 1,000 g/mol [70, 71], thus lower compared to hemicellulose and a pK_a value of 3 to 11 [45].

2.1.4 Residual Components

The three main components, cellulose, hemicellulose, and lignin, make up more than 90 % of the dry solids in woody biomass. The remaining 10 % are pectins and proteins, as well as smaller molecules, such as extractives and inorganic substances. Pectins are polysaccharides consisting of D-galacturonic acid, D-galactose, L-arabinose, and L-rhamnose residues, while proteins are polymeric structures consisting of amino acids. Extractives are a class of components that can be extracted from wood with organic solvents to get terpenes, fats, waxes, and phenols, or with hot water to get tannins and salts. They account for 2 to 5 % of the dry solids in wood and about 20 to 40 % of the dry bark [3, 45]. The inorganic constituents of wood are entirely contained in the ash and amount to 0.1 to 1 % of the ash. Inorganics mainly comprise Al, Ca, Fe, K, Mg, Mn, Na, P, and Zn [3].

2.2 Hydrothermal Pretreatment of Hemicellulose in Wood Hydrolyzates

Various hydrothermal pretreatments for biomass conversion exist, depending on the process conditions, as illustrated in Figure 7. At temperatures of 150–200 °C and pressures of around 2.5 MPa, the pretreatment is called hydrothermal carbonization (HTC) and is generally characterized by forming a high-calorific solid phase. At slightly higher temperatures and pressures, aqueous phase reforming (APR) produces hydrogen that reacts via heterogeneous catalytic reactions to hydrogenate degradation products of biomass. Between 250 and 370 °C and at pressures above the equilibrium vapor pressure of water, an energy-dense bio-crude can be obtained by hydrothermal liquefaction (HTL). Beyond the critical point, supercritical water gasification (SCWG) is favored, leading to a methane-rich (near the critical region) or hydrogen-rich (temperatures above 600 °C) combustible gas. [82]

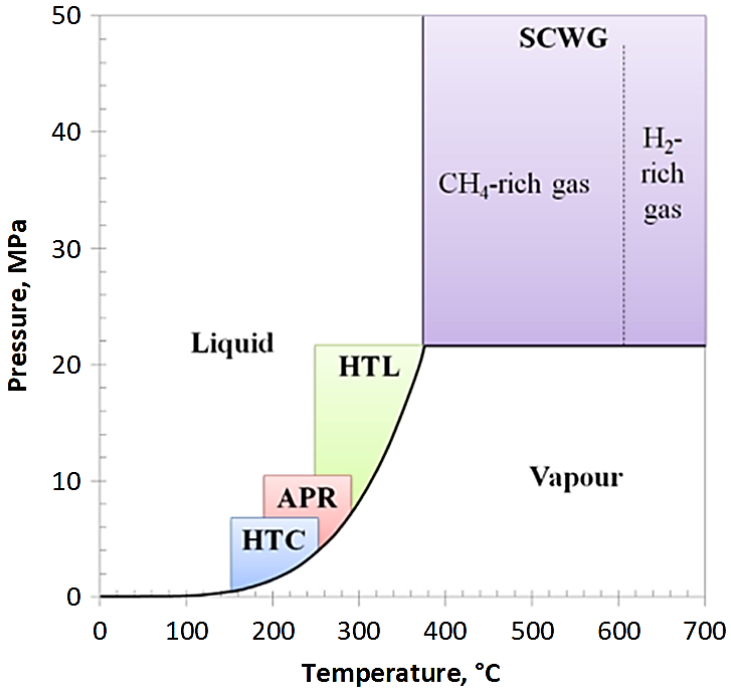

Figure 7: Hydrothermal processing regions according to the pressure–temperature phase diagram of water [82]

The hydrothermal pretreatment of wood hydrolyzates is performed in the HTC region but without the aim of producing a solid fuel. For this reason, relatively short residence times are crucial to prevent polymerization reactions that lead to the formation of solids. Hence, it is not a typical HTC process. However, under selected process conditions, this pretreatment enables the depolymerization of the remaining hemicellulose oligomers, formed during pulping, into value-added soluble products, such as monomeric sugars, furans, and carboxylic acids (Figure 8) [83]. On the other hand, under harsh operational conditions, the formation of humins by polymerization reactions can occur, which may cause problems in the following processes, such as increased fouling or inhibition [84–86]. Within this thesis, the hydrothermal pretreatment of organosolv BWH for converting oligomeric hemicellulose to xylose without the formation of furanic compounds is examined to a certain extent.

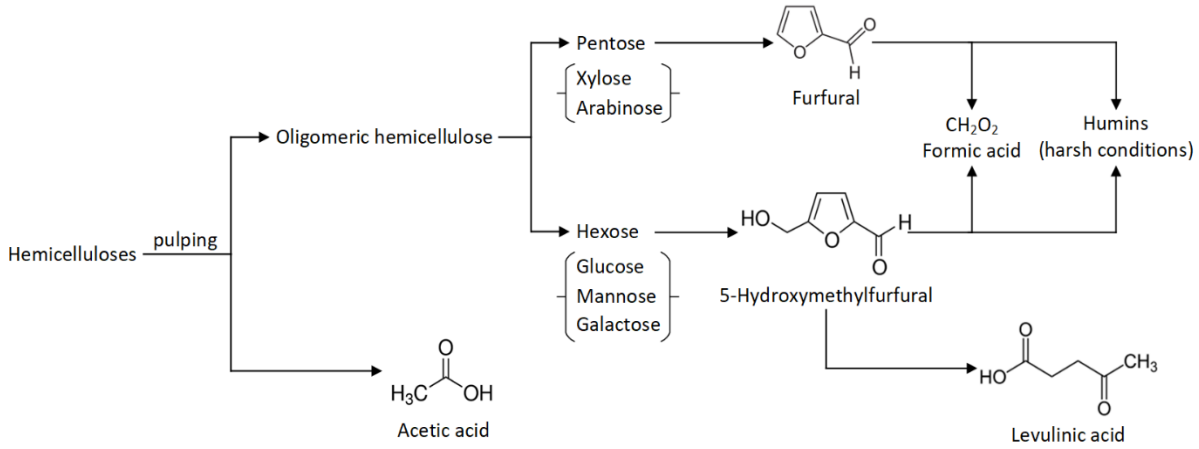

Figure 8: Reaction pathways in the hydrothermal pretreatment of hemicellulose to sugars and degradation products (based on [83])

In principle, hydrothermal pretreatment has some advantages, such as that (i) the process does not require any additional chemicals other than water, which reduces equipment capacity and corrosion, (ii) it is a simple and economical operation, and (iii) the ability to break down the structure of the hemicellulose oligomers and thus reduce sugar losses. For that reason, this pretreatment has been considered a sustainable process suitable for the fractionation of oligomeric hemicellulose into valuables according to the biorefinery approach [48, 87, 88]. Researchers put in efforts to develop hydrothermal processes that reflect these potential benefits and achieve high yields on the desired products without the formation of chemical successors.

Li et al. [89] developed a selective catalytic hydrothermal pretreatment of corncob into xylose and furfural using solid acid catalysts ($SO_4^{2-}/TiO_2 - ZrO_2/La^{3+}$). The prepared catalyst had high thermal stability and strong acid sites. The highest furfural yield of 6.2 g/100 g was obtained at a temperature of 180 °C and a residence time of 120 min with a 6.8 g/100 g xylose yield at a corncob-to-water ratio of 10:100. This confirmed the possibility of a hydrolytic splitting of biomass into platform chemicals by solid acids. Thus, to realize the process, chemicals had to be added, which makes it disadvantageous from an economic and environmental point of view.

Chemical-free processes are of higher interest since no additional input streams or its recovery is necessary and the resulting product stream contains few or no inhibitors. Cheng et al. [90] developed a laboratory scale batch hot water pretreatment and a pilot scaled continuous hydrothermal pretreatment to convert bioenergy sorghum bagasse into monomeric sugars without adding any agents. The aim was to obtain both glucose and xylose at temperatures of 160–190 °C and a residence time of 10 min. In addition, during pilot scale tests, the influence of subsequent disk milling was studied. Maximum yields of glucose and xylose of 82.6 % and 70.8 %, respectively, were achieved when sorghum bagasse was pretreated at 180 and 190 °C followed by disk milling. Laboratory experiments resulted in 5–15 % higher yields than pilot scale experiments. Hence, it could be shown that high yields of monomeric sugars are attainable without adding chemicals to the pretreatment.

Further research has to focus on increasing the yields or rather converting the entire oligomeric sugars into monomeric sugars without the formation of furans. Köchermann et al. [87] studied the kinetics of hydrothermal furfural production from xylose containing organosolv BWH and MSs at temperatures between 160 and 200 °C. The results obtained show that the almost complete conversion of oligomeric hemicellulose to xylose without a notable furfural production appears to be possible. This approach is continued in the thesis in research part III (Section 1.2).

2.3 Recovery Methods of Hemicellulose from Wood Hydrolyzates

In the previous sections, pulping and hydrothermal processes that result in different hydrolyzate streams containing considerable amounts of dissolved biomass components were discussed. For the material use of the hemicellulose present in the wood hydrolyzates, these have to be efficiently separated from other solutes. Methods that could be suitable for this purpose are precipitation, preparative chromatography, liquid phase adsorption, and membrane filtration. It depends on the desired properties of the hemicellulose, e.g., molecular weight and purity, which technology best meets the requirements. As described above, the recovery of hemicellulose from wood hydrolyzates is likely to be achieved not with a standalone separation technology but with a combination of methods. In this section, the mentioned suitable separation technologies, including their advantages and disadvantages, are presented and discussed. Due to their extensive use within the thesis, the major focus is on the recovery processes liquid phase adsorption and membrane filtration.

2.3.1 Precipitation

Precipitation using organic solvents (e.g., ethanol, methanol, and acetone) is a simple and one of the main methods for recovery and purification of hemicellulose. The solvents must be miscible with water in any ratio and reduce, due to their low dielectric constant, the solvation of the hemicellulose in the wood hydrolyzates. Because of its chemical properties, ethanol is the most commonly used solvent [31]. By adjusting the ethanol content, the hemicellulose can be fractionated according to its molecular weights [91]. Song et al. [92] described the relationship between yield and average molecular weight in terms of the ethanol content used during the precipitation of hemicellulose from spruce hot-water extracts (Figure 9). The

hemicellulose yield increased with increasing ethanol content, and the average molecular weight decreased. Hence, the ethanol consumption becomes high if a high yield is required. Lignin is precipitated much lower than the hemicellulose and may be part of lignin-hemicellulose complexes. Other investigations [93–95] regarding the precipitation and fractionation of hemicellulose from different hydrolysate streams with ethanol confirm that hemicellulose recovery is higher at higher ethanol contents. However, besides the ability to control the molecular weight of the precipitated hemicellulose, this method exhibits some disadvantages. The precipitated hemicellulose has to be separated from a huge volume of ethanol by, e.g., filtration, and, in addition, the consumed ethanol has to be purified and recirculated by, e.g., distillation or NF. Despite the high materials and process technology expenditure, the hemicellulose fraction still contains lignin and other wood components [8, 92, 96].

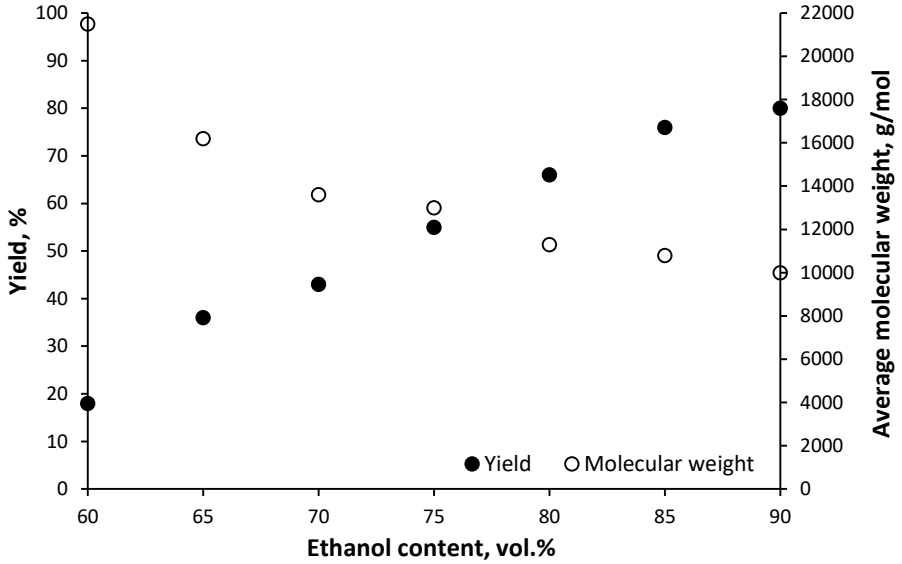

Figure 9: Yield and average molecular weight of hemicellulose precipitated from hot-water spruce extracts at different ethanol contents (based on [92])

Supercritical anti-solvents, e.g., CO_2, can also be used for the precipitation of hemicellulose from wood hydrolyzates. This method offers a more sustainable alternative to ethanol since CO_2 has special physico-chemical properties at the critical point (p = 7.38 MPa, T = 31.8 °C). It is non-toxic, non-flammable, inert, cheap, and easily to remove from the product stream [31]. Haimer et al. [97, 98] investigated the precipitation of hemicellulose from DMSO/water mixtures using CO_2 as an anti-solvent. Results were obtained that indicate that the precipitation rate and thus the particle size and shape, as well as the purity can be controlled by temperature and pressure. Hence, this method is suitable for providing specific forms of hemicellulose. However, the process involves pressures of 6–11 MPa and is, therefore, more complex and demanding.

As mentioned above, precipitation of hemicellulose from untreated wood hydrolyzates requires large amounts of solvents and therefore may not be economical and ecological. Using combined separation techniques, such as membrane filtration for the volume reduction and precipitation of the concentrate rich in hemicellulose, has attracted some interest. Xu et al. [99] reported that

UF and subsequent ethanol precipitation led to a higher hemicellulose content and average molecular weight than precipitation alone. This process solution could be useful if solid hemicellulose or higher purity than obtained by just UF are required [6].

2.3.2 Preparative Chromatography

Preparative chromatography allows for selective and high hemicellulose recovery at high purity. Different types of columns have been studied, such as anion-exchange [100], size-exclusion [101], affinity [102], and centrifugal partition [103] chromatography, whereas the first two are the most commonly used. The principle of anion-exchange chromatography is based on the ion exchange mechanism and of size-exclusion chromatography on the different molecular weights or, more correctly, on the hydrodynamic volume. During the chromatographic separation, the product fraction is diluted due to elution with an additional solvent. Hence, similar to precipitation, a combination of membrane filtration and preparative chromatography could be beneficial. Due to the lower feed volume during the chromatography, less eluent would be required, and the purity of the hemicellulose could be increased compared to membrane filtration alone. A separation cascade consisting of microfiltration to remove solids, UF for the pre-concentration of hemicellulose, and final purification by size-exclusion chromatography was investigated by Andersson et al. [101]. Process water from a thermomechanical pulp mill was used as an input stream. Recovery of hemicellulose of greater than 99 % and a purity of approx. 82 % could be achieved at an optimal sample volume and flow rate of 20 % and 25 mL/min, respectively. In terms of the economic feasibility, it was concluded that alternative processes such as diafiltration are probably more suitable in dependence on the product requirements. However, the need for salts, such as borate, NaOH, or NaCl, which act as buffers in the eluent, and the difficulty in upscale are still obstacles to an industrial application of this technology [15, 31]. In addition, the salts that are used for the buffers have to be recovered.

2.3.3 Liquid Phase Adsorption

2.3.3.1 Fundamentals

Liquid phase adsorption is a thermal separation process characterized by the selective addition of solutes from a bulk fluid on solids. The process occurs through the interaction of the active, high-energy centers on the surface of the solids with the atoms, molecules, or ions of a mobile phase. The adsorption active phase in which the addition takes place is called adsorbent. The component in the bulk fluid phase prior to adsorption is called adsorptive, and the component which is bound to the adsorbent, is called adsorpt. Adsorbate is the complex of adsorpt and adsorbent. Desorption describes the remobilization of already bound adsorpt. The relations are shown schematically in Figure 10 (a). [27]

Adsorption-desorption processes consist of a complex interaction of different convective and diffusive mass transport mechanisms, which are coupled with the actual adsorption/desorption as well as heat transport and heat conduction mechanisms. These usually proceed in the following seven sub-steps (Figure 10 (b)) [104]:

(1→2) The adsorptive attains the boundary layer of the adsorbent by convective and diffusive mass transport,
(2→3) The adsorptive permeates through the boundary layer by diffusive mass transport,
(3→4) The adsorptive penetrates into the pores of the adsorbent by different diffusion mechanisms, some take place simultaneously and some sequentially,
(4→5) The actual adsorption is the exothermic addition of the adsorptive to the adsorbent,
(5→6) The released heat of adsorption is transported, mainly by heat conduction, to the surface of the adsorbent,
(6→7) The energy transport through the boundary layer is equivalent to (2→3), and
(7) The output of the released energy into the bulk fluid phase by convection and heat conduction.

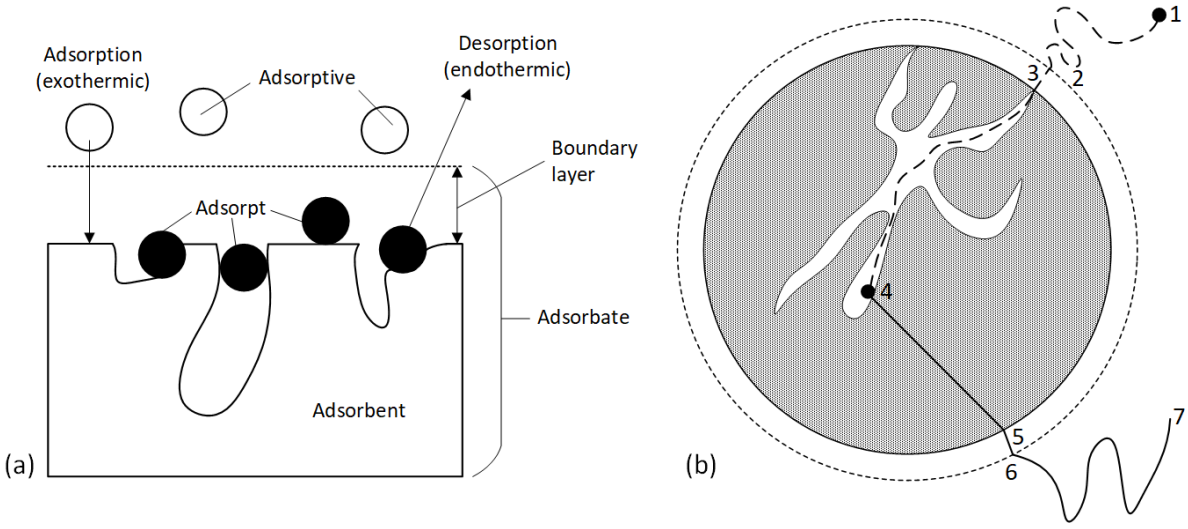

Figure 10: (a) Basic terms and (b) sub-steps of the adsorption process (based on [104])

Liquid phase adsorption is typically classified according to its bonding enthalpies in chemisorption and physisorption [37]. In the case of *chemisorption*, the adsorpt-adsorbent bond is based on an electron transfer; this means it is a chemical bond. Hence, the binding energies are in the magnitude of reaction enthalpies. Kümmel and Worch [105] indicate values between 60 and 450 kJ/mol. Since chemisorption is an irreversible process, it is used almost exclusively in the field of control filters to remove problematic compounds beforehand. The adsorbent cannot be regenerated after fully loaded and must, therefore, be disposed of. On the other hand, if the adsorpt-adsorbent bond is based on intermolecular forces without electron transfer, i.e., dipole, dispersion (van der Waals' interactions), or induction forces dominate, the term *physisorption* is used. The binding energies are less than 50 kJ/mol [105]. In most technical adsorption processes, physisorption dominates since the regeneration of the loaded adsorbent is feasible under technically and economically sensible conditions. Thus, a cyclic adsorption-desorption process without the exchange of adsorbent can be realized. The affinity between adsorptive and adsorbent depends mainly on the properties of the bulk fluid or rather the contained molecules and the used adsorbent materials. Characteristics of the various adsorbent materials are presented in Section 2.3.3.2, and for the adsorptive, the following properties can influence physisorption [106]:

- Increasing hydrophobicity increases the adsorbability
- Functional Groups
  - Hydroxyl group (R-OH) reduce the adsorbability
  - Amino group (R-NH_2) greatly reduce the adsorbability
  - Sulfonic acid groups (R-SO_3H) usually reduce the adsorbability
  - Nitro group (R-NO2) improve the adsorbability
- A low pH results in a higher adsorbability of acidic substances
- A high pH results in a higher adsorbability of basic substances

As with all thermal separation processes, the driving force behind adsorption is an externally imposed imbalance in chemical potential. Hence, during adsorption and desorption processes, an equilibrium between the adsorbate phase and the adsorptive concentration in the bulk fluid aspires. The position of the equilibrium is described by thermodynamics and the speed with which the equilibrium is reached by kinetics. However, thermodynamic equilibrium is characterized by a certain coverage of the adsorbent surface at a constant adsorptive concentration. In this state, the adsorption rate is equal to the desorption rate. As the thermodynamic equilibrium is approached, adsorbed molecules release from the adsorbent surface and change into the bulk fluid. Therefore, the net adsorption rate slows down near the equilibrium [107].

Thermodynamic equilibrium in liquid phase adsorption depends on the concentration of the adsorptive in the bulk fluid and on the process temperature. To determine the loading or capacity of the adsorbent in equilibrium, one of the two parameters must be kept constant. This results in three options to present the thermodynamic equilibrium of the adsorption in a two-dimensional plot. The types of representation are isotherms, isosters, and isobars. The most common is the isotherm, where the process temperature is kept constant, and the adsorbent capacity is plotted over the adsorptive concentration. Usually, a higher adsorptive concentration results in a higher capacity, while a higher process temperature at the same adsorptive concentration results in a lower capacity. According to Brunauer et al. [108] adsorption isotherms can be classified into five fundamental types, as illustrated in Figure 11.

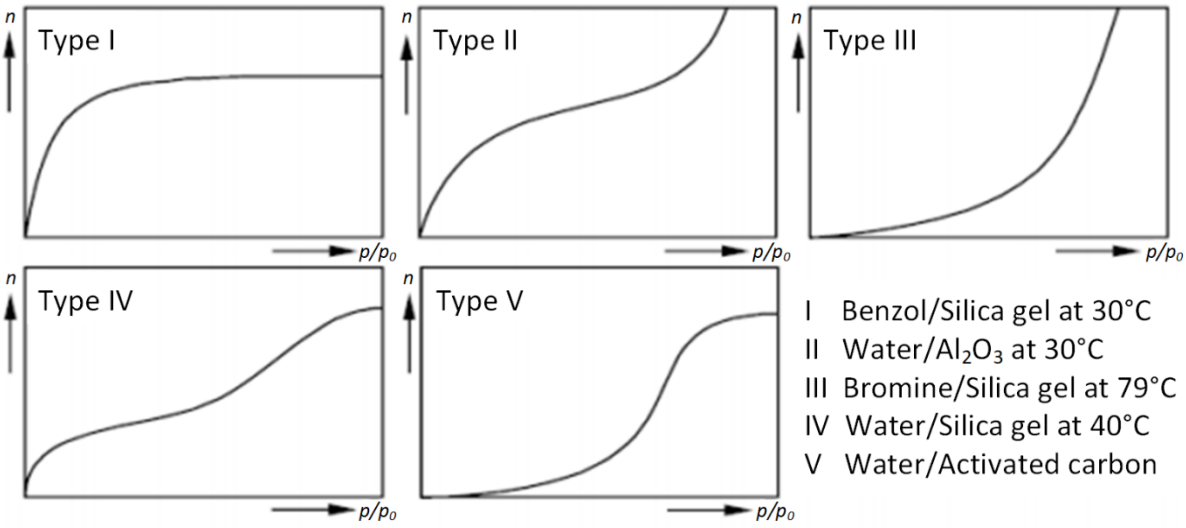

Figure 11: Categories of adsorption isotherms (based on [108])

After an initial linear increase, Type I isotherms reach a plateau value that can be interpreted as the maximum adsorbate concentration. These isotherms correspond to monolayer adsorption and are mathematically described by the Langmuir equation. Microporous adsorbents exhibit a Type I isotherm. Type II isotherms describe adsorption in non-porous and macroporous adsorbents. After reaching an intermediate plateau and exceeding a critical concentration, the monolayer changes into multilayer adsorption, followed by condensation in the pores. The BET equation allows a mathematical formulation of the isotherm type. Type III isotherms indicate only weak interactions between the adsorbent surface and the first adsorpt layer. Thus, multilayers are already formed before the first adsorpt layer is completely built up. A mathematical description is available via the Freundlich equation. Type IV isotherms follow an undulating course with an intermediate plateau. They are characterized by multilayer formation and can be mathematically solved by various approaches; one possibility is the BET equation. Type V isotherms are s-shaped and represent a combination of type III (Freundlich) and I (Langmuir) isotherms. The isotherm models used in the adsorption studies (research part I – Section 1.2) are presented in more detail in Section 3.2.1.3 [27, 104].

The simplest case for the determination of equilibrium and isotherm models is the single-component process. In industrial practice, this case occurs only very rarely; usually, multi-component processes are predominant. Wood hydrolyzates are, as presented above, multi-component systems. During the adsorption, the various adsorptives compete for the active sites on the adsorbent. A number of multi-component isotherm models exist for the mathematical description, which are based either on the equivalent single-component isotherms or empirical models.

In a batch reactor system, the equilibrium results from the adsorptive concentration in the bulk fluid and on the adsorbent. As adsorption time progresses, the system approaches maximum adsorption capacity and thus equilibrium. On the other hand, when using a continuous column, adsorption occurs along a fixed adsorbent bed. Over the operation time, the active adsorption zone relocates deeper in the adsorbent bed, as illustrated in Figure 12. Saturation or breakthrough of the adsorbent bed occurs when the adsorptive concentration C in the output stream corresponds to the adsorptive concentration C_0 in the input stream, i.e., C/C_0 is equal to 1.

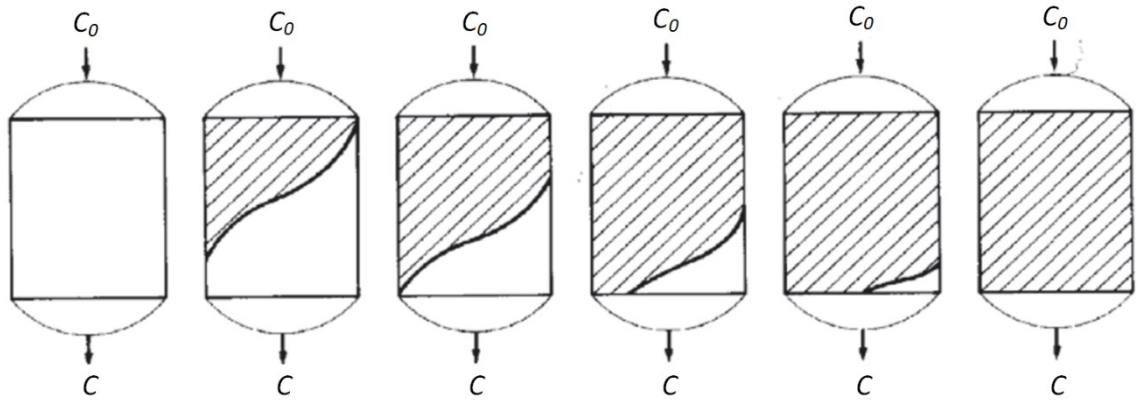

Figure 12: Relocation of the active adsorption zone over operation time [109]

Exemplified breakthrough curves are presented in Figure 13. During the adsorption of multi-component mixtures, various adsorptives compete for the active sites on the adsorbent. Poorly adsorbable substances, which quickly occupy the active adsorption sites in the fixed bed, can be displaced by strongly adsorbable substances. Consequently, the concentration of the poorly adsorbable substances in the outlet stream can be greater than the inlet concentration, as shown by the type 1 breakthrough curve. The type 2 breakthrough curve is to be expected for the strongly adsorbable substances [110].

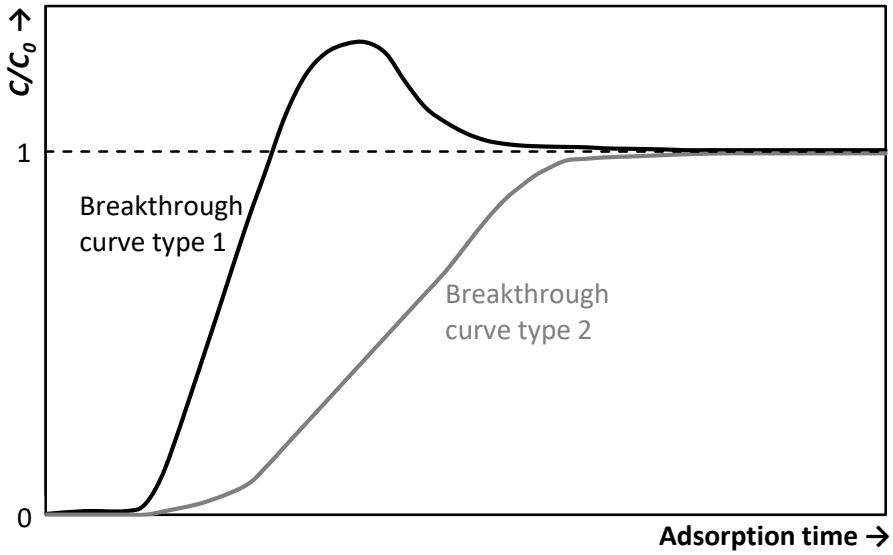

Figure 13: Breakthrough curves of a multi-component adsorptive mixture (based on [110])

2.3.3.2 Adsorbent Materials

Adsorbents are porous solids that differ in their pore surface, pore geometry, and chemical composition. Within this thesis, different classes of adsorbents were studied. In the following section, essential properties of industrial adsorbent materials, more precisely of activated carbon, zeolites, and polymeric resins, for separation processes in biorefineries are briefly presented.

Activated Carbon

Activated carbon is the most widely used adsorbent. It is defined as a carbonaceous product with a porous structure (pore volume > 0.2 cm^3/g) and a large internal surface area (> 400 m^2/g) with pore diameters between 0.3 and a few thousand nanometers on which molecules attach [104]. Commercial carbons are produced from various materials, such as charcoal, peat, wood, fruit nuts, lignite, petroleum coke, bituminous coal, and coconut shells. Depending on the raw material and later technical use, thermal or chemical activation is applied. Thermal activation consists of two process steps, first carbonization and then activation. Carbonization is realized by heating the raw material to 400 to 500 °C in an oxygen-free atmosphere to remove the volatile matter. The carbonized particles are then activated by exposing them to an oxidizing agent, usually steam or carbon dioxide, at 800 to 1000 °C [37]. This technique is usually used for the activation of coal and coconut shell. This forms a porous, three-dimensional graphite lattice and a large surface area by removing the pore blocking pyrolysis materials created during the carbonization step [27]. Chemical activation is generally used to activate peat and wood-

based raw materials. The raw material is impregnated with a strong dehydrating agent, typically phosphoric acid or zinc chloride, mixed into a paste, and then heated to 500 to 800 °C. Activated carbon produced by chemical activation generally exhibits a very open pore structure, commonly referred to as macroporous, ideal for the adsorption of large molecules [27].

The possible applications of activated carbon in liquid phase adsorption and the relatively low price (0.25–2 €/kg [104]) are convincing advantages of this adsorbent. Activated carbons used for liquid phase adsorption are designed to have pore sizes larger than 30 Å to decrease the mass transfer resistance of large size adsorptives [27]. In addition, they exhibit high binding energies to organic compounds, such as fatty acids, alcohols, and esters, due to the hydrophobic properties of the surface. Therefore, activated carbons show high capacities at low fluid concentrations of organic substances in the liquid phase [104]. A disadvantage compared to other materials is the poor mechanical stability and abrasion resistance. In addition, a material loss of approximately 10 % is associated with each thermal desorption step [111].

Zeolites

Zeolites are naturally occurring or synthesized microporous crystalline aluminosilicate materials with a defined framework. The framework consists basically of silicon ($[SiO_4]^{4-}$) and aluminum ($[AlO_4]^{5-}$) tetrahedrons, which are cross-linked to each other by oxygen atoms. Clusters of these primary building units form secondary building units, which are further linked to form the entire tertiary structure of a zeolite framework [27]. This framework has a very regular structure of cages interconnected by windows in each cage. The size of the window aperture depends on the number of tetrahedra. So far, approx. 40 naturally occurring zeolites were discovered, and approx. 200–300 synthetic zeolites were produced [104]. The structural formula of a zeolite unit can be represented by:

$$M_{x/n}\left[(AlO_2)_x(SiO_2)_y\right] \cdot zH_2O \tag{2-1}$$

Where M is the cation such as Na^+, K^+, Ca^{2+}, Mg^{2+}, and NH^{4+}, x and y are integers with $y/x \geq 1$, n is the valence of the cation, and z is the number of water molecules in each unit cell [37]. The aluminum atom provides an anion on the framework, which is compensated by an exchangeable cation. The position of the cation on the framework mainly influences the adsorptive properties. Another important factor influencing the properties of the zeolite is the Si/Al ratio. The transition from a hydrophilic to a hydrophobic surface occurs at a Si/Al ratio between 8 and 10 [112]. Hence, when preparing a zeolite for a specific application, the appropriate Si/Al ratio and cation type must be selected. Zeolites are usually manufactured by hydrothermal synthesis (up to 200 °C) of sodium aluminosilicate from sodium hydroxide, sodium silicate, and sodium aluminate. This is followed by ion exchange with cations and drying of the crystals, which can be pelletized with a binding agent to form macroporous pellets [27].

One main advantage of this material is the possibility of producing adsorbents with both hydrophilic and hydrophobic properties. Hydrophobic zeolites have low water absorption and selectively adsorb non-polar organic components from liquid streams [113]. In addition, zeolites are thermally very stable and only change into another phase between 700 and 1000 °C [114]. This means they can be regenerated or burned free even after

irreversible loading. Disadvantages are probably the higher price (1–4 €/kg, for special materials up to 20 €/kg [104]) and the lack of acid resistance. At low pH, aluminum is dissolved away from the framework. With an increasing silicon content, the resistance to strong acids can increase, which is associated with a decreasing resistance to strong bases [104].

Polymeric Resins

Polymeric resins are synthetically produced polymers with a large inner surface. Commercial adsorbents are usually made from styrene and divinylbenzene or acrylic acid esters and divinylbenzene, as well as phenyl-formaldehyde resins. Other than this, agarose, ethylene glycol dimethacrylate, and vinylpyridine are also used as adsorbents. In contrast to ion exchange resins, adsorbent polymers do not have any functional groups such as sulfonyl groups. Therefore, the adsorption process can be described by physisorption only. Polymeric resins are usually available in the form of spherical beads with a particle size between 0.2 to 1 mm. Each bead consists of many small microbeads that are connected and form a macroporous structure. These microbeads in turn, are made of microgel particles ranging in size between 0.01 to 15 µm [115]. The degree of cross-linking determines the microporous structure of these microparticles and provides a high surface area and structural strength. To produce polymeric adsorbents, a monomer (e.g., styrene or acrylic acid ester) is copolymerized using cross-linking agents (e.g., divinylbenzene). Inert materials are then added, which are miscible with the monomers, do not significantly affect chain growth, and can be extracted or evaporated from the polymerizate with the formation of pores [105]. By varying the type and concentration of the monomers, inert materials, the proportion of cross-linking agents, the reaction conditions, and the post-cross-linking, the pore structures, the inner surface, and the polarity of the polymeric adsorbent can be controlled. [27, 104]

Polymeric resins are mainly used in liquid phase adsorption processes. Due to their hydrophobic characteristics, they are well suited to remove aromatic or chlorinated hydrocarbons, such as phenols or organic pesticides, from process and wastewaters [116]. Their distinct advantages are greater physical, chemical, and biological stability, improved biocompatibility, complete immiscibility with the adsorbate medium, elimination of emulsification, and an increased potential for re-use [117]. The desorption of loaded resin can be realized by extraction, pH shift, or temperature swing processes. For the last option, the limited temperature resistance of maximum 120 to 250 °C must be considered [116]. The main drawbacks of polymeric resins are that they tend to shrink and swell during cyclic operations and that they are costlier than commonly available adsorbents (3–5 times more expensive compared to activated carbon [118]) [27]. However, in some applications, the better performance compensates for the higher costs.

2.3.3.3 Removal of Lignin

The adsorption of BWH aims to remove lignin from the feed solution to reduce fouling and thus increase the filtration capacity during subsequent membrane filtration. Factors that must be considered when selecting suitable adsorbent materials are, e.g., the selectivity for lignin over hemicellulose and derived sugars, maximum adsorption capacity, the desorption process and associated chemical and energy consumption, amount and type of waste resulting, as well

as costs. In addition, since membrane filtration does not necessarily separate hemicellulose from lignin in the required purity [119], it may be necessary to remove the lignin beforehand, e.g., by adsorption. Hence, the pretreatment of BWH by adsorption not only removes the lignin and thus enhances the membrane filtration but can also contribute to higher purity of the resulting product stream. Another advantage of adsorption is that it removes the lignin but does not alter its structure. Thus, this could be used for lignin-based products after subsequent desorption and recovery.

Lignin is a hydrophobic molecule that can be adsorbed on non-polar adsorbents. On the other hand, hemicellulose has hydrophilic properties and, therefore, shows little or no affinity. The utilization of activated carbons for this purpose has been extensively investigated. Mohan and Karthikeyan [120] studied the adsorptive uptake of lignin and tannin from diluted aqueous solutions by activated charcoal. Color removal of lignin and tannin increased gradually to 86 and 74 % at the end of 1 h contact time. Moreover, as one of the few they presented the desorption of lignin from activated carbon with 1 M NaOH solution yielding no desorption and 1 M HCl solution yielding less than 7 % desorption. From this, it can be followed that most of the adsorpt molecules bind to the adsorbent through strong chemisorption interaction. Montané et al. [121] studied the removal of lignin-related products from an oligosaccharide-rich almond shell hydrolyzate by three commercially available activated carbons. Adsorption for lignin-related products was higher than for oligosaccharides, and the selectivity toward lignin adsorption was better when the activated carbon was highly microporous and had small mesopore diameters, a low volume of mesopores, a low concentration of basic surface groups to limit oligosaccharide adsorption, and acidic surface groups to favor the adsorption of the lignin-related products. The average retention for lignin was 64 % and for carbohydrates 21 %. Liu et al. [122], Shen et al. [123], and Gütsch and Sixta [124] investigated the removal of ligneous material from prehydrolysis liquor of a kraft-based dissolving pulp production process by adsorption on activated carbons. An overall lignin removal of 75 to 85 % was obtained, while that of oligomeric and monomeric sugars was between less than 20 and 33 %. In addition, Gütsch and Sixta [124] evaluated regeneration possibilities of the spent activated carbons. The desorption of lignin by dissolution using various lignin solvents led to a lignin removal of maximum 21 %. This value is not sufficient for a cyclic operation. On the other hand, thermal treatment efficiently regenerated the spent activated carbons at temperatures exceeding 800 °C. The strong interactions between the adsorbent and the adsorbed compounds make activated carbon an efficient adsorption material. At the same time, these are the major drawbacks. The regeneration and recovery and thus the potential use of the adsorbed components are challenging or even impossible. In addition, a material loss of approximately 10 % is associated with each thermal regeneration step [111].

The use of inorganic adsorbents, especially zeolites, appears to overcome the mentioned disadvantages, particularly the relatively high loss of sugars. However, very few studies have investigated removing phenolic compounds and none of lignin from hydrolyzate streams by inorganic adsorbents. Ranjan et al. [111] examined the adsorption of phenolics from biomass hydrolysates on zeolites: 97 % removal of phenolics and a minimal loss of sugars were obtained. It was also found that zeolites with high silica content adsorb phenolics more

efficiently from hydrolyzates due to increased hydrophobicity. The desorption of lignin-loaded zeolites has not yet been studied.

Polymeric resins have become a promising choice for efficiently removing aromatic impurities. Especially the possibility to recover adsorbed substances by solvent washing is beneficial in comparison to activated carbon and inorganic adsorbents [36]. Chen et al. [125] investigated the separation of phenolic compounds from aqueous phase products of hydrothermal liquefaction of rice straw by modified XAD4 resins. Optimal desorption of all adsorbed components was achieved with 55 wt.% of aqueous ethanol solution. The total content of phenolic compounds in aqueous solution increased from 18 to 78 % after separation. Schwartz and Lawoko [126] removed 90 % of acid-soluble lignin, and 100 % of furan derivatives from acid hydrolyzed hemicellulose using XAD4 resin. Regeneration was performed at room temperature with 75 % acetone with an efficiency of 85 % with respect to acid-soluble lignin. Lehto and Alén [127] studied the adsorption of non-carbohydrate materials from hardwood autohydrolyzates by XAD4 resins. The resin treatment removed roughly half of the initial dissolved lignin and almost all the furanic compounds. Neither oligomeric hemicellulose nor its derived sugars were removed in significant amounts from the aqueous phase. Koivula et al. [128] used XAD7HP and XAD16N adsorbents to remove foulants from wood autohydrolyzates aiming at the reduction of membrane fouling. XAD7HP resin was able to remove approx. 50 % ligneous material but also 30 % of the hemicellulose in the hydrolyzate. For XAD16N, the results were 70 and 50 %, respectively. This means in this case the treatment was not selective to lignin. They explained the carbohydrate losses, at least partly, with the formation of lignin-hemicellulose complexes. Heinonen et al. [38] investigated the separation and recovery of lignin from monosaccharide-rich hydrolyzates of lignocellulose by six commercial polymeric adsorbents. In comparative batch tests, the resin XAD16N was proven to be the most efficient and was studied in more detail in column tests. A good separation efficiency could be obtained with a 95 % monosaccharide recovery yield limit, and the lignin removal level was 80 %. Practically all of the adsorbed lignin could be recovered with a 50 wt.% aqueous ethanol solution. The process, developed on a laboratory scale, was successfully scaled up (scale-up factor: 420).

As presented in the brief review, the removal of lignin and phenolic compounds from various aqueous solutions by adsorption on activated carbons, zeolites, and polymeric resins, has been investigated to a certain extent. However, single- and multi-component adsorption isotherms regarding the uptake of lignin and hemicellulose are insufficiently described, and BWH from organosolv pulping as feed solution has never been used. In addition, knowledge about the removal of lignin in continuous cyclical operation and the technical and economic assessment is limited. These contents were investigated in the Publications I and V.

2.3.4 Membrane Filtration

2.3.4.1 Fundamentals

Membrane filtration is a separation process that is based on the selective transport of individual components through a semi-permeable membrane. In most cases, the driving force is a pressure difference between the two sides of the membrane resulting in a liquid flow through the membrane pores. The various dissolved components in the feed solution are separated by the membrane according to their molecular size and the size of the pores. Typical pressure-driven membrane processes are microfiltration (MF), UF, NF, and reverse osmosis (RO). In all four processes the feed solution is separated into a filtrate or permeate, which consists of molecules small enough to pass through the membrane, and a concentrate or retentate, which contains all the particles and/or molecules that are retained by the membrane due to their larger size or repulsive charge. Regardless of the type of filtration used, the process is usually operated in cross-flow, i.e., the feed solution flows tangentially over the membrane surface, which has the advantage of reducing the formation of a fouling layer and enabling a continuous process. The other possibility is dead-end filtration, where the feed solution is pumped orthogonally against the membrane [54, 129].

There are no uniform definitions for the four types of filtration, but often the pore size and/or the MWCO of the membrane are used for categorization. The MWCO is commonly described as the molecular weight of the solute that is 90 to 95 % retained by the membrane [130]. Since not only the membrane resistance is decisive for the separation but also the mass transport at the membrane-liquid interface, which mainly depends on geometrical and process parameters, a concrete characterization is difficult [131]. This means that membranes from different manufacturers with the same pore size or MWCO can show different separation performances for certain components. Table 2 categorizes the pressure-driven membrane processes MF, UF, NF, and RO according to their pore diameter, MWCO, applied pressure, as well as separation and transport modes. Within this thesis, mainly UF and NF processes are investigated and, therefore, only these are presented below in more detail.

Table 2: Categorization of the pressure-driven membrane processes microfiltration, ultrafiltration, nanofiltration, and reverse osmosis (based on [129] and [132])

Process	Pore diameter [µm]	MWCO [kDa]	TMP [MPa]	Separation and mass transport
Microfiltration	10^{-1}–10^{1}	> 250	0.05–0.2	Size exclusion, convection
Ultrafiltration	10^{-2}–10^{-1}	1–250	0.1–1	Size exclusion, convection
Nanofiltration	10^{-3}–10^{-2}	0.1–1	0.5–6	Size and Donnan exclusion, convection and diffusion
Reverse osmosis	10^{-4}–10^{-3}	< 0.1	1–10	Solution and diffusion

In UF, the components to be retained by the membrane are macromolecules with molecular weights between 1000 and several hundred thousand Dalton (Da) and/or submicron particles. Usually, the osmotic pressure of the feed solution is negligible and, therefore, relatively low hydrostatic pressure differences are used. The principle of the UF process and mass transport is depicted in Figure 14 (a). UF membranes are mostly asymmetric with a thin mesoporous skin

layer on the surface facing the feed solution and a macroporous substructure. Due to this structure, the flux through the pore membrane can adequately be described by the so-called pore-flow model [130]. This means the mass transport through the UF membrane is convective (*conv)*. Based on Darcy's law, the permeate flux across the membrane (J) is written as a function of the TMP (Δp), dynamic viscosity (η), and membrane resistance (R_m).

$$J = J_{conv} = \frac{\Delta p}{\eta \cdot R_m} \tag{2-2}$$

For the determination of R_m it is assumed that the membrane pores are cylindrical channels with the same hydraulic diameter (d_h), the membrane has the thickness Δz, and the flow in the pores is laminar and can be described by Hagen-Poiseuille's law [41]. The flux can then be expressed by Eq. (2-3).

$$J = \frac{d_h^2 \cdot \Delta p}{32 \cdot \eta \cdot A_m \cdot \Delta z} \cdot n_p \cdot \pi \cdot \frac{d_h^2}{4} \tag{2-3}$$

Where A_m is the membrane surface area and n_p the number of pores. Including the membrane porosity $\varepsilon \left(= V_p/V_{tot} = \left(n_p \cdot \pi \cdot d_h^2\right)/(4 \cdot A_m)\right)$, which represents the free volume of the membrane material, gives Eq. (2-4).

$$J = \frac{\varepsilon \cdot d_h^2 \cdot \Delta p}{32 \cdot \eta \cdot \Delta z} \tag{2-4}$$

However, the assumptions made above generally do not apply in practice. In many cases, UF membranes have a certain pore size distribution and structures, which resemble a bed of packed spherical particles or connected cavities with different geometrical configurations. The permeate flux through these membranes can be better described by the Kozeny-Carman equation [129] as presented in Eq. (2-5).

$$J = \frac{\varepsilon^3 \cdot \Delta p}{k \cdot \eta \cdot a_s^2 \cdot (1-\varepsilon)^2 \cdot \Delta z} \tag{2-5}$$

Where k is a dimensionless constant taking the non-cylindrical pore geometry and the tortuous path into account and a_s $\left(= A_p/\left(V_{tot} - V_p\right)\right)$ is the specific pore surface.

During the filtration of real liquid mixtures, membrane fouling usually occurs, i.e., the deposition and accumulation of particles or solutes, so-called foulants, on the membrane surface or inside the membrane pores by different mechanisms. The formation of a fouling layer increases the thickness of the active separation layer and changes the retention characteristics of the membrane. This applies to dead-end as well as cross-flow filtration. Hence, to describe the mass transport through a covered membrane, the membrane resistance R_m has to be supplemented by the fouling resistance R_f (Eq. (2-6)) [130].

$$J = \frac{\Delta p}{\eta \cdot (R_m + R_f)} \tag{2-6}$$

R_m is material dependent and assumed to be constant, while R_f depends on the solute characteristics (e.g., conformation, charge, hydrophilicity, and solute concentration) and operating conditions (e.g., temperature, pressure, and shear rate) and can be both reversible and irreversible. In the course of a filtration process, the permeate flux decreases due to the formation of a fouling layer on the membrane surface, until a steady-state is reached. This steady-state is characterized by the fact that the mass flow of solutes transported to the fouling layer corresponds to the mass flow of the solutes transported away by diffusive or dynamic effects. Typically, the steady-state flux increases with increasing TMP, temperature, cross-flow velocity (CFV), and decreasing solute concentration in the feed stream. However, if the fouling layer is compressible, the flux will only increase to a certain level with increasing TMP and then level off, the so-called critical flux [133]. Beyond this critical flux no further significant increase can be achieved.

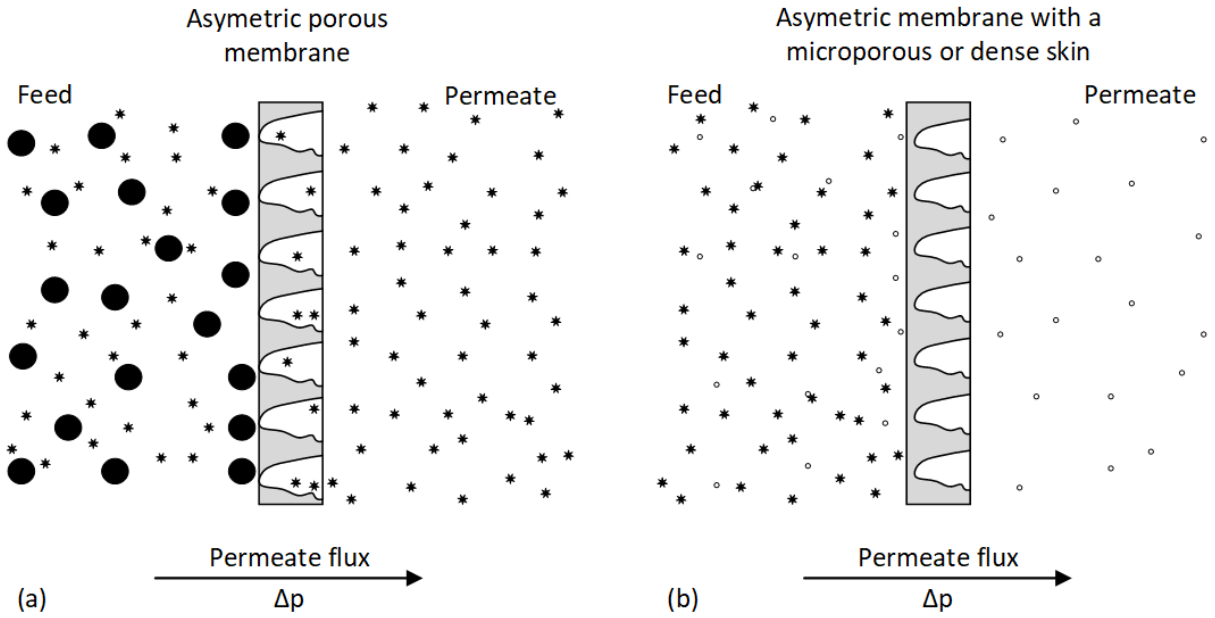

Figure 14: The principle and mass transport in (a) ultrafiltration and (b) nanofiltration (based on [129])

NF is one of the newest pressure-driven membrane processes and has come on the market during the last few decades [27]. In NF, particles, macromolecules, and low molecular weight compounds, such as monomeric sugars and carboxylic acid, are separated from a solvent, usually water. The feed solution may have a significant osmotic pressure. Hence, the applied pressure difference is generally about an order of magnitude higher than UF. The principle of the NF process and mass transport is depicted in Figure 14 (b). NF membranes are mostly asymmetric with a microporous or more or less dense skin layer and a macroporous substructure. Due to this structure, the mass transport in NF is based on both diffusion (*diff*) through the membrane matrix and convection through the pores [129].

$$J_i = J_{i,diff} + J_{i,conv} \tag{2-8}$$

The mathematical description for the convective mass transport is already presented above and the diffusive part can be described by the solution-diffusion model. The diffusive mass transport is based on a gradient of the chemical potential across the membrane and relies on the following simplifications [134]:

- The membrane is considered a continuum,
- The fluids on either side of the membrane are in chemical equilibrium with the membrane material at the interface, and
- The pressure within a membrane is uniform, and the chemical potential gradient across the membrane is expressed only as a concentration gradient.

The driving force for the permeating component *i* of a liquid mixture is the chemical potential μ_i on both sides of the membrane. Restricting the chemical potential to pressure and molar concentration gradients as driving force and for incompressible phases it can be expressed by Eq. (2-9) [135].

$$\mu_i = \mu_i^0 + RT\ln(\gamma_i c_i) + \upsilon_i(p - p_i^0) \tag{2-9}$$

Where μ_i^0 is the chemical potential at a reference pressure p_i^0, R is the universal gas constant (8.314 J/(mol K)), T is the temperature, c_i is the molar concentration, γ_i the activity coefficient linking concentration with activity, and υ_i is the molar volume. Assuming that the mass transport across the membrane is only by diffusion, the general form for calculating the molar permeate flux $\dot{n}_i$ of component *i* is given by Eq. (2-10).

$$\dot{n}_i = -x_{i,m} \cdot L_i \cdot \frac{\mathrm{d}\mu_i}{\mathrm{d}z} \tag{2-10}$$

Where $\mathrm{d}\mu_i/\mathrm{d}z$ is the gradient of chemical potential which appears over the membrane thickness, $x_{i,m}$ is the molar fraction of component *i* dissolved in the membrane, and L_i is a proportionality coefficient that represents the mobility or flexibility of component *i* in the membrane and is not necessarily constant. The negative sign indicates the mass transport from high to low concentrations. With the help of the Nernst-Einstein equation, L_i can be written as a function of the thermodynamic diffusion coefficient D_i according to Eq (2-11).

$$D_i = R \cdot T \cdot L_i \tag{2-11}$$

The molar permeate flux can then be expressed by Eq. (2-12).

$$\dot{n}_i = -x_{i,m} \cdot \frac{D_i}{RT} \cdot \frac{\mathrm{d}\mu_i}{\mathrm{d}z} \tag{2-12}$$

From the model equation, it can be deduced that molar permeate flux and selectivity depend not only on the difference of the chemical potential, i.e., the driving force but also on the solubility of the components in the membrane and the diffusion of these components through the membrane [130]. A distinct property of NF membranes compared to the above mentioned filtration types is that they often carry positive or negative electrical charges. Therefore, the separation properties are not only determined by the MWCO and the dissolution of components in the membrane but also by the surface charge, which affects the permeability of charged components, such as salt ions. Due to these electrical interactions between ions and the surface charge of the membrane, NF membranes are capable of separating, for example, monovalent from multivalent ions [129]. Hence, the permeate flux for charged membranes then expands in addition to the diffusive and convective part by one for the electric charge (ψ).

$$J_i = J_{i,diff} + J_{i,conv} + J_{i,\psi} \tag{2-13}$$

For the derivation of J_ψ the chemical potential must be extended by the term $Z_iF\varphi$, which includes the influence of an electric field on the permeating ions, according to Eq (2-14) [41].

$$\mu_{el,i} = \mu_i + Z_iF\varphi \tag{2-14}$$

Where $\mu_{el,i}$ is the electrochemical potential, Z_i is the ion valence, F is Faraday's constant, and φ is the electrical potential. For neutral components, because of $Z_i = 0$, the electrochemical potential corresponds to the chemical potential, and J_ψ is eliminated from Eq. (2-13).

Another parameter which is of interest to describe the practical application of UF and NF is the retention of certain components. The true retention (R_{true}) is calculated by Eq. (2-15).

$$R_{true} = \left(1 - \frac{C_p}{C_m}\right) \cdot 100\% \tag{2-15}$$

Where C_p and C_m are the concentration of the component in the permeate and at the membrane surface, respectively. As it is complicated to measure concentrations at the membrane surface, the observed retention (R_{obs}) according to Eq. (2-16) is more practicable [70].

$$R_{obs} = \left(1 - \frac{C_p}{C_f}\right) \cdot 100\% \tag{2-16}$$

Where C_f is the concentration of the component in the feed solution. The true retention is always higher than the observed retention. This is because retained substances accumulate in the membrane-liquid interface, resulting in a concentration gradient from the bulk solution to the membrane surface. This phenomenon is referred to as concentration polarization. In this study, the observed retention was used and denoted by R.

2.3.4.2 Membrane Materials and Structures

Synthetic membranes for MF, UF, NF, and RO can be classified based on their structure into porous membranes, homogenous dense membranes, and dense membranes carrying electrical

charges or selective functional groups. Furthermore, the structure of the membranes may be symmetric, i.e., the structure is identical over the cross-section of the membrane, or asymmetric, i.e., the structure varies over the cross-section of the membrane. Materials used can be of organic and/or inorganic nature, and the membranes can be manufactured as flat sheets/spiral-wound, tubes/capillaries, or hollow fibers. [129]

This study focuses specifically on UF and NF membrane technology. UF membranes usually have a porous asymmetric structure, i.e., the pore diameters increase by a factor of 10–1000 from one side of the membrane to the other. On the other hand, NF membranes have a dense asymmetric structure, i.e., they consist of a 0.1–5 µm thick skin layer on a highly porous 100-300 µm thick substructure, and can carry positive or negative electrical charges [129]. Inorganic materials, especially ceramics, such as TiO_2, SiO_2, ZrO_2, and Al_2O_3, have become increasingly important in the last 25–30 years and are well-established for the production of UF membranes and are also increasingly used in NF applications [136]. However, their advantages of higher temperature and chemical resistance, longer service life, and better cleaning options are offset by the more complex membrane production and significantly higher investment costs. Organic UF and NF membranes are commonly used in the industry [131], as well as in the experiments carried out within this thesis. For the production of organic membranes, an almost limitless variety of polymers and polymer blends are available. Typical polymers used to produce UF and NF membranes include polysulfone, polyethersulfone, polyamide, polypiperazine amide, polyimide, composite fluoro polymers, and cellulose acetate. Substructures often consist of polyethersulfone, polyester, polypropylene, and polyacrylonitrile. However, many other polymeric and hybrid materials are under investigation [137, 138].

The selection of the proper membrane material and structure depends mainly on the composition of the solution to be processed and on the operating conditions applied during the membrane filtration. When processing aqueous solutions membrane materials with a hydrophilic character are usually advantageous, as the use of very hydrophobic materials tends to result in lower throughputs at similar MWCO and increased membrane fouling by organic molecules due to the better adsorption of these molecules on the membrane surface [139]. Moreover, the chemical resistance of the membrane material becomes more important for the processing of solutions with extreme pH (< 2 or > 10) or in the presence of oxidizing agents.

2.3.4.3 Concentration Polarization and Membrane Fouling

The performance of pressure-driven membrane filtration is mostly hindered by concentration polarization (CP) and membrane fouling. While CP is a natural consequence of the semi-permeability and selectivity of a membrane [140], membrane fouling can depend on many factors, including membrane characteristics (hydrophilicity, surface topography, charge, MWCO, pore size distribution), solute characteristics (conformation, charge, hydrophilicity, solute concentration), and operating conditions (pressure, temperature, shear rate) [129, 141]. Membrane fouling can be classified into external fouling, i.e., on the membrane surface, and internal fouling, i.e., on the interior of the membrane pores. CP and membrane fouling are schematically illustrated in Figure 15 and are explained in more detail below.

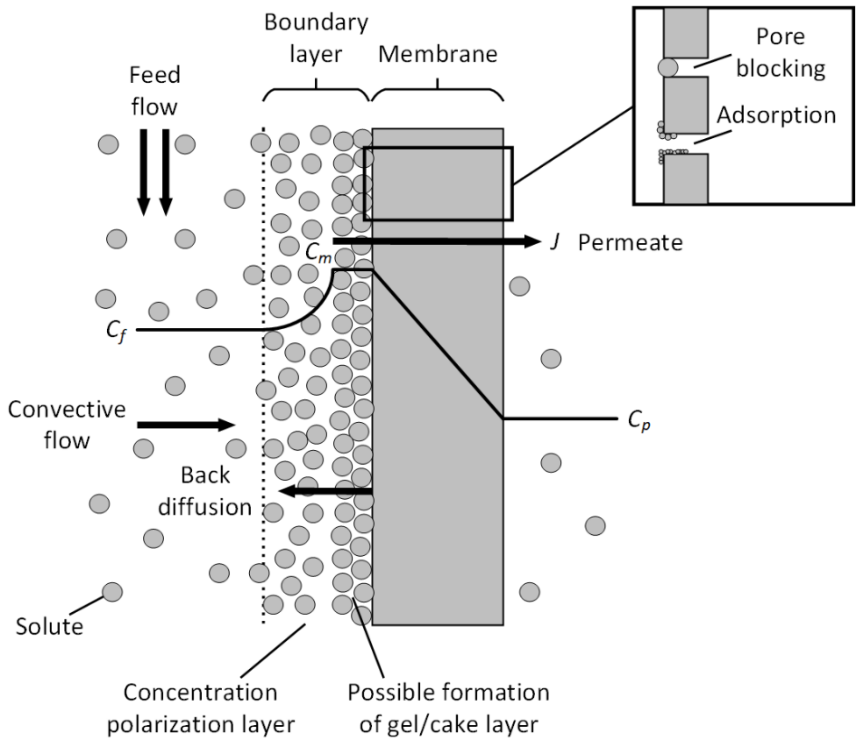

Figure 15: Schematic illustration of concentration polarization and membrane fouling (based on [142] and [41])

Theoretical fouling models for different solutions [143–145] and predictive models [146–148] have been developed to allow diagnostics and preventive measures. However, wood hydrolyzates are complex mixtures containing a multitude of components, and there are several solute-solute and solute-membrane interactions. Therefore, it is difficult to simulate the filtration process, considering all factors, with MSs.

Different compounds have been reported to foul the membranes during the filtration of wood hydrolyzates. In many cases, lignin, its phenolic degradation products, wood extractives, and furanic compounds have been identified as potential foulants in UF and NF of process waters from the pulp and paper industry [42, 128, 149–151].

Concentration Polarization

CP is a reversible phenomenon that occurs due to the semi-permeability and selectivity of a membrane. When a liquid mixture is brought to the membrane surface, some components will permeate the membrane while others are retained. This leads to an accumulation of retained materials and a depletion of the permeating components in the boundary layer adjacent to the membrane surface. The diffusive transport of the molecules in the boundary layer back into the feed solution is relatively slow and causes a concentration gradient [129]. Thereby, the concentration in the boundary layer can reach 20 to 50 times the concentration in the feed solution. As a consequence, the resistance of transport across the membrane increases, and thus, permeate flux decreases. The increase in resistance can be attributed in part to the increased viscosity and osmotic pressure. Increased osmotic pressure hinders the effect of the applied TMP. Compared to membrane fouling, CP achieves steady-state after a certain process time [6].

CP is particularly relevant in UF, where the membrane retains mainly macromolecules and particles. Since the applied TMP is generally relatively low during the UF process, increased osmotic pressure due to CP may significantly decline flux. More important, however, is that the diffusive back transport of the retained components into the feed solution is rather slow due to their high molecular weight, and the solubility of the retained molecules is often exceeded so that precipitation will occur. This can result in a more or less dense solid layer on the membrane surface, affecting the separation characteristics of the membrane by reducing permeate flux and increasing the rejection of lower molecular weight components [129].

External Fouling

The deposition of particles and macromolecules, as well as the precipitation of solutes on the membrane surface, is called external fouling. It can be classified into the formation of a cake or gel layer [152]. A cake layer is formed when particles accumulate on the membrane surface. A prerequisite for the cake layer to build up is that the particles are larger than the pores. The gel layer formation occurs when the solubility of the organic substances in the CP layer is exceeded and the attractive forces become greater than the repulsive forces. At this point, the permeate flux reaches a limit independent of the applied TMP. Both fouling mechanisms result in additional resistance to the permeate flux but are generally of reversible nature, making them a less problematic form of fouling [153].

Internal Fouling

Fouling caused by the deposition, as well as the adsorption of solutes and smaller particles on the interior of the membrane pores, is called internal fouling. It can be classified into pore blocking and adsorption [152]. Pore blocking occurs due to the complete or partial closure of membrane pores by particles and solutes that are just large enough to be retained by the membrane. It usually happens at the beginning of a filtration process, when the membrane surface is still free of deposits. The incoming particles and solutes can directly interact with the membrane pores. The largest pores are blocked first, resulting in a highly permeate flux decline at the start of the filtration [27]. Adsorption is primarily influenced by the affinity between the membrane material and the solutes. The interactions between the two phases can be divided into physisorption and chemisorption, as presented in Section 2.3.3.1, as well as electrostatic attraction forces. Consequence is the narrowing of the effective pore diameter, which results in a higher filtration resistance of the membrane [154]. Hence, both fouling mechanisms contribute to an additional resistance and can thus reduce permeate flux and increase retention. The more distinct this resistance is on the membrane, the more it decreases its reusability, and cleaning costs increase.

2.3.4.4 Ultrafiltration for the Recovery of Hemicellulose

The UF of BWH aims for the isolation and concentration of hemicellulose from lignin and smaller molecules to add value to the material. Designing and optimizing the UF process is generally a trade-off between high permeate flux, high retention, and high purity. Whereby high retention and high purity are challenging to reconcile with each other. A high permeate flux is desirable because the capital and operating costs are inversely proportional [57]. High retention is desirable to reduce the cost of the raw material, and high purity, as well as concentration, is

usually required in subsequent conversion processes [27]. These process responses mainly depend on the operating parameters TMP, temperature, pH, and CFV. In addition, the membrane material and structure also has an influence. Hence, after choosing an appropriate membrane, the operating parameters must be optimized in terms of maximum permeate flux and hemicellulose retention, as well as minimal lignin retention.

As presented in Section 2.1.2 and 2.1.3, hemicellulose dissolved in wood hydrolyzates has higher molecular weights than lignin, except an overlap in the lower range. The isolation of hemicellulose out of process water from a thermomechanical pulp mill using UF was studied by Persson and Jönsson [70]. They used different polymeric membranes with MWCOs between 1 and 10 kDa to investigate the influence of TMP and solution concentration on hemicellulose and lignin retention, as well as permeate flux and fouling of the membranes. High hemicellulose retention above 90 % was achieved at lignin retention of 30 to 50 %. Permeate flux declined by approx. 60 % because the membranes showed high susceptibility to fouling. Krawczyk et al. [155] studied the influence of TMP, CFV, temperature, and concentration on the UF of a high-viscosity solution containing hemicellulose from wheat bran. A tubular ceramic membrane with a MWCO of 10 kDa was used. An acceptably high permeate flux of up to 62 L/(m²h), high hemicellulose retention of 96 %, and no significant membrane fouling was observed. Low TMP, high CFV, and high temperature seemed to be beneficial. Furthermore, the permeate flux was decreased significantly with increasing feed concentration. This demonstrated that the membrane performance is strongly associated with the viscosity of the feed solution. In the study of Al Manasrah et al. [119] the performance of three regenerated cellulose UF membranes with MWCOs ranging from 5 to 30 kDa was evaluated with respect to the recovery of hemicellulose from spruce sawdust extract. In addition, a diafiltration technique was used to obtain more purified hemicellulose in the retentate. The smallest pore size membrane retained almost 90 % of the hemicellulose up to a volume reduction of 70 %. Diafiltration separated the oligomeric hemicellulose fraction from the monomeric sugars, hence increasing its purity. Purification of hemicellulose from lignin was only to a certain extent possible. They concluded that to improve hemicellulose purity, an additional purification method, such as adsorption, is required. This approach, i.e., improving the UF of wood hydrolyzates to recover hemicelluloses by pretreatment with polymeric adsorbents, was addressed by Koivula et al. [128]. Adsorption pretreatment with the polymeric resins XAD7HP and XAD16N was found to be effective in increasing permeate flux and reducing fouling during the UF of pine/eucalyptus hydrolyzate. Unfortunately, in addition to potential foulants such as lignin, significant amounts of hemicellulose were lost during the pretreatment. Thuvander and Jönsson [71] studied a filtration cascade consisting of MF and UF to recover hemicellulose from the process water from thermomechanical pulping of spruce. MF (ceramic membrane, pore size = 0.1 µm) was used to remove large contaminants, such as suspended matter and colloidal extractives, and UF (spiral-wound membrane, MWCO = 5 kDa) to concentrate and purify the hemicellulose from low molecular weight contaminants. The content of colloidal extractives in the wood hydrolyzate was greatly reduced by MF while maintaining a high proportion of high molecular weight hemicellulose. This MF pretreatment increased the initial permeate flux during the subsequent UF step from 90 to over 200 L/(m²h).

In addition to the determination of technical measures and parameters, economic considerations are also necessary to develop a UF process. Optimizing the costs is generally a trade-off between high permeate flux and a low energy requirement [27]. Studies regarding cost estimates of hemicellulose recovery from wood hydrolyzates by UF cannot be found in the literature. However, there are some calculations for specific production costs for the recovery of lignin by UF. Jönsson and Wallberg [56] and Arkell et al. [55] evaluated costs for the lignin recovery from hardwood and softwood black liquor, respectively. In the first study, a plant dimension of 200 m^3/h of the pulping liquor was assumed, and the utilization of tubular ceramic membranes with a MWCO of 15 kDa. Specific production costs of 33 EUR/t of lignin were calculated. The second study assumed a feed flow rate of 100 m^3/h with full-scale spiral-wound NF modules with a MWCO of 1 kDa resulting in 46 EUR/t of lignin. Cost estimation for the recovery of lignin from organosolv spent liquor was conducted by Alriols et al. [156]. They considered a liquor flow of 6000 L/h and a UF cascade consisting of a 5 kDa, 10 kDa, and 15 kDa (ceramic tubular membranes) stage. Obtained lignin fractions entail a cost of 52 EUR/t of product.

The brief overview reveals that there are already some studies concerning hemicellulose recovery from wood hydrolyzates. However, the major part of these investigations was carried out using conventional methods of experimentation. This means changing one of the independent factors while maintaining the others at fixed levels. This ignores the interaction effects between the examined factors, affecting the performance of the UF process. To overcome these problems, statistical tools such as the design of experiments can be applied, where all the studied factors are varied simultaneously over a set of experimental runs. By the additional use of multiobjective optimization the optimal set of process parameters in terms of maximum permeate flux and hemicellulose retention, as well as minimal lignin retention, can be determined (Publication II). In addition, there is no technical and economic assessment for the recovery of hemicellulose from wood hydrolyzates by UF (Publication V).

2.3.4.5 Nanofiltration for the Recovery of Hemicellulose Derived Sugars

NF aims to purify and concentrate monomeric C5 sugars from hydrothermally pretreated BWH. The hydrothermal pretreatment of wood hydrolyzates is already presented in Section 2.2. Before further conversion (e.g., fermentation and hydration) of the C5 sugars to high value-added products, potential inhibitors, such as carboxylic acids, furans, and phenolic compounds, must be separated. Since NF has similarities to UF, the design requirements are the same as described above. In contrast, the solution pH is of greater importance as it affects the charged species and the functional groups of the membrane [27]. However, especially in NF, fouling can cause severe flux reductions and hence a loss in process performance [42]. This is mainly due to the higher retention of the membranes and thus an increased osmotic pressure difference.

Tight NF membranes can retain up to 99 % of monosaccharides [27] and remove water and other non-sugars without adding chemicals and phase changes. Sjöman et al. [157] recovered xylose by NF from two artificial hemicellulose hydrolyzate feeds. The filtration experiments were first made at different temperatures and TMPs in reflux mode and afterward for 20 h at 50 °C and 3.0 MPa in concentration mode. Three thin-film composite membranes with MWCOs from 150 to 300 Da were used. Within the short-term filtration experiments a promising separation potential for xylose recovery and purification could be observed. Flux

values were relatively low with 10 to 16 L/(m²h). During the long-term filtration, fouling and compaction effects were detected by a decrease in permeate flux of about 10–25 %. Weng et al. [73] studied the separation and concentration of C6 and C5 sugars of hydrolyzates obtained from dilute acid hydrolysis of rice straw using NF at varying process parameters. Appropriate operation conditions found were a low pH (2.9) and temperature (25 °C), as well as medium TMPs (2.5–3.4 MPa). Average retentions for glucose, arabinose, and xylose of 95.2, 86.1, and 85.7 % were achieved. For furans and carboxylic acids, even negative retentions were observed. At the end of the NF process, the permeate flux changed from initially 16 to 2 L/(m²h). This flux decline was mainly due to reversible fouling, as it was possible to restore the permeate flux by membrane cleaning with a combination of de-ionized water (DIW) and 0.01 M NaOH. Removal of furfural and concentration of monosaccharides were investigated by Qi et al. [158] using two commercial NF membranes (MWCOs of 100 to 150 Da) with synthetic glucose–xylose–furfural solution as a model. The effects of the process parameters feed pH and concentration, as well as temperature on permeate flux and retention of the three solutes, were studied. In addition, the effects of the two filtration modes, concentration, and diafiltration, were also investigated. Again, low pH and temperature increased retention, and increasing feed concentration decreased retention. Concentration experiments greatly increased the concentrations of xylose and glucose, while furfural concentration increased to some extent. This process could be improved by diafiltration for further removal of furfural. The influence of varying operation conditions and feed concentration for the separation of acetic acid from glucose and xylose out of a model hydrolyzate solution by using NF and RO membranes were investigated by Zhou et al. [159]. Parameter studies came to a similar conclusion as Weng et al. [73] and Qi et al. [158]. However, they proposed using RO instead of NF membranes for simultaneous acetic acid separation and sugar concentration. The reason is that RO membranes showed nearly complete retention of glucose and xylose at all process conditions and low retention for acetic acid at low pH. Gautam and Menkhaus [42] evaluated RO and NF membranes for their ability to separate fermentation inhibitors (carboxylic acids and furans) from sugars while simultaneously concentrating the sugars. A pure sugar solution and a biomass hydrolyzate from pine wood chips were used as a feed streams. A performance and fouling analysis demonstrated that when treating real biomass substrates, NF is recommended due to lower rejections of inhibitors and hence less fouling caused by osmotic pressure. Last but not least, Huang et al. [160] developed a process model to simulate an integrated forest biorefinery manufacturing pulp and other co-products. Their model included NF to concentrate pre-extraction hydrolyzate sugars. The simulation results showed that pre-extraction is a potential method to recover hemicellulose prior to kraft cooking.

As outlined above, some research has already been conducted on the recovery of xylose from synthetic and/or authentic biomass hydrolyzates. In the majority of the known studies, membrane fouling is presented as problem. Still, the contribution of the individual fouling mechanisms to the performance losses is not specified in more detail. In addition, the influence of hydrothermal pretreatment of wood hydrolyzates and the associated degradation of existing components, as well as the formation of new potential foulants and inhibitors on the NF process, has not yet been considered (Publication III). Technical and economic assessment for the valorization of xylose from wood hydrolyzates by NF is also lacking (Publication V).

3. Materials and Methods

An overview of the materials and methods applied for the adsorption, UF, hydrothermal pretreatment, and NF experiments are provided in the following sections. Moreover, the approach for the technical and economic process assessment is described. More detailed information can be found in the corresponding Publications I–V.

3.1 Materials

3.1.1 Beechwood Hydrolyzates

The lignocellulose biorefinery pilot plant of the Fraunhofer Center for Chemical-Biotechnological Processes (CBP) in Leuna (Germany) provided the BWHs. During the investigations for this thesis, the organosolv process for the pulping of beechwood into cellulose, hemicellulose, and lignin was further developed and optimized. Hence, BWHs from different batches with different concentrations were used for the experimental work. In the following, the varying process conditions for the extraction of the BWHs are described.

During organosolv pulping 70 kg oven-dry weight (odw) of debarked beechwood chips were fractionated in a 500 L batch reactor with forced circulation at 170 °C and 2.0 MPa for 130 min (H-factor = 1,500) using 224 kg of an ethanol-water mixture (1:1 w/w) and 0.8 % sulfuric acid (based on wood odw) as a catalyst. Afterward, the spent liquor (SL) was displaced by fresh ethanol-water wash liquor (WL, 1:1 w/w) and washed at 100 °C, 2.0 MPa, and a WL-to-solid ratio of 10:1 w/w for 60 min to extract remaining lignin. Subsequently, two more displacement washing steps were performed with water. The remaining pulp fraction was discharged and dewatered using a screw press. About 90 % of the dissolved lignin in the displaced SL and/or WL was precipitated either by dilution with water [65] or by evaporation of ethanol at reduced pressure [161] and recovered by filtration. From the remaining liquid phase, ethanol was recovered by rectification, and the residual liquid product is considered BWH. It contains oligomeric hemicellulose and its hydrolysis products, such as monomeric sugars, furans, and carboxylic acids, as well as residual lignin and its phenolic derivatives.

BWHs were taken from five different batches: (i) BWH 1 results from the further processing of both SL and WL and lignin precipitation by dilution, (ii) BWH 2, 3, and 4 results from the further processing of SL and a varying proportion of WL and lignin precipitation by evaporation, and (iii) BWH 5 results from the further processing of only SL and lignin precipitation by evaporation. The compositions of the five BWHs used in the studies in Publications I–V are presented in Table 3. Physicochemical properties of the components in the BWHs are depicted in Section 2.1. The pH for BWH 1 and 2 is 2.5 and 2.6, respectively, and for BWH 3, 4, and 5 1.9. Before their use, they were filtered by vacuum filtration using a 4 µm filter paper (Macherey-Nagel) to remove larger particles and suspended solids from the liquid fraction. Afterward, they were stored at 4 °C up to their use.

Table 3: Concentration of oligomeric hemicellulose, glucose, xylose, 5-hydroxymethylfurfural (5-HMF), furfural, acetic acid, and lignin in beechwood hydrolyzate (BWH) 1, 2, 3, 4, and 5

Components		BWH 1	BWH 2	BWH 3	BWH 4	BWH 5
Oligomeric hemicellulose	[g/L]	1.6	4.0	10.3	19.8	22.8
Glucose	[g/L]	0.3	0.6	1.7	3.9	2.8
Xylose	[g/L]	2.6	6.2	13.3	25.3	34.2
5-HMF	[g/L]	n.d.	0.4	0.6	1.6	0.8
Furfural	[g/L]	0.6	0.8	0.1	0.2	n.d.
Acetic acid	[g/L]	1.5	4.1	3.8	7.8	3.9
Lignin*	[g/L]	3.1	1.6	3.2	n.d.	4.8

* all components that contribute to the UV absorbance at 280 nm

3.1.2 Adsorption Equipment and Adsorbents

Adsorption equipment, i.e., batch reactor and fixed-bed column, used for the experimental work, has a laboratory scale and is described below. Furthermore, the adsorbents used are specified.

3.1.2.1 Batch Reactor

The experimental setup for the batch reactor consists of an 800 mL round bottom beaker placed in a water bath and agitated by a magnetic stirrer/hot plate (Heidolph, model: MR Hei-Standard). The temperature was measured by a Pt100 element inserted into the beaker. For sampling, a defined amount of the solution-adsorbent-suspension was taken from the beaker by a pipette and filtered by vacuum filtration using filter paper Whatman No. 2 (pore size = 8 µm). Except for sampling, the beaker was covered throughout the trials.

3.1.2.2 Fixed-Bed Column

The experimental setup for the fixed-bed column consists of a 1 L round bottom beaker placed in a water bath and agitated by a magnetic stirrer/hot plate (Heidolph, model: MR Hei-Standard) and a peristaltic pump (Ismatec, model: ISM596D), which fed the feed solution to an insulated glass column with an inner diameter of 1.5 cm and a length of 20 cm (YMC Europe, model: ECO15/200V4V). The temperature was measured by a Pt100 element inserted into the beaker, and the beaker was covered throughout the trials.

3.1.2.3 Adsorbents

Five adsorbents were tested, four polymeric resins and one zeolite. The studied resins are the hydrophobic styrene-divinylbenzene (PS-DVB) based Amberlite XAD4 and XAD16N (Sigma Chemical Corporation), and SEPABEADS SP700 (Mitsubishi Chemical Corporation), as well as the uncharged polyacrylate (PA) based Amberlite XAD7HP (Sigma Chemical Corporation). XAD4 is applicable for the adsorption of small hydrophobic molecules from polar solvents, e.g., organics of relatively low to medium molecular weight. XAD16N can adsorb hydrophobic compounds up to the molecular weight of 40,000 g/mol. SP700 is recommended to recover materials from fermentation broths, particularly the extraction and concentration of small oligomers. XAD7HP can be used to adsorb organic compounds up to the molecular weight of 60,000 g/mol. The studied zeolite HiSiv1000, (Honeywell UOP Molecular Sieve), has a

crystalline, inorganic silica-alumina structure (Si/Al ratio less than 20), also referred to as “high silica zeolite”. HiSiv1000 has strong adsorption characteristics to larger molecules (approx. 100 g/mol) with a hydrophobic character. Physicochemical characteristics of the adsorbents are listed in Table 4.

The adsorbents were initially cleaned or activated before their use. Resins were rinsed with DIW to remove preservatives like sodium chloride and sodium carbonate salts and other contaminants. As long as these preservatives and contaminants are present, the conductivity of the rinsing water increases. Hence, the rinsing was continued until the conductivity of the rinsing water no longer increased (typical adsorbent-to-water ratio 1:55 w/v). After the rinsing of the resins, they were dried for 24 h at 80 °C. Pretreatment of the zeolite was performed at 360 °C in an air atmosphere for 16 h to remove any organic contamination in the adsorbent pores. The prepared adsorbents were stored in oven-dried flasks up to their use.

Table 4: Physicochemical characteristics of the studied polymeric resins and zeolite as provided by manufacturers

Adsorbent	Structure	Surface area (m^2/g)	Pore diameter (Å)	Porosity (mL/g)	Particle size (mm)	Density (g/mL)
XAD4	PS-DVB	750	100	0.98	0.25-0.84	1.02
XAD7HP	PA	450	90	1.14	0.25-0.84	1.05
XAD16N	PS-DVB	800	100	1.82	0.25-0.84	1.02
SP700	PS-DVB	1200	90	2.20	0.25-0.70	1.01
HiSiv1000	SiO_2/Al_2O_3	353	8	-	Powder < 0.1	0.53

3.1.3 Flow Tube Reactor for Hydrothermal Pretreatment

The flow tube reactor for the hydrothermal pretreatment experiments has a laboratory to pilot scale Figure 16. It is made of stainless steel, has a total length of 860 mm, an inner diameter of 20 mm, and a wall thickness of 5 mm. The total reaction volume, including the inlet and outlet section, is about 300 mL. The feed solution is fed by a membrane pump (ProMinent, model: Orlita MfS 35/10) and first quickly heated up to the desired reaction temperature by an electrical furnace. Afterward, the process liquor enters the tube reactor, where a three-zone heating jacket maintains the temperature. After leaving the reactor, rapid cooling takes place by a water-cooled heat exchanger. The residence time was determined and adjusted using a Coriolis mass flow meter (Siemens, model: MASS 2100 DI 1.5 and MASS 6000). With the help of a back pressure regulator (Badger Meter, model: RC200), the pressure for the trials was adjusted.

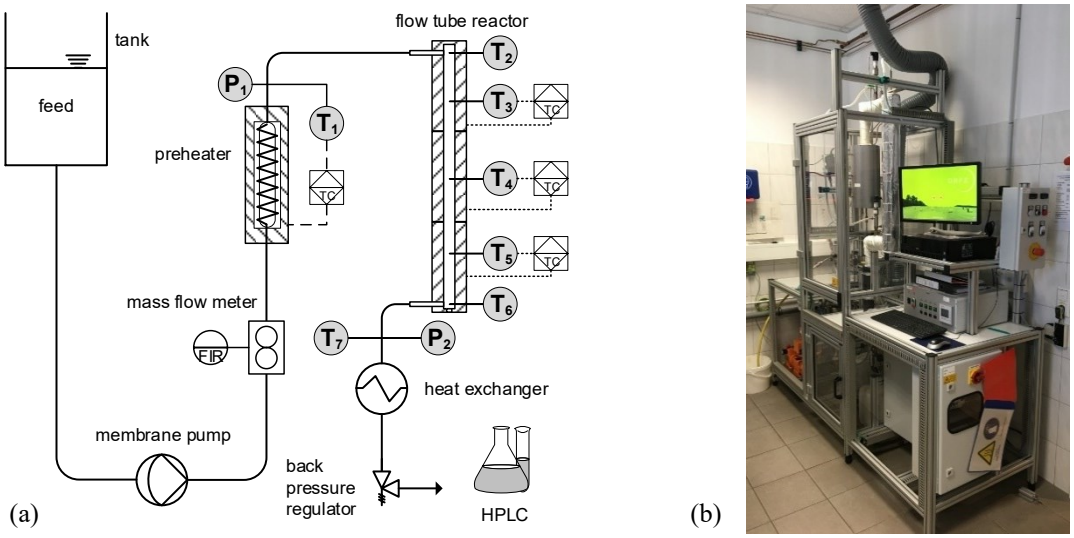

Figure 16: (a) Schematic and (b) picture of the flow tube reactor for hydrothermal pretreatment experiments

3.1.4 Membrane Filtration Equipment and Membranes

Membrane filtration was investigated on a laboratory scale, using a dead-end filtration system, and on a pilot scale, using a cross-flow filtration system. Both test rigs are described below. Furthermore, the filtration materials, i.e., the tested UF and NF membranes, are specified.

3.1.4.1 Dead-end Filtration System

The dead-end filtration system with a stationary mixer consists of a 1 L double-jacket feed tank and, a 0.4 L stirred cell (Andreas Junghans, model: JU-A296-000:00-02) pressurized with nitrogen (Figure 17). The active membrane surface area was 0.0044 m². The TMP was adjusted by a pressure control valve and measured by a pressure sensor (WIKA, model: A-10). A stirrer/hot plate (Heidolph Instruments, model: MR Hei-Standard) set the desired stirring speed and temperature within the stirred cell. In addition, the temperature of the feed tank was measured with a Pt100 element and maintained constant by a water circulation thermostat (Peter Huber Kältemaschinenbau, model: CC-304B). The permeate flux (J) through the membrane, calculated according to Eq. (3-1), was obtained by collecting permeate over time in a volumetric cylinder placed on a balance (Wägetechnik Wehle, model: MIS2.FLIA-7008.01).

$$J = \frac{V_p}{A_m \cdot t} \tag{3-1}$$

In this equation V_p is the volume of the permeate, A_m is the membrane surface area, and t is time.

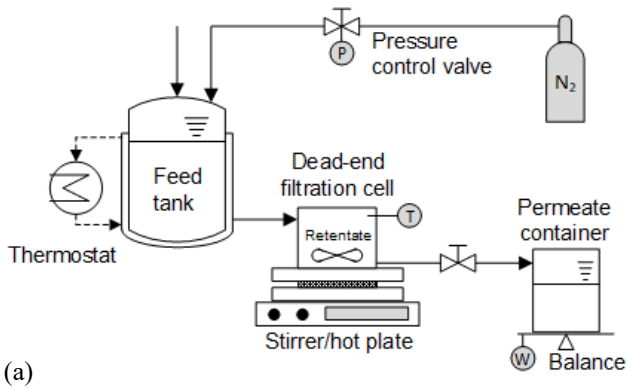

(a)

(b)

Figure 17: (a) Schematic and (b) picture of the dead-end filtration system for membrane filtration experiments

3.1.4.2 Cross-flow Filtration System

The cross-flow filtration system, shown in Figure 18, consists of a plate-and-frame membrane module (Alfa Laval, model: LabStak M20), a 20 L double-jacket feed tank, a diaphragm pump (Hydra-Cell, model: G10-E), and a shell and tube heat exchanger (Brazetek, model: BT-ST-55-B-1). The TMP (Δp) was adjusted by pressure control valves installed on the retentate side and measured using pressure sensors (Baumer, model: PBMN 25B) installed on the feed (p_f) and retentate (p_r) side of the membrane module. As the pressure on the permeate side was atmospheric, the TMP is the average of the feed side and retentate side pressures according to Eq. (3-2).

$$\Delta p = \frac{p_f + p_r}{2} \tag{3-2}$$

The flow rate was regulated with the pump equipped with a frequency converter (Hitachi, model: NE-S1) and measured on the retentate side (Meister Strömungstechnik, model: DMIK). The temperature was controlled using a chiller with a heating function (Peter Huber Kältemaschinenbau, model: Unichiller 025w-H) connected to the heat exchanger and measured using a Pt100 element behind the pump. The permeate flux, according to Eq. (3-1), was determined with a volumetric cylinder and a balance (Kern & Sohn, model: PLS 8000-2A).

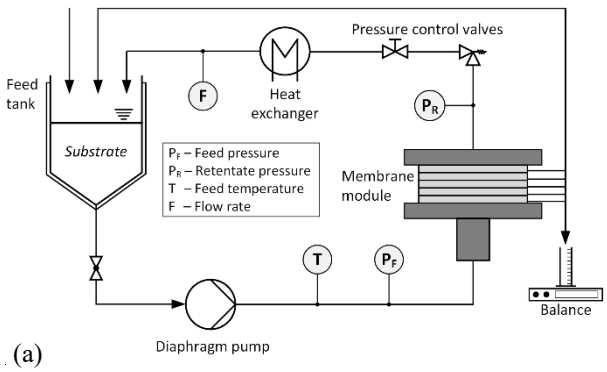

(a)

(b)

Figure 18: (a) Schematic and (b) picture of the cross-flow filtration system for membrane filtration experiments

3.1.4.3 Membranes

As described above, UF was investigated to recover and concentrate hemicellulose while removing lignin from BWH. Based on the considered components' physicochemical properties, six commercial polymeric UF flat-sheet membranes were tested (Table 5). These membranes differ in their skin layer material and thus the surface properties, as well as the MWCOs. An important characteristic is the hydrophilicity of the membranes. GR90PP has a hydrophobic surface, ETNA01PP, UFX5pHt, and UH004 are made of hydrophobic materials modified to be hydrophilic, RC70PP has naturally hydrophilic properties, and UA60 is a tight thin-film membrane.

For the concentration of hemicellulose derived xylose and the removal of potential inhibitors (e.g., furanic components and carboxylic acids), four commercially available NF flat-sheet membranes with MWCOs between 150 and 400 Da were tested. An overview of the NF membranes and their properties according to the manufacturers is given in Table 5.

Fresh membranes were cut according to the geometry of the filtration system used and installed. A new set of membranes was first thoroughly flushed with DIW to remove surface preserving agents and then with a 1 wt.% P3-Ultrasil-53 solution (ECOLAB) to remove pore stabilizers and remaining chemicals. Afterward, the detergent was replaced by DIW, and the membranes were compacted for at least 8 h.

Table 5: Properties of the tested ultrafiltration (UF) and nanofiltration (NF) membranes as provided by manufacturers

Filtration	Membrane	Manufacturer	Skin layer material	MWCO (Da)	pH range
UF	ETNA01PP	Alfa Laval	Composite fluoro polymer	1,000	1-11
	UFX5pHt	Alfa Laval	Polysulfone	5,000	1-13
	GR90PP	Alfa Laval	Polyethersulfone	5,000	1-13
	RC70PP	Alfa Laval	Regenerated cellulose acetate	10,000	1-10
	UA60	TriSep	Polypiperazine amide	1,000-3,500	1-12
	UH004	Microdyn-Nadir	Polyethersulfone	4,000	0-14
NF	NF	Alfa Laval	Polyamide	300	2-10
	DK	GE Osmonics	Polyamide	150-300	2-10
	TS40	TriSep	Polypiperazine amide	200-300	2-11
	NF90	Dow	Polyamide	200-400	2-11

3.2 Methods

3.2.1 Adsorption Experiments and Isotherms

Adsorption experiments were conducted to (i) identify appropriate adsorbents for efficient removal of lignin and recovery of hemicellulose (oligomeric hemicellulose + monomeric sugars) from BWH, (ii) determine single and multi-component adsorption isotherms, (iii) investigate the effect of flow rate and dynamic lignin adsorption capacity in a fixed-bed column, and (iv) to show the possibility of regeneration of the adsorbents. For points (i) and (ii) BWH 1, and for points (iii) and (iv) BWH 3 was used.

3.2.1.1 Experimental Procedure

At first, adsorbent screening and modeling of isotherms were realized using single- and binary-component MSs to reduce complexity and work with well-defined compositions. In the MSs, phenol (Carl Roth, purity ≥ 99.5 %), with a concentration of 3.1 g/L, was chosen to represent lignin and xylose (Carl Roth, purity ≥ 98.5 %), with a concentration of 4.2 g/L, was chosen to represent hemicellulose in BWH 1. Experiments were performed using the batch reactor at a temperature of 25 °C, agitated at 500 rpm, and for a residence time of 180 min. The pH of the MSs was adjusted to 6.0 as several studies have shown that this leads to a preferred uptake of phenols due to the predominant existence as neutral molecules. Hence, the interaction between the adsorbents and phenols is mainly physical van der Waals' forces [162–164]. For adjusting the pH, a 5 M NaOH (VWR Chemicals, purity ≥ 98.9 %) or 1 M HCl (Carl Roth, molar concentration = 1 mol/L) solution was used. After the temperature of the adsorbate solution was stabilized, the adsorbents were added with the adsorbent-to-solution (A:S) ratios of 1:5, 1:10, 1:15, 1:20, 1:25 and 1:33 w/v (g/mL). The moment the adsorbents were added to the adsorbate solution was considered time zero for the experiments. To identify equilibrium time and concentration, small volume liquid samples of 3 mL were collected at predetermined time intervals and analyzed regarding their concentration of phenol and xylose. Equilibrium time and concentration were reached after no change in concentration of adsorptive in solution were detected. These experiments were carried out to study the effects of adsorbent dose and contact time as well as to identify the most suitable adsorbent materials. Furthermore, to calculate the model parameters of single- and multi-component adsorption isotherms.

As the next step, adsorbent screening and equilibrium studies were conducted using BWH 1. The experimental procedure was identical to that for MSs. But instead, the samples were analyzed for lignin and hemicellulose. The isotherm model parameters obtained from MS experiments were applied to the adsorption process using BWH 1 to predict and interpret the mechanisms which are predominant during the adsorption of lignin and hemicellulose. The precision of the prediction was statistically evaluated. On the one hand, this was done to determine if generic adsorption isotherms from defined MSs can be applied to authentic wood hydrolyzates, and on the other hand, to represent the dimension of deviations. In addition, multi-component isotherm model parameters were re-determined using equilibrium data from experiments with BWH 1. Due to the multi-component character of BWH 1, the model parameters were calculated directly and not by the single-component isotherms. The obtained isotherm models and parameters were also statistically evaluated.

The effect of flow rate and dynamic lignin adsorption capacity was investigated using the fixed-bed column and a process temperature of 50 °C. The volume of the adsorbent bed was 26.5 mL (h_{bed} = 15 cm, d_{bed} = 1.5 cm), and the adsorbent was packed to the column as an aqueous slurry. As adsorbent, the SP700 was used. The effect of different flow rates on the adsorption of lignin onto the adsorbent was studied with the four flow rates 1, 2, 3, and 4 mL/min corresponding to 2.3, 4.5, 6.8, and 9.1 bed volumes (BV) per hour, respectively. To determine the maximum amount of lignin that can be adsorbed onto SP700 30 BV of BWH 3 were fed through the column. Each BV was collected and taken as a sample for analysis.

Desorption of lignin or rather regeneration of the adsorbent SP700 was investigated with a 20 wt.% and a 50 wt.% ethanol (Carl Roth, purity ≥ 99.8 %) solution as well as with a 0.5 M NaOH (VWR Chemicals, purity ≥ 98.9 %) solution. To compare the desorption experiments with each other, it was necessary to load the adsorbent with the same amount of lignin. Therefore, the SP700 was mixed with BWH 3 in the batch reactor in an A:S ratio of 1:10 w/v. Process conditions were a temperature of 25 °C, a stirring speed of 500 rpm, and a residence time of 120 min. Afterward, the loaded adsorbent was packed to the column and washed with 3 BV of DIW to remove remaining BWH 3. Then 10 BV of the respective ethanol or NaOH solution were fed through the column with a flow rate of 2 mL/min (4.5 BV/h). Each BV, this means from the washing as well as from the desorption step, was collected and taken as a sample for analysis.

3.2.1.2 Fundamental Calculations

The removal of phenol and xylose from MSs as well as lignin and hemicellulose from BWH 1 and 3 onto the adsorbents was calculated according to Eq. (3-3).

$$Removal = \frac{C_0 - C_t}{C_0} \times 100\% \tag{3-3}$$

Where C_0 refers to the initial concentration and C_t to the pollutant concentration at time t.

The equilibrium adsorption capacity q_e was calculated from the mass balance equation according to Eq. (3-4):

$$q_e = \frac{(C_0 - C_{eq}) \cdot V_0}{m} \tag{3-4}$$

Where C_{eq} refers to the equilibrium concentration, V_0 to the volume of adsorbate solution, and m to the mass of used adsorbent.

The efficiency of the desorption of lignin from the adsorbent was evaluated by Eq. (3-5):

$$Desorption = \frac{C^{des}_{lignin,eq} \cdot V_{desorbent}}{(C^{ads}_{lignin,0} - C^{ads}_{lignin,eq}) \cdot V_{BWH3}} \cdot 100\% \tag{3-5}$$

Where $C^{des}_{lignin,eq}$ is the equilibrium lignin concentration during the desorption process, $C^{ads}_{lignin,0}$ and $C^{ads}_{lignin,eq}$ are the initial and equilibrium lignin concentration during the adsorption process, $V_{desorbent}$ is the volume of the desorbent in contact with the adsorbent, and V_{BWH3} is the volume of BWH 3 in contact with the adsorbent.

3.2.1.3 Single- and Multi-Component Isotherm Models

In the scope of adsorption experiments, single- and multi-component adsorption isotherms were modeled. The model equations and parameters used are shown in Publication I and in Table 6.

In single-component systems, the non-competitive isotherm equations Freundlich (Eq. (3-6)), Langmuir (Eq. (3-7)), and Redlich-Peterson (Eq. (3-8)) were used. The Freundlich isotherm is an empirical equation employed to describe a non-ideal and reversible adsorption. The model

can be adopted for multilayer adsorption, with non-uniform distribution of adsorption heat and affinities over the heterogeneous surface [165]. The Langmuir isotherm, which is based on defined model assumptions and is mathematically derived from those, assumes monolayer adsorption, which can only occur at a fixed number of definite localized sites that are identical, with no lateral interactions and steric hindrance between the adsorbed molecules. Each molecule possesses constant enthalpy and equal affinity [165, 166]. The Redlich-Peterson isotherm incorporates three parameters into an empirical equation. The isotherm model combines elements from both the Langmuir and Freundlich equation, and the mechanism of adsorption is a hybrid one and does not follow ideal monolayer adsorption. The exponent β_{RP} predetermines the limits of the isotherm. When β_{RP} tends to zero, Redlich-Peterson approaches the Freundlich isotherm model, and when β_{RP} is close to one, Redlich-Peterson approaches Langmuir condition [167].

When more than one potential adsorbate is present in the aqueous solution, there can be interaction and/or competition for adsorption on the same active sites between the various components. Hence, there is a possibility that adsorption of one component may affect the adsorption of other components. For the characterization of multi-component systems, the equivalent models of the applied single-component isotherms were used. That means, extended Freundlich (Eq. (3-9) and (3-10)), non-modified competitive Langmuir (Eq. (3-11)), modified competitive Langmuir (Eq. (3-12)), extended Langmuir (Eq. (3-13)), non-modified competitive Redlich-Peterson (Eq. (3-14)), and modified competitive Redlich-Peterson (Eq. (3-15)) were applied [164, 168].

Model parameters of single- and multi-component isotherm equations were determined by the nonlinear regression method and the open-source software GNU Octave. The nonlinear least-squares solver *"lsqcurvefit"* within the optimization package was used.

Table 6: Applied single- and multi-component adsorption isotherms

Isotherm model	Model equation	Model parameters	Eq.
Single-component			
Freundlich	$q_e = K_F C_{eq}^{n}$	$K_F; n$	(3-6)
Langmuir	$q_e = Q_0 \frac{K_L C_{eq}}{1 + K_L C_{eq}}$	$K_L; Q_0$	(3-7)
Redlich-Peterson	$q_e = \frac{K_{RP} C_{eq}}{1 + a_{RP} C_{eq}^{\beta_{RP}}}$	$K_{RP}; a_{RP}; \beta_{RP}$	(3-8)
Multi-component			
Extended Freundlich	$q_{e,i} = \frac{K_{F,i} C_{eq,i}^{n_i + x_i}}{C_{eq,i}^{x_i} + y_i C_{eq,j}^{z_i}}$	$x_i; y_i; z_i$	(3-9)
	$q_{e,j} = \frac{K_{F,j} C_{eq,j}^{n_j + x_j}}{C_{eq,j}^{x_j} + y_j C_{eq,i}^{z_j}}$	$x_j; y_j; z_j$	(3-10)
Non-modified competitive Langmuir	$q_{e,i} = \frac{Q_{0,i} K_{L,i} C_{eq,i}}{1 + \sum_{j=1}^{N} K_{L,j} C_{eq,j}}$	-	(3-11)
Modified competitive Langmuir	$q_{e,i} = \frac{\frac{Q_{0,i} K_{L,i} C_{eq,i}}{n_{L,j}}}{1 + \sum_{j=1}^{N} K_{L,j} \left(\frac{C_{eq,j}}{n_{L,j}}\right)}$	$n_{L,j}$	(3-12)
Extended Langmuir	$q_{e,i} = \frac{Q_{0,i} K_{L,i} C_{eq,i}}{1 + \sum_{j=1}^{N} K_{L,j} C_{eq,j}}$	$K_{L,i}; Q_{0,i}$	(3-13)
Non-modified competitive Redlich-Peterson	$q_{e,i} = \frac{K_{RP,i} C_{eq,i}}{1 + \sum_{j=1}^{N} a_{RP,j} C_{eq,j}^{\beta_{RP,j}}}$	-	(3-14)
Modified competitive Redlich-Peterson	$q_{e,i} = \frac{K_{RP,i} \frac{C_{eq,i}}{n_{RP,i}}}{1 + \sum_{j=1}^{N} a_{RP,j} \left[\frac{C_{eq,j}}{n_{RP,j}}\right]^{\beta_{RP,j}}}$	$n_{RP,j}$	(3-15)

3.2.1.4 Model Validation and Statistical Evaluation

For the validation and statistical evaluation of the various single and multi-component equilibrium models, the error function Marquardt's percent standard deviation (*MPSD*) was calculated according to Eq. (3-16):

$$MPSD = 100 \times \sqrt{\frac{1}{N - P} \sum_{i=1}^{n} \left(\frac{q_{e,i}^{exp} - q_{e,i}^{cal}}{q_{e,i}^{exp}} \right)^2} \tag{3-16}$$

Where N is the number of data points, P is the degree of freedom of the isotherm equations, $q_{e,i}^{exp}$ is the experimentally determined equilibrium adsorption capacity, and $q_{e,i}^{cal}$ is the calculated equilibrium adsorption capacity. The model, which fits the best to the experimental data, is the one with the lowest *MPSD*.

3.2.2 Ultrafiltration Experiments and Process Optimization

In the first part of the UF experiments, the influence of the process parameters TMP, temperature, and pH on the separation of hemicellulose from remaining lignin in BWH was investigated. In addition, to consider the influence of different MWCOs and polymeric materials, six UF membranes were screened. For this purpose, statistical design of experiments was applied, whereby all examined factors are varied simultaneously over a set of experimental runs. The response surface methodology (RSM), developed by Box and Wilson [169], with a central composite design (CCD), was used since nonlinear relationships between the studied factors are suspected [170]. This methodological approach results in empirical regression models that represent a mathematical correlation between the process parameters and the responses (i) permeate flux, (ii) hemicellulose retention, and (iii) lignin retention. The estimation of optimized TMP, temperature, and pH in terms of maximum permeate flux and hemicellulose retention, as well as minimal lignin retention, is a multiobjective problem within certain constraints. Pareto optimization (PO) was chosen as an appropriate method to solve this problem. Thereby, a frontier of competitive designs was developed in which no design can improve one criterion without diminishing at least one other criterion [171]. BWH 2 was used during the experimental work.

The second part of the UF experiments includes investigations regarding the influence of adsorption pretreatment on filtration capacity and solute retention. For this purpose, both untreated and adsorption pretreated BWH 3 were tested.

3.2.2.1 Response Surface Methodology

RSM with a CCD with three factors (n) and five levels was applied to investigate the influence of the effective factors TMP (X_1), temperature (X_2), and pH (X_3) on the permeate flux, hemicellulose retention, and lignin retention (Publication II). The operating ranges and the levels of the considered variables are shown in Table 7.

Table 7: Actual and coded levels of the factors used for the experimental design

Factors	Symbol	Actual values of coded levels				
		-α	-1	0	+1	+α
Transmembrane pressure (MPa)	X_1	0.4	0.4	0.7	1.0	1.0
Temperature (°C)	X_2	25	25	40	55	55
pH value (-)	X_3	2.5	2.5	5	7.5	7.5

The process variables are studied in five coded levels, -α, -1, 0, +1, and +α, each corresponding to an actual variable value. The actual variable's highest and lowest values are +1 and -1, respectively, and represent the orthogonal design points of a full factorial design (2^n). The midrange is 0 and represents the center or the replicate point (n_c), which determines the experimental error. The coded levels -α and +α form the CCD and thus depict the second-order polynomial. The coded level -α defines the negative distance between the star points and the center point and +α the positive distance. In this study, the α value is 1, meaning the star points are face-centered. The number of experimental runs (N) is calculated according to Eq. (3-17).

$$N = 2^n + 2n + n_c \tag{3-17}$$

As mentioned above, three independent variables n and four replicate points n_c were selected, resulting in 18 experimental runs. In Table 8 the CCD experimental matrix is presented. For the development of empirical models that correlate the particular responses to the three independent variables, a second-order polynomial equation described by Eq. (3-18) was established.

$$Y = b_0 + \sum_{i=1}^{n} b_i X_i + \sum_{i=1}^{n} b_{ii} X_{ii}^2 + \sum_{i=1}^{n-1} \sum_{j=i+1}^{n} b_{ij} X_i X_j \tag{3-18}$$

Where Y is the predicted response, b_0 is a constant coefficient, b_i is a linear coefficient, b_{ii} is a quadratic coefficient, b_{ij} is an interaction coefficient, and X_i and X_j are the coded values of the factors. Hence, if three variables are considered, the second-order polynomials, using the coded factors, are expressed by Eq. (3-19).

$$\begin{aligned} Y = {} & b_0 + b_1 X_1 + b_2 X_2 + b_3 X_3 + b_{11} X_{11}^2 + b_{22} X_{22}^2 \\ & + b_{33} X_{33}^2 + b_{12} X_1 X_2 + b_{13} X_1 X_3 + b_{23} X_2 X_3 \end{aligned} \tag{3-19}$$

The statistical analysis of the models was performed by analysis of variance (ANOVA) with an F-test to obtain the mathematical/statistical correlation between input and output parameters. To verify the goodness of fit of the individual models, each model term was tested statistically, confirming the significance of F-values with $p \leq 0.05$. The values of the coefficient of determination R^2, adjusted R^2, and predicted R^2 are obtained to check the quality of the suggested polynomial. For the development of the experimental plan and the statistical analysis of the experimental results, the software Design-Expert (Stat-Ease Inc., Version 11) was used.

Table 8: Central composite design of experiments and the responses permeate flux (J), hemicellulose retention ($R_{hemicellulose}$), and lignin retention (R_{lignin}) for the ultrafiltration membranes UA60 and UH004

Run	Factors			Observed responses – UA60			Observed responses – UH004		
no.	TMP (X_1)	T (X_2)	pH (X_3)	J (L/(m²h))	$R_{hemicellulose}$ (%)	R_{lignin} (%)	J (L/(m²h))	$R_{hemicellulose}$ (%)	R_{lignin} (%)
1	-1	-1	-1	23.7	73.1	42.4	22.6	60.3	28.2
2	+1	-1	-1	31.9	95.7	46.6	28.7	83.1	33.3
3	-1	+1	-1	32.2	68.8	36.0	23.8	50.8	26.5
4	+1	+1	-1	52.6	83.0	43.9	36.2	78.4	26.1
5	-1	-1	+1	22.6	72.1	46.8	25.6	47.9	41.9
6	+1	-1	+1	32.9	90.7	47.5	36.8	70.2	30.2
7	-1	+1	+1	33.0	51.8	37.9	32.3	44.5	33.7
8	+1	+1	+1	52.1	64.7	45.1	54.5	60.5	33.7
9	-α	0	0	30.0	66.9	36.3	24.3	41.3	24.6
10	+α	0	0	37.7	91.4	43.3	47.5	59.0	28.6
11	0	-α	0	29.2	95.9	41.6	30.3	56.8	30.7
12	0	+α	0	37.8	79.0	39.9	37.5	58.7	24.9
13	0	0	-α	34.4	83.9	38.9	27.7	58.8	26.2
14	0	0	+α	35.5	66.4	47.0	38.1	44.4	35.7
15	0	0	0	32.2	86.2	40.2	34.9	55.2	29.0
16	0	0	0	32.1	81.2	41.7	35.2	57.4	27.8
17	0	0	0	31.3	84.0	40.8	36.5	54.5	27.7
18	0	0	0	32.6	86.7	38.8	35.1	55.6	27.6

The experimental runs of the CCD were executed using the cross-flow filtration system in total reflux mode. This means the retentate and permeate were recycled to the feed tank. The flow rate of the feed solution was 10 L/min, which corresponds to a CFV of 1.1 m/s and a Reynolds number (Re) of 820. The filtration area of each membrane was 0.036 m^2, and for each set of experiments, fresh membranes were used. Before (PWF_b) and after (PWF_a) the filtration experiments the pure water flux (PWF) of each UF membrane was measured at 0.7 MPa and 40 °C. Through the assessment of the PWF reduction (PWF_r), according to Eq. (3-20), the severity of fouling was quantified.

$$PWF_r = \frac{PWF_b - PWF_a}{PWF_b} \cdot 100\% \tag{3-20}$$

For the filtration process, 10 L of BWH 2 was filled into the feed tank and then circulated at 0.7 MPa and 40 °C until a steady-state was achieved to maintain a constant concentration during the experiments. Subsequently, an experimental set was conducted, including six experimental points. Every experimental point was held for at least 1 h before permeate was collected for 1 min in a volumetric cylinder to calculate the permeate flux. Simultaneously to the permeate flux measurements, small amounts of samples (10 mL) were taken from the feed and permeate to determine concentrations and retentions.

To illustrate the experimental procedure, after filling in the BWH 2 in more detail, the run-in period, steady-state flux, and flux measurements for the membranes UA60 and UH004 are exemplified in Figure 19 (a), and the hemicellulose and lignin concentrations in the feed and permeate in Figure 19 (b). An experimental set is shown, which consists of six experimental points (run no. 1, 13, 10, 16, 7, and 6 – see Table 8). Steady-state was reached when the permeate flux changed very little or not at all over time due to the formation of a deposited layer by concentration polarization as well as by reversible and irreversible fouling. Because of the recirculation of the retentate and permeate into the feed tank and the removal of negligibly small amounts of samples, it can be assumed that the retentate concentration corresponds to the feed concentration. On this basis, the influence of the process parameters TMP, temperature, and pH on the permeate flux and the hemicellulose and lignin concentrations in the feed and permeate could be determined. A detailed discussion of the results shown as an example, as well as the reasons and explanations for them can be found in Section 4.2.3.

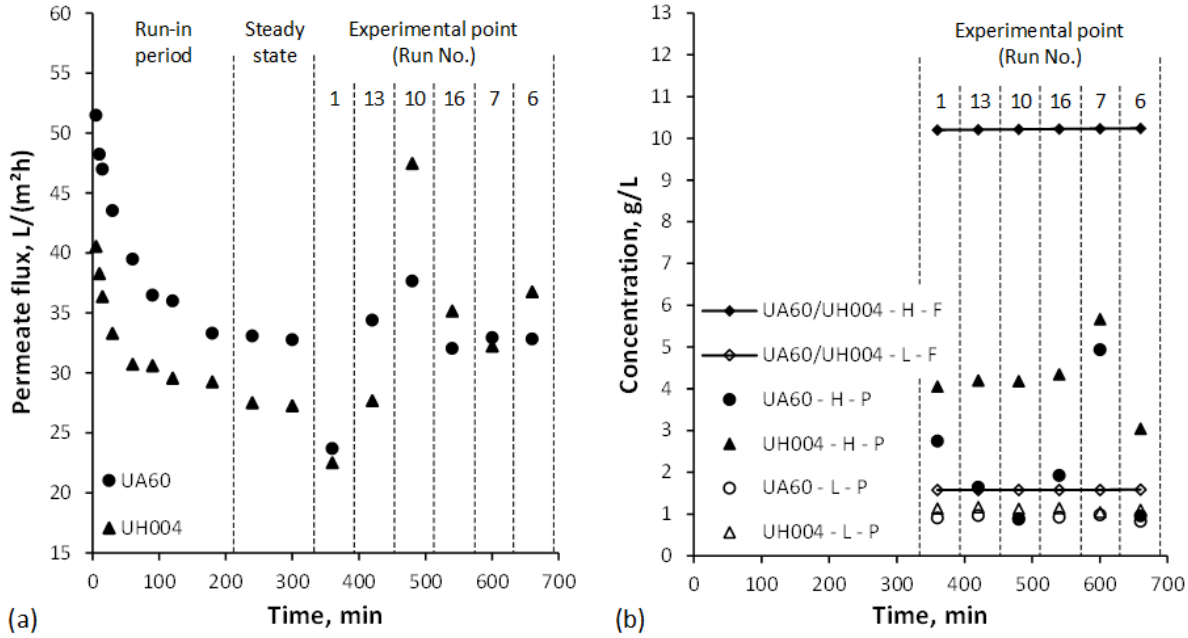

Figure 19: Example of an experimental set including (a) permeate flux run-in period until reaching steady-state and six experimental points (run no.) and (b) hemicellulose (H) and lignin (L) concentrations in the feed (F) and permeate (P) for six experimental points

3.2.2.2 Pareto Optimization

The aim of PO was the simultaneous determination of optimized TMP, temperature, and pH in terms of maximum permeate flux and hemicellulose retention, as well as minimal lignin retention. The empirical model equations (Table 15), established using RSM, can be expressed as objective functions within the PO. Hence, the optimization of the UF process is multiobjective, which can be generally formulated as:

$$\begin{aligned} &\min_x F(x) = [f_1(x), f_2(x), \dots f_i(x)]^T, (i \geq 2) \\ &s.t. \\ &g_u(x) \leq 0 \ (1 \leq u \leq r) \\ &h_v(x) = 0 \ (1 \leq v \leq s) \\ &x_{lb} \leq x_t \leq x_{ub} \ (1 \leq t \leq i_x) \end{aligned} \tag{3-21}$$

Where $F(x)$ is a vector composed of i objective functions $f_k(x)$. The functions $g_u(x)$ and $h_v(x)$ are related with the r inequality and s equality constraints, respectively, and x_{lb} and x_{ub} are the lower and upper bound constraint vectors on x of dimension i_x. $x \in \mathbb{R}^n$ is the vector of decision variables to be optimized, and n is the number of decision variables. The feasible design space is defined as $X = \{x \in \mathbb{R}^n | g_u(x) \leq 0 (1 \leq u \leq r) \ and \ h_v(x) = 0 \ (1 \leq v \leq s)\}$, and the feasible objective space is defined as $Z = \{z \in \mathbb{R}^i | z = F(x), x \in X\}$. If an objective function $f_i(X)$ is to be maximized, then an equivalent objective function $-f_i(X)$ is considered to be minimized. A design vector $x^* \in X$ is Pareto optimal, if there does not exist any other point $x \in X$, such that $f_k(x^*) \geq f_k(x)$ for all $k \in \{1, 2, \dots, i\}$, and there exists at least one $k \in \{1, 2, \dots, i\}$ such that $f_k(x^*) > f_k(x)$. Hence, a Pareto solution is Pareto optimal if and only if there does not exist another solution that is not worse in all objectives and is strictly better in at least one objective [172]. The Pareto optimal set in the design space refers to the set of Pareto optimal solutions. The corresponding set of Pareto optimal solutions in the objective space is referred to as the Pareto front [171].

No assumptions about the relative importance of the three objective criteria were made a priori. This means it is up to the decision-maker to assess the trade-offs between the different criteria and select an appropriate solution from the determined Pareto front. The calculation of the Pareto solution set was conducted with MATLAB (MathWorks) using genetic algorithms. To obtain a dense solution set, 200 points on the Pareto front were calculated. As the objective functions were determined in terms of coded variables, the constrained design space was defined by a lower bound (x_{lb}) for TMP, temperature, and pH of -1 and by an upper bound (x_{ub}) for TMP, temperature, and pH of +1. To ensure that no part of the Pareto front fails to be considered in the optimization process, the algorithm starts by obtaining anchor points corresponding to the minimum values of each single-objective functions [173]. The three-dimensional Pareto front is determined by the interpolation of the calculated Pareto points, without extrapolated points, and assuming that linear interpolation shows the truth.

Within the decision-making process using PO, trade-offs between the individual objectives have to be considered carefully. The aim is to determine a single or a smaller set of solutions from a potentially large amount of possible solutions. For this purpose, the utopia point (UP) method was used for strategically selecting a solution from the obtained Pareto optimal solution set [171]. The point $F^0(x) \in Z$ is a UP, if for each $k \in \{1, 2, \dots, i\}$, $F_k^0(x) = \min_x \{F_k(X) | x \in X\}$. Hence, it provides an "ideal" solution to the optimization problem, which is unattainable. The closest feasible solution, in terms of the Euclidian distance, to the UP is called the compromise point (CP) and has valuable characteristics such as feasibility, Pareto optimality, and independence of irrelevant alternatives [174].

3.2.2.3 Influence of Adsorption Pretreatment on the Ultrafiltration Process

BWH 3 was pretreated for the experiments by continuous adsorption in the fixed-bed column, as described in Publication V. The adsorbent used, dimension of the fixed-bed, and process temperature were equal to the experimental work described in Section 3.2.1.1. The flow rate for the adsorption and desorption was 2 mL/min (4.5 BV/h). At first, 6 BV of BWH 3 were fed to the adsorption column, and subsequent, it was regenerated by 5 BV of a 50 wt.% ethanol solution. This was repeated until 600 mL of pretreated BWH 3 were collected.

The separation of hemicellulose from remaining lignin in adsorption pretreated and untreated BWH 3 by UF was realized using the dead-end filtration system. A fresh membrane (TriSep UA60) was used in each trial. For the filtration experiments, 600 mL of the respective feed solution were filled into the feed tank/stirred cell and concentrated to a volume reduction (*VR*) of 0.8. *VR* was calculated according to Eq. (3-22) as the ratio between the mass of the feed (m_f) and the mass of the permeate (m_p) since differences in density can be neglected.

$$VR = \frac{m_p}{m_f} \tag{3-22}$$

Samples were collected from the feed and permeate to determine the concentrations and retentions. Furthermore, to assess the severity of fouling caused by the filtration of pretreated and untreated BWH 3, PWF_r was determined. All filtration steps were operated at process parameters previously identified as being optimal (Δp = 0.95 MPa, T = 55 °C, pH = 2.6) and a stirring speed of 500 rpm.

3.2.3 Hydrothermal Pretreatment Experiments

Based on Köchermann et al. [87], a newly designed hydrothermal process was developed, which, in comparison to previous studies, enables the conversion of the remaining oligomeric hemicellulose in BWH 4 to monomeric xylose without the formation of chemical successors, such as furans, and the addition of catalysts (Publication III). Experimental work was carried out using the flow tube reactor at a pressure of 5.0 MPa for all trials. RSM with a face-centered CCD, with the two variables temperature and residence time, was used to study appropriate combinations of process parameters for maximum conversion of oligomeric hemicellulose to monomeric xylose. The levels of the examined process parameters are shown in Table 9. The center point was replicated three times and the factorial points twice. The software Design-Expert (State-Ease Inc., Version 11) was used to statistically evaluate and create the empirical model for predicting appropriate process conditions to reach maximum xylose concentrations.

Table 9: Actual values and coded levels of the factors used for the experimental design

Factors	Symbol	Actual values of coded levels		
		-1	0	+1
Temperature (°C)	X_1	160	170	180
Residence time (min)	X_2	2.5	7.5	12.5

3.2.4 Nanofiltration Experiments – Filtration Performance and Fouling

In the first part of the NF experiments, the influence of hydrothermal pretreatment of BWH 4 on the separation of oligomeric hemicellulose derived xylose from fermentation inhibitors (acetic acid, furfural, and 5-HMF) by four commercial NF membranes was investigated. Using a MS as a reference, untreated BWH 4, and hydrothermally pretreated BWH 4 (HPBWH 4), a comprehensive evaluation of membrane performance and fouling were completed to verify the feasibility of the NF process. The performance of the NF membranes was assessed by the determination of permeate flux, retentions, and selectivity. Fouling behavior was described by the resistance-in-series model [175]. Besides, the cleaning and regeneration of the NF membranes were considered. The methodological procedure is presented in more detail in Publication III.

The MS was prepared with the aim of reproducing replicates of BWH 4 and HPBWH 4. Therefore, 50 g/L xylose (Sigma-Aldrich, purity ≥ 99 %), 8 g/L acetic acid (VWR Chemicals, purity ≥ 99 %), 6 g/L glucose (VWR Life Science, purity ≥ 99.5 %), and 2 g/L furfural (Sigma-Aldrich, purity ≥ 99 %) were dissolved in DIW. To adjust the pH to 2.7 a 1 M HCl (Carl Roth, molar concentration = 1 mol/L) solution was used. The pH of BWH 4 of 1.9 was also adjusted to 2.7 with a 5 M NaOH (VWR Chemicals, purity ≥ 98.9 %) solution. The MS was used to quantify performance and fouling characteristics without the influence of the complex hydrolyzate streams containing oligomeric hemicellulose, inhibitory compounds, and unknown species.

The second part of the NF experiments included a parameter screening of TMP and temperature to achieve an energetically favorable process with high xylose recovery rates. Hydrothermally pretreated BWH 2 (HPBWH 2) from the lignocellulose biorefinery pilot plant of Fraunhofer Center CBP was used as feed solution.

3.2.4.1 Performance Analysis

NF performance experiments were executed using the cross-flow filtration system in concentration mode in a single filtration step. This implies that the permeate was discharged into an external tank, and the retentate was recycled to the feed tank. This was done to investigate the performance of the NF membranes when increasing the concentration of organic substances in the feed solutions. The feed flow rate was 10 L/min corresponding to a CFV of 1.1 m/s and a Reynolds number of 820. The active filtration area for each NF membrane was 0.036 m^2. At the beginning of each experimental run, the PWF was measured at 3.0 MPa and 25 °C in triplicate, and $MgSO_4$ retention twice at 0.9 MPa, 25 °C, and a concentration of 2000 ppm.

For the concentration process, 10 L of the feed solution was filled into the feed tank. The filtration was operated at a TMP of 3.0 MPa and a temperature of 25 °C. The permeate was withdrawn continuously until a *VR* of 0.4–0.5. The permeate flux through the membranes was obtained after predetermined time intervals by collecting the permeate for 1 min. Simultaneously, samples (10 mL) were taken from the feed, retentate, and permeate to determine concentrations and retentions. In addition, the separation factor α was calculated according to Eq. (3-23).

$$\alpha_{inh/xyl} = \frac{C_{inh,p}/C_{xyl,p}}{C_{inh,f}/C_{xyl,f}} = \frac{1 - R_{obs,inh}}{1 - R_{obs,xyl}} \quad (3\text{-}23)$$

Where $C_{inh,p}$ and $C_{xyl,p}$ are the concentrations of inhibitors and xylose in the permeate, respectively, and $C_{inh,f}$ and $C_{xyl,f}$ are the concentrations of inhibitors and xylose in the feed, respectively. The separation factor $\alpha_{inh/xyl}$ indicates the separation of all considered inhibitors with respect to xylose. Separation factors of the individual inhibitors (acetic acid, furfural, and 5-HMF) to xylose are determined in the same way.

3.2.4.2 Fouling Analysis

Fouling experiments were also done using the cross-flow filtration system but in total reflux mode to investigate the susceptibility to fouling for the various NF membranes and feed solutions. Process parameters were equal to the performance analysis.

For the quantification of the fouling mechanisms, the resistance-in-series model [139, 175, 176] based on Darcy's law was used. In this model, the permeate flux (J) is written as a function of the TMP, the dynamic viscosity, and the total resistance (R_{tot}).

$$J = \frac{\Delta p}{\eta \cdot R_{tot}} \quad (3\text{-}24)$$

When filtering DIW, R_{tot} involves only the membrane resistance (R_m). This resistance is an intrinsic membrane characteristic that does not change during the filtration process or by changing the feed solution. R_m can be calculated according to Eq. (3-25) via PWF measurements before the filtration of one of the feed solutions.

$$R_m = \frac{\Delta p}{\eta_{DIW} \cdot PWF_b} \quad (3\text{-}25)$$

During the filtration of MS, BWH 4, and HPBWH 4, fouling can be caused by several mechanisms, such as concentration polarization (R_{cp}), gel and/or cake layer formation ($R_{g/c}$), and adsorption and/or pore blocking ($R_{a/p}$) [177]. These individual resistances can be summarized as a total fouling resistance (R_f), formulated in Eq. (3-26).

$$R_{tot} = R_m + R_f = R_m + R_{cp} + R_{g/c} + R_{a/p} \quad (3\text{-}26)$$

To determine R_f, the filtration of MS, BWH 4, or HPBWH 4 was operated until a steady permeate flux (J_{spf}) was reached [178]. The dynamic viscosity of the bulk solution (μ_b) was used for the calculation according to Eq. (3-27).

$$R_f = \frac{\Delta p}{\eta_b \cdot J_{spf}} - R_m \quad (3\text{-}27)$$

Based on this sum parameter, the single resistances could be identified. For this purpose, subsequent to the experiments with MS, BWH 4, or HPBWH 4, they were replaced by DIW,

and the PWF (PWF_{a1}) was measured. From this information, the newly resulting fouling resistance R_{f1} consisting of $R_{g/c}$ and $R_{a/p}$ can be determined (Eq. (3-28)).

$$R_{f1} = \frac{\Delta p}{\mu_{DIW} \cdot PWF_{a1}} - R_m = R_{g/c} + R_{a/p} \tag{3-28}$$

Fouling by concentration polarization is excluded since there are no solutes in the DIW, which can cause a concentration polarization layer. Hence, R_{cp} can be calculated by subtracting R_{f1} from R_f (Eq. (3-29)).

$$R_{cp} = R_f - R_{f1} \tag{3-29}$$

Then, the fouled NF membranes were rinsed with DIW at high shear rates (Δp = 0.4 MPa, T = 25 °C, CFV = 2.7 m/s, Re = 2020). It was assumed that under these conditions, the gel/ cake layer is washed off, and fouling by adsorption/pore blocking remains [179, 180]. Afterward, the PWF of the rinsed membrane (PWF_{a2}) was measured again with DIW. The resistance of the rinsed membrane can be understood as $R_{a/p}$ (Eq. (3-30)).

$$R_{a/p} = \frac{\Delta p}{\eta_{DIW} \cdot PWF_{a2}} - R_m \tag{3-30}$$

Finally, $R_{g/c}$ can be calculated by subtracting $R_{a/p}$ from R_{f1} (Eq. (3-31)).

$$R_{g/c} = R_{f1} - R_{a/p} \tag{3-31}$$

After the fouling experiments, the NF membranes were cleaned with the 1 wt.% P3-Ultrasil-53 solution (Δp = 0.4 MPa, T = 40 °C, CFV = 1.1 m/s, t = 30 min) and PWF (PWF_{a3}) and $MgSO_4$ retention were measured again to control the possibility of cleaning and regeneration of the NF membranes. The resistance of the cleaned NF membranes R_{cm} was calculated equivalent to R_m according to Eq. (3-25).

3.2.4.3 Influence of Transmembrane Pressure and Temperature

For the experiments, BWH 2 was hydrothermally pretreated converting oligomeric hemicellulose to monomeric xylose. The process was realized in a continuous pilot scale plug flow reactor made of Inconel 625 high-grade steel with a total length of 2150 mm, an internal diameter of 40 mm, and a reaction volume of about 2.15 L at the lignocellulose biorefinery pilot plant of Fraunhofer Center CBP. Based on the findings of the previous hydrothermal pretreatment experiments, the reactor was fed at a flow rate of 20 L/h, resulting in a residence time of 9 min, and operated at a pressure of 16.2 MPa and a temperature of 180 °C.

The filtration experiments were performed with the cross-flow system in total reflux. A fresh membrane (Alfal Laval NF) was used in each trial. For the parameter screening studies, 10 L of HPBWH 2 were circulated at a flow rate of 14 L/min, corresponding to a CFV of 1.5 m/s and a Reynolds number of 1130. The TMP was varied between 1.0 and 4.0 MPa at 25 °C, and

the temperature was varied between 25 and 55 °C at 3.0 MPa. Small amounts of samples (10 mL) were taken from the feed, retentate, and permeate to determine the concentrations and retentions. At appropriate process conditions, the HPBWH 2 was concentrated to a *VR* of 0.8.

3.2.5 Analytical Methods

In this section, the methods for analysis and characterization of liquid samples from BWHs on the one hand, and solid membrane materials on the other hand are presented. High-performance liquid chromatography (HPLC), gas chromatography (GC), UV/VIS spectroscopy, and viscosity measurements were applied for liquid samples. To characterize UF and NF membranes, atomic force microscopy (AFM) and BET analysis were applied.

3.2.5.1 High Performance Liquid Chromatography

The concentration of oligomeric hemicellulose, glucose, xylose, 5-HMF, and furfural was determined using an AZURA HPLC system (Knauer Wissenschaftliche Geräte GmbH) equipped with a binary pump system, an autosampler, a column oven, a diode array detector (DAD), and a refractive index detector (RID). The frozen samples were thawed at ambient temperature and prepared as follows: oligomeric hemicellulose was hydrolyzed to monomeric sugars by mixing the samples with a 72 % H_2SO_4 (Merck, purity ≥ 96 %) solution in a ratio of 28:1 v/v (based on Sluiter et al. [181]). Afterward, they were heated to 121 °C for 40 min and then cooled down to 30 °C for 30 min. The pH of the resulting acid hydrolyzate was adjusted to 5.0 with $CaCO_3$ (Carl Roth, purity ≥ 99.9 %). The sample was then transferred to a 1.5 mL centrifugation tube with a filter inlet (pore size: 0.2 µm) and centrifuged for 10 min at 10 °C and 15,000 rpm. The filtrate was diluted with ultrapure water in a ratio of 1:10 to 1:100 and transferred to a 1.5 mL tube with a 1 mL inlet, and stored at 4 °C. For the analysis, an autosampler (at 10 °C) was used to inject 15 µL of the sample into a MetaCarb 87P column (300 mm × 7.8 mm) equipped with a pre-column (30 mm × 7.8 mm) heated to 70 °C. Ultrapure water was used as the mobile phase under isocratic conditions and a flow rate of 0.35 mL/min. Glucose and xylose were detected using the RID, and 5-HMF and furfural were quantified with the DAD set at 280 nm. The concentration of oligomeric hemicellulose was determined as a concentration difference of xylose concentration after total hydrolysis. All HPLC measurements were conducted at least in duplicate.

3.2.5.2 Gas Chromatography

Acetic and formic acid analysis was performed on a 7890 A GC system with a flame-ionization detector (FID) from Agilent technologies. The headspace sampling was realized using an autosampler. For the analysis, 3 mL of the sample, 1 mL of the internal standard (2-methyl butyric acid, 184 mg/L), 0.5 mL of methanol, and 2.5 mL of sulfuric acid (diluted 1:5 v/v) were placed in a headspace vial and closed with an aluminum crimp cap with the PTFE/silicone septum. The injection mode was split at 1:10, and the injector temperature was kept at 220 °C. For the separation, a DBFFAP column (60 m × 0.25 mm × 0.5 µm) was used. The GC system was operated as follows: an initial temperature of 40 °C and hold for 20 min and a linear ramp of 10 °C/min until 200 °C and hold for 10 min. The FID was heated to 260 °C. All GC measurements were conducted at least in triplicate.

3.2.5.3 UV/VIS Spectroscopy

For phenol and lignin concentration analysis, a UV/VIS spectrophotometer (VWR, model: UV-6300PC) was used with a quartz cuvette of 1 cm diameter. The measurements of phenol were carried out at 254 nm. Samples were diluted with ultrapure water in a ratio of 1:10 v/v. The absorbance of lignin was detected at 280 nm [55, 128] after diluting the sample with ultrapure water so that the absorbance was between 1.0 and 0.3. Thereby, it has to be pointed out that some wood extractives and carbohydrate degradation products (e.g., furfural and 5-HMF) also absorb UV light at 280 nm [38]. This can lead to an overestimation of the lignin concentration. As the use of the absorption rate is unpractical for further calculations, the values were converted into a mass concentration by Eq. (3-32).

$$C_{lignin} = \frac{A_{280} \cdot d}{\alpha \cdot l} \tag{3-32}$$

Where A_{280} is the absorbance value at 280 nm, α is the absorptivity factor [110 L/(g cm)] as an average value for several wood species according to TAPPI [182], l is the length of the cuvette, and d is the dilution factor. All UV/VIS spectrophotometer measurements were conducted with ultrapure water as a blank sample and at least in duplicate.

3.2.5.4 Viscosity Measurement

Viscosity measurements were performed on a DV-II+ Pro Extra viscometer from Brookfield. Due to the relatively low viscosity of the liquid samples, a UL adapter with an Yula 15(E)Z spindle was used. Measurement parameters were set and values readout with the software Rheocalc from Brookfield. The samples were tested in triplicate at a shear rate interval of 1-200 s^{-1} and a temperature of 25 °C. The results were evaluated by mathematical modeling of the shear rate-dependent viscosities using the Ostwald-de Waele power law.

3.2.5.5 Atomic Force Microscopy

In Publications II and III, AFM was used to measure the surface roughness of the flat-sheet membranes tested. A Keysight 5600LS SPM AFM equipped with an Agilent MAC Mode III controller and manufacturer-supplied software was used. Measurements were performed in the tapping mode with silicon-doped probes of type PPP-NCH. The probes had a force constant of 10–130 N/m, a resonant frequency of 204–497 kHz, a tip height of 10–15 µm, and a cantilever thickness of 4 µm, a length of 125 µm, and a width of 30 µm. Operating conditions were in air under atmospheric pressure at ambient temperature. The in-plane horizontal (X- and Y-axis) scales were 5 µm × 5 µm, and the vertical Z-axis varied with respect to the surface roughness of each membrane. The roughness value root-mean-square roughness (Rq) was obtained from processing image data using Gwyddion software [183].

3.2.5.6 BET Analysis

The average pore width, total pore volume, and BET surface area of the flat-sheet membranes used in Publication III were determined by isothermal N_2 adsorption/desorption at -196.53 °C (77 K) using an autosorb iQ2 (Quantachrome Instruments) surface and porosity analyzer. For the sample preparation, the skin layer of the flat-sheet membranes was mechanically separated

from their support. Afterward, the skin layer was cleaned with DIW, then air-dried, and degassed with N_2 at 45 °C (2 °C/min) for 480 min under a vacuum of 10^{-3} mm Hg to dry and unclog pores. For each NF membrane, approximately 200 mg of the skin material was placed into a standard bulb cell with an inner diameter of 9 mm. The amount of N_2 adsorbed was measured in the p/p_0 range of 0.005–0.973. The specific surface area was calculated using the BET method [184] from the linear region of the adsorption curves.

3.2.6 Process Assessment

When developing new processes/process cascades or transferring established processes to new applications, technical and economic assessment should be considered right from the beginning to identify technical and non-technical gaps and barriers at an early stage [185]. In the scope of this work, the results of the experimental studies were integrated into such an assessment (Publications IV and V). For the technical assessment, flowsheet simulation was applied to calculate mass and energy balances as well as sizing of the equipment. The economic assessment was realized by the determination of specific production costs.

Two purification cascades for the separation and valorization of hemicellulose from organosolv BWH were assessed (Figure 1). Purification cascade 1 consists of an adsorption process to remove lignin from the BWH and UF for the concentration of hemicellulose and simultaneous removal of remaining lignin fragments and smaller molecules. On the other hand, purification cascade 2 consists of hydrothermal pretreatment of the BWH to convert remaining hemicellulose oligomers into monomeric xylose and NF to separate fermentation inhibitors and increase the concentration of xylose. To enable comparability, both purification cascades were scaled to the same plant size and input concentration. A plant capacity to process 50,000 dry metric tonnes of beechwood annually, resulting in 258,400 metric tons of BWH [43], was assumed to be a reasonable size for a demonstration plant [186, 187]. The input concentration corresponds to BWH 5, and an output concentration of 200 g/L of the desired components seems attainable [58]. Moreover, it was assumed that the processes would be located in Germany at an existing chemical site, where all required utilities and wastewater treatment could be provided, and the operating time would be 8,000 hours per year. The required utilities for the process configurations are high pressure steam (HPS) at 2.2 MPa, low pressure steam (LPS) at 0.23 MPa, cool water (CW) with an inlet temperature of 20 °C, and electricity (EE).

3.2.6.1 Flowsheet Simulation

The software Aspen Plus® was chosen as an appropriate tool for flowsheet simulation. The input data of the single process simulations were mainly from the experimental results, complemented by information from literature as indicated. Liquid activity coefficients were calculated with the NRTL (Non-Random Two Liquids) property method because of its good performance to represent highly non-ideal mixtures [188]. All unit operations were simulated with a common simplification as continuous processes [189–191]. The physical property database *BIODFMS3* [192], was used for physical properties of the main lignocellulosic components (e.g., cellulose, hemicellulose, lignin) [193].

3.2.6.2 Mass Balance

In mass balancing, all input ($\dot{m}_{input}$) and output ($\dot{m}_{output}$) streams were determined and described in terms of their mass and material composition. Mass balancing is based on the conservation of mass at steady-state according to Eq. (3-33).

$$\sum \dot{m}_{input} = \sum \dot{m}_{output} \tag{3-33}$$

With the knowledge from the mass balancing, the developed processes could be examined for their applicability, and equipment could be dimensioned. For further characterization of the processes, yields (Y) were calculated according to Eq. (3-34).

$$Y = \frac{m_{i,product}}{m_{i,0}} \cdot 100\% \tag{3-34}$$

Where $m_{i,0}$ is the initial mass of component i and $m_{i,product}$ is the mass of component i in the product stream. The replacement or renewal of consumables, such as adsorbent (lifetime > 5 years [194]) and membrane materials (lifetime 1-1.5 years [195–197]), were not considered in the mass balance. These were included in the economic calculations.

3.2.6.3 Energy Balance

Energy balance is based on the conservation of energy according to Eq. (3-35).

$$\sum \dot{E}_{input} = \sum \dot{E}_{output} \tag{3-35}$$

Where $\dot{E}_{input}$ is the energy content of all input streams and $\dot{E}_{output}$ is the energy content of all output streams. Included forms of energy were thermal, electrical, mechanical, and chemical energy.

The energy demands of both purification cascades were determined using Aspen Plus® except for the electrical power of the pumping system of the adsorption and desorption process as well as of the feed and recirculation pump for UF and NF process. Electrical power requirements for the pumping system of the adsorption and desorption process result from the adsorbent bed's hydraulic characteristics. The pressure drop at various temperatures and flow rates for each meter of bed depth of SP700 in down flow operation is shown in Figure 20 [198].

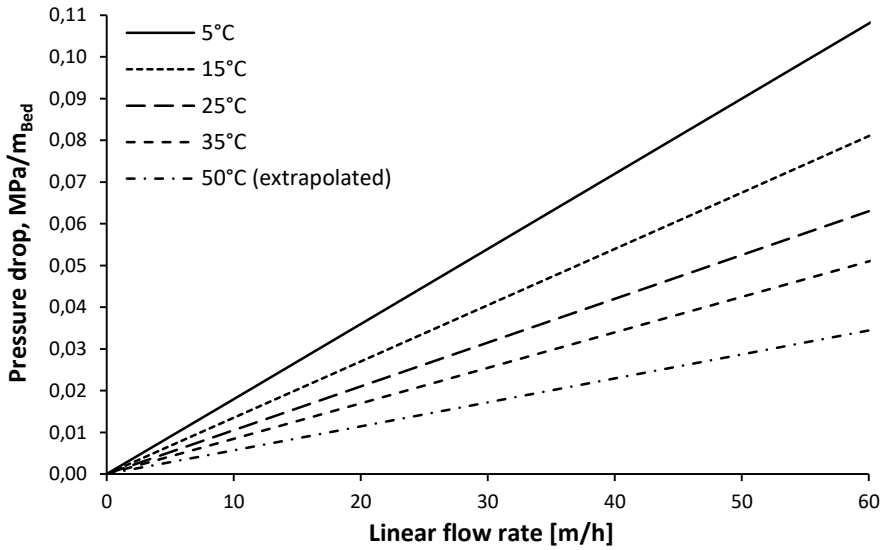

Figure 20: Approximate pressure drop at various temperatures and flow rates for each meter of bed depth of SP700 (based on [198])

The energy required in the UF and NF for the feed pump ($\dot{E}_{feed\ pump}$), delivering the inlet pressure of the system, and the recirculation pump ($\dot{E}_{recirc\ pump}$), compensating for the frictional pressure losses and maintaining a certain circulation flow, was calculated according to Eq. (3-36) and Eq. (3-37), respectively [27, 55, 56].

$$\dot{E}_{feed\ pump} = \left(\frac{\Delta p \cdot \dot{V}_{feed}}{\eta_{pump} \cdot \left(VR \cdot \dot{V}_{feed}\right)}\right) \cdot \dot{V}_p = \left(\frac{\Delta p}{\eta_{pump} \cdot VR}\right) \cdot \dot{V}_p \tag{3-36}$$

$$\dot{E}_{recirc\ pump} = \left(\frac{\Delta p_{f,av} \cdot \dot{V}_{mod}}{\eta_{pump} \cdot \left(J_{av} \cdot A_{mod}\right)}\right) \cdot \dot{V}_p \tag{3-37}$$

Where $\dot{V}_{feed}$ is the feed volume flow of the filtration system, $\dot{V}_{mod}$ is the feed volume flow in a membrane module, $\dot{V}_p$ is the permeate volume flow, A_{mod} is the membrane area of a membrane module, η_{pump} is the pump efficiency (0.8), and J_{av} and $\Delta p_{f,av}$ are the average permeate flux and the average frictional pressure drop in a membrane module during the concentration to the aimed VR. J_{av} and $\Delta p_{f,av}$ correspond to Eq. (3-38) and Eq. (3-39), respectively [199].

$$J_{av} = \frac{\int_0^{VR} J\, dVR}{VR} = a + \frac{b}{2} \cdot VR + \frac{c}{3} VR^2 + \frac{d}{4} VR^3 \tag{3-38}$$

$$\Delta p_{f,av} = \frac{\int_0^{VR} \Delta p_f\, dVR}{VR} = a + \frac{b}{2} \cdot VR + \frac{c}{3} VR^2 + \frac{d}{4} VR^3 \tag{3-39}$$

Third-degree polynomials were fitted to the influence of VR on permeate flux and frictional pressure drop (Δp_f). The average values are obtained by integrating the regression equations.

For a more detailed energetic assessment, the energy efficiency (η_E) was determined (Eq. (3-40)) defined as the energy output in the purified product stream ($\dot{E}_{product} = \dot{m}_{product} \cdot LHV_{product}$) divided by the energy input, including all material streams ($\dot{E}_{input,material} = \sum \dot{m}_{input,i} \cdot LHV_{input,i}$) as well as heat ($\dot{E}_{heat}$) and electrical power ($\dot{E}_{electricity}$) demands.

$$\eta_E = \frac{\dot{E}_{product}}{\dot{E}_{input,material} + \frac{\dot{E}_{heat}}{\eta_{heat}} + \frac{\dot{E}_{electricity}}{\eta_{electricity}}} \tag{3-40}$$

The calculations were based on the following estimations: (i) lower heating value (*LHV*) of the input, and the purified product streams were obtained from Aspen Plus®, and (ii) process heat and electrical power are provided by a natural gas-fired combined heat and power plant (CHP) with a thermal efficiency (η_{heat}) of 51 % and an electrical efficiency ($\eta_{electricity}$) of 39 % [200].

3.2.6.4 Sizing of Equipment

Within this investigation the sizing of the equipment was estimated either via volume flow rate, electrical power and/or specific dimensions obtained from the flowsheet simulations using Aspen Plus®.

The dimensions of buffer tanks, pumps, the tube bundle reactor for hydrothermal pretreatment, adsorption columns, and membrane plants were determined based on the volume flow and information from manufacturers. To estimate the capacity of buffer tanks for the feed, intermediates, and product streams, the volume input per unit of time, the residence time (48 h), and a volume correction factor (f_{VC} = 1.2) were considered. For the sizing of the pumps, the exiting volume flow and a specific factor that takes the applied pressure level into account were used. The tube bundle reactor for hydrothermal pretreatment was designed based on the inflowing volume, residence time, and information from manufacturers. Regarding the adsorption column, the flow rate and the assumption of a diameter-to-height ratio of 1:5 for the column were used for dimensioning. In addition, the manufacturer's information for the adsorbent SP700 was included. At least three columns are needed. The total membrane areas required for UF and NF were estimated using Eq. (3-41).

$$A_m = 1.2 \cdot \left(\frac{\dot{V}_{feed}}{J_{av}} \right) \tag{3-41}$$

A factor of 1.2 was used to include the extra area needed for cleaning and maintenance.

The demand of electrical power is needed for dimensioning the agitators in the buffer tanks. The estimate of the dimension results from the volume of the respective buffer tank and an assumed power requirement of 20 W/m³ [201].

Sizes of heat exchangers and the rectification column (recovery of desorbate solution) were determined directly using the equipment sizing package in Aspen Plus®. The dimension of the heat exchangers is described by their transfer area, which results from the heat flow, the incoming and outgoing temperatures, and the heat transfer coefficient. For the rectification

column, the capacity is determined as a function of the type and number of trays, the height and diameter of the column sections, and the operating pressure.

3.2.6.5 Costing

The mass and energy balances from the flowsheet simulation of both purification cascades as well as sizing of the equipment were used to conduct the costing. Specific production costs were calculated using a simplified approach based on VDI Guideline 6025 [44]. All relevant costs were assigned to the cost group's capital-linked costs, consumption-linked costs, operation-linked costs, and other costs. The capital-linked costs were determined based on equipment costs. The design, dimensioning, and quantitative determination of the equipment was carried out in the flowsheet simulation. The estimation of equipment costs was done according to the data and methods described by Peters et al. [202] and Chauvel et al. [203]. The chemical engineering plant cost index (CEPCI) and ProcessNet Chemieanlagen-Index Deutschland (PCD) [204] were used as cost indices to update the costs to the base year 2020. Plant-specific surcharge factors were used to account for direct costs and indirect costs leading to fixed-capital investments (FCI). The annuity method was used to calculate depreciation and interest into equal annual payments. The consumption-linked costs are based on the use and prices of raw materials, auxiliary materials, process energy, and disposal costs. Operation-linked costs contain estimations for labor and maintenance. Operating staff was assumed based on typical requirements in the chemical industry according to plant capacity and the degree of automation [202]. The wage costs were calculated on an hourly basis [205]. Operating supervision was estimated with a 15 % surcharge based on the operating staff cost. Other costs include administration, insurance, and uncertainties, which were calculated with overhead rates. General assumptions for the costing are summarized in Table 10. Specific production costs were calculated by dividing the total annual production costs by the annual quantity of products.

Table 10: Main assumptions for costing

Parameter	Value	Unit
Average cost of capital	4	% p.a.
Assessment period	20	Years
Maintenance, repairs	5	% of FCI p.a.[a]
Administration	20	% of labor costs p.a.[a]
Insurance, uncertainties	1.5	% of FCI p.a.[a]
Labor costs	28.5	EUR/h[b]
UF/NF membrane	30	€/m² [c]
Membrane housing	50	€/m² [c]
Adsorbent material	5,100	€/m³ [c]

[a][202]; [b][205]; [c]information from manufacturers and industry

4. Results and Discussion

In this section, the results of the four general research parts, namely (I) separation and recovery of lignin from BWH by adsorption, (II) UF of BWH for concentrating hemicellulose and removal of lignin, (III) NF of hydrothermally treated BWH for concentrating hemicellulose derived xylose and removal of inhibitory components, and (IV) demonstration and assessment of purification cascades for the separation and valorization of hemicellulose and derived xylose from BWH, are presented and discussed.

4.1 Adsorption for the Separation and Recovery of Lignin

In Section 4.1.1 results of adsorbent screening and in Section 4.1.2 results of single- and multi-component isotherm modeling using MSs are presented. Next, Sections 4.1.3 and 4.1.4 illustrate the results of the adsorption processes with BWH 1 and discuss the applicability of the isotherm models from MSs to real and complex wood hydrolyzates. Finally, Sections 4.1.5 and 4.1.6 give a brief excursus regarding lignin uptake from BWH 3 in a continuous fixed-bed column and desorption of lignin from the adsorbents, respectively. More detailed information can be found in the corresponding Publications I and V.

4.1.1 Adsorbent Screening with Model Solutions

4.1.1.1 Effect of Adsorbent-to-Solution Ratio

The effect of the adsorbent dose was determined using A:S ratios of 1:5, 1:10, 1:15, 1:20, 1:25, and 1:33 w/v (Figure 21). A comparison of the five tested adsorbents and A:S ratios was made based on phenol and xylose removal from binary-component solutions according to Eq. (3-3). The relative removal of phenol and xylose increases with an increasing A:S ratio. This increase can be explained by the increase in surface area and the number of active sites of the adsorbents. Typically, at one A:S ratio, the removal rate of the adsorbates becomes constant due to the aggregation of adsorption sites and thus a decrease in total available adsorbent surface area and an increase in diffusion path length. Except for XAD4, the phenol removal became constant between an A:S ratio of 1:5–1:10 w/v. Thus, even higher removal rates appear to be possible for higher dosage of XAD4. XAD7HP and SP700 were able to remove phenol almost completely from the binary MS. SP700 has an aromatic PS-DVB matrix; hence phenol as an aromatic molecule has a strong affinity. XAD4 and XAD16N adsorbents are also PS-DVB based but show lower surface areas and porosities and are, therefore, most probably less efficient. XAD7HP is an uncharged PA based adsorbent with an aliphatic surface and has naturally higher hydrophilicity than PS-DVB adsorbents and, thus lower affinity towards aromatic molecules. Nevertheless, in contrast to other studies [38, 128, 206] XAD7HP was the most efficient resin for the adsorption of phenol during the batch experiments. One reason might be the much better distribution and thus higher wetting of the adsorbent particles in the MS due to the weakly polar characteristics. Another explanation could be the better uptake of materials with low molecular weights. The SiO_2/Al_2O_3-based HiSiv1000 adsorbent has a hydrophobic character distinguished by 12-member oxygen rings. The zeolite has free diameters of 7–7.4 Å.

Aromatic phenol molecules have a molecular size of approx. 6 Å and can thus be recovered easily by HiSiv1000. However, the zeolite is much less selective and efficient compared to the resins.

The removal rate of xylose can be considered constant for the polymeric adsorbents at an A:S ratio of 1:10 w/v. SP700 showed the lowest removal of xylose with 4.4 % at A:S = 1:5 w/v and XAD7HP the highest removal rate with 7.8 % at A:S = 1:5 w/v. The removal of xylose using zeolite HiSiv1000 did not become constant at the maximum A:S ratio of 1:5 w/v. However, maximum removal of 16.9 % was detected at A:S = 1:5 w/v. These results can be explained by the previously shown chemical structures and characteristics of the adsorbents.

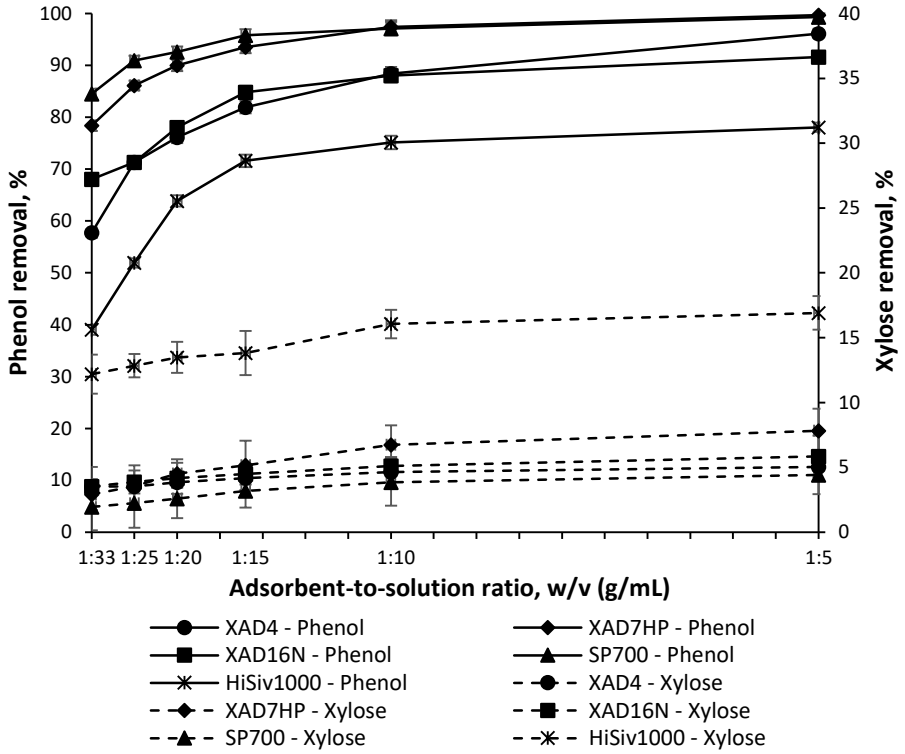

Figure 21: Effect of adsorbent-to-solution ratio on the removal of phenol and xylose from a binary-component phenol-xylose solution after a contact time of 180 min (Error bars represent the standard deviation)

4.1.1.2 Effect of Contact Time

The effect of contact time was evaluated for all five adsorbents at an A:S ratio of 1:5 w/v. The phenol and xylose removal were determined at predefined time intervals from 0 to 180 min. Figure 22 illustrates that within the first 8 min the adsorption rate was very fast, and afterward, it gradually decreased. This is due to the initially high difference in concentration between the adsorbate solution and adsorbent surface, which decreases with adsorption time until reaching the equilibrium concentration. The experimental conditions, which means mixing the solutions using a magnetic stirrer, may cause abrasion of the adsorbent materials. This would increase the adsorption rate over time due to smaller particle sizes. However, no apparent abrasion could be observed for the polymeric resins, and the zeolite was already powdery (Table 4). The equilibrium time for the removal of phenol by the studied adsorbents was found to be between

15 and 90 min, and for the removal of xylose between 60 and 90 min under the experimental conditions. XAD7HP and SP700 have reached equilibrium in the shortest time.

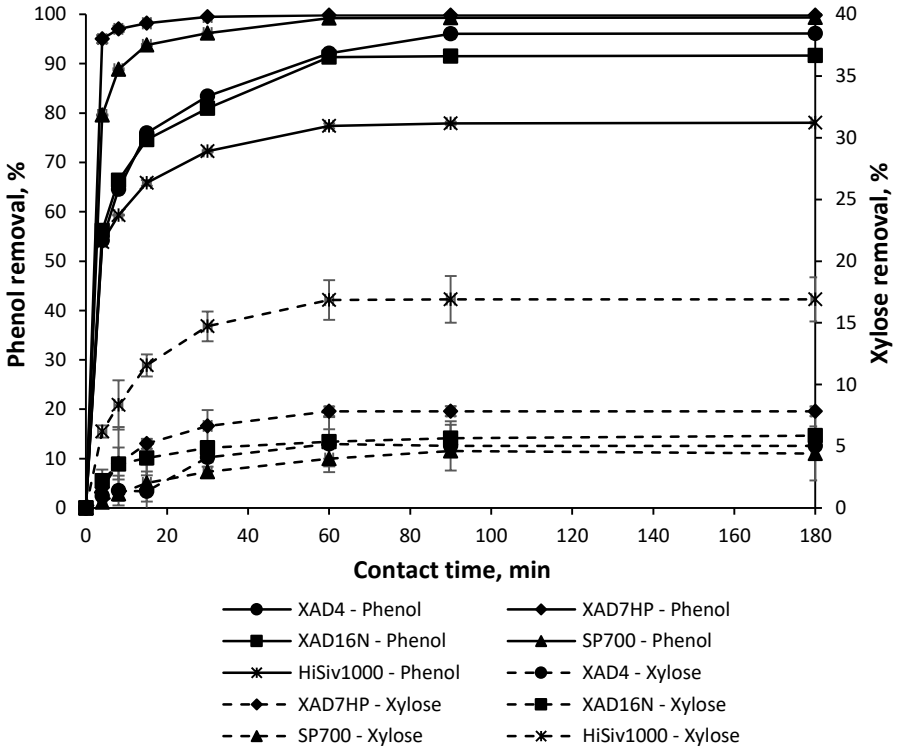

Figure 22: Effect of contact time on the removal of phenol and xylose from a binary-component phenol-xylose solution at an adsorbent-to-solution ratio of 1:5 w/v (Error bars represent the standard deviation)

4.1.1.3 Selection of Adsorbents

The results above and the dimensionless separation factor R_L derived from the Langmuir-Isotherm were used to select the two most appropriate adsorbents for the separation problem. The separation factor R_L is expressed in Eq. (4-1) and determined from single-component MSs.

$$R_L = \frac{1}{1 + K_L C_0} \tag{4-1}$$

K_L is the constant of the non-competitive Langmuir-Isotherm (Eq. (3-7)). R_L values indicate whether the adsorption process is favorable ($0 < R_L < 1$), linear ($R_L = 1$), unfavorable ($R_L > 1$), or irreversible ($R_L = 0$) [207]. The closer the value is to 0, the more favorable the process is. The studies on the A:S ratio have shown that the most efficient phenol uptake was reached at a ratio of 1:5 w/v and the lowest xylose uptake at a ratio of 1:33 w/v (Figure 21). However, since the focus is the maximum removal of phenol from the aqueous solutions and xylose uptake increased only very slightly with increasing A:S ratio, the A:S ratio of 1:5 w/v was chosen for further studies. The studies on the effect of constant time have shown that all adsorbents reached equilibrium after 90 min at the latest (Figure 22), The R_L values (Table 11) of phenol uptake for all adsorbents were in the range of 0.08–0.71, indicating that adsorption of phenol on the studied adsorbents is a favorable process. The lowest R_L values can be observed for XAD7HP and SP700 with 0.08. For xylose, the R_L values were between 0.89 and 0.94, indicating

insignificant adsorption of xylose on the studied adsorbents. The highest R_L values can be determined for XAD4 and SP700 with 0.94. Nevertheless, the two polymeric adsorbents, XAD7HP and SP700, were further considered since the focus is the maximum removal of phenol from the aqueous solutions (Publication I).

Table 11: Langmuir constant K_L and separation factor R_L

	K_L (L/g)	R_L
XAD4		
Phenol	1.13	0.22
Xylose	0.02	0.94
XAD7HP		
Phenol	3.84	0.08
Xylose	0.02	0.93
XAD16N		
Phenol	0.13	0.71
Xylose	0.02	0.92
SP700		
Phenol	3.59	0.08
Xylose	0.01	0.94
HiSiv1000		
Phenol	0.45	0.42
Xylose	0.03	0.89

4.1.2 Isotherm Modeling with Model Solutions

4.1.2.1 Single-Component Models

Single component models were applied to get the best-fit model and thus to interpret the mechanisms during the adsorption process. The calculated parameters of the isotherms are presented in Table 12. According to the *MPSD* the uptake of phenol by XAD7HP and SP700 can be fitted best by the Freundlich equation (Figure 23 (a)). Hence, multilayer adsorption, with non-uniform distribution of adsorption heat and affinities, seems to be predominant. Nevertheless, Langmuir and Redlich-Peterson equations also provide a satisfying graphical fit to the experimental data points. The determination of the adsorption isotherms for the uptake of xylose by XAD7HP and SP700 is associated with distinct uncertainties due to the high liquid phase concentrations at all investigated A:S ratios. These high liquid phase concentrations are related to the very low adsorptions rates. According to *MPSD*, it seems that the Langmuir equation exhibits the best fitting for XAD7HP and SP700 (Figure 23 (b)). However, the high standard deviations of the experimental data illustrate that Freundlich and Redlich-Peterson isotherm models could be applicable, too.

The Langmuir parameter K_L can be used to quantify the interaction between adsorptive and adsorbent. The K_L values for phenol are higher than for xylose; consequently interactions between phenol and adsorbents are more stable than interactions between xylose and the adsorbents. XAD7HP and SP700 show similar results for K_L regarding the adsorption of phenol and xylose [164].

Table 12: Parameters of the single-component isotherm models for the adsorption of phenol and xylose from a single-component solution by XAD7HP and SP700

Single component isotherm model	Parameter	XAD7HP		SP700	
		Phenol	Xylose	Phenol	Xylose
Freundlich	K_F ((g/g)/(g/L)$^{1/n}$)	0.095	6E-04	0.135	4E-04
	n	0.436	1.023	0.562	1.072
	MPSD	18.99	1.067	8.015	1.701
Langmuir	Q_0 (g/g)	0.108	0.036	0.137	0.032
	K_L (L/g)	3.835	0.018	3.585	0.014
	*MPS*D	43.87	1.060	17.76	1.690
Redlich-Peterson	K_{RP} (L/g)	113.5	0.006	0.985	0.006
	α_{RP} (L/g)$^{\beta}$	1184	8.100	6.887	9.790
	β_{RP}	0.542	0.008	0.619	0.158
	MSPD	25.55	1.234	11.28	3.569

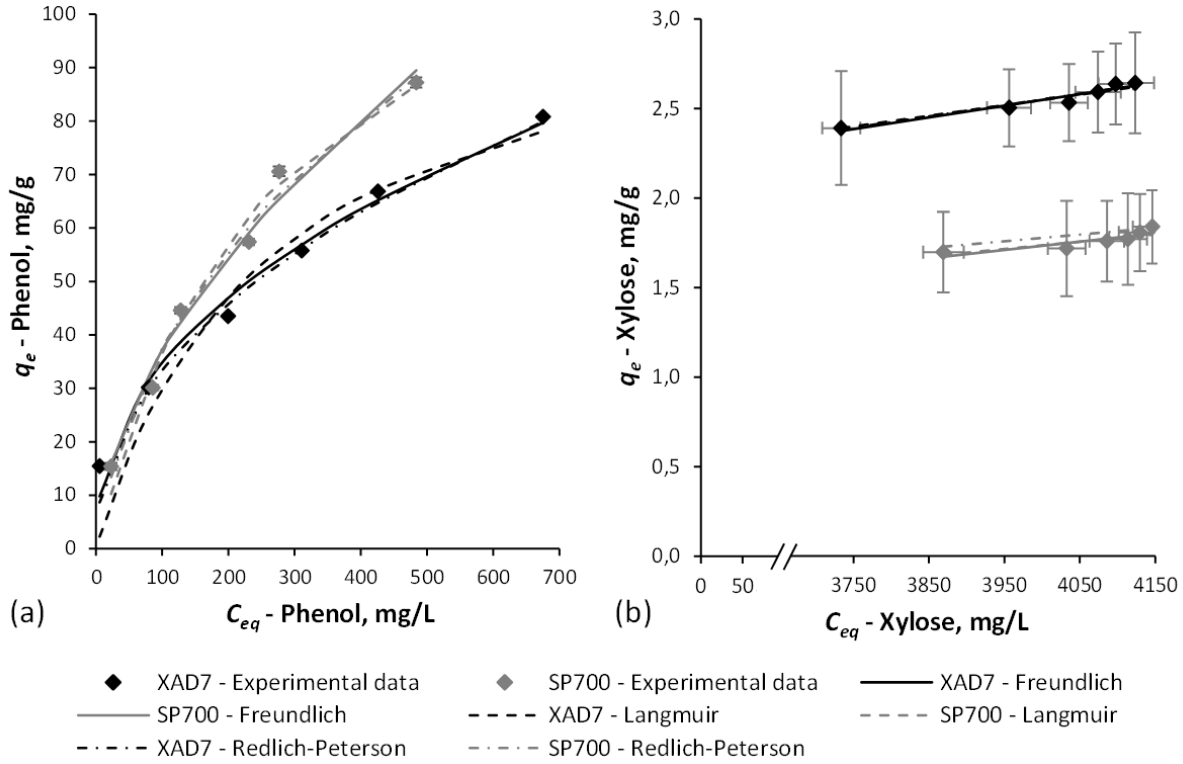

Figure 23: Single-component isotherm models (a) for phenol uptake by XAD7HP and SP700 and (b) for xylose uptake by XAD7HP and SP700 from single-component solutions (Error bars represent the standard deviation)

4.1.2.2 Multi-Component Models

The simultaneous adsorption data of phenol and xylose onto the studied resins were applied to the multi-component isotherm models extended Freundlich, non-modified competitive Langmuir, modified competitive Langmuir, extended Langmuir, non-modified competitive Redlich-Peterson, and modified competitive Redlich-Peterson. The resulting model parameters of all multi-component adsorption isotherms are given in Table 13. A comparison of the experimental and calculated equilibrium adsorption capacities of phenol and xylose uptake by XAD7HP and SP700 is presented in Figure 24 (a)–(d). Thereby, the bisecting line represents the measured adsorption process, and the 10, 20, and 30 % error lines indicate the deviation of the calculated results from the experiments. Hence, the closer the calculated results are distributed around the bisecting line, the better fits the model.

The extended Freundlich model was best fitted to the experimental data and had the lowest *MPSD* for the phenol uptake by both resins in a binary mixture with xylose. This is also illustrated in Figure 24 (a) and (c), where most of the data points calculated with the extended Freundlich model are falling within the 10 % error lines around the bisecting line. The multi-component non-modified competitive Langmuir model shows a poor fit to the experimental data and high values for the *MPSD*. The use of the interaction term $n_{L,j}$ improves the fit. The extended Langmuir model shows no improvement in fitting and has a larger *MPSD* than the modified Langmuir model. The non-modified competitive Redlich-Peterson model shows suitable fitting and a low *MPSD* for the uptake of phenol by XAD7HP. By introducing the interaction term $n_{RP,j}$ in the modified Redlich-Peterson model, the fitting changed for the worse. For phenol uptake by SP700, the contrary was observed; modified Redlich-Peterson provided suitable fitting and non-modified Redlich-Peterson was worse.

The determination of the multi-component adsorption isotherms for xylose uptake in a binary mixture with phenol is associated with particular uncertainties due to the high liquid phase concentrations at all investigated A:S ratios. The multi-component extended Freundlich isotherm gives the best results. This is exemplified by very low *MPSD* values in Table 13 and in Figure 24 (b) and (d), where all data points are on the bisecting line. However, it must be taken into account that some calculated data points of the extended Freundlich model are distributed around the 10 and 20 % error line. This is because of higher standard deviations due to a more unstable adsorption process compared to the phenol uptake. This instability is due to the initially high concentration difference between the adsorbate solution and the adsorbent surface, which only changed slightly during xylose adsorption onto XAD7HP and SP700. In contrast to the adsorption of phenol, the determined single- and multi-component isotherms for the xylose uptake, namely Langmuir and extended Freundlich, differ in their characteristics. However, when transferring the results from the batch adsorption experiments to a continuous fixed-bed column, the adsorption process should be described using equivalent models and parameters. This is because in columns exist regions where the pure component is predominant and regions where component profiles overlap. Hence, in this case as multi-component isotherm extended Freundlich is approved due to the above mentioned facts, and as single-component isotherm Freundlich equation due to low *MPSD* values (Table 12).

Table 13: Parameters of the multi-component isotherm models for the adsorption of phenol and xylose from a binary-component solution by XAD7HP and SP700

Multi-component isotherm model	Parameter	XAD7HP		SP700	
		Phenol	Xylose	Phenol	Xylose
Extended Freundlich	x_i	-2.419	1.729	-0.546	-3.414
	y_i	-5E-07	0.003	1.317	-0.002
	z_i	7.803	0.023	-5.381	3.925
	MPSD	14.35	0.806	6.054	1.036
Non-modified competitive Langmuir	*MPSD*	29.75	38.89	12.83	32.72
Modified competitive Langmuir	$n_{L,j}$	0.855	0.586	0.917	0.653
	MPSD	32.89	37.33	13.30	26.20
Extended Langmuir	$Q_{0,I}$ (g/g)	0.344	0.002	0.854	0.002
	$K_{L,I}$ (L/g)	21.39	10.48	20.37	20.24
	*MPS*D	54.15	17.70	37.27	10.22
Non-modified competitive Redlich-Peterson	*MPSD*	19.12	89.59	73.16	13.85
Modified competitive Redlich-Peterson	$n_{RP,j}$	0.945	0.122	0.197	0.454
	MPSD	21.96	86.86	31.65	53.02

These results support the theory that the multi-component extended Freundlich isotherms apply to those systems where each component individually follows the single-component Freundlich isotherm. The extended Freundlich equation assumes that the adsorption of each component in a multi-component system has an exponential distribution of adsorption energy and that the coverage by each adsorbate molecule at each energy level is given by the extended Langmuir isotherm [208]. In binary or in general in multi-component solutions, three types of effects on the adsorption can occur [209]:

I. Synergism – Effect of the mixture is greater than that of each of the individual effects of the components in the mixture.
II. Antagonism – Effect of the mixture is less than that of each of the individual effects of the components in the mixture.
III. Non-interaction – Effect of the mixture is neither more nor less than that of each of the individual effects of the components in the mixture.

The effect of interaction between phenol and xylose in a binary mixture could be interpreted by the ratio of the adsorption capacity of one adsorbate (Q_{mix}) in the binary mixture to the same adsorbate when present alone (Q_0). Thus defined [210]:

- $Q_{mix}/Q_0 > 1$, synergism
- $Q_{mix}/Q_0 = 1$, non-interaction
- $Q_{mix}/Q_0 < 1$, antagonism

In this study, Q_{mix}/Q_0 was calculated as 1.00 and 1.11 for phenol and xylose with XAD7HP, as well as 0.99 and 0.62 for phenol and xylose with SP700. Hence, the binary mixture shows no effect on the phenol adsorption in both adsorbents, whereas it showed a slightly synergistic effect on the xylose adsorption with XAD7HP and an antagonistic effect with SP700.

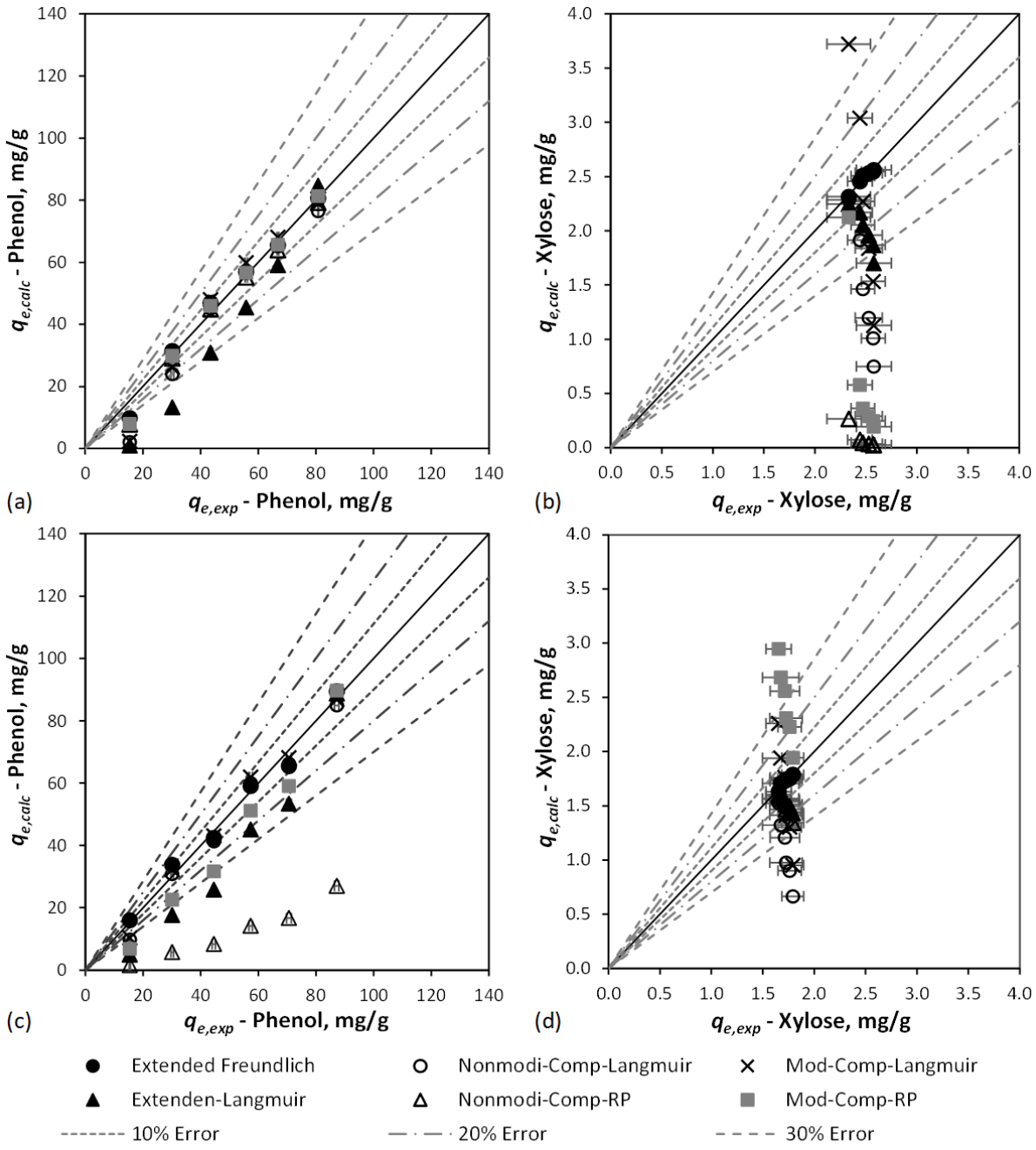

Figure 24: Comparison of experimental and calculated equilibrium adsorption capacity (q_e) of (a) phenol uptake by XAD7HP, (b) xylose uptake by XAD7HP, (c) phenol uptake by SP700, and (d) xylose uptake by SP700 from a binary-component solution (Error bars represent the standard deviation)

4.1.3 Adsorbent Screening with Beechwood Hydrolyzate

To validate the selection of adsorbents using MSs, all five adsorbents were tested again using BWH 1 at an A:S ratio of 1:5 w/v for 180 min – see Figure 25. Equilibrium for the removal of lignin was reached after 90 min at the latest. Again, the adsorbents Amberlite XAD7HP and SEPABEADS SP700 showed the best separation characteristics. This means 93.4 and 94.8 % of lignin could be removed. A decrease in adsorption capacity compared to phenol removal in MS experiments can be explained by the presence of many other hydrophobic components (e.g.,

furans) in BWH 1.By their adsorption, active sites on the adsorbents are occupied and thus are no longer accessible to lignin. The maximum removal or rather losses of hemicellulose amounted to 6.9 % for XAD7HP and 8.0 % for SP700. These results are similar to those using MSs. Hence, using a binary phenol-xylose MS the appropriate adsorption materials can be selected regarding their application in the uptake of lignin from BWH 1. However, the adsorption capacities have to be determined individually for each solution or wood hydrolyzate.

As mentioned in Section 3.2.1.1, the pH of BWH 1 was adjusted from 2.5 to 6.0 using a 5 N NaOH solution to enable comparability between MS and BWH 1 experiments. Dissolved lignin in organosolv BWH is a highly complex macromolecule (Section 2.1.3) consisting of several phenolic compounds such as phenol ($pK_a = 9.99$), syringol ($pK_a = 9.98$), catechol ($pK_a = 9.48$), guaiacol ($pK_a = 9.93$) and vanillin ($pK_a = 7.40$) linked together by hydrogen bonds formed mainly by carboxylic acids ($pK_a = 3–4$) [32]. Hence, when the pH is increased the carboxylic acids are dissociated, which results in a partial breakdown of the hydrogen bonds, thus destabilizing the lignin network. The phenolic compounds are still predominant as molecular species. Accordingly, it is to be expected that at a pH of 6.0 the adsorption rate of the smaller lignin molecules is higher due to a better accessibility and mass transfer within the adsorbent particles. The increased negative charge of the lignin molecules has no or just a minor influence on the adsorption due to the nonpolar characteristics of the adsorbents.

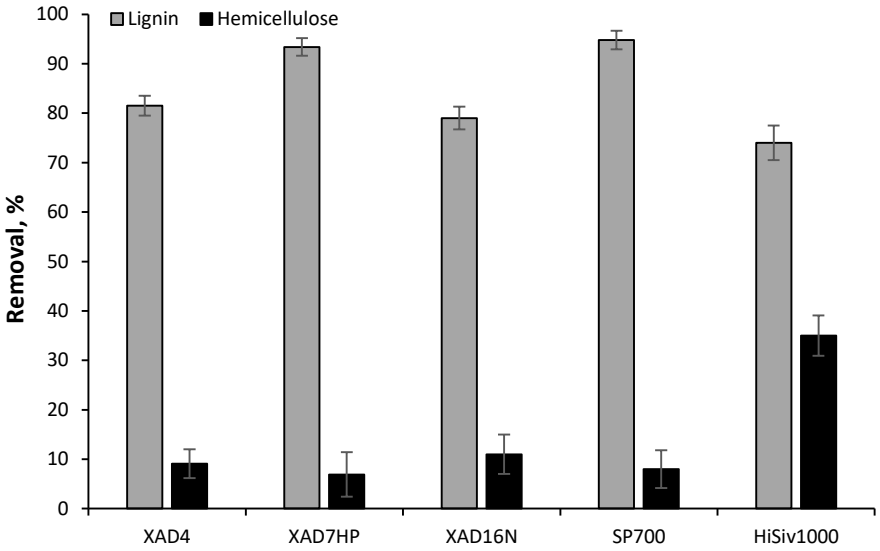

Figure 25: Adsorbent screening for the removal of lignin and hemicellulose from beechwood hydrolyzate 1 (Error bars represent the standard deviation)

4.1.4 Application and Evaluation of Isotherms to Beechwood Hydrolyzate

The isotherm model parameters from MS experiments (Table 12 and Table 13) were applied to predict and interpret the adsorption mechanisms, which are predominant during the adsorption of lignin and hemicellulose from BWH 1 by XAD7HP and SP700. The precision of the prediction and thus interpretation was analyzed by calculating the *MPSD* according to Eq. (3-16). Thereby, $q_{e,i}^{exp}$ is the experimentally determined equilibrium adsorption capacity from BWH 1 and $q_{e,i}^{cal}$ is the calculated equilibrium adsorption capacity determined by

experimental data from BWH 1 and isotherm model parameters from MS experiments. In addition, multi-component isotherm parameters were re-determined using equilibrium data from BWH 1 experiments. The model parameters were calculated directly and not by the single-component isotherms due to the character of the biomass substrate. Validation of these isotherm models was executed by calculating the *MPSD*, too. Thereby, $q_{e,i}^{exp}$ is the experimentally determined equilibrium adsorption capacity from BWH 1 and $q_{e,i}^{cal}$ is the calculated equilibrium adsorption capacity determined by experimental data and isotherm model parameters from BWH 1. All *MPSD* values for multi-component equilibrium modeling using isotherm parameters from MS and BWH 1 are displayed in Table 14. Moreover, the multi-component isotherms of lignin and hemicellulose adsorption onto XAD7HP and SP700 using model parameters from BWH 1 are illustrated in Figure 26. The methodological approach and results are presented in more detail in Publication I.

The application of the multi-component isotherm model parameters determined by MSs to the adsorption processes in BWH 1 resulted in very high values for *MPSD*. This applies to all model equations as well as for both adsorbents. The re-determined model parameters using BWH 1 resulted in significantly lower values for the *MPSD*. In the case of lignin adsorption, this seems to be mainly due to the lower equilibrium concentration compared to phenol. The reason for this may be, on the one hand, the strong affinity of the adsorbents towards other degradation products with a hydrophobic character present in BWH 1. These components, which are probably smaller in their molecular sizes compared to lignin, can lead to a blocking or occupation of the particle pores, which are then no longer accessible. On the other hand, lignin is very heterogeneous and consists of a wide range of molecules of different sizes, shapes, and functionalities. Hence, the surface groups of the lignin molecules differ, which may significantly influence the degree of affinity with the adsorbents. Regarding the adsorption of the hemicellulose, the differences between the *MPSD* values of applied MS model parameters compared to BWH 1 model parameters are smaller due to the general low equilibrium concentrations during the uptake of sugars. Nevertheless, the differences in *MPSD* could be explained by the variety of the molecular weight distribution of the hemicellulose. It is believed that the smaller molecules are mainly adsorbed, while the larger ones remain in the fluid phase [121].

Adsorption of lignin onto XAD7HP and SP700 correlates best with the extended Freundlich model depicted by the lowest *MPSD* and Figure 26 (a) and (c). Model parameters for XAD7HP are $K_F = 0.056$, $n = 0.798$, $x_i = -0.846$, $y_i = 0.611$ and $z_i = -0.392$ and for SP700 $K_F = 0.052$, $n = 0.716$, $x_i = -7.244$, $y_i = 0.019$ and $z_i = -0.220$. The non-modified competitive Redlich-Peterson model shows a very poor fit to the experimental data and high values for the *MPSD*. Despite the introduction of the interaction term $n_{RP,j}$ of the modified competitive Redlich-Peterson model, the fitting and the *MPSD* got even worse. The non-modified competitive Langmuir isotherm, which corresponds to the extended Langmuir equation if the model parameters are determined directly (Table 6), shows considerably lower *MPSD* values and a better fitting. The modified competitive Langmuir model with the interaction term $n_{L,j}$ also shows improvement.

Table 14: Comparison of Marquardt's percentage standard deviation (*MPSD*) for the multi-component equilibrium modeling of lignin and hemicellulose uptake by the adsorbents XAD7HP and SP700 using isotherm model parameters determined by model solutions (MSs) and beechwood hydrolyzate 1 (BWH 1)

Multi-component isotherm model	Model parameter source	XAD7HP		SP700	
		Lignin *MPSD*	Hemicellulose *MPSD*	Lignin *MPSD*	Hemicellulose *MPSD*
Extended Freundlich	MS	112	32.4	33.3	36.5
	BWH 1	0.90	2.35	1.65	0.94
Non-mod. comp. Langmuir	MS	147	36.7	173	44.9
	BWH 1	30.8	23.1	39.4	21.7
Mod. comp. Langmuir	MS	136	46.7	106	67.4
	BWH 1	29.8	32.1	37.5	20.6
Extended Langmuir	MS	135	44.9	128	54.5
	BWH 1	30.8	23.1	39.4	21.7
Non-mod. comp. Redlich-Peterson	MS	172	93.5	193	227
	BWH 1	139	77.4	163	72.0
Mod. comp. Redlich-Peterson	MS	139	65.9	151	82.2
	BWH 1	189	69.3	209	58.1

From Figure 26 (b) and (d) and by the lowest *MPSD* in Table 14 it can be seen that the hemicellulose uptake by XAD7HP and SP700 is best represented by the extended Freundlich model, too. Model parameters are $K_F = 0.550$, $n = -2.973$, $x_j = -3.431$, $y_j = 0.012$ and $z_j = -0.920$ and $K_F = 0.052$, $n = -1.884$, $x_j = -0.659$, $y_j = 0.034$ and $z_j = -1.561$, respectively. The non-modified and modified competitive Redlich-Peterson model provide very poor fit. Non-modified competitive or rather extended Langmuir and modified competitive Langmuir show a more adequate but still not satisfying correlation to the experimental results.

From these considerations, it can be concluded that by means of MSs used in this study, the multi-component isotherm models and thus the adsorption mechanisms for the uptake of lignin and hemicellulose from BWH 1 by XAD7HP and SP700 can be predicted relatively accurately. Nevertheless, the isotherm model parameters of the MSs do not adequately describe the specific adsorption process of BWH 1 onto the resins. Hence, they have to be determined individually. An extension of the MS or rather of the model by a third component, e.g., furfural, could still improve the fit of the applied model parameters.

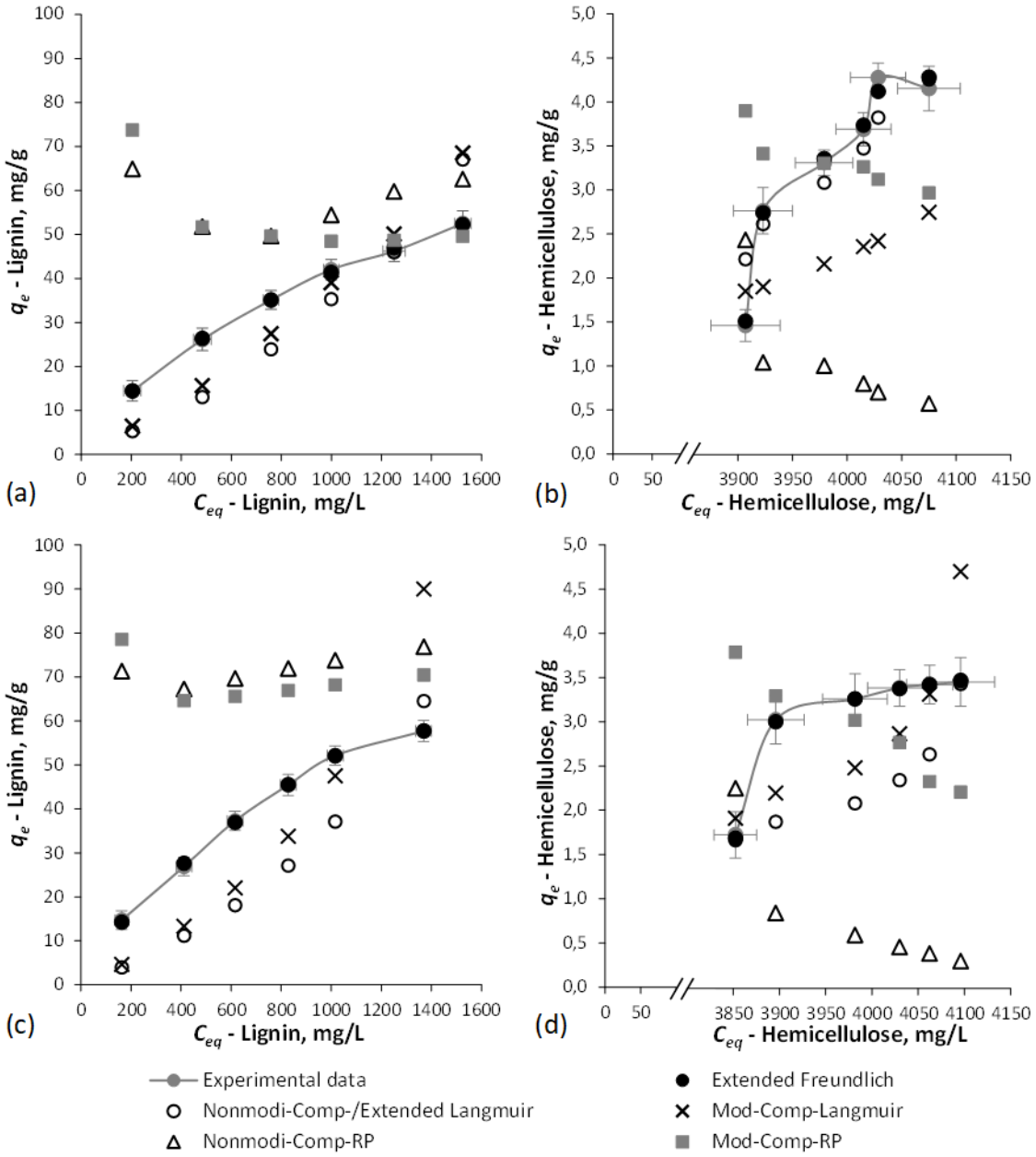

Figure 26: Comparison of the multi-component isotherms determined by using model parameters from BWH 1 of (a) lignin uptake by XAD7HP, (b) hemicellulose uptake by XAD7HP, (c) lignin uptake by SP700, and (d) hemicellulose uptake by SP700 in BWH 1 (Error bars represent the standard deviation)

4.1.5 Adsorption of Lignin in a Fixed-Bed Column

The effect of flow rate on the adsorption of lignin on SP700 in a continuous fixed-bed column was studied using BWH 3 and is presented in Figure 27. As can be seen, the flow rate has no effect on the adsorption of lignin within the investigated range. The manufacturer (Mitsubishi Chemical Corporation) of the SP700 recommends a flow rate between 0.5 and 5 BV/h [198]. Based on this information and economic considerations, 4.5 BV/h was chosen for further investigations.

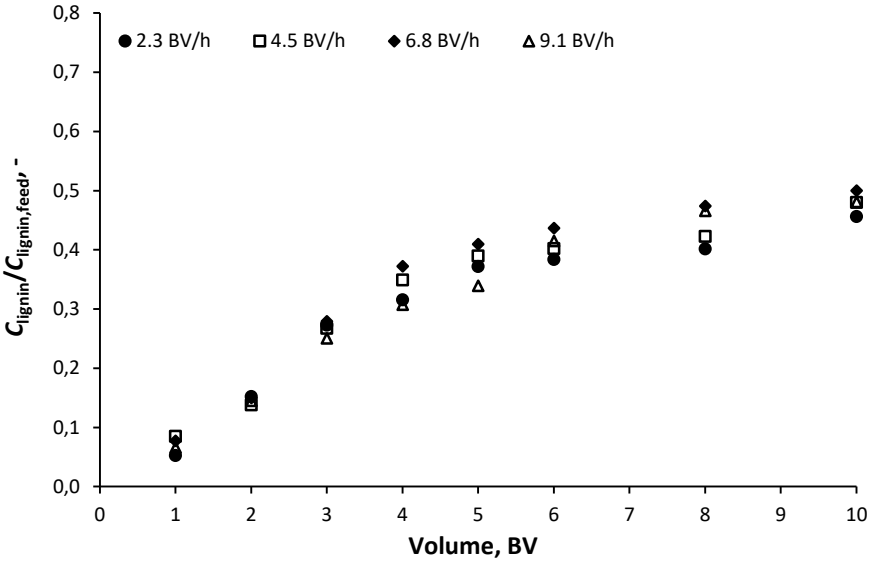

Figure 27: Effect of flow rate on the breakthrough curve of lignin with SP700 adsorbent bed

The dynamic adsorption capacity of lignin, hemicellulose, and furans (5-HMF + furfural) on SP700 in a continuous fixed-bed column at a flow rate of 4.5 BV/h is represented by its breakthrough curves in Figure 28 (a). The breakthrough curve of lignin showed a prolonged and atypical shape. Montané et al. [121] and Heinonen et al. [38] have described similar behavior during the adsorption of lignin on activated carbon and the resin Amberlite® XAD-16N, respectively. The reason might be the heterogeneous nature of the lignin, meaning it consists of a wide variety of fragments of different molecular sizes and shapes, eluting in irregular intervals. After feeding 30 BVs of BWH 3 through the SP700 column, the outlet lignin concentration did not reach the feed level. The hemicellulose concentration increased to the feed level within the first BV. Hence there is no or just minor adsorption on SP700. The course of the breakthrough curve between BV 0 and 1 could not be determined due to dead volumes in the experimental setup. For the furans, breakthrough was observed just a few BVs after the hemicellulose. The feed concentration level for the furans was reached after 3 BVs. Due to their hydrophobic nature, the adsorbent material was expected to be more selective regarding these components. Furans and lignin probably compete during the adsorption, and the higher concentration of lignin in the BWH 3 could cause that the furans are displaced from the solid phase.

Based on the experimentally obtained breakthrough curves in Figure 28 (a), the efficiency of the adsorption process was evaluated in terms of cumulative lignin removal and hemicellulose recovery yield (Figure 28 (b)). The adsorbed amount of lignin, which was used to determine the cumulative lignin removal yield values, was calculated as the area under the lignin loading curve from the first to the thirtieth BV. On the other hand, the adsorbed amount of hemicellulose used in the determination of the cumulative hemicellulose recovery values was calculated as the area above the hemicellulose loading curve from the first BV to the point at which the hemicellulose concentration reached the feed level. The loading curves were represented by four-degree polynomials fitted to the experimental determined breakthrough curves.

A lignin removal of at least 80 % was defined as a benchmark (Publication V). This was achieved after adding 6 BVs of BWH 3 and is associated with a hemicellulose recovery of 99.5 %. Due to the short column (h_{bed} = 15 cm), the results correspond to a process with a very low number of theoretical plates (NTP) and thus a low efficiency.

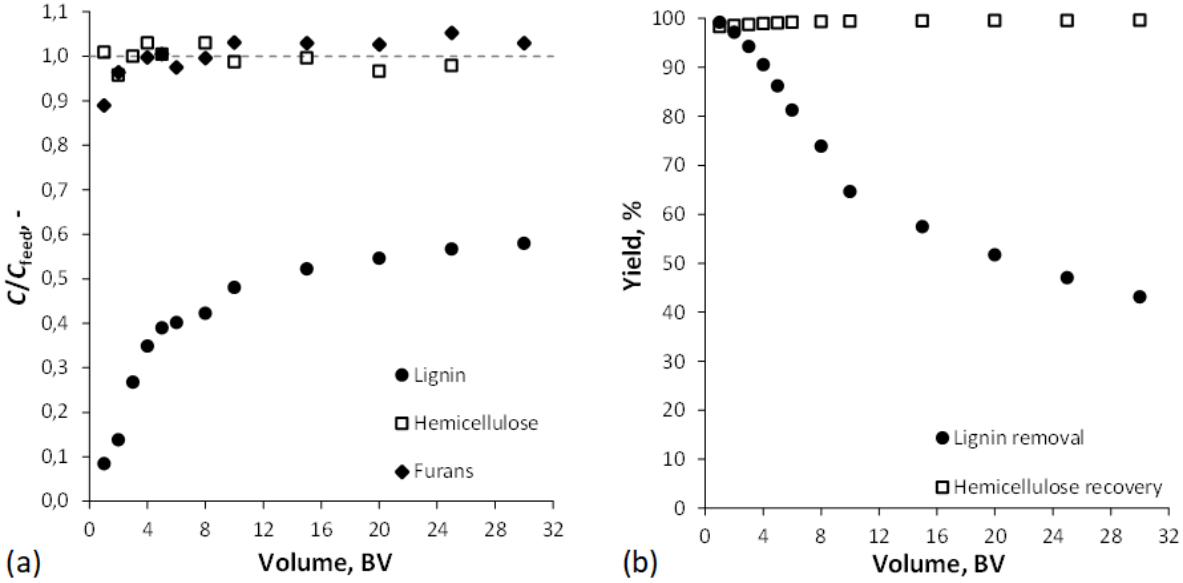

Figure 28: (a) Breakthrough curves of lignin, hemicellulose, and furans and (b) lignin removal and hemicellulose recovery as function of the bed volumes fed through the SP700 adsorbent bed with 4.5 BV/h

4.1.6 Desorption Studies

The desorption of lignin or rather regeneration of the SP700 adsorbent bed was investigated with a 20 and 50 wt.% ethanol solution, as well as with a 0.5 M NaOH solution (Figure 29). Before the solutions were fed to the column, the loaded adsorbent was rinsed with 3 BV of DIW. No significant removal was observed in the samples from this first washing step.

The most efficient of the tested desorbents was the 50 wt.% ethanol solution. Within 5 BVs 95 % and within 10 BVs practically all of the adsorbed lignin could be removed. Thereby, the lignin concentration in the desorbent solution was consistently lower than that of BWH 3. Using the 20 wt.% ethanol solution, the desorption of lignin was just 39 % after 5 BVs and 52 % after 10 BVs, and lignin was less concentrated. Hence, the desorption process could not be carried out efficiently. From alkaline pulping, it is well known that the solubility of lignin is high in an alkaline pH range [3, 34]. For this reason, the 0.5 M NaOH solution was also tested as desorbent. With NaOH 76 % of the adsorbed lignin could be removed within 5 BVs and 79 % within 10 BVs. This means the desorbent performed in between the 20 and 50 wt.% ethanol solution.

Based on the investigations, it can be summarized that the adsorbent SP700 enables both the efficient separation of lignin from hemicellulose from an authentic wood hydrolyzate and the recovery of adsorbed lignin for further use. The recovery of the desorbent (50 wt.% ethanol solution) for reuse could be done by distillation or nanofiltration and is essential for developing

an economic and ecological process. The separation of lignin from the desorbent solution was not examined.

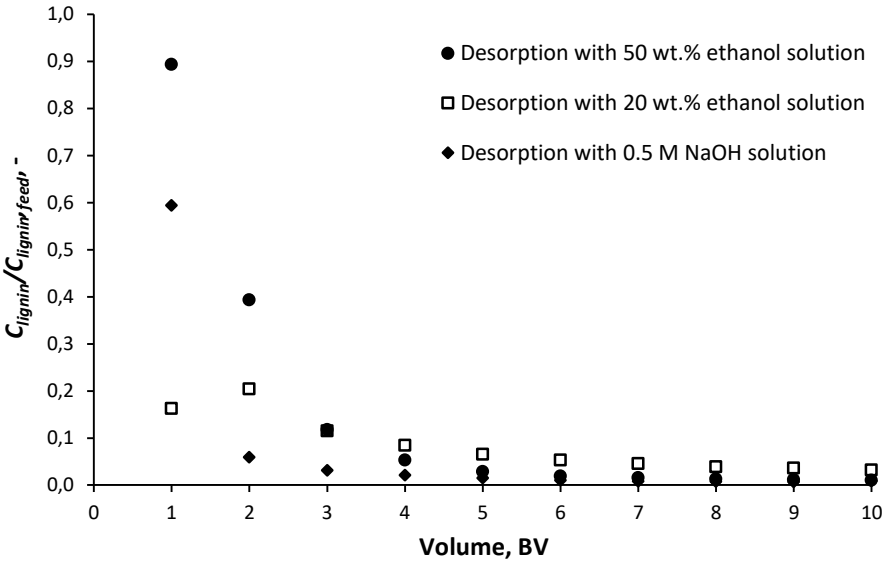

Figure 29: Desorption of lignin with a 20 wt.% ethanol solution, a 50 wt.% ethanol solution, and a 0.5 M NaOH solution from the SP700 adsorbent bent fed at a flow rate of 4.5 BV/h

4.2 Ultrafiltration for Concentrating Hemicellulose and Removal of Lignin

Results and discussion of the UF experiments are subdivided into five sections. Section 4.2.1 presents the results of membrane screening, and Section 4.2.2 describes the characterization of appropriate UF membranes. Next, Sections 4.2.3 and 4.2.4 illustrate the results of the statistical experiments by RSM and process optimization by PO using BWH 2. Finally, in Section 4.2.5, the influence of pretreatment of BWH 3 by adsorption on polymeric resins is discussed. More detailed information can be found in the corresponding Publications II and V.

4.2.1 Membrane Screening

A simple membrane screening was carried out to select from the six investigated UF membranes the two that were least susceptible to fouling during the filtration of BWH 2. The PWF reduction and permeate flux decline from the beginning of the filtration process until reaching a stationary operating point were used as measures to evaluate fouling. The preliminary tests were conducted at a TMP of 0.7 MPa, a temperature of 40 °C, and a CFV of 1.1 m/s. In most applications, it has been shown that hydrophilic membranes are less sensitive to fouling than hydrophobic membranes during the filtration of wood hydrolyzates [149,150,211]. However, the chemical and mechanical stability of the hydrophilic membranes is in general inferior to the hydrophobic ones. Hence, a compromise could be hydrophobic membranes modified to be hydrophilic. In this investigation, varying skin layer materials and thus surface properties (Table 5) consider these differences. In addition, the influence of the pore sizes was studied using membranes with MWCO from 1 to 10 kDa.

PWF_b and PWF_a for the calculation of PWF_r are average values from three measurements each. The regenerated cellulose membrane RC70PP exhibits the lowest PWF_r with 15.9 %. This is

mainly due to its strong hydrophilic characteristics and the largest MWCO. PWF_r for the other membranes increase in the following order: UA60 (38.7 %) > UH004 (46.7 %) > GR90PP (71.9 %) > ETNA01PP (76.2 %) > UFX5pHt (84.3 %). Hence, it seems that polymeric material, surface properties, and MWCO have no significant influence on PWF_r. Of these membranes with non-natural hydrophilic properties, UA60 and UH004 have the lowest values for PWF_r. Thus, they are least susceptible to fouling using BWH 2 as a feed solution.

The flux decline of the membranes is displayed in Figure 30 and presented as the ratio between the permeate flux J during the filtration of BWH 2 at time t and PWF_b. For GR90PP, ETNA01PP, and UFX5pHt, i.e., hydrophobic and modified hydrophilic membranes with MWCOs between 1 and 5 kDa, the flux was less than 15 % of PWF_b after 10 min and around 5 % after 180 min of filtration. Hence, no significant differences in dependence on the surface properties and MWCOs could be observed. All three membranes are highly prone to fouling when using BWH 2 as feed solution. This could be an indication that surface hydrophilization may be insufficient and fouling occurs in the non-hydrophilic substructure of the membranes. The regenerated cellulose membrane RC70PP exhibits low flux loss of maximum 30 % after 240 min compared to PWF_b. This is due to its strong hydrophilicity and the high MWCO. However, the same characteristics resulted in low hemicellulose retention in a range of 7 to 35 % within the RSM experimental design. Moreover, the RC70PP showed severe signs of wear due to the lower chemical and mechanical stability. UA60 and UH004 had similar flux declines. Both have flux losses of 27 to 30 % within the first 5 min and reach up to 17 to 19 % of PWF_b after 240 min of filtration. The membranes UA60 and UH004 were considered in the further examinations based on the screening results (Publication II).

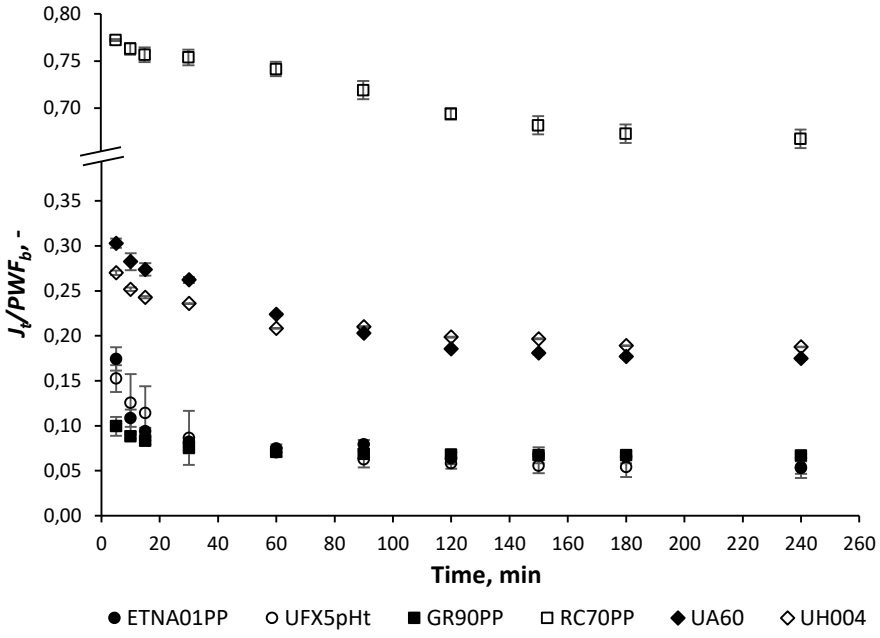

Figure 30: Flux decline during the ultrafiltration of beechwood hydrolyzate 2 using the membranes ETNA01PP, UFX5pHt, GR90PP, RC70PP, UA60, and UH004 (Error bars represent the standard deviation)

4.2.2 Membrane Characterization

4.2.2.1 Membrane Surface Roughness

The AFM images displaying the surface roughness of the UF membranes UA60 and UH004 are shown in Figure 31 (a) and (b). Both UF membranes have relatively even surface structures within the measured area. The *Rq* values for UA60 and UH004 are 11.6 and 1.7 nm, respectively, indicating smooth surfaces. In comparison with each other, the surface roughness of the membrane UA60 is, of course, much higher than that of UH004.

Membranes with rough surfaces have higher fouling potentials than membranes with smooth surface roughness [212, 213]. "Valley" regions on rough membranes are likely to be of irregular shape and may become clogged. Depending on the particle size of insoluble solids and the molecular size of the solutes in the feed solution, the "pore-like valleys" may not be completely plugged but become clogged, restricting the flow through that "valley". Furthermore, particles are preferentially transported into the "valleys", and thus a densely packed resistance layer can be formed, which reduces the flow through the membrane. On smooth membranes, such particles would probably be more evenly spaced and not be concentrated in the "pore-like valleys", resulting in a less overall flux decline. Vrijenhoek et al. [214] have shown that based on the Carman-Kozeny equation, the resistance of a single layer of 140 nm particles to pure water permeation is over 1000 times more than that of the clean membrane. This implies that a cake layer of only 1 nm thickness would create approximately a 10 % permeate flux decline [215]. Thus, membrane surface roughness is an important physical property to provide a qualitative prediction about relative fouling behavior and flux losses when using feed solutions containing small insoluble solids (as when using BWH). However, as the areas measured were small and the MWCO of the UF membranes are slightly different, the obtained roughness values can only be used as estimates, and a definite correlation between roughness and fouling or rather flux losses is associated with uncertainties.

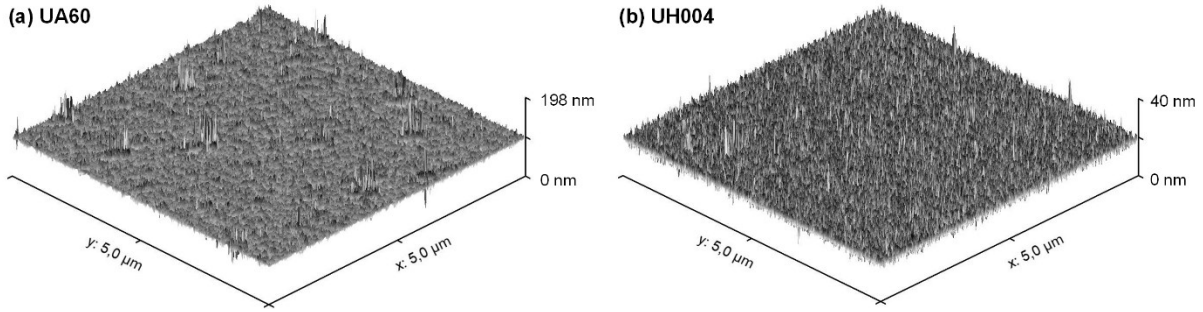

Figure 31: Atomic force microscope images showing surface roughness of the ultrafiltration membranes (a) UA60 and (b) UH004

4.2.2.2 Hydrophilicity

Hydrophilicity is one significant surface parameter affecting membrane fouling because of the hydrophobic nature of most foulants. Contact angle measurements can quantify hydrophilicity. For UA60, a contact angle between 30 to 50° is estimated by the manufacturer, and for UH004, a contact angle of 42° can be found in the literature [216]. In general, hydrophilic surfaces have

a contact angle of 0–90°, and the smaller the angle, the more hydrophilic the surface. At values above 90°, the surfaces are considered hydrophobic. Hence, both UF membranes are hydrophilic, and UA60 is probably more hydrophilic than UH004. The fouling potential of the membranes increases with decreasing hydrophilicity because of the higher binding affinities of hydrophobic components, such as lignin and its phenolic degradation products in the BWHs.

PWF_b and PWF_a for the UF of BWH 2 for UA60 and UH004 were 143.4 L/(m^{2}h) and 87.9 L/(m^{2}h), respectively, and 166.6 L/(m^{2}h) and 83.6 L/(m^{2}h), respectively. The higher PWF_b of UH004 compared to UA60 is presumably due to the higher MWCO, and differences in hydrophilicity might be less important. However, PWF_r, already presented in Section 4.2.1, indicates that the membrane UA60 is less susceptible to fouling when using BWH 2 as a feed solution because it is probably more hydrophilic compared to UH004. The fouling potential for UA60 seems to be lower despite higher surface roughness. From this, it can be concluded that the differences in surface roughness between the UF membranes have no significant influence.

4.2.3 Response Surface Methodology

4.2.3.1 Regression Model Equations and Analysis of Variance

The observed responses [(i) permeate flux, (ii) hemicellulose retention, and (iii) lignin retention] for the UF membranes UA60 and UH004 from the CCD experiments studying the influence of three independent variables [TMP (X_1), temperature (X_2), and pH (X_3)] are shown in Table 8. With these data, the coefficients of the polynomial equation, as explained in Section 3.2.2.1, were determined by fitting. The resulting coefficients and thus the obtained regression model equations in terms of coded variables are presented in Table 15. The greater the value of the respective factor in the model equations, the significantly greater the influence on the response. Moreover, the positive signs in the models indicate the synergetic effects of the factor, whereas the negative signs indicate antagonistic effects.

The statistical significance of the developed regression models was tested using ANOVA. For this, the statistical estimators *F*-value, *p*-value, R^2, adjusted R^2, and predicted R^2 were computed [217]. The results are presented in Table 15. The corresponding model or variable is significant if the *F*-value is larger and the *p*-value is smaller than 0.05. The ANOVA results for the three observed responses showed high *F*-values between 12.0 and 32.8 and low *p*-values of maximum 0.0058 for UA60 and high *F*-values between 13.5 and 58.6 and low *p*-values of maximum 0.0012 for UH004. Hence, the obtained regression models are highly significant and give a good prediction of the experimental data. Beneath these two estimators, the coefficient of determination R^2, which is the proportion of variation in the response attributed to the regression model and should be close to 1, was considered. The R^2 values of the developed regression models for UA60 and UH004 are between 0.92 and 0.99, indicating that they can explain 92-99 % of the data variation. However, Koocheki et al. [218] postulated that a large value of R^2 does not always imply that a regression model is suitable, and such inference can only be made based on a similarly high value of adjusted R^2. The values of adjusted R^2 are between 0.86 and 0.97, thus approving a high significance of the models and indicating a good agreement between the experimental and predicted values for the observed responses. For good fitting, the differences between adjusted R^2 and predicted R^2 should be less than 20 % [219].

The developed regression models meet this requirement, with the values of predicted R^2 between 0.75 and 0.88. The models offer variability in the prediction of responses of 75–88 % beyond the experimental range of process conditions. Concluding, the models are adequate for predicting the observed responses for both UF membranes in the range of the experimental variables.

Table 15: Empirical models in terms of coded variables for the responses permeate flux (J), hemicellulose retention ($R_{hemicellulose}$), and lignin retention (R_{lignin}) and analysis of variance (ANOVA) for the ultrafiltration membranes UA60 and UH004

Regression equation	UA60			UH004		
	J (L/(m²h))	$R_{hemicellulose}$ (%)	R_{lignin} (%)	J (L/(m²h))	$R_{hemicellulose}$ (%)	R_{lignin} (%)
Factors						
b_0	+34.1	+84.1	+41.9	+35.5	+52.8	+28.0
b_1	+6.57	+9.31	+2.71	+8.43	+9.56	+1.35
b_2	+6.74	-8.02	-2.20	+3.12	-1.43	-3.59
b_3	+0.14	-5.88	+1.64	+5.73	-7.49	+5.16
b_{11}	–	-4.51	–	+0.31	+0.25	-1.31
b_{22}	–	+3.77	–	-1.69	+7.87	-0.08
b_{33}	–	-8.49	–	-2.67	+1.70	+3.05
b_{12}	+2.65	-1.75	–	+3.30	-1.56	+2.85
b_{13}	+0.10	-0.68	–	+0.73	-0.15	-4.13
b_{23}	+0.05	-3.66	–	+3.09	-1.23	+2.60
ANOVA						
F-value	27.1	32.8	12.0	25.7	13.5	58.6
p-value	< 0.0001	< 0.0001	0.0058	0.0001	0.0012	< 0.0001
R^2	0.94	0.97	0.92	0.97	0.95	0.99
adj. R^2	0.90	0.94	0.86	0.93	0.87	0.97
pred. R^2	0.80	0.84	0.76	0.81	0.75	0.88

4.2.3.2 Interaction of Factors

Contour plots are presented to examine the interaction of the variables on the responses permeate flux, hemicellulose retention, and lignin retention for the two UF membranes UA60 and UH004. They are displayed in Figure 32, Figure 33, and Figure 34 (a)–(f) as a function of the operating variables TMP and temperature at pH 2.5, 5, and 7.5.

Permeate Flux

Permeate flux is one of the most important parameters to evaluate the performance of a UF process. Moreover, the capital and operating costs are inversely proportional to the permeate flux [57]. The results for the UF membranes UA60 and UH004 are displayed in Figure 32 (a)-(c) and (d)-(f), respectively.

The permeate fluxes of the UF membranes were generally relatively low with values between 23.4 and 50.3 L/(m^{2}h) using UA60 and 14.8 and 55.8 L/(m^{2}h) using UH004. Krawczyk et al. [155] and Puro et al. [220] obtained comparable values. With regard to the membrane UA60, the influences of both TMP (b_1 = 6.57) and temperature (b_2 = 6.74) on the permeate flux are of similar significance, whereas for UH004, the influence of TMP (b_1 = 8.43) is about 2.7-fold

that of temperature (b_2 = 3.12). Hence, a high value of TMP and temperature is preferred for achieving a high permeate flux, whereas the influence of temperature is less important for UH004. As UF is a pressure-driven process, an increasing TMP leads to an increase in the permeate flux. As can be seen from Table 15, this increase is linear for UA60 and nearly linear for UH004. Likewise, an increase in temperature leads to an increase in the permeate flux, too; this trend can be explained by the declining viscosity (η) of BWH 2, which enhances the liquid flow through the membranes and thus the permeate flux according to the proportionality $J \sim 1/\eta \sim 1/e^{1/T}$. Moreover, in the case of the polypiperazine amide membrane UA60, increased temperature can cause changes in the surface structure, leading to an increment of the membrane pore size and thus to a higher permeate flux [221]. There is a relevant interaction between TMP and temperature for both UF membranes.

It is observed that the effect of pH on the permeate flux is not significant for UA60 (b_3 = 0.14) and significant for UH004 (b_3 = 5.73) with a quadratic variable (b_{33} = -2.67) in the regression model. Hence, for UH004, the permeate flux increases with an increasing pH of about 6 and then flattens off. This might be explained by an increase in the negative surface charge of the hydrophilized polyethersulfone membrane because of the ionization of functional groups as well as adsorbed ions or other charged molecules, which in turn can lead to elevated electrostatic repulsion and thus reduced fouling tendencies. The increase in the surface charge finds a maximum plateau in the neutral range [41]. For UH004, there is a recognizable interaction between temperature and pH.

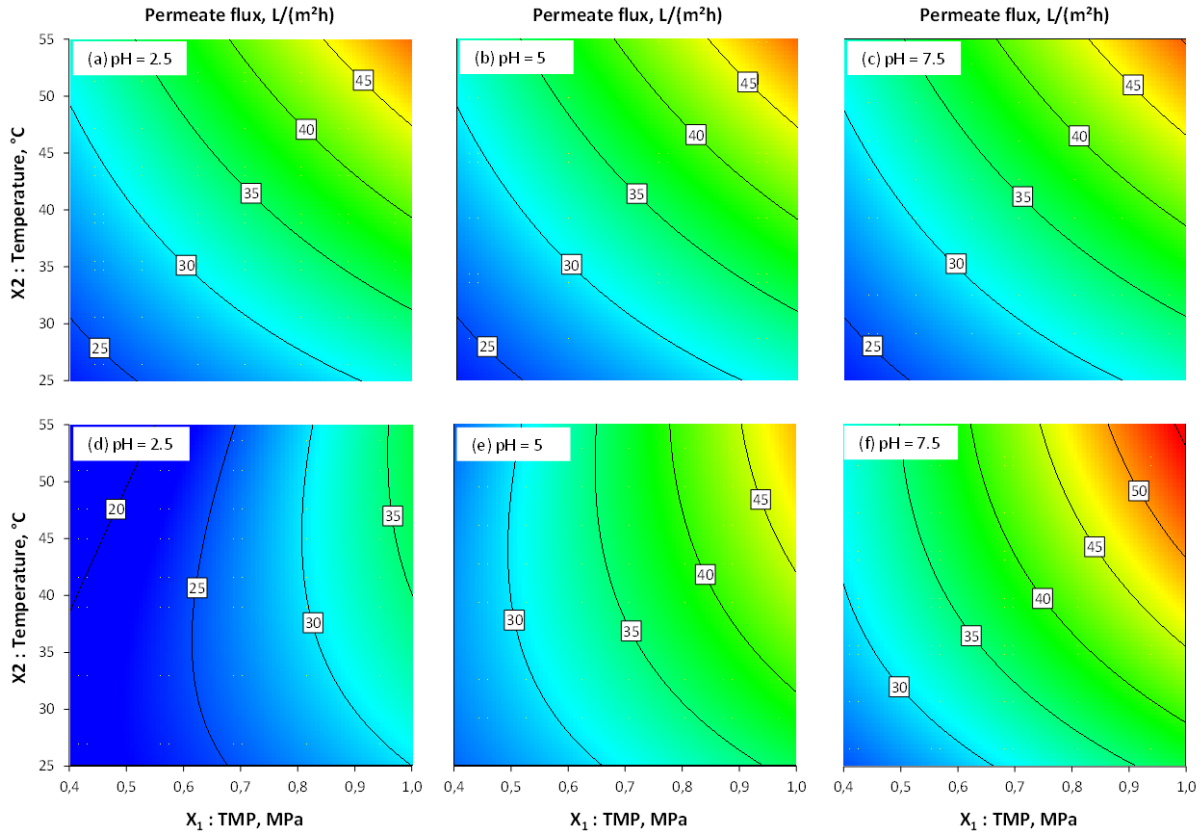

Figure 32: Contour plots of the permeate flux as a function of the influence factors transmembrane pressure (TMP) and temperature at pH values of 2.5, 5, and 7.5 for the ultrafiltration membranes (a)–(c) UA60 and (d)–(f) UH004

Hemicellulose Retention

The influence of TMP, temperature, and pH on the hemicellulose retention for the UF membranes UA60 and UH004 is illustrated in Figure 33 (a)–(c) and (d)–(f), respectively.

High hemicellulose retention of up to 100 % for UA60 and up to 81.4 % for UH004 was determined. Similar results were discovered by Persson and Jönsson [70] and Al Manasrah et al. [119]. For UA60, the calculated rejection values above 100 % can be observed in Figure 33 (b). This is a consequence of the developed regression models and has no physical meaning. For UA60, the influences of TMP (b_1 = 9.31) and temperature (b_2 = -8.02) are of similar significance but with opposite effects. In the case of UH004, TMP is also highly significant (b_1 = 9.56) and temperature has no or just a minor influence (b_2 = -1.43). Hence, the hemicellulose retention increases with increasing TMP and decreasing temperature. The concentration of suspended solids, possible extractives, and macromolecules in the immediate vicinity of the membrane surface increases with increasing TMP as a consequence of the rising permeate flux and thus can lead to the formation of a cake- and/or gel-like layer that acts as an additional permeation barrier and thus increases hemicellulose retention [70]. The rise in hemicellulose retention with decreasing temperature can have different reasons: one could be that lower temperature results in lower diffusion coefficients, which hinder the diffusive return of deposited material from the membrane surface to the bulk solution. In addition, at a constant permeate flux, lower temperature results in higher solute concentrations at the membrane surface, which may cause more fouling. Both factors would lead to an increased permeation barrier against the hemicellulose and thus a higher rejection. The proportionality $D_i \sim T$ supports these explanations. As discussed before, the structural changes of the membrane surface could also be a reason for higher hemicellulose retention. A slight interaction between TMP and temperature can be observed for both UF membranes.

The influence of pH on UA60 (b_3 = -5.88) as well as on UH004 (b_3 = -7.49) is significant. As mentioned above, a pH change of the BWH 2 might also change the membrane surface charge. The decrease in retention for the uncharged hemicellulose could be because of the increased MWCO of the membranes, resulting from the greater intramembrane electrostatic repulsion at the negatively charged state at a higher pH [222]. The quadratic variable for the effect of pH on the regression model for UA60 has a great impact (b_{33} = -8.49). The hemicellulose retention is a little influenced up to a pH of about 4, as most components are still in their uncharged molecular form. With the increasing dissociation of various components in the BWH 2, the charge differences increase and result in a distinct decrease in hemicellulose retention. For UH004, the quadratic variable has just a little impact (b_{33} = 1.70). For UA60, there is a recognizable interaction between temperature and pH.

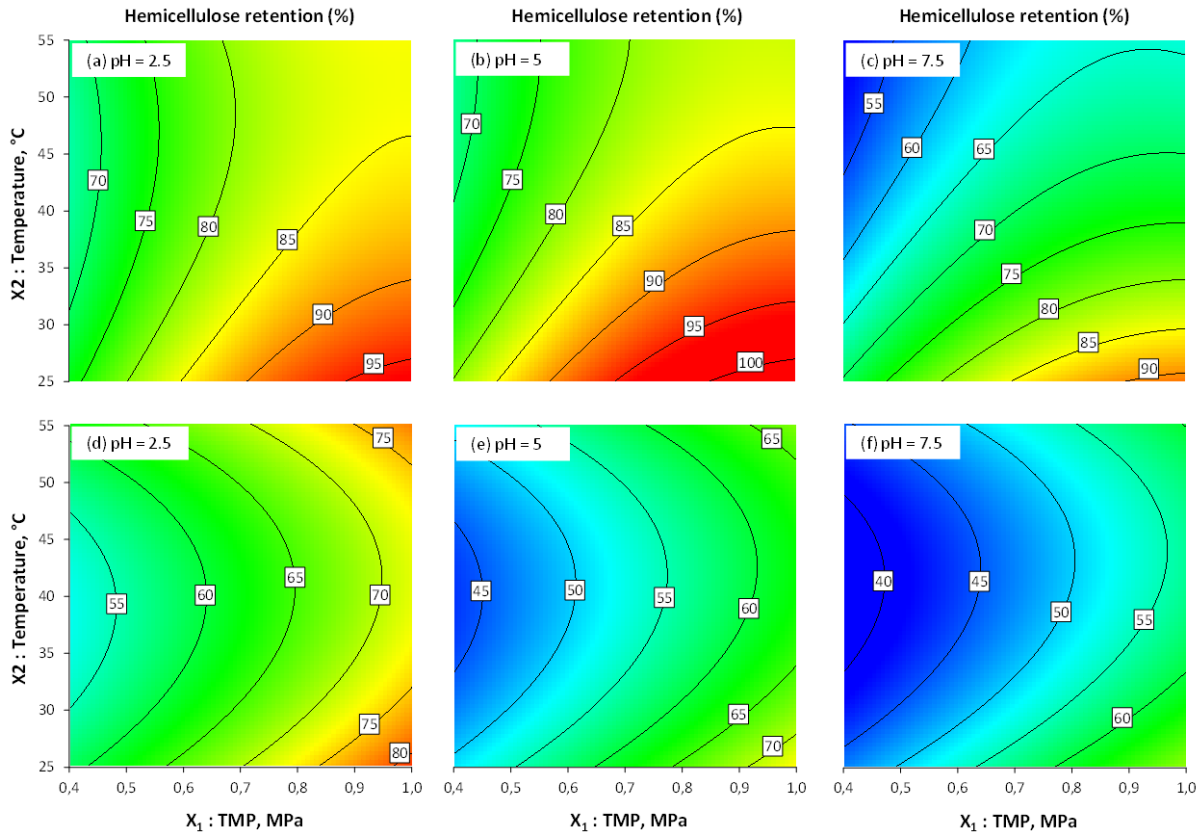

Figure 33: Contour plots of the hemicellulose retention as a function of the influence factors transmembrane pressure (TMP) and temperature at pH values of 2.5, 5, and 7.5 for the ultrafiltration membranes (a)–(c) UA60 and (d)–(f) UH004

Lignin Retention

The contour plots for lignin retention for the UF membranes UA60 and UH004 are displayed in Figure 34 (a)–(c) and (d)–(f), respectively.

Lignin retention is between 35.3 and 48.4 % when using UA60 and 10.1 and 41.3 % when using UH004. Jönsson et al. [57] and Al Manasrah [119] observed higher lignin retention. Thus, it can be assumed that lignin in their investigations had a higher molecular weight and is therefore retained more. Persson and Jönsson [70] depicted results in a similar range. Because of the overlap of the hemicellulose and lignin molar masses (Section 2.1.3) as well as the presence of lignin-hemicellulose complexes [119], a complete separation of hemicellulose from lignin via UF seems impossible. Concerning UA60, the influence of TMP (b_1 = 2.71) and temperature (b_2 = -2.20) is of similar significance but with opposite effects. Using UH004, the influence of TMP (b_1 = 1.35) is 2.7 times smaller than the influence of temperature (b_2 = -3.59). Hence, increasing TMP and decreasing temperature result in an increase in lignin retention, whereas the influence of TMP is less important for UH004. The explanations for these phenomena are the same as for hemicellulose retention and already discussed above. From Table 15, it can be seen that there is no interaction between TMP and temperature for UA60 and a relevant term for UH004.

In case of UA60, the effect of pH is less significant (b_3 = 1.64), whereas for UH004, the influence of pH (b_3 = 5.16) is highly significant. Hence, the lignin retention tends to increase

with increasing pH. This might be because most of the organic acids (pK_a = 3–4) dissociate into negatively charged molecules, which minimizes their ability to form hydrogen bonds with lignin, stabilizing their network [128]. Hence, the lignin macromolecules decompose into smaller units with a high negative charge. The negative charge of the membrane surface increases with increasing pH. This results in strong repulsive forces and thus higher lignin retention. The quadratic variable (b_{33} = 3.05) in the regression equation because of the influence of pH is not relevant for a value of approx. less than 4.0. For UH004, there are recognizable interactions between TMP and pH as well as between temperature and pH.

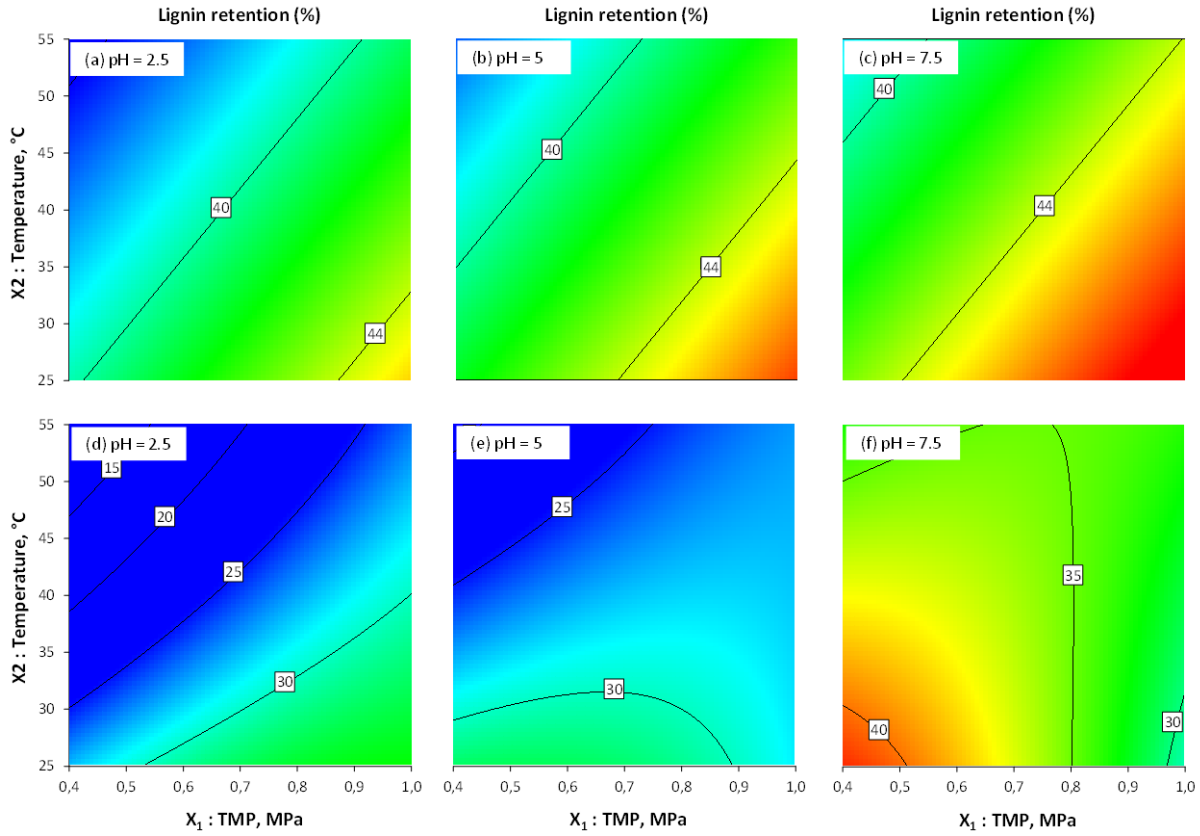

Figure 34: Contour plots of lignin retention as a function of the influence factors transmembrane pressure (TMP) and temperature at pH values of 2.5, 5, and 7.5 for the ultrafiltration membranes (a)–(c) UA60 and (d)–(f) UH004

4.2.4 Pareto Optimization

The Pareto solution set, with a population size of 200, and the three-dimensional Pareto front determined by the interpolation of the Pareto points for the membranes UA60 and UH004 are displayed in Figure 35 (a) and (b). In addition, within the figures, the Pareto points for the maximum permeate flux, maximum hemicellulose retention, and minimal lignin retention as well as UP and CP are marked. Each Pareto front contains the Pareto optimal solutions indicating a trade-off between the maximum permeate flux, as well as hemicellulose retention, and minimal lignin retention. From Section 4.2.3.2, it is evident that these objectives strongly compete with each other. If the decision-maker wishes to emphasize the highest possible permeate flux and hemicellulose retention, the lignin retention rises, too, and vice versa.

The Pareto front for UA60 shows a convex region between two concave regions. The convex region has a visible bulge, which is called knee. This region is most likely interesting for the decision-maker [223]. The knee points are most preferred or rather applied for the decision-maker as an "optimal compromise" as a small improvement in one of the objectives requires an unfavorably large sacrifice for the other objectives. Hence, moving away in any direction of the knee points may not be very attractive. A different interpretation of knee points can also be found in refs [224] and [225]. The Pareto front for UH004 shows no concave and/or convex behavior within the three-dimensional space. Hence, the Pareto front is more or less a flat surface. Half of the calculated Pareto points are located on the left edge. Another set of points, which spans the Pareto front, is located at the upper-right edge.

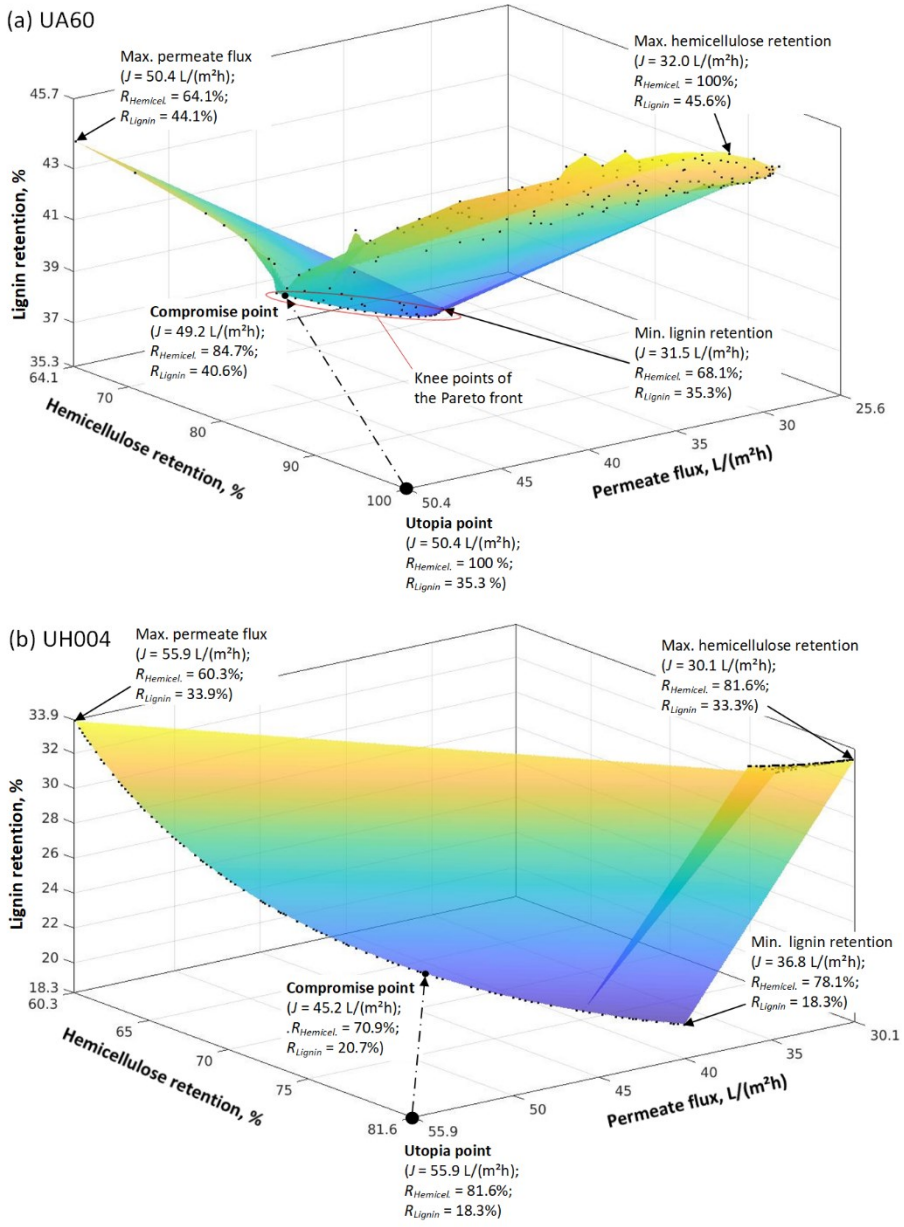

Figure 35: Pareto solution sets (n_{PP} = 200) and interpolated Pareto front for the maximization of the regression equations of permeate flux and hemicellulose retention and for the minimization of lignin retention for the ultrafiltration membranes (a) UA60 and (b) UH004

Optimal operating points within the Pareto solution sets were identified for both membranes by the UP method. The UP is located at the maximum permeate flux, maximum hemicellulose retention, and minimum lignin retention in the range of values studied (Figure 35 (a) and (b)). The CP or the optimal value within this study corresponds to the Pareto solution, which has the least Euclidean distance to the UP. For UA60, the optimal operation conditions are thus a TMP of 0.98 MPa, temperature of 55 °C, and pH of 2.5, which would lead to a permeate flux of 49.2 L/(m^2h), hemicellulose retention of 84.7 %, and lignin retention of 40.6 %. The optimal process parameters for UH004 are a TMP of 1.0 MPa, a temperature of 55 °C, and a pH of 4.1, from which a permeate flux of 45.2 L/(m^2h), hemicellulose retention of 70.9 %, and lignin retention of 20.7 % are expected.

Hence, for UA60, it is possible to obtain a retentate with a high hemicellulose content and little losses but still a relevant amount of lignin. For optimal operation conditions with UH004, the pH has to be adjusted, meaning an addition of chemicals (e.g., NaOH). Although less lignin is held back, the lower hemicellulose retention and permeate flux lead to the conclusion that the use of UA60 is recommended for the process investigated, as described in more detail in Publication II.

4.2.5 Influence of Pretreatment with Adsorption

Adsorption previous to the UF process was employed to remove hydrophobic components, mainly lignin, and thus reduce fouling of the UA60 membrane. Figure 36 (a) presents the permeate flux for the filtration of untreated and by adsorption pretreated BWH 3. Pretreatment by adsorption significantly increased the permeate flux from an average value of 22.2 to 60.8 L/(m²h). This is partly due to the removal of lignin and its degradation products, which have been shown to foul the membrane [226]. Another explanation for the increased flux values is provided by Puro et al. [150]: Wood extractives, which might be preferentially attached to the membrane surface in the absence of lignin, have both hydrophobic and hydrophilic moieties and, when the hydrophobic part is attached on the membrane, the hydrophilic part faces the aqueous phase making the membrane surface more hydrophilic and thus improving the permeate flux. However, fouling caused by the filtration of BWH 3 was quantified by calculating the PWF_r. Without adsorption prior to the UF the PWF_r was 27 %, and with adsorption prior to the UF 8 %. Hence, adsorption as a pretreatment for the UF of BWH minimizes membrane fouling. Similar findings were made by Koivula et al. [128] and Persson et al. [149].

The influence of the pretreatment by adsorption on the retention of hemicellulose and lignin is shown in Figure 36 (b). Adsorption reduced the average retention from 90 to 79 % for hemicellulose and 41 to 19 % for lignin (Publication V). This means higher losses of hemicellulose but simultaneously a purer retentate stream. Reasons might be reduced interactions between hydrophobic lignin and other unidentified components with the UF membrane and thus less formation of a deposited layer and less pore plugging or narrowing. The final retentate concentration (VR = 0.8) using the pretreated feed solution was 96.4 g/L for hemicellulose and 1.1 g/L for lignin.

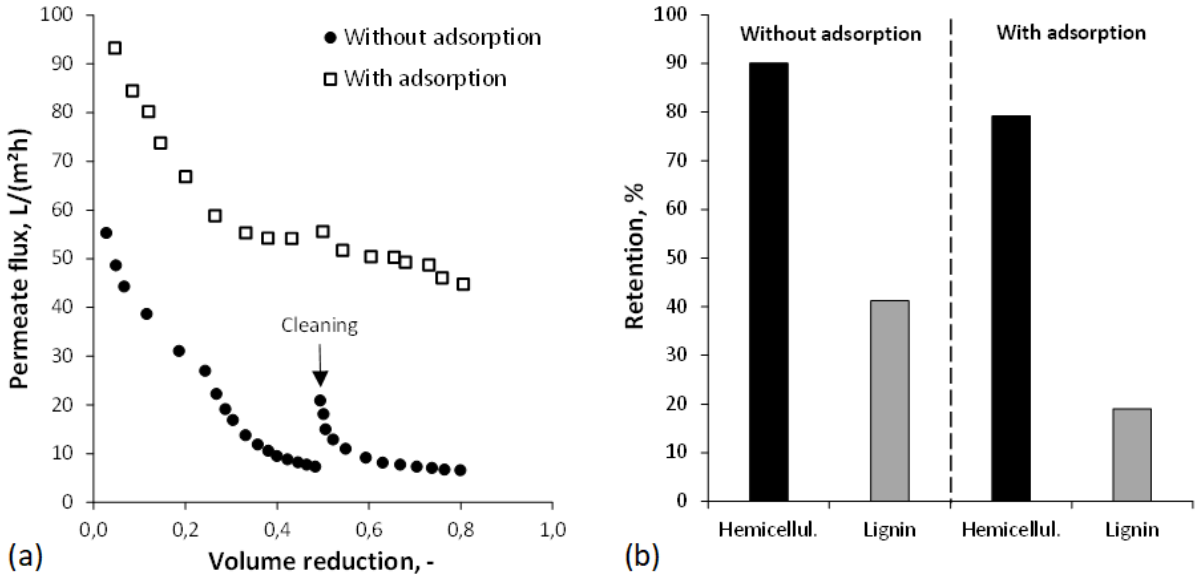

Figure 36: (a) Permeate flux and (b) retention for hemicellulose and lignin during the ultrafiltration of beechwood hydrolyzate 2 with and without pretreatment by adsorption

4.3 Hydrothermal Pretreatment of Beechwood Hydrolyzate

The empirical correlations between the concentrations of oligomeric hemicellulose, xylose, furfural, and cellulose with reaction temperature and residence time are presented in Figure 37 (a)–(d). For each component, a modified model was chosen, whereby only significant coefficients ($p < 0.05$) were taken into account as described in Publication III. ANOVA for every model demonstrated high significance, as was evident from the *F*-test with a very low probability.

As shown in Figure 37 (a), hydrothermal pretreatment of BWH 4 with process parameters in the blue area resulted in the hydrolytic splitting of the oligomeric hemicellulose. To reduce the amount of oligomeric hemicellulose within the investigated parameter range, the process temperature or residence time must be increased. This context is not new and was already described in the literature [84, 87]. However, as indicated in Figure 37 (b) and (c), the interaction between reaction temperature and residence time showed a significant influence on the conversion products of oligomeric hemicellulose. While short residence times at elevated temperatures led to high yields of xylose, at long reaction times and moderate temperatures, furfural was formed. The same accounts for the remaining cellulose in the BWH 4 (Figure 37 (d)), which was hydrolyzed to glucose under more severe process conditions. However, cellulose is a crystalline polymer and much more stable than hemicellulose [227]. Therefore, a complete conversion of cellulose would be associated with increased xylose degradation to furfural.

Appropriate process conditions for maximizing the xylose concentration were determined by the desirability function [228] based on the model equations. The BWH 4 was treated at the determined favorable reaction temperature of 180 °C and a residence time of 3.1 min (Publication III) to obtain the HPBWH 4 for the subsequent NF tests. The composition of HPBWH 4 consists of 0.0 g/L oligomeric hemicellulose, 6.1 g/L glucose, 45.0 g/L xylose,

1.5 g/L 5-HMF, 0.7 g/L furfural, and 8.0 g/L acetic acid. Hence, the oligomeric hemicellulose is completely broken down at low furfural concentrations. The deviations between the model predicted and experimental concentration values were 0.0 % for oligomeric hemicellulose, 13.1 % for glucose, 7.1 % for xylose, 0.7 % for 5-HMF, and 0.3 % for furfural.

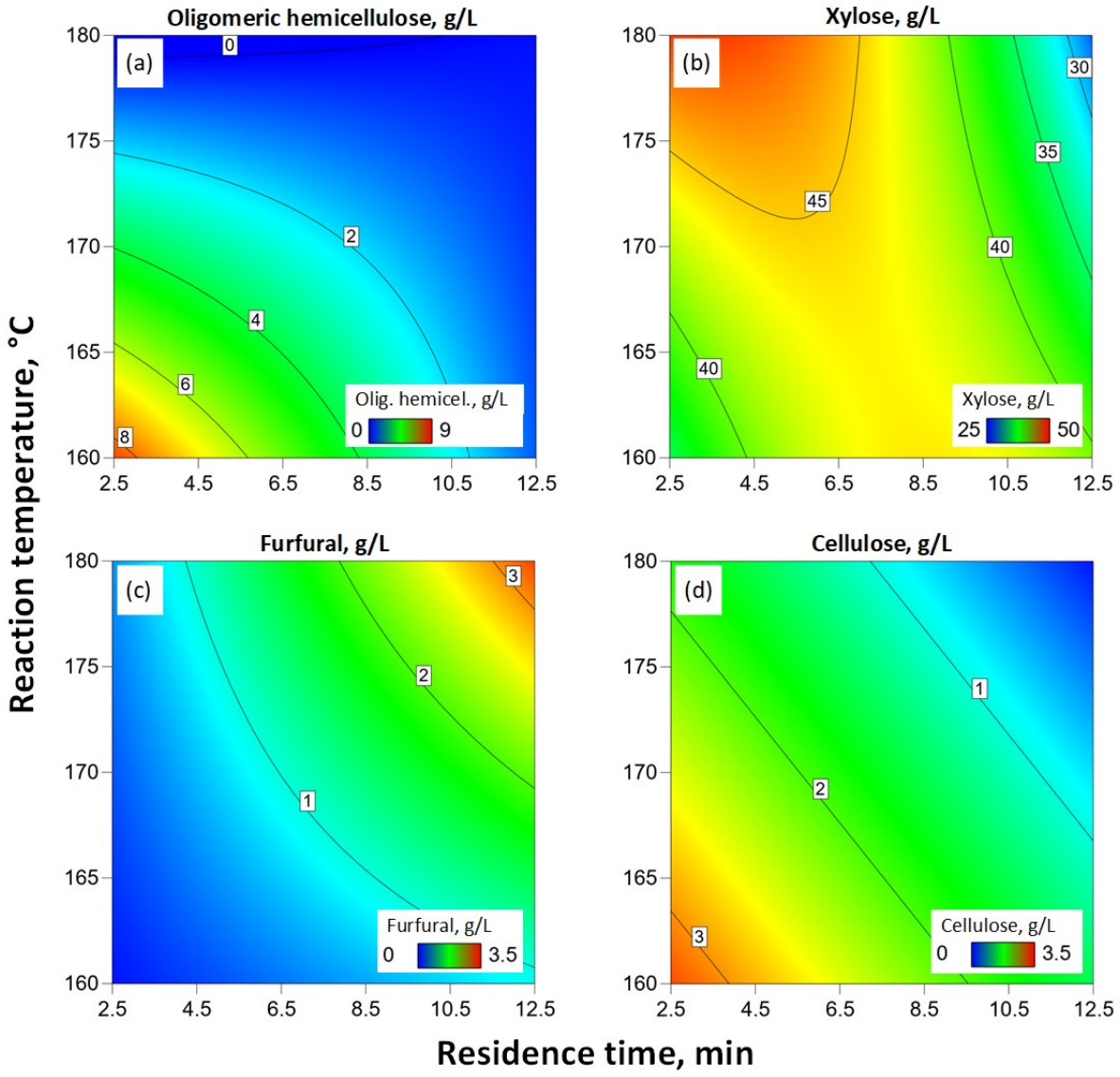

Figure 37: Contour plots of a) oligomeric hemicellulose, b) xylose, c) furfural, and d) cellulose concentration as a function of reaction temperature and residence time

4.4 Nanofiltration for the Purification and Concentration of Xylose

In Section 4.4.1, characteristics of the four tested NF membranes are presented. Next, Sections 4.4.2 and 4.4.3 illustrate the performance and fouling analysis results, respectively, using MS, BWH 4, and HPBWH 4 as feed solutions. Finally, Section 4.4.4 gives a brief excursus regarding the influence of TMP and temperature on permeate flux and solute retentions using HPBWH 2. More detailed information can be found in the corresponding Publications III and V.

4.4.1 Membrane Characterization

4.4.1.1 Pure Water Flux and Salt Retention

PWF_b amounts for the NF membranes NF, DK, TS40, and NF90 95.3 L/(m²h), 96.9 L/(m²h), 104.9 L/(m²h), and 90.2 L/(m²h), respectively, and followed the order TS40 > DK > NF > NF90. The PWF_b can be correlated to the hydrophilic properties of the membranes, which contact angle measurements can quantify. For this research part, the results of those measurements for the four NF membranes are also taken from the literature [42, 229] and displayed in Table 16. The correlation between contact angle and hydrophilicity of the membrane surface as well as the susceptibility to fouling by hydrophobic components is already described in Section 4.2.2.2. The contact angles of the NF membranes increase contrariwise to the PWF_b. Thus, the tendency can be seen that the lower the hydrophilicity of the membrane surface, the smaller the PWF_b. However, it must be noted that a direct correlation between different contact angles and PWF is only valid for membranes of the same thickness and porosity.

Salt retention of the NF membranes is expressed as the retention of $MgSO_4$. For NF, DK, TS40, and NF90, the $MgSO_4$ retention amounts 98.4, 98.3, 98.6, and 99.2 %, respectively, and followed the order NF90 > TS40 > NF > DK. Hence, despite the highest MWCO of 200-400 Da, NF90 appears to be the densest of the four NF membranes. The differences between the other NF membranes are slightly lower. Another explanation might be the differences in surface charge. From the results, it would be expected that NF90 has the lowest isoelectric point and, therefore, probably the strongest electrostatic repulsion against the dissociated $MgSO_4$. However, since the surface charge of the NF membranes could not be quantified, it is not considered within this study.

4.4.1.2 Pore and Surface Characteristics

Pore characteristics and surface roughness also influence the flow properties and selectivity of a membrane. Usually, larger pore sizes lead to higher permeate fluxes and less fouling. The pore characteristics of the four NF membranes, implying average pore width, total pore volume, and BET surface area, are given in Table 16. The determined average pore widths are in the range of 6.6–10.4 nm. They are not in good agreement with the MWCO values of the NF membranes summarized in Table 5 but are in reasonable compliance with the measured salt retentions. Hence, DK has the largest pores, and NF90 has the smallest pores. The total pore volumes of the NF membranes are in the range of 0.022–0.044 cm³/g, indicating a dense bulk architecture without many pores [230]. In addition, the BET surface areas of all NF membranes are small, as can be seen in Table 16, which closely relates to the pore volume. Depending on the proportion between the pore characteristics and the molecular weight of potential foulants, the pores can become completely blocked or narrowed. Moreover, physical and chemical interactions between insoluble solids and the membrane, as well as bridging effects between a small molecule on the membrane surface and a larger insoluble molecule are problematic, too [42].

Table 16: Root-mean-square roughness calculated from atomic force microscopy, average pore width, total pore volume, and BET surface area calculated from N_2 physisorption (77 K), and contact angle for the nanofiltration membranes taken from literature

Membrane	Root-mean-square roughness (nm)	Average pore width (nm)	Pore volume (cm^3/g)	BET surface area (m^2/g)	Contact angle (°)
NF	5.8	8.7	0.041	18.9	49[a]
DK	15.5	10.4	0.044	16.7	45[a]
TS40	44.2	7.4	0.034	18.4	22[b]
NF90	38.8	6.6	0.029	17.6	52[b]

[a][229], [b][42]

AFM images displaying the surface roughness of the four NF membranes are shown in Figure 38 a)–d), and *Rq* roughness values are listed in Table 16. The *Rq* value for the membrane NF is 5.8 nm, indicating the lowest surface roughness compared to the others. On the other hand, TS40 shows the highest surface roughness with 44.2 nm and just behind NF90 with 38.8 nm. DK has an average value of 15.5 nm. The correlation between surface roughness and the performance as well as the susceptibility of a membrane to fouling is already described in Section 4.2.2.1.

Since the sample quantities and the membrane areas measured were small, the obtained average pore width, pore volume, specific surface area, and roughness values can only be used as estimates, and a definite correlation between the membrane characteristics and fouling or permeate flux decline is associated with uncertainties.

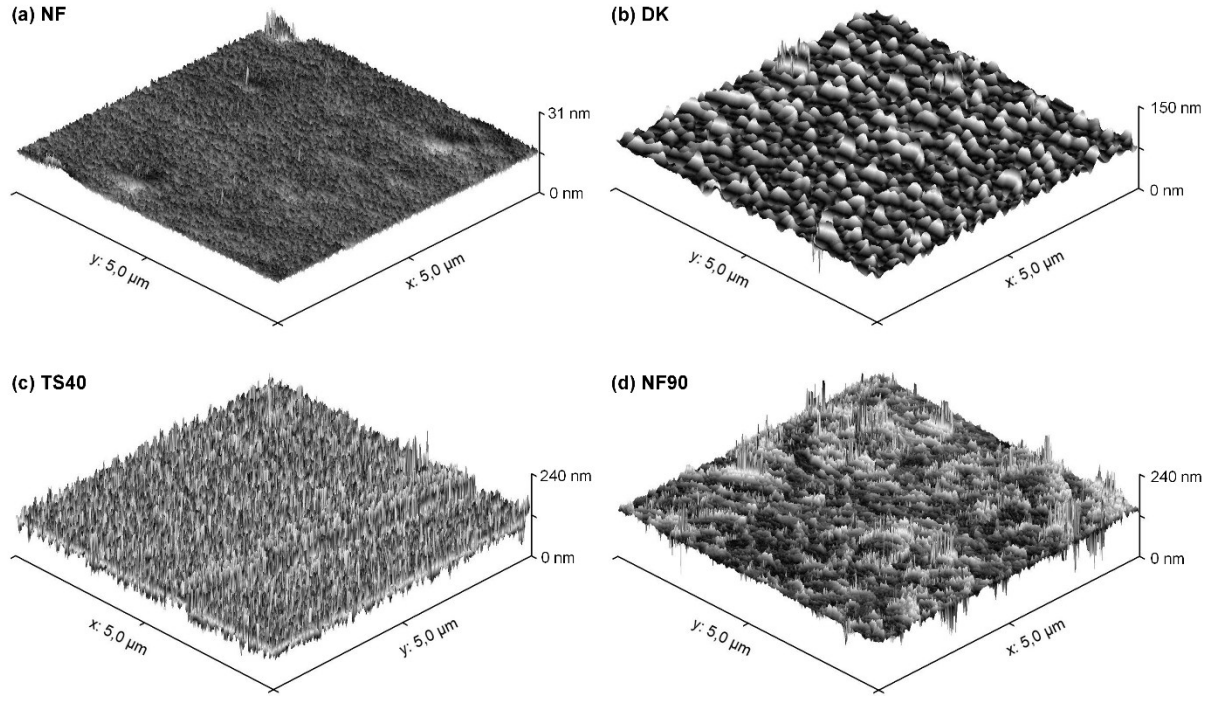

Figure 38: Atomic force microscopy images showing surface roughness of the nanofiltration membranes a) NF, b) DK, c) TS40, and d) NF90

4.4.2 Performance Analysis

For the performance evaluation, the permeate flux profiles up to a *VR* of 0.4–0.5, the retention of oligomeric hemicellulose, glucose, xylose, 5-HMF, furfural, and acetic acid in the concentrated solutions, and the separation factors in terms of xylose are considered.

4.4.2.1 Permeate Flux Performance

The permeate flux profiles of the four NF membranes when concentrating MS, BWH 4, or HPBWH 4 are presented in Figure 39 a)–c), respectively. It can be seen that the flux performances of the membranes are always in the same order, regardless of the feed stream used. The membrane NF showed the highest and most sustained flux values in all applications, and NF90 showed the lowest permeate fluxes. When using NF90 in combination with BWH 4 or HPBWH 4, the experiments even had to be stopped at a *VR* of approx. 0.2 due to insufficient flux values. The best flux performance by NF may be attributed to the largest specific surface area and the relatively high pore width. NF90 has only a slightly lower specific surface but the smallest pore width. For DK and TS40, similar flux results can be observed. Hence, differing pore widths and specific surface areas appear to compensate each other for their effect on the permeate flux. The contact angle does not appear to influence the permeate flux profiles to a large extent.

All four NF membranes showed lower flux values when processing BWH 4 or HPBWH 4 instead of MS. This is mainly due to the much more complex composition of the feedstocks and the presence of hydrophobic phenolic compounds derived from lignin [73, 231]. Moreover, for the real biomass feed streams, it can be observed that the permeate flux first asymptotically approaches a limiting value and then drops again. This could be caused by changes in the solubility of certain components or a significant increase in osmotic pressure due to the volume reduction. From Figure 39 c), it can be seen that the hydrothermal pretreatment of BWH 4 has a clear positive influence on the flux performance of the NF membranes. Average flux increases of 27, 14, 15, and 33 % can be achieved for the membranes NF, DK, TS40, and NF90, respectively. Higher flux values may be due to the partial or complete breakdown of cellulose and oligomeric hemicellulose to monomeric sugars during the hydrothermal pretreatment of BWH 4. This reduces the potential for forming a deposited layer on the membrane surface and thus the possibility of pore plugging and/or narrowing. A more detailed description of the fouling mechanism is presented below. Nevertheless, the formation of polymeric structures such as humins by furfural resinification (furfural reacts with itself, self-polymerization) and/or condensation (furfural reacts with xylose, cross-polymerization) during the hydrothermal pretreatment [84–86] can negatively affect the permeate flux. Since furfural is present in relatively low concentrations in BWH 4 and due to the hydrothermal conditions, as described above, there is no significant new formation of furfural, polymerization reaction probably only occurs to a small extent. Hence, the positive effects of the depolymerization of the oligomeric sugars appear to superimpose the negative effects of the polymerization reactions as well as the formation of other impurities.

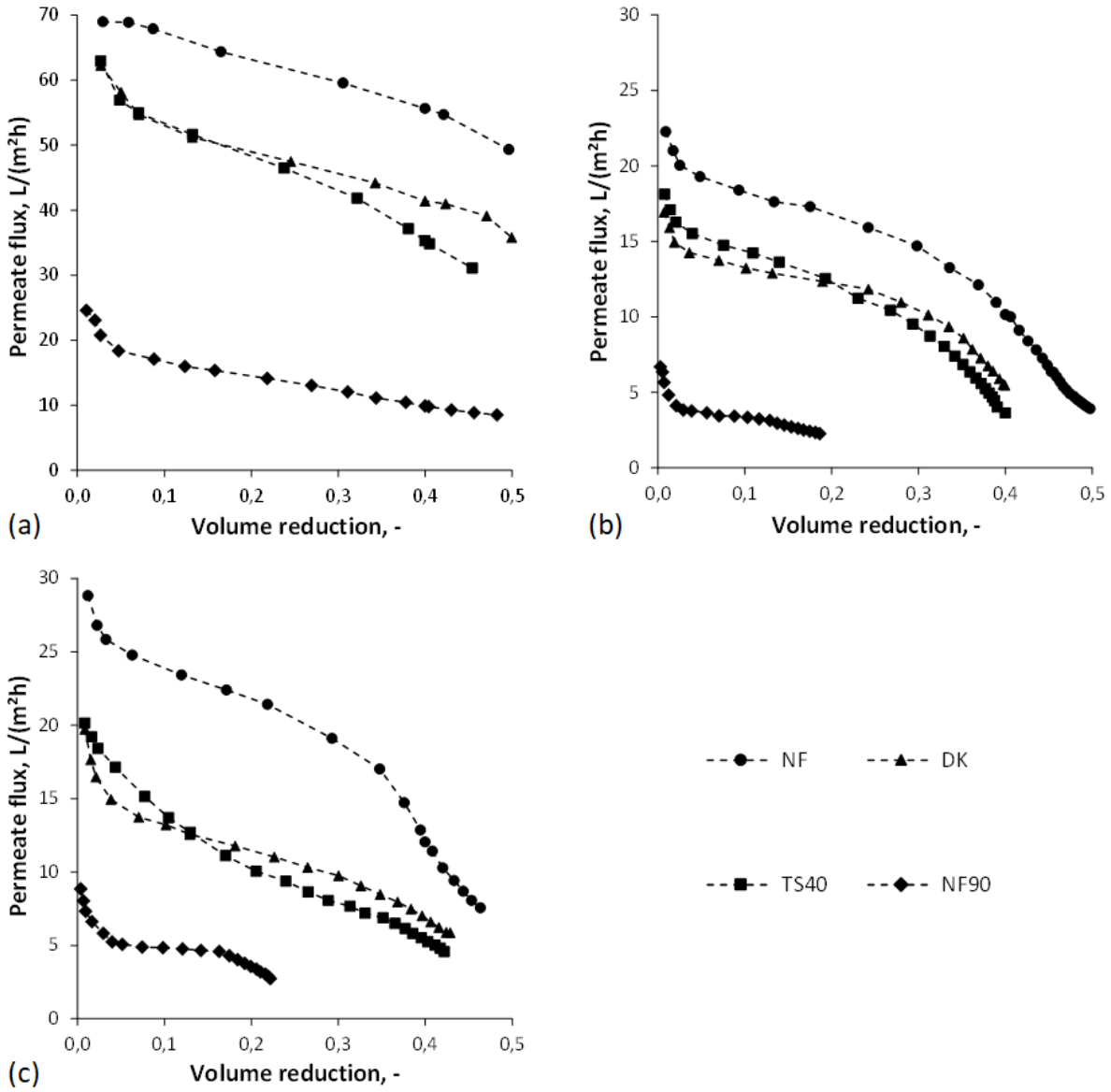

Figure 39: Permeate flux profiles for the nanofiltration membranes NF, DK, TS40, and NF90 during the concentration of (a) model solution, (b) beechwood hydrolyzate 4, and (c) hydrothermally treated beechwood hydrolyzate 4

4.4.2.2 Separation Performance

Besides the permeate flux profiles, the retention of sugars, especially xylose, and the permeation of the inhibitory compounds 5-HMF, furfural, and acetic acid, are also important measures for evaluating membrane performance. Figure 40 a) shows glucose, xylose, furfural, and acetic acid retention for the four NF membranes concentrating MS. NF90 showed high retentions above 99 % for glucose as well as xylose. In contrast, for the other three NF membranes, glucose and xylose retention is in a similar range between 95 and 96 % and between 84 and 87 %, respectively. Unfortunately, along with the high sugar retention of NF90, furfural and acetic acid were also highly retained with 42 and 51 %, respectively. On the other hand, NF and DK showed very small retentions for both components, acetic acid, even with negative values. Thereby, the negative values can be explained by two possible mechanisms: (i) under the experimental conditions (pH = 2.7) approximately 0.9 % of the acetic acid is dissociated

and exists as negatively charged acetate; the positively charged membranes (isoelectric point ~ 4) could attract negatively charged acetate and thus lead to negative retentions for acetic acid [232]; (ii) the retention of acetic acid might be altered by intermolecular interactions with xylose and other organics, as shown in the literature [232, 233]. Hence, as expected, the highest xylose losses and the lowest inhibitor retentions agree with those NF membranes with the highest fluxes and pore width.

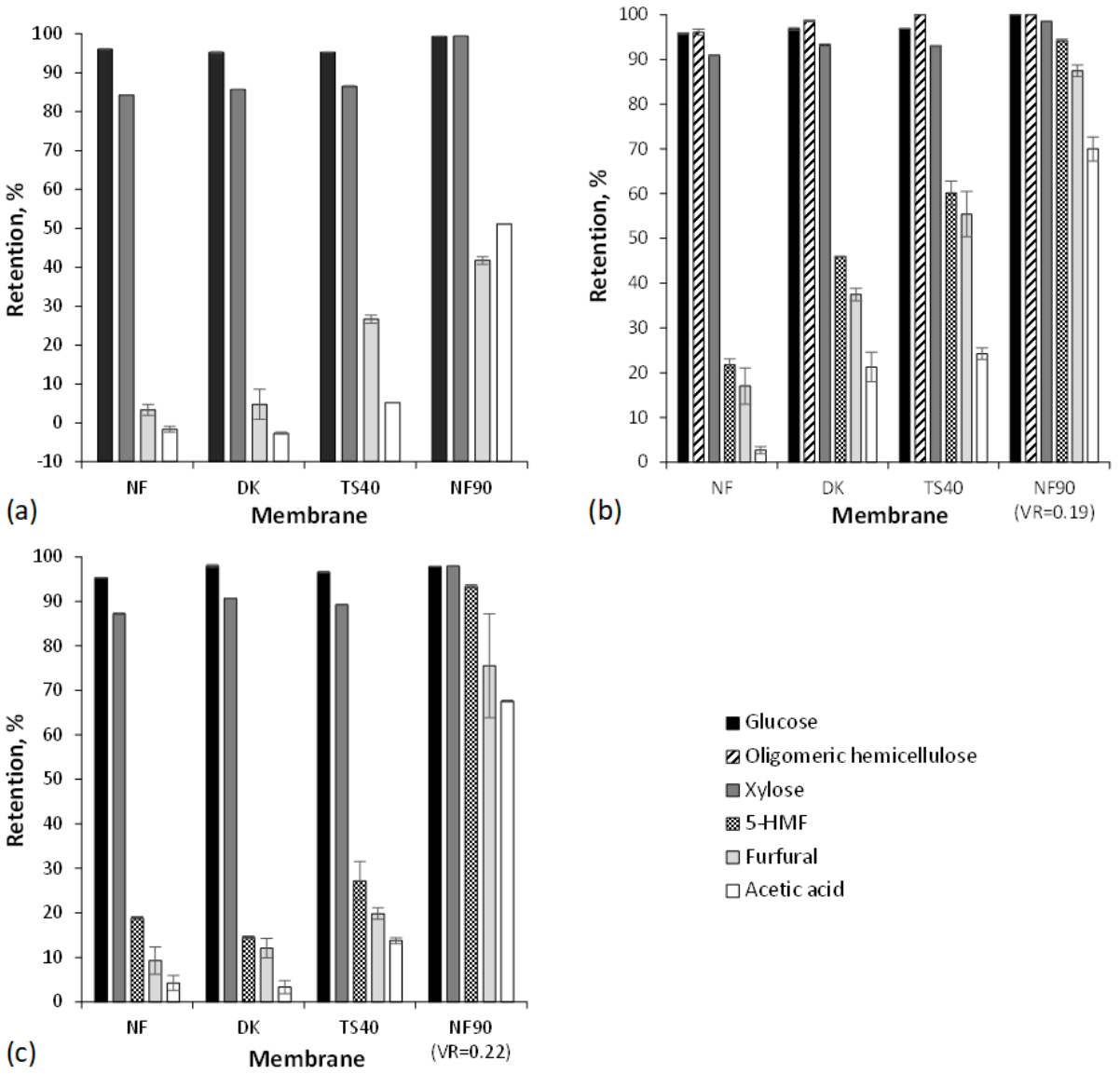

Figure 40: Retention of glucose, oligomeric hemicellulose, xylose, 5-HMF, furfural, and acetic acid for the nanofiltration membranes NF, DK, TS40, and NF90 during the concentration (VR = 0.4) of (a) model solution, (b) beechwood hydrolyzate 4, and (c) hydrothermally treated beechwood hydrolyzate 4 (Error bars represent the standard deviation)

When processing the real biomass feed stream BWH 4 or HPBWH 4 to a VR of 0.4 (0.2 for NF90 with BWH 4 or HPBWH 4), as shown in Figure 40 b) and c), the retention for all analyzed components increased compared to MS. During the filtration of BWH 4 with NF90, 100 % glucose and oligomeric hemicellulose and 99 % xylose were retained, and 70-94 % of the inhibitory components. NF retained 96 % glucose and oligomeric hemicellulose and

91 % xylose and only 22 % 5-HMF, 17 % furfural, and 3 % acetic acid, which is desirable concerning subsequent conversion processes. The other NF membranes (DK and TS40) performed in between. The reason for the higher retentions might be the interaction between the oligomeric hemicellulose/monomeric sugar molecules and other soluble organics to more complex structures. In addition, the interaction between hydrophobic phenolics and other unidentified components with the NF membranes results in a deposited layer and thus pore plugging or narrowing. The results of the hydrothermal pretreatment of the BWH 4 indicate that pore plugging or narrowing is less compared to the utilization of BWH 4 since the retentions of the analyzed components mostly decrease. This could be due to decreased fouling tendencies as a result of the hydrothermal treatment. The retention for glucose, xylose, 5-HMF, furfural, and acetic acid decreased by -1–2 %, 1–4 %, 1–33 %, 8–36 %, and -2–18 %, respectively. This positive influence is the most evident for TS40 and DK and the least for NF90 and NF. Hence, due to the hydrothermal pretreatment of BWH 4, the sugar losses during the NF process increased but at simultaneously higher xylose concentrations and lower retentions of 5-HMF, furfural, and acetic acid, which results in a cleaner retentate.

The separation factor α was calculated to evaluate the separation performance of the four NF membranes. As seen from Eq. (3-23), higher values indicate the desired separation of inhibitors while retaining a higher concentration of xylose [159]. In Table 17, the separation factors of the inhibitory components 5-HMF, furfural, and acetic acid and the combination of all inhibitors over xylose are shown. For the sake of completeness, the separation factors of glucose and oligomeric hemicellulose over xylose are also calculated. NF90 is best suited for high xylose retention and NF for low inhibitor retention. Regardless of the feed solution used, the highest separation factors for inhibitors over xylose were reached for NF90 caused by the nearly complete xylose retention. Moreover, higher separation factors can be observed when using BWH 4 compared to HPBWH 4. As expected, there is very little separation between glucose and oligomeric hemicellulose over xylose, with separation factors between 0.0 and 1.2. Hence, NF membranes with small pores, low surface roughness, and high hydrophilicity should be used for the separation of xylose from inhibitors out of wood hydrolyzate streams.

Table 17: Separation factor α for xylose (xyl) from glucose (glu), oligomeric hemicellulose (olig hemi), 5-HMF, furfural (fur), acetic acid (acetic), and inhibitors (inh = 5-HMF + fur + acetic) during concentration (VR = 0.4) of model solution (MS), beechwood hydrolyzate 4 (BWH 4), and hydrothermally treated beechwood hydrolyzate 4 (HPBWH 4)

Membrane	Feed	$\alpha_{glu/xyl}$	$\alpha_{olig\ hemi/xyl}$	$\alpha_{5\text{-}HMF/xyl}$	$\alpha_{fur/xyl}$	$\alpha_{acetic/xyl}$	$\alpha_{inh/xyl}$
NF	MS	0.3	-	-	6.2	6.5	6.4
	BWH 4	0.5	0.4	8.6	9.1	11	10
	HPBWH4	0.4	-	6.3	7.1	7.5	7.3
DK	MS	0.3	-	-	6.7	7.2	7.1
	BWH 4	0.5	0.2	8.0	9.2	12	11
	HPBWH4	0.2	-	9.2	9.4	10	10
TS40	MS	0.4	-	-	5.4	7.0	6.7
	BWH 4	0.5	0.0	5.7	6.3	11	9.8
	HPBWH4	0.3	-	6.8	7.5	8.0	7.8
NF90	MS	1.2	-	-	100	84	88
	BWH 4 (VR = 0.19)	0.0	0.0	3.9	8.5	20	17
	HPBWH 4 (VR = 0.22)	1.0	-	3.2	12	15	13

4.4.3 Fouling Analysis

The usage of the resistance-in-series model, where the permeate flux through the membrane is analyzed based on the hydraulic resistance to the filtration, allows identifying overall fouling as the sum of different contributions related to the specific fouling mechanisms concentration polarization, gel/cake layer formation, and adsorption/pore blocking. The permeate flux and total resistance versus time for the filtration of MS, BWH 4, and HPBWH 4 using the four NF membranes are shown in Figure 41 a)–d). Single resistances for the membranes, concentration polarization, gel/cake layer formation, and adsorption/pore blocking and their share of the total resistance are listed in Table 18. The initial rapid permeate flux decline could be explained by an osmotic pressure ($\Delta\pi_p$) increase [234]. A rough calculation is provided by the van 't Hoff equation (Eq. (4-2)) with R as the universal gas constant and T as the temperature.

$$\Delta\pi_p = \left(C_f - C_p\right) \cdot R \cdot T \tag{4-2}$$

After 5 min of operation, an osmotic pressure of 0.8–1.4 MPa, depending on the NF membrane and feed solution, counteracts the applied TMP of 3.0 MPa. If the osmotic pressure became equal to the TMP, the permeate flux would decline to 0 L/(m²h). Within the first 15 min of filtration, a comparatively high permeate flux decline can be observed, attributed to fouling by adsorption and/or pore blocking on the clean membrane surface [235]. Another reason might be the continued compaction of the NF membranes. After that, the permeate flux approaches the steady-state. However, a decrease in permeate flux was relatively small. The permeate flux decline correlates with the increase in total resistance. This implies an initial increase in total resistance, followed by a gradual decrease in slope during the experimental runs. Using NF90, the total resistance was initially larger due to the smallest pore width, less hydrophilicity, and

high surface roughness. The total resistance of DK and TS40 is approx. 2.5 times lower, while it is approx. 3.3 times lower for NF but increases with a similar rate to NF90. Hence, NF is the least susceptible to fouling for the considered application. The total resistance is the lowest when filtering MS and the highest for BWH 4. As was already apparent from the performance analysis, the hydrothermal pretreatment of BWH 4 has a positive effect on membrane fouling. The total resistance to the filtration of HPBWH 4 is approx. 1.4 times smaller than that of BWH 4. A detailed discussion regarding the positive influence of hydrothermal pretreatment of BWH 4 on the NF process is presented in Publication III.

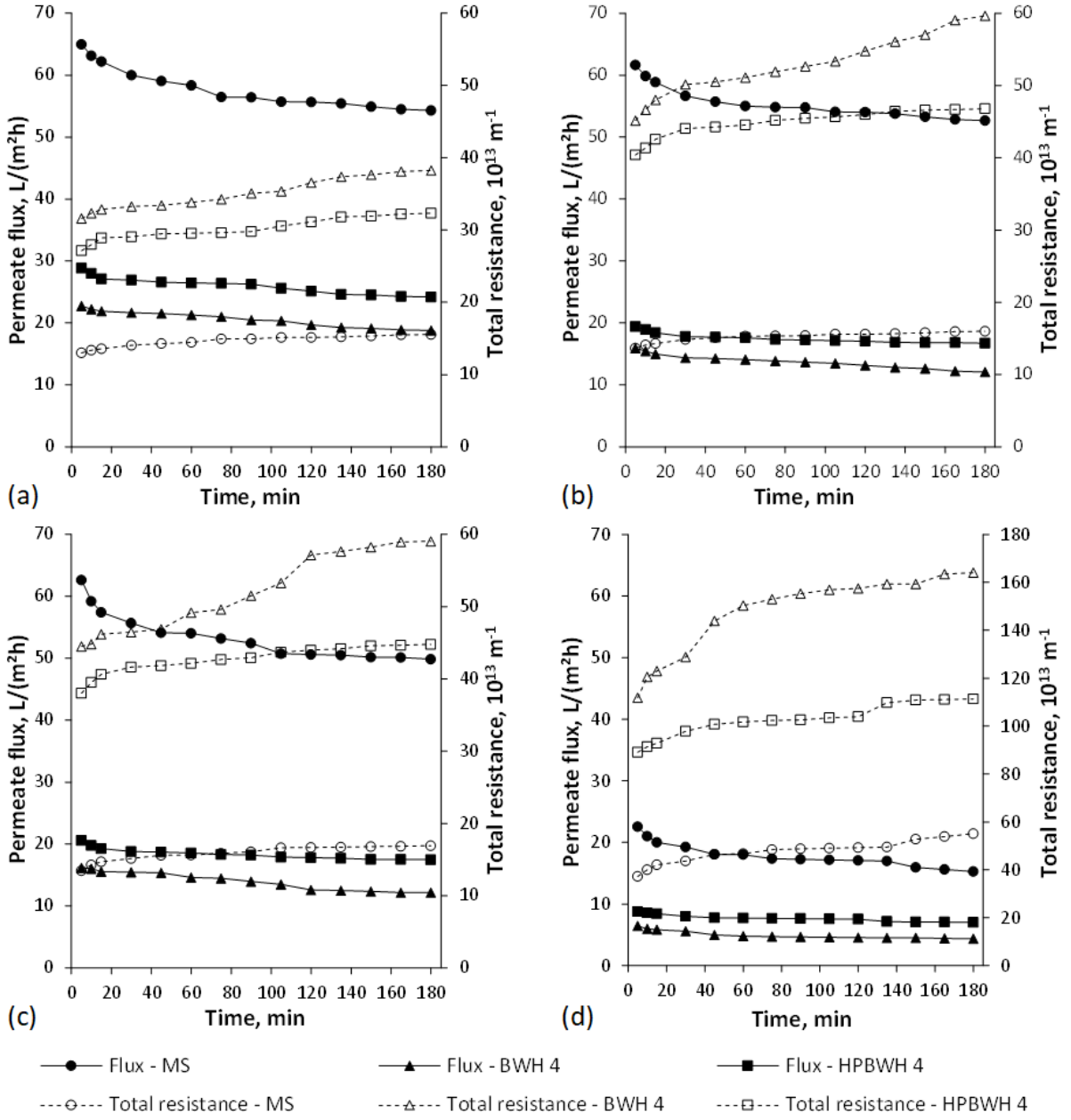

Figure 41: Permeate flux and total resistances versus time for the filtration of model solution (MS), beechwood hydrolyzate 4 (BWH 4), and hydrothermally treated beechwood hydrolyzate 4 (HPBWH 4) using the nanofiltration membranes a) NF, b) DK, c) TS40, and d) NF90

4.4.3.1 Concentration Polarization

The percentage of the concentration polarization resistance on the total resistance accounted for 37–73 % for MS, 71–82 % for BWH 4, and 71–77 % for HPBWH 4. The concentration polarization resistance is greater for BWH 4 by a factor of approximately 3–8 and 2–6 for HPBWH 4 compared to that for MS. This factor is only temporary during the processing of the different feed streams and is the most dominant concerning the total resistance, excluding the membrane resistance. NF90 exhibits the highest concentration polarization resistances and the smallest increase between the different feed solutions. On the contrary, the membrane NF shows the smallest concentration polarization resistances, and DK the largest increment between the concentration polarization resistances of MS, BWH 4, and HPBWH 4. These phenomena can be attributed to the respective membrane characteristics. The reason for the lower concentration polarization resistances for the filtration of MS and HPBWH 4 compared to BWH 4 is quite clear. The total retentate concentration of soluble and insoluble components in the BWH 4 is higher than that in HPBWH 4 and even higher than that in MS, as shown in Figure 40 a)–c). Lower concentrations of compounds result in reduced concentration polarization effects and permeate flux decline by gel layer formation and osmotic pressure. The lower concentration polarization between BWH 4 and HPBWH 4 can be explained by the partial or complete degradation of oligomeric cellulose and hemicellulose to monomeric sugars, which reduces the potential for the formation of a concentrated layer of oligomers on the membrane surfaces.

Concentration polarization cannot be avoided if the filtration aims to concentrate a particular component with little loss. However, concentration polarization could be minimized if only the desired component is retained and/or if problematic components (e.g., furans and phenolic components) are removed or even not generated before the concentration process. Alternatively, the CFV could be set so that a turbulent flow results. An ideal membrane, where only the desired sugars are retained, and all non-sugar components permeate, would provide a higher purity of sugars and allow a higher maximum concentration of sugars. Some of the examined NF membranes could transfer a large proportion of the inhibitory components into the permeate and concentrate the sugars in the retentate. Nevertheless, the NF membranes have to be further modified to get higher sugar concentrations in the retentate, better separation of sugar from inhibitory components, and to achieve lower fouling resistances [236, 237]. Another approach could be to configure the pulping process so that problematic components are produced less or to further pretreat the BWH 4 or HPBWH 4, for example, by adsorption on resins, as presented in Section 4.1 and 4.2.5, to remove problematic components.

4.4.3.2 Gel and/or Cake Layer Formation

The share of the gel/cake layer resistance on the total resistance was of little importance compared to the membrane and concentration polarization resistance. The gel/cake layer resistance for BWH 4 tends to be higher than that for HPBWH 4 and even higher than that for MS. Since BWH 4 and HPBWH 4 were prefiltered before the NF process to remove particles and suspended solids, cake formation can be mostly excluded. The formation of the gel layer is, as already shown above, largely dependent on the concentration polarization. Hence, the

results and possible reasons and explanations are similar. This implies that NF90 is the most and NF the least prone to gel/cake layer formation.

4.4.3.3 Adsorption and/or Pore Blocking

The share of the adsorption/pore blocking resistance is also of little importance compared to membrane and concentration polarization resistance. Contrary to the expectations, the adsorption/pore blocking resistance values for MS are usually the highest before BWH 4 and HPBWH 4. A possible explanation for this phenomenon could be the shielding of the membrane surface by the real biomass feed streams, which discouraged adsorption/pore blocking through problematic components. This shielding could result from either direct interactions of dissolved organic components with the surface or indirect interactions between certain adsorbed species on the surface and repulsion of remaining soluble components in the bulk solution above the membrane [42]. As a result, the intensity of adsorption/pore blocking for BWH 4 and HPBWH 4 is more or less relatively small. The reason for this could be that the concentration of hydrophobic components, such as lignin, its phenolic degradation products (especially residual insoluble solids), and furans (e.g., 5-HMF and furfural), which are the most responsible for fouling by adsorption/pore blocking [128, 142], has changed little during the hydrothermal pretreatment.

Table 18: Resistances of the membrane (R_m), concentration polarization (R_{cp}), gel and/or cake layer formation ($R_{g/c}$), and adsorption and/or pore blocking ($R_{a/p}$) and their percentage on the total resistance ($R_{tot} = R_m + R_{cp} + R_{g/c} + R_{a/p}$) for the filtration of model solution (MS), beechwood hydrolyzate 4 (BWH 4), and hydrothermally treated beechwood hydrolyzate 4 (HPBWH 4) using the nanofiltration membranes NF, DK, TS40, and NF90

Mem-brane	Feed	R_m		R_{cp}		$R_{g/c}$		$R_{a/p}$	
		[10^{13} m^{-1}]	[%]	[10^{13} m^{-1}]	[%]	[10^{13} m^{-1}]	[%]	[10^{13} m^{-1}]	[%]
NF	MS	7.3	47	6.3	41	0.8	5	1.1	7
	BWH 4	7.4	19	27	71	2.9	8	0.9	2
	HPBWH 4	7.5	23	23	71	1.3	4	0.8	2
DK	MS	7.2	45	6.0	37	0.9	6	1.9	12
	BWH 4	7.4	12	47	79	3.5	6	1.8	3
	HPBWH 4	7.3	16	36	77	1.6	3	1.7	4
TS40	MS	7.1	42	7.4	44	0.8	5	1.6	9
	BWH 4	7.1	12	48	81	3.3	6	0.6	1
	HPBWH 4	7.1	16	35	77	2.4	5	0.8	2
NF90	MS	7.8	14	40	73	4.6	8	2.9	5
	BWH 4	7.8	5	134	82	18	11	3.8	2
	HPBWH 4	7.7	7	86	77	15	14	2.3	2

4.4.3.4 Membrane Cleaning

The effect of cleaning the NF membranes with the 1 wt% P3-Ultrasil-53 solution (pH = 9) is presented as the ratio between R_m and R_{cm} (Figure 42). The closer this value is to 1, the more the membrane resistance after cleaning after the fouling experiments corresponds to the initial resistance. As can be seen, with few exceptions, the membrane resistances decreased and almost

returned to their initial resistances (R_m/R_{cm} > 0.97). For the NF membrane DK in combination with BWH 4 (R_m/R_{cm} = 0.91) and HPBWH 4 (R_m/R_{cm} = 0.92), cleaning was comparatively less effective. However, the regeneration of the NF membranes examined does not tend to depend on the feed solutions used. Hence, the MS and the real biomass substrates do not contain any components or foulants that resist the alkaline cleaning using P3-Ultrasil-53. A possible reason why the initial PWF of the NF membranes could not be restored may be a result of continued compaction of the NF membranes during the process, which in turn increased the membrane resistance over time.

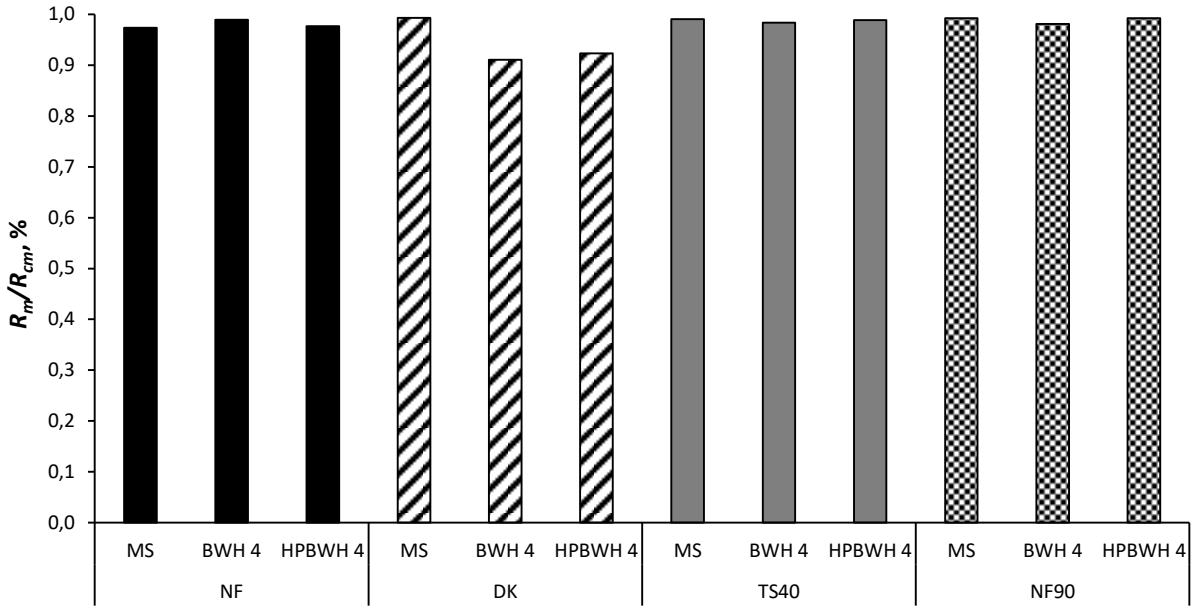

Figure 42: Ratio between the initial membrane resistance (R_m) and the membrane resistance after cleaning (R_{cm}) with a 1 wt% P3-Ultrasil-53 solution (pH = 9) after the fouling experiments

4.4.4 Influence of TMP and Temperature on Permeate Flux and Retentions

The influence of TMP and temperature on the NF process was studied using HPBWH 2 as described in Section 3.2.4.3. HPBWH 2 consists of 1.5 g/L oligomeric hemicellulose, 8.2 g/L xylose, and 0.7 g/L furfural. Hence, 63 % of the hemicellulose oligomers were converted to monomeric xylose, and furfural formation was observed to a low extent, proving low sugar degradation.

In Figure 43 (a), screening experiments with TMPs of 1 to 4 MPa and their influence on permeate flux and retentions are shown. Typically, the permeate flux increases with increasing TMP linearly until a certain level, the so-called critical flux [133]. Beyond this critical flux, no further significant increase can be achieved. The critical flux was determined to lie between 2 and 3 MPa. The deviation from the linear increase of permeate flux with TMPs over 2 MPa indicates the transition to the limiting flux phase. The cause for the flux limitation may be concentration polarization and gel/cake layer formation [238]. This flux limitation cannot be avoided using real wood hydrolyzates, but the choice of a fitting TMP permits that the mass accumulation on the membrane surface has a minor effect on the process efficiency. In general, the retentions of the solutes increased as the TMP increased. More significantly for furans (5-HMF + furfural) and acetic acid than for xylose and even oligomeric hemicellulose. Reasons

might be an increased solvent flux due to increased pressure since water is more permeable than the solutes and the formation of a fouling layer that acts as an additional permeation barrier and thus increases solute rejection [178,232].

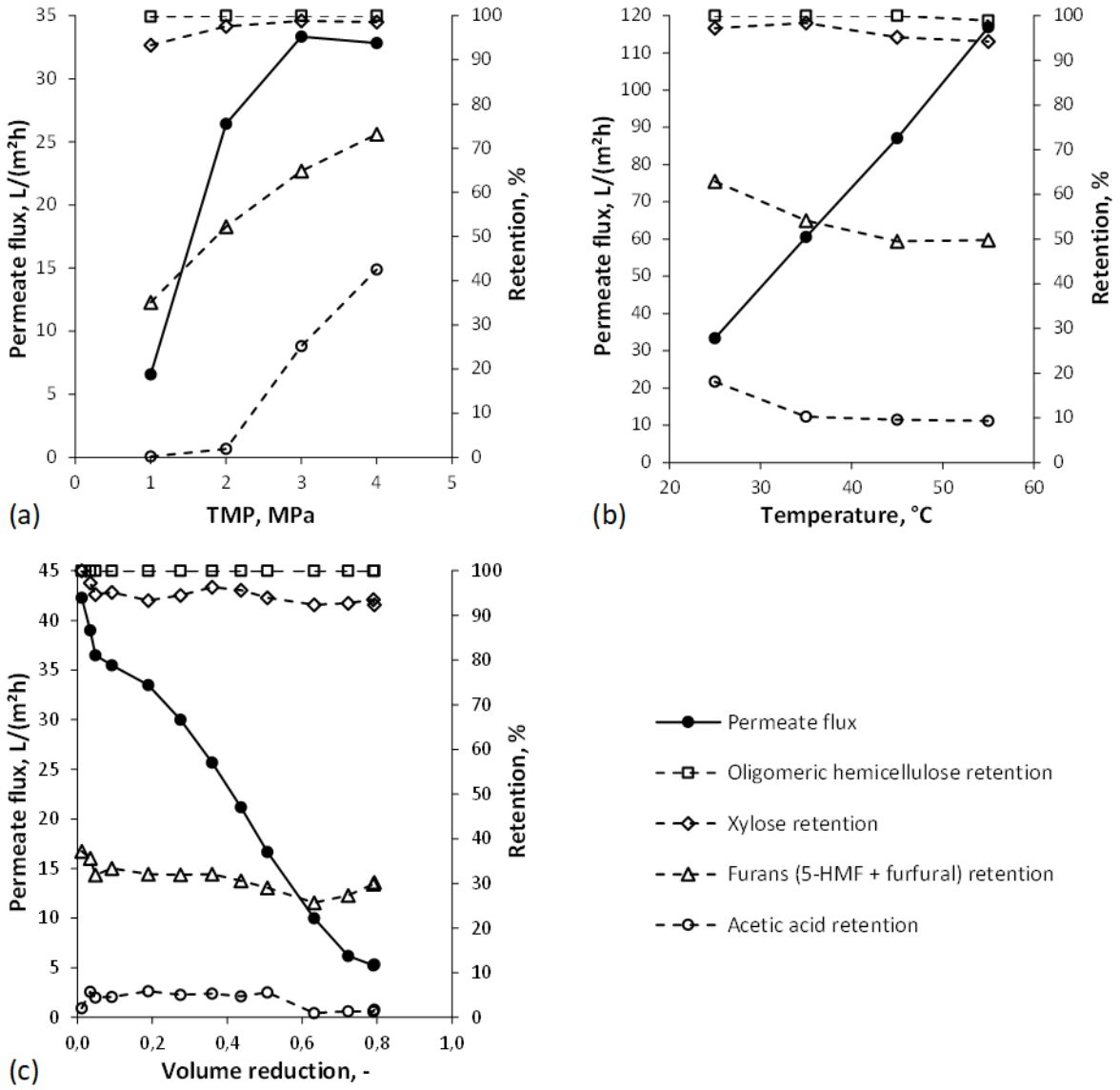

Figure 43: (a) Influence of transmembrane pressure (TMP) on permeate flux and retention (T = 25 °C), (b) influence of temperature on permeate flux and retention (Δp = 3 MPa), and (c) concentration of hydrothermally pretreated beechwood hydrolyzate 2 (Δp = 2 MPa, T = 35 °C)

The influence of temperature on permeate flux and retentions is shown in Figure 43 (b). The permeate flux increases linearly within the studied temperature range. This trend can be explained by a declining viscosity of the feed solution, which enhances the liquid flow through the membrane and thus the permeate flux according to the proportionality $J \approx 1/\eta \approx 1/e^{1/T}$. The decrease in solute retentions can be attributed to several mechanisms: (i) increased diffusion of the solutes results in an enhanced transport through the membrane, (ii) Nilsson et al. [239] proposed that the increase of uncharged solutes in the mass transfer is greater than that of water with increasing temperature, and (iii) increased temperature can cause

changes in the surface structure of thin-film composite membranes leading to an increment of membrane pore size and MWCO [221].

Appropriate process conditions chosen on the beforehand parameter screening were a TMP of 2 MPa and a temperature of 35 °C (Publication V). The HPBWH 2 was concentrated by NF to a *VR* of 0.8. The results of the concentration experiments are depicted in Figure 43 (c). Permeate flux started with 42.3 L/(m²h) and decreased continuously since the feed became more concentrated due to rejected solutes until reaching a value of 5.3 L/(m²h). The average permeate flux was 22.5 L/(m²h). Average retentions for oligomeric hemicellulose, xylose, furans, and acetic acid were 100, 95, 31, and 4 %, respectively. This resulted in an oligomeric hemicellulose and xylose concentration in the retentate of 7.5 and 39.3 g/L, respectively, and a reduction of the inhibitor-to-xylose ratio by 70 %.

4.5 Comparative Process Assessment

The two purification cascades assessed are presented in a block diagram in Figure 1. A comparison of both cascades was performed. It should be mentioned that the examinations carried out in this section are of a conceptual character and are based on the experimental work in Sections 4.1 to 4.4. For the assessment and comparing of both purification cascades, mass balances including product yields, energy balances including energy efficiencies, and specific production costs were calculated. However, at first, the input data and assumptions of the Aspen Plus® flowsheet simulations, as well as the dimensions of the main unit operations, are described. More detailed information can be found in the corresponding Publications IV and V. In addition, an environmental assessment of the adsorption process, hydrothermal pretreatment, and nanofiltration is presented in Publication IV.

4.5.1 Process Description

As described above (Section 3.2.6), purification cascade 1 consists of an adsorption process and subsequent UF. The experimental input data for the flowsheet simulation are mainly taken from Sections 4.1.5, 4.1.6, and 4.2.5. For the adsorption process, a continuous fixed-bed column loaded with the adsorbent SP700 is specified. The column, operated in down-flow, is fed by a flow rate of 4.5 BV/h, corresponding to a velocity of 39 m/h with a bed diameter of 1.2 m and a height of 6.1 m. Hence, the pressure drop is approx. 0.13 MPa according to Figure 20. The process temperature is 50 °C. After adding 6 BVs of BWH to the adsorbent bed, 80 % lignin is removed, and 99.5 % hemicellulose (oligomeric hemicellulose + monomeric sugars) is recovered. Desorption of lignin is operated with 5 BVs of a 50 wt.% ethanol solution with the same process parameters and assumptions as of the adsorption process. The desorbate solution is recovered by a rectification column with a recovery rate ≥ 99.5 % [189]. The column has 22 trays and operates below 0.2 MPa overhead pressure [189], and a pressure drop of 0.8 kPa/stage is assumed [240]. A Murphree efficiency of 75 % was set in the rectification column [12]. An 80 wt.% ethanol solution is drawn off at the top of the column. The product stream from the adsorption is fed to the UF operated as a feed-and-bleed system [56]. Process conditions are a TMP of 0.95 MPa, a temperature of 55 °C, and a CFV of 1.1 m/s. Retention for hemicellulose is 79 % and for lignin 19 %. Assuming that BWH 5 is used as feedstock, a

VR of approx. 0.76 is necessary to achieve a hemicellulose concentration of 200 g/L in the purified product stream. An average permeate flux and frictional pressure drop of 61.7 L/(m²h) and 0.102 MPa, respectively, follows. The membrane surface area accounts for 625 m².

Purification cascade 2, also described in Section 3.2.6, consists of hydrothermal pretreatment and subsequent NF. The hydrothermal pretreatment is operated in a tube bundle reactor at a pressure of 2.0 MPa, a reaction temperature of 180 °C, and a residence time of 3.1 min. The design of the tube bundle reactor is based mainly on information from manufacturers. It consists of 107 tubes of 0.025 m in diameter and 5 m in length each and is flowed through at a velocity of 0.025m/s. Almost the entire hemicellulose oligomers are hydrolyzed to xylose, of which a minor proportion reacts further to furfural. At the reactor outlet, the reaction product passed through a heat exchanger preheating the feed solution and cooling down the reactor outlet to 60 °C. In the subsequent NF, operated as feed-and-bleed system, xylose with 95 %, furans with 31 %, and acetic acid with 4 % is retained at a TMP of 2.0 MPa, a temperature of 35 °C, and a CFV of 1.5 m/s. Assuming that BWH 5 is used as feedstock, a *VR* of approx. 0.72 is necessary to achieve a xylose concentration of 200 g/L in the purified product stream. An average permeate flux and frictional pressure drop of 24.2 L/(m²h) and 0.118 MPa, respectively, follows. The membrane surface area accounts for 1628 m².

4.5.2 Mass Balance

In purification cascade 1, 7.6 t/h of a 200 g/L concentrated hemicellulose solution can be produced out of initially 32.3 t/h BWH 5 with a hemicellulose sugar (oligomeric hemicellulose + monomeric sugars) concentration of 57 g/L (Table 19). Hence, the hemicellulose yield along purification cascade 1 is 83 %. In addition to BWH 5, other input streams are water and ethanol, each with 16.2 t/h, for the desorption of lignin. The recovery of the desorbate solution by rectification, as described above, results in a requirement for water of 12.2 t/h and fresh ethanol, including the losses during the desorption process, of 0.2 t/h. One metric ton of hemicellulose (dry matter = 100 %) causes 25.3 m³ of wastewater. This high volume is mainly due to the large water input during the organosolv pulping, as described in Section 3.1.1, and should be reduced.

In purification cascade 2, 8.9 t/h of a 200 g/L concentrated xylose solution can be produced out of initially 32.3 t/h BWH 5 with a hemicellulose sugar (oligomeric hemicellulose + monomeric sugars) concentration of 57 g/L (Table 19). Hence, the xylose yield along purification cascade 2, considering the initial mass as the sum of oligomeric hemicellulose and xylose, is 97 %. The advantage of this cascade is that no other input streams, such as additional chemicals, are needed. A wastewater quantity of 13.7 m³ per metric ton of xylose (dry matter = 100 %) is produced. The reason for this high volume is the same as described for purification cascade 1.

The comparison between the two concepts shows that for purification cascade 2 more of the product xylose can be obtained with less wastewater due to the generally higher product yield. Hemicellulose losses in purification cascade 1 are mainly during the UF process because of lower retentions of the valuable components.

Table 19: Mass balance and (production) costs of purification cascade 1 and 2

Purification cascade and main streams	Mass input	Mass output	(Production) costs
	[t/h]		[EUR/t]
Purification cascade 1			
Beechwood hydrolysate 5	32.3 (10.3 MW)	0.0	
Process water	12.2	0.0	0.15[a]
Ethanol	0.2 (1.7 MW)	0.0	550[b]
Wastewater	0.0	37.1	2.5[a]
Purified hemicellulose ($C_{hemicel.}$ = 200 g/L)	0.0	7.6 (7.0 MW)	135.1[c]
Purification cascade 2			
Beechwood hydrolysate 5	32.3 (10.3 MW)	0.0	
Wastewater	0.0	23.4	2.5[a]
Purified xylose (C_{xylose} = 200 g/L)	0.0	8.9 (7.9 MW)	71.4[c]

[a][202]; [b][241]; [c]calculated

4.5.3 Energy Balance

Energy requirements and utility consumption of the purification cascades are shown in Table 20. Within purification cascade 1 the highest utility demands are LPS and CW, mainly for the recovery of ethanol after desorption but also for the adsorption and desorption process itself. The UF process consumed most of the electrical power.

In purification cascade 2, the hydrothermal pretreatment requires the total HPS, and the electricity demand is mainly for the NF process. In a comparative Aspen Plus® simulation, where the xylose concentration was realized by multiple-effect evaporation, the heat demand is higher by a factor of 3.4 and the electricity demand lower by a factor of 0.3.

The energy efficiency was determined for both purification cascades as defined in Section 3.2.6.3. For the purification of hemicellulose in cascade 1 the energy efficiency accounts for 24 %, and for the purification of xylose in cascade 2 56 %. The significantly lower value of purification cascade 1 compared to purification cascade 2 can be explained by two circumstances. On the one hand, because of the higher energy input by the material stream ethanol (LHV = 26.7 MJ/kg) and the additional heat required for ethanol recovery. On the other hand, because of different retention values for furans, acetic acid, and lignin during combined adsorption and UF compared to single step NF. Meaning, that the overall yielding of the three components has a lower degree in purification cascade 1 than purification cascade 2. This results in a higher energetic loss but also in a more purified product stream. However, by implementing an adsorption step in purification cascade 2, the separation could be improved. The associated decrease in energy efficiency could be compensated by the targeted recovery of lignin as a by-product stream after desorption.

Table 20: Energy/utility requirements and costs of purification cascade 1 and 2

Process utility	Purification cascade 1	Purification cascade 2	Costs
	[MW]		
Electrical power	0.2	0.3	150 EUR/MWh[a]
Cool water	7.2	0.0	0.043 EUR/t[b]
Low pressure steam	8.8	0.0	25 EUR/t[b]
High pressure steam	0.0	1.6	25 EUR/t[b]

[a][242]; [b][9]

4.5.4 Costing

FCI and annual costs for the two purification cascades are summarized in Table 21. The costs for the equipment are 2,424 kEUR for purification cascade 1 and 1,737 kEUR for purification cascade 2. The most expensive components for purification cascade 1 are the rectification column for ethanol recovery (638 kEUR), the adsorption columns (422 kEUR), and UF (50 kEUR). For purification cascade 2, the costs are determined by the reactor for hydrothermal pretreatment (265 kEUR) and the NF (130 kEUR). To calculate the FCI a surcharge factor of 4.5 was used for equipment costs to account for the indirect and direct costs of a liquid treatment plant.

Table 21: Investments and annual costs of purification cascade 1 and 2

		Purification cascade 1	Purification cascade 2
Fixed-capital investment	[kEUR]	10,962	7,855
Capital-linked costs	[kEUR/a]	809	581
Depreciation	[kEUR/a]	550	395
Interest	[kEUR/a]	259	186
Consumption-linked costs	[kEUR/a]	5,002	2,279
Raw material	[kEUR/a]	-	-
Auxiliary and operating material	[kEUR/a]	1,080	49
Energy supply	[kEUR/a]	3,180	1,762
Disposal costs	[kEUR/a]	742	468
Operation-linked costs	[kEUR/a]	1,984	1,828
Labor costs	[kEUR/a]	1,436	1,435
Maintenance	[kEUR/a]	548	393
Other costs	[kEUR/a]	452	405
Administration	[kEUR/a]	287	287
Insurance	[kEUR/a]	110	79
Uncertainties	[kEUR/a]	55	39

Since no costs are assumed for the BWH [43], the consumption-linked costs, mainly energy supply, account for a large share of the total costs. For purification cascade 1, this cost position is with 61 % the largest cost driver. Mainly due to the high LPS demand within ethanol recovery. Consumption-linked costs, mainly for the HPS required for the hydrothermal

pretreatment, is with a share of 45 % the main cost driver in purification cascade 2. Shortly after, with a share of 36 %, are the operation-linked costs, mainly labor.

Specific production costs of the two purification cascades differ significantly (Table 22). The costs for the purified hemicellulose in cascade 1, at 135.1 EUR/t, are almost twice as high as compared to 71.4 EUR/t for the production of a purified xylose stream in cascade 2. This difference is mainly, as already mentioned above, on the one hand, due to the higher product yield and thus higher product volume in cascade 2 compared to cascade 1. On the other hand, due to a more extensive process and energy requirement in cascade 1 compared to cascade 2. The selling price for hemicellulose from lignocellulosic biomass is 1,500 to 3,500 EUR/t [243] and that for xylose (98 % pure D-xylose) is 2,000 to 3,000 EUR/t [244]. Hence, the integration of the investigated purification cascades into the production process for hemicellulose and xylose, respectively, seems reasonable. However, for a comprehensive economic assessment, the entire process chain from the raw material to the final product would have to be examined. In addition, concrete quality requirements would have to be defined for the final product with regard to its further use.

Table 22: Specific production costs of purified hemicellulose and xylose product stream

		Purification cascade 1	Purification cascade 2
Capital-linked costs	[EUR/$t_{product}$]	13.3	8.1
Consumption-linked costs	[EUR/$t_{product}$]	81.9	32.0
Operation-linked costs	[EUR/$t_{product}$]	32.5	25.6
Other costs	[EUR/$t_{product}$]	7.4	5.7
Production costs	[EUR/$t_{product}$]	135.1	71.4

5. Summary, Conclusions, and Future Work

In the following section, the main insights of the thesis are summarized in terms of their contribution to the specified aims and conclusions are drawn. Furthermore, recommendations for future research are elaborated.

5.1 Summary

WBBs generate process streams containing dissolved hemicellulose, lignin, and degradation products. The hemicellulose and derived monomeric C5 sugars have a high potential for use as resources in bio-based chemistry. For this purpose, they have to be separated from other biomass components and concentrated into a purified product solution suitable for further conversion. The BWH from which the hemicellulose is to be separated originates from organosolv pulping. Within the scope of this work, the separation and valorization of hemicellulose from BWH by adsorption and membrane filtration were experimentally investigated and assessed.

An adsorption process was developed that allows the separation of residual lignin from hemicellulose out of BWH. At first, four polymeric resins (XAD4, XAD7HP, XAD16N, SP700) and one zeolite (HiSiv1000) were compared in batch experiments, and competitive adsorption isotherms were modeled. Of the five tested adsorbents, the PA based XAD7HP and the PS-DVB based SP700 were found to be the most efficient. The extended Freundlich isotherm best described the lignin adsorption onto XAD7HP and SP700. This means that the adsorbents can still remove lignin from BWH after its surface is already covered with it. As a next step, the resin SP700 was studied in more detail in continuous column tests. A lignin removal of at least 80 % was defined as the benchmark. This was achieved after feeding 6 BVs of BWH to the column and is associated with a hemicellulose recovery of 99.5 %. The desorption of lignin was investigated with a 20 wt.% and a 50 wt.% ethanol solution, as well as with a 0.5 M NaOH solution. The most efficient desorbate solution was the 50 wt.% ethanol solution. Within 10 BVs practically all of the adsorbed lignin could be removed from the resin.

UF of BWH was developed for the concentration of hemicellulose with simultaneous removal of lignin. To estimate appropriate process parameters, the statistical approach RSM and multiobjective optimization by the determination of Pareto frontiers were used. By means of RSM, the multidimensional correlations of TMP, temperature, and pH with the performance parameters permeate flux, hemicellulose retention, and lignin retention were determined. Using UA60, the UF process was mostly influenced by TMP and temperature. The pH has just a little or no effect. For UH004, TMP was the most significant factor influencing the UF process, followed by pH and then temperature with little or no effect. Based on the empirical model equations, PO and decision-making by the UP method were applied to determine the process conditions for high permeate flux and hemicellulose retention, as well as low lignin retention. The estimated optimum parameters for UA60 were found to be a TMP of 0.98 MPa, a temperature of 55 °C, and a pH of 2.5, which would lead to a permeate flux of 49.2 L/(m²h), hemicellulose retention of 84.7 %, and lignin retention of 40.6 %. For UH004, a TMP of

1.0 MPa, a temperature of 55 °C, and a pH of 4.1, from which a permeate flux of 45.2 L/(m²h), hemicellulose retention of 70.9 %, and lignin retention of 20.7 % are expected. For optimal operation conditions with UH004, the pH has to be adjusted. Hence, its adoption is not recommended, as additional chemicals have to be added, which is unfavorable from an economic and environmental point of view. However, due to the overlap of the molecular weights of hemicellulose and lignin as well as the presence of hemicellulose-lignin complexes in the BWH a complete separation of both components by UF seems impossible. In addition to the process optimization, the influence of adsorption of BWH previous to the UF was investigated. This pretreatment significantly increased the permeate flux from an average value of 22.2 to 60.8 L/(m²h). This is due to the removal of lignin and other hydrophobic components. Adsorption reduced the average hemicellulose retention from 90 to 79 % and the average lignin retention from 41 to 19 %. This means higher losses of hemicellulose but simultaneously a purer retentate stream.

In NF, the influence of hydrothermal pretreatment of BWH and membrane characteristics on the separation of xylose from fermentation inhibitors (acetic acid, furfural, and 5-HMF) was investigated. At first, a hydrothermal process was developed using RSM to study appropriate process parameters (temperature and residence time) for the maximum conversion of the oligomeric fraction of hemicellulose to xylose. At a temperature of 180 °C and a residence time of 3.1 min almost 100 % of the hemicellulose oligomers were converted to xylose. Then, the NF process using a MS, BWH, and HPBWH as well as four different membranes (NF, DK, TS40, NF90) was assessed by a performance evaluation and fouling analysis. The hydrothermal conversion step positively affects the performance of the NF membranes and reduces fouling. When HPBWH was used, the permeate flux increased depending on the NF membrane by 14-33 %. Due to higher xylose concentrations and lower inhibitor retentions, a cleaner retentate could be obtained compared to the use of BWH. Reduced fouling is probably mainly due to the degradation of the oligomeric sugar molecules to monomers, which minimizes the potential of concentration polarization and the formation of a gel/cake layer on the membrane surface. In addition, to design an energetically favorable process, appropriate process parameters for the NF of HPBWH were determined. A *VR* of 80 % was reached at a TMP of 2.0 MPa and a temperature of 35 °C resulting in an average permeate flux of 22.5 L/(m^{2}h) and retentions for xylose, furans, and acetic acid of 95, 31, and 4 %, respectively. This resulted in an increase in xylose concentration by a factor of 4.8 and a reduction of the inhibitor-to-xylose ratio by 70 %.

Based on the findings of the experimental work, two purification cascades were simulated on an industrial scale using Aspen Plus®. Purification cascade 1 consists of an adsorption process to remove foulants from the BWH and UF for the concentration of hemicellulose and simultaneous removal of remaining lignin. Purification cascade 2 consists of hydrothermal pretreatment of the BWH to hydrolyze the remaining hemicellulose oligomers into xylose and NF to separate potential fermentation inhibitors and increase xylose concentration. In the first cascade, 80 % of the lignin was removed by adsorption, and 7.6 t/h of a purified hemicellulose solution with a concentration of 200 g/L was obtained using UF. In cascade 2, almost the entire oligomeric fraction of the hemicellulose was hydrothermally converted to xylose and purified by NF to 8.9 t/h of a xylose solution with a concentration of 200 g/L. The energy efficiency of

the cascades was 24 and 56 %, respectively. Furthermore, the estimation of specific production costs showed that hemicellulose could be recovered from BWH at the cost of 135.1 EUR/t and xylose at 71.4 EUR/t. Thus, it can be concluded that the combination of hydrothermal pretreatment and NF has a high potential for economic implementation in WBBs.

5.2 Conclusions

The results presented in this thesis demonstrate the challenges for the separation and valorization of hemicellulose and its derived sugars from wood hydrolyzates. Due to the multi-component nature of the feed solutions, the provision of a purified hemicellulose or xylose solution cannot be achieved by a standalone separation technique. A suitable separation cascade depends on the wood hydrolyzates used, the dissolved components, and the product requirements. In conclusion, adsorption on polymeric resins efficiently removes lignin from wood hydrolyzates, and enhances filtration capacity and decreases fouling in subsequent membrane filtration. The purification and concentration of hemicellulose and xylose by UF and NF, respectively, have high potential in future biorefineries as they are more cost-efficient and environmentally friendly. However, due to the overlap of molecular weights of the components of interest, a complete separation of individual substances seems impossible, and fouling is still a challenge. The combination of NF with prior hydrothermal pretreatment of the wood hydrolysates has the advantage of higher availability of monomeric sugars in solution and has a positive effect on the filtration process. Promising applications are those that connect processes that benefit from each other in terms of product yields, capacity, and reduced fouling. Hence, the findings of this thesis illustrate the possibility to make hemicellulose from wood hydrolyzates usable by means of adsorption and membrane filtration, thus extending their application in the processing of real biomass substrates.

5.3 Future Work

To establish adsorption and membrane filtration processes for the separation and valorization of hemicellulose from wood hydrolyzates on an industrial scale, open questions and challenges still need to be addressed in the future. These mainly concern the application of the purified products obtained, the improvement of the individual processes and process knowledge, the development of entire separation cascades, and upscaling.

The hemicellulose produced during experiments can be used in various product applications. So far, only a few investigations have been carried out to identify the most promising applications for this process stream and formulate specific requirements that the fractionated hemicellulose must meet for further utilization. More extensive studies concerning these issues should be carried out.

For further improvement and a better understanding of the individual processes, the following work could be continued: (i) Adsorption can be improved by finding non-conventional methods for desorption such as sonic/microwave energy, which would reduce the adsorption-desorption-cycle time as well as equipment and energy requirements. For a better process understanding, adsorption kinetics have to be modeled, and predictive model tools can play a key role in

process design. (ii) For the further development of UF, on the one hand, the molecular interactions of the dissolved biopolymers in the wood hydrolyzates have to be studied in more detail, and on the other hand, membranes with a narrower pore size distribution are needed to increase the separation efficiency. (iii) Since NF membranes are often severely fouled, fouling resistant membranes must be developed, and efficient cleaning is necessary.

To produce a pure hemicellulose or xylose stream, or even a solid/crystalline product, entire separation cascades must be developed. There are already various approaches and ideas for combining different sustainable separation processes into one cascade. For example, one possibility, e.g., could be the combination of an adsorption step, a membrane filtration cascade, chromatographic methods, and concentration by drying. However, the proof of the developed concepts is mostly still pending.

The experimental work in this study was carried out on a laboratory to technical scale. This scale enables intensive research on the individual processes and the identification of suitable materials and process parameters, as well as appropriate process configurations. However, pilot to demonstration scale experiments are required as a next step to verify the results and refine the process design. In addition, long-term performance tests for adsorption and membrane materials, as well as for continuous cyclic operation, are needed. Such investigations can be the basis for a more precise determination of process costs and the integration of the developed separation processes into existing industrial plants.

6. References

[1] International Panel of Climate Change (IPCC), Climate Change 2007: The Physical Science Basis: Contribution of Working Group I to the Fourth Assessment Report of the Intergovernmental Panel on Climate Change [Solomon, S., D. Qin, M. Manning, Z. Chen, M. Marquis, K.B. Averyt, M. Tignor and H.L. Miller (eds.)], Cambridge University Press, Cambridge, United Kingdom and New York, NY, USA, 2007.

[2] M. Fatih Demirbas, Biorefineries for biofuel upgrading: A critical review, Applied Energy 86 (2009) S151-S161.

[3] H. Sixta, Handbook of Pulp, Wiley-VCH Verlag GmbH, Weinheim, Germany, 2006.

[4] T. KOBAYASHI, A. USHIDA, I. KOURAKATA, K. SETO, T. HIWATASHI, T. SATO, T. NARUMI, Washing Effect of Microbubble Mixture on the Soiled Model Attached on a Metal Surface, JAPANESE JOURNAL OF MULTIPHASE FLOW 34 (2020) 254–263.

[5] M. Ebrahimi, D. Humpert, S. Schönherr, P. Czermak, Keramische Membrantechnologie für die Verfügbarmachung biogener Stoffströme, Chemie Ingenieur Technik 93 (2021) 154–167.

[6] E. Strand, Enhancement of Ultrafiltration Process by Pretreatment in Recovery of Hemicelluloses from Wood Extracts, Lappeenranta University of Technology, Lappeenranta, 2016.

[7] M. Leschinsky, H.K. Weber, R. Patt, H. Sixta, Formation of insoluble components during autohydrolysis of eucalyptus globulus, Lenzinger Berichte 87 (2009) 16–25.

[8] H.-J. Huang, S. Ramaswamy, U.W. Tschirner, B.V. Ramarao, A review of separation technologies in current and future biorefineries, Separation and Purification Technology 62 (2008) 1–21.

[9] J. Michels, ‘‘Lignocellulose Biorefinery – Phase 2” – final scientific and technical report of all project partners, DECHEMA Gesellschaft für Chemische Technik und Biotechnologie, 2014.

[10] B. Rößiger, R. Röver, G. Unkelbach, D. Pufky-Heinrich, Production of Bio-Phenols for Industrial Application: Scale-Up of the Base-Catalyzed Depolymerization of Lignin, GSC 07 (2017) 193–202.

[11] S. Willför, A. Sundberg, A. Pranovich, B. Holmbom, Polysaccharides in some industrially important hardwood species, Wood Sci Technol 39 (2005) 601–617.

[12] R. Nitzsche, M. Budzinski, A. Gröngröft, Techno-economic assessment of a wood-based biorefinery concept for the production of polymer-grade ethylene, organosolv lignin and fuel, Bioresource Technology 200 (2016) 928–939.

[13] J. Michels, Pilot Project ‘‘Lignocellulose Biorefinery” – final scientific and technical report of all project partners, DECHEMA Gesellschaft für Chemische Technik und Biotechnologie, 2009.

[14] P. Gatenholm, M. Tenkanen, Hemicelluloses: Science and Technology, American Chemical Society, Washington, DC, 2003.

[15] D.S. Naidu, S.P. Hlangothi, M.J. John, Bio-based products from xylan: A review, Carbohydrate Polymers 179 (2018) 28–41.

[16] N.M.L. Hansen, D. Plackett, Sustainable films and coatings from hemicelluloses: A review, Biomacromolecules 9 (2008) 1493–1505.

[17] J. Hartman, A.-C. Albertsson, M.S. Lindblad, J. Sjöberg, Oxygen barrier materials from renewable sources: Material properties of softwood hemicellulose-based films, J. Appl. Polym. Sci. 100 (2006) 2985–2991.

[18] K.S. Mikkonen, M. Tenkanen, Sustainable food-packaging materials based on future biorefinery products: Xylans and mannans, Trends in Food Science & Technology 28 (2012) 90–102.

[19] R. Deutschmann, R.F.H. Dekker, From plant biomass to bio-based chemicals: Latest developments in xylan research, Biotechnology advances 30 (2012) 1627–1640.

[20] M. Söderqvist Lindblad, A.-C. Albertsson, E. Ranucci, M. Laus, E. Giani, Biodegradable polymers from renewable sources: Rheological characterization of hemicellulose-based hydrogels, Biomacromolecules 6 (2005) 684–690.

[21] D.U. Lima, R.C. Oliveira, M.S. Buckeridge, Seed storage hemicelluloses as wet-end additives in papermaking, Carbohydrate Polymers 52 (2003) 367–373.

[22] R. Nitzsche, J. Köchermann, A. Gröngröft, M. Kraume, Nanofiltration of Organosolv Hemicellulose Hydrolyzate: Influence of Hydrothermal Pretreatment and Membrane Characteristics on Filtration Performance and Fouling, Ind. Eng. Chem. Res. 60 (2021) 916–930.

[23] E. de Jong, H. Stichnothe, G. Bell, H. Jørgensen, Bio-Based Chemicals - A 2020 Update, IEA Bioenergy Task 42, 2020.

[24] P. Barbaro, F. Liguori, C. Moreno-Marrodan, Selective direct conversion of C 5 and C 6 sugars to high added-value chemicals by a bifunctional, single catalytic body, Green Chem. 18 (2016) 2935–2940.

[25] S. Dutta, S. De, B. Saha, M.I. Alam, Advances in conversion of hemicellulosic biomass to furfural and upgrading to biofuels, Catal. Sci. Technol. 2 (2012) 2025.

[26] van der Waal, J.C., de Jong, E., Avantium chemicals: The high potential for the levulinic product tree, Industrial biorenewables, a practical viewpoint (2016) 97–120.

[27] S. Ramaswamy, H. Hua-Jiang, B.v.(E.) Ramarao, Separation and purification technologies in biorefineries, Wiley John Wiley & Sons Ltd, Chichester, West Sussex, United Kingdom, 2013.

[28] M.-G. Ma, N. Jia, J.-F. Zhu, S.-M. Li, F. Peng, R.-C. Sun, Isolation and characterization of hemicelluloses extracted by hydrothermal pretreatment, Bioresource Technology 114 (2012) 677–683.

[29] S.S. Madaeni, K. Tahmasebi, S.H. Kerendi, Sugar Syrup Concentration Using Reverse Osmosis Membranes, Eng. Life Sci. 4 (2004) 187–190.

[30] S.S. Madaeni, S. Zereshki, Reverse osmosis alternative: Energy implication for sugar industry, Chemical Engineering and Processing: Process Intensification 47 (2008) 1075–1080.

[31] F. Peng, P. Peng, F. Xu, R.-C. Sun, Fractional purification and bioconversion of hemicelluloses, Biotechnology advances 30 (2012) 879–903.

[32] E. Koivula, M. Kallioinen, S. Preis, L. Testova, H. Sixta, M. Mänttäri, Evaluation of various pretreatment methods to manage fouling in ultrafiltration of wood hydrolysates, Separation and Purification Technology 83 (2011) 50–56.

[33] H. Kumar, R. Alén, G. Sahoo, Characterization of hardwood soda-AQ lignins precipitated from black liquor through selective acidification, Bioresources 11 (2016) 9869–9879.

[34] W. Zhu, H. Theliander, Precipitation of lignin from softwood black liquor: an investigation of the equilibrium and molecular properties of lignin, Bioresources 10 (2015) 1696–1714.

[35] C. Wu, L. Bing, S. Li, D. Yu, D. Wang, Effect of coagulating agents on lignin and oligosaccharide contents in pre-hydrolysis liquor obtained in the production of dissolving pulp from poplar residual slabs, Bioresources 11 (2016) 87–94.

[36] M. Caetano, C. Valderrama, A. Farran, J.L. Cortina, Phenol removal from aqueous solution by adsorption and ion exchange mechanisms onto polymeric resins, Journal of colloid and interface science 338 (2009) 402–409.

[37] R.T. Yang, Adsorbents: Fundamentals and Applications, John Wiley & Sons, Inc, Hoboken, NJ, USA, 2003.

[38] J. Heinonen, Q. Sanlaville, H. Niskakoski, J. Tamper, T. Sainio, Separation and recovery of lignin from hydrolysates of lignocellulose with a polymeric adsorbent, Separation and Purification Technology 186 (2017) 125–134.

[39] T. Persson, H. Krawczyk, A.-K. Nordin, A.-S. Jönsson, Fractionation of process water in thermomechanical pulp mills, Bioresource Technology 101 (2010) 3884–3892.

[40] G. Schild, H. Sixta, L. Testova, Multifunctional Alkaline Pulping, Delignification and Hemicellulose Extraction, Cellulose Chemistry and Technology (2010) 35–45.

[41] T. Melin, R. Rautenbach, Membranverfahren: Grundlagen der Modul- und Anlagenauslegung, 3rd ed., 2007.

[42] A. Gautam, T.J. Menkhaus, Performance evaluation and fouling analysis for reverse osmosis and nanofiltration membranes during processing of lignocellulosic biomass hydrolysate, Journal of Membrane Science 451 (2014) 252–265.

[43] R. Nitzsche, A. Gröngröft, J. Köchermann, K. Meisel, H. Etzold, M. Verges, M. Leschinsky, J. Bachmann, B. Saake, S. Torkler, K. Patzsch, B. Rößiger, D. Pufky-Heinrich, G. Unkelbach, Platform and fine chemicals from woody biomass: Demonstration and assessment of a novel biorefinery, Biomass Conv. Bioref. 48 (2020) 793.

[44] Verein Deutscher Ingenieure, Economic calculation systems for capital goods and plants, Beuth Verlag GmbH, Düsseldorf 03.100.01, 91.140.10, 2012.

[45] E. Sjöström, Wood Chemistry, Elsevier, 1993.

[46] Z. Zhang, M.D. Harrison, D.W. Rackemann, W.O.S. Doherty, I.M. O'Hara, Organosolv pretreatment of plant biomass for enhanced enzymatic saccharification, Green Chem. 18 (2016) 360–381.

[47] P. Alvira, E. Tomás-Pejó, M. Ballesteros, M.J. Negro, Pretreatment technologies for an efficient bioethanol production process based on enzymatic hydrolysis: A review, Bioresource Technology 101 (2010) 4851–4861.

[48] N. Mosier, C. Wyman, B. Dale, R. Elander, Y.Y. Lee, M. Holtzapple, M. Ladisch, Features of promising technologies for pretreatment of lignocellulosic biomass, Bioresource Technology 96 (2005) 673–686.

[49] M. FitzPatrick, P. Champagne, M.F. Cunningham, R.A. Whitney, A biorefinery processing perspective: Treatment of lignocellulosic materials for the production of value-added products, Bioresource Technology 101 (2010) 8915–8922.

[50] M. Galbe, G. Zacchi, Pretreatment: The key to efficient utilization of lignocellulosic materials, Biomass and Bioenergy 46 (2012) 70–78.

[51] A. Brandt, J. Gräsvik, J.P. Hallett, T. Welton, Deconstruction of lignocellulosic biomass with ionic liquids, Green Chem. 15 (2013) 550.

[52] K. Zhang, Z. Pei, D. Wang, Organic solvent pretreatment of lignocellulosic biomass for biofuels and biochemicals: A review, Bioresource Technology 199 (2016) 21–33.

[53] M. Verges, Verfahrenstechnische Untersuchung des Ethanol-Wasser-Organosolvaufschlusses von Lignocellulose in einer integrierten Pilotanlage, Dissertation, Universität Stuttgart zur Erlangung, 2019.

[54] H. Krawczyk, Separation of Biomass Components by Membrane Filtration - Process Development for Hemicellulose Recovery, Lund University, 2013.

[55] A. Arkell, J. Olsson, O. Wallberg, Process performance in lignin separation from softwood black liquor by membrane filtration, Chemical Engineering Research and Design 92 (2014) 1792–1800.

[56] A.-S. Jönsson, O. Wallberg, Cost estimates of kraft lignin recovery by ultrafiltration, Desalination 237 (2009) 254–267.

[57] A.-S. Jönsson, A.-K. Nordin, O. Wallberg, Concentration and purification of lignin in hardwood kraft pulping liquor by ultrafiltration and nanofiltration, Chemical Engineering Research and Design 86 (2008) 1271–1280.

[58] L. Ahsan, M.S. Jahan, Y. Ni, Recovering/concentrating of hemicellulosic sugars and acetic acid by nanofiltration and reverse osmosis from prehydrolysis liquor of kraft based hardwood dissolving pulp process, Bioresource Technology 155 (2014) 111–115.

[59] K. Li, L. Kollberg, H. Almqvist, B. Xu, C. Hulteberg, Maximizing yield of liquid-lignin from membrane filtration retentate of kraft black liquor, Industrial Crops and Products 169 (2021) 113657.

[60] M. Mänttäri, J. Lahti, H. Hatakka, M. Louhi-Kultanen, M. Kallioinen, Separation phenomena in UF and NF in the recovery of organic acids from kraft black liquor, Journal of Membrane Science 490 (2015) 84–91.

[61] O.Y. Abdelaziz, K. Ravi, M. Nöbel, P. Tunå, C. Turner, C.P. Hulteberg, Membrane filtration of alkali-depolymerised kraft lignin for biological conversion, Bioresource Technology Reports 7 (2019) 100250.

[62] Y. Wang, S. Azhar, M.E. Lindström, G. Henriksson, Stabilization of Polysaccharides During Alkaline Pre-Treatment of Wood Combined with Enzyme-Supported Extractions in a Biorefinery, Journal of Wood Chemistry and Technology 35 (2014) 91–101.

[63] P. Tomani, The LignoBOOST Process, Cellulose Chemistry and Technology 44 (2010) 53–58.

[64] T. Kleinert, K. v. Tayenthal, Über neuere Versuche zur Trennung von Cellulose und Inkrusten verschiedener Hölzer, Z. Angew. Chem. 44 (1931) 788–791.

[65] S. Laure, M. Leschinsky, M. Fröhling, F. Schultmann, G. Unkelbach, Assessment of an organosolv lignocellulose biorefinery concept based on a material flow analysis of a pilot plant, Cellulose Chemistry and Technology 48 (2014) 793–798.

[66] F.G. Calvo-Flores, J.A. Dobado, Lignin as renewable raw material, ChemSusChem 3 (2010) 1227–1235.

[67] N. Brosse, Lignin: properties and applications in biotechnology and bioenergy, Nova Science Publishers, Hauppauge, N.Y, 2012.

[68] A. Teleman, M. Nordström, M. Tenkanen, A. Jacobs, O. Dahlman, Isolation and characterization of O-acetylated glucomannans from aspen and birch wood, Carbohydrate Research 338 (2003) 525–534.

[69] R. Alén, Biorefining of forest resources, Papermaking science and technology, 2011.

[70] T. Persson, A.-S. Jönsson, Isolation of hemicelluloses by ultrafiltration of thermomechanical pulp mill process water—Influence of operating conditions, Chemical Engineering Research and Design 88 (2010) 1548–1554.

[71] J. Thuvander, A.-S. Jönsson, Extraction of galactoglucomannan from thermomechanical pulp mill process water by microfiltration and ultrafiltration—Influence of microfiltration membrane pore size on ultrafiltration performance, Chemical Engineering Research and Design 105 (2016) 171–176.

[72] P. Stenius, Surface chemistry and charge of cellulosic fibres, 2011.

[73] Y.-H. Weng, H.-J. Wei, T.-Y. Tsai, T.-H. Lin, T.-Y. Wei, G.-L. Guo, C.-P. Huang, Separation of furans and carboxylic acids from sugars in dilute acid rice straw hydrolyzates by nanofiltration, Bioresource Technology 101 (2010) 4889–4894.

[74] S.K. Dutta, S. Chakraborty, Pore-scale dynamics of enzyme adsorption, swelling and reactive dissolution determine sugar yield in hemicellulose hydrolysis for biofuel production, Scientific reports 6 (2016) 38173.

[75] G.W. Gokel, Dean's Handbook of Organic Chemistry, 2nd ed., McGraw-Hill Professional, New York, 2004.

[76] N. Mogi, E. Sugai, Y. Fuse, T. Funazukuri, Infinite Dilution Binary Diffusion Coefficients for Six Sugars at 0.1 MPa and Temperatures from (273.2 to 353.2) K, J. Chem. Eng. Data 52 (2007) 40–43.

[77] C.R. Wilke, P. Chang, Correlation of diffusion coefficients in dilute solutions, AIChE J. 1 (1955) 264–270.

[78] C.L. Yaws, Yaws' handbook of thermodynamic and physical properties of chemical compounds physical, thermodynamic and transport properties for 5,000 organic chemical compounds, Knovel, 2003.

[79] M.S. Karunarathna, R.C. Smith, Valorization of Lignin as a Sustainable Component of Structural Materials and Composites: Advances from 2011 to 2019, Sustainability 12 (2020) 734.

[80] I. Carrillo, C. Vidal, J.P. Elissetche, R.T. Mendonça, Wood anatomical and chemical properties related to the pulpability of Eucalyptus globulus: A review, Southern Forests: a Journal of Forest Science 80 (2017) 1–8.

[81] R. El Hage, N. Brosse, L. Chrusciel, C. Sanchez, P. Sannigrahi, A. Ragauskas, Characterization of milled wood lignin and ethanol organosolv lignin from miscanthus, Polymer Degradation and Stability 94 (2009) 1632–1638.

[82] M. Déniel, G. Haarlemmer, A. Roubaud, E. Weiss-Hortala, J. Fages, Energy valorisation of food processing residues and model compounds by hydrothermal liquefaction, Renewable and Sustainable Energy Reviews 54 (2016) 1632–1652.

[83] H.A. Ruiz, M. Hedegaard Thomsen, H.L. Trajano, Hydrothermal Processing in Biorefineries // Hydrothermal processing in biorefineries: Production of bioethanol and high added-value compounds of second and third generation biomass, Springer International Publishing; Springer, Cham, 2017.

[84] J. Köchermann, J. Schreiber, M. Klemm, Conversion of d -Xylose and Hemicellulose in Water/Ethanol Mixtures, ACS Sustainable Chem. Eng. (2019).

[85] I. van Zandvoort, Y. Wang, C.B. Rasrendra, E.R.H. van Eck, P.C.A. Bruijnincx, H.J. Heeres, B.M. Weckhuysen, Formation, molecular structure, and morphology of humins in biomass conversion: Influence of feedstock and processing conditions, ChemSusChem 6 (2013) 1745–1758.

[86] X. Hu, S. Kadarwati, S. Wang, Y. Song, M.M. Hasan, C.-Z. Li, Biomass-derived sugars and furans: Which polymerize more during their hydrolysis?, Fuel Processing Technology 137 (2015) 212–219.

[87] J. Köchermann, J. Mühlenberg, M. Klemm, Kinetics of Hydrothermal Furfural Production from Organosolv Hemicellulose and d -Xylose, Ind. Eng. Chem. Res. 57 (2018) 14417–14427.

[88] H.A. Ruiz, R.M. Rodríguez-Jasso, B.D. Fernandes, A.A. Vicente, J.A. Teixeira, Hydrothermal processing, as an alternative for upgrading agriculture residues and marine biomass according to the biorefinery concept: A review, Renewable and Sustainable Energy Reviews 21 (2013) 35–51.

[89] H. Li, A. Deng, J. Ren, C. Liu, Q. Lu, L. Zhong, F. Peng, R. Sun, Catalytic hydrothermal pretreatment of corncob into xylose and furfural via solid acid catalyst, Bioresource Technology 158 (2014) 313–320.

[90] M.-H. Cheng, B.S. Dien, D.K. Lee, V. Singh, Sugar production from bioenergy sorghum by using pilot scale continuous hydrothermal pretreatment combined with disk refining, Bioresource Technology 289 (2019) 121663.

[91] K. SWENNEN, C. COURTIN, B. VANDERBRUGGEN, C. Vandecasteele, J. DELCOUR, Ultrafiltration and ethanol precipitation for isolation of arabinoxylooligosaccharides with different structures, Carbohydrate Polymers 62 (2005) 283–292.

[92] T. Song, A. Pranovich, B. Holmbom, Separation of polymeric galactoglucomannans from hot-water extract of spruce wood, Bioresource Technology 130 (2013) 198–203.

[93] J. Bian, F. Peng, P. Peng, F. Xu, R.-C. Sun, Isolation and fractionation of hemicelluloses by graded ethanol precipitation from Caragana korshinskii, Carbohydrate Research 345 (2010) 802–809.

[94] F. Peng, J.-L. Ren, F. Xu, J. Bian, P. Peng, R.-C. Sun, Comparative study of hemicelluloses obtained by graded ethanol precipitation from sugarcane bagasse, Journal of agricultural and food chemistry 57 (2009) 6305–6317.

[95] D. Zasadowski, J. Yang, H. Edlund, M. Norgren, Antisolvent precipitation of water-soluble hemicelluloses from TMP process water, Carbohydrate Polymers 113 (2014) 411–419.

[96] Z. Liu, P. Fatehi, S. Sadeghi, Y. Ni, Application of hemicelluloses precipitated via ethanol treatment of pre-hydrolysis liquor in high-yield pulp, Bioresource Technology 102 (2011) 9613–9618.

[97] E. Haimer, M. Wendland, A. Potthast, T. Rosenau, F. Liebner, Precipitation of Hemicelluloses from DMSO/Water Mixtures Using Carbon Dioxide as an Antisolvent, Journal of Nanomaterials 2008 (2008) 1–5.

[98] E. Haimer, M. Wendland, A. Potthast, U. Henniges, T. Rosenau, F. Liebner, Controlled precipitation and purification of hemicellulose from DMSO and DMSO/water mixtures by carbon dioxide as anti-solvent, The Journal of Supercritical Fluids 53 (2010) 121–130.

[99] C. Xu, S. Willför, K. Sundberg, C. Petterson, B. Holmbom, Physicochemical characterization of spruce galactoglucomannan solutions: Stability, surface activity and rheology, Cellulose Chemistry and Technology 41 (2008) 51–62.

[100] C. Assor, B. Quemener, J. Vigouroux, M. Lahaye, Fractionation and structural characterization of LiCl-DMSO soluble hemicelluloses from tomato, Carbohydrate Polymers 94 (2013) 46–55.

[101] A. Andersson, T. Persson, G. Zacchi, H. Stålbrand, A.-S. Jönsson, Comparison of diafiltration and size-exclusion chromatography to recover hemicelluloses from process water from thermomechanical pulping of spruce, Applied biochemistry and biotechnology 137-140 (2007) 971–983.

[102] K. Bunnell, C.-S. Lau, J.O. Lay, J. Gidden, D.J. Carrier, Production and Fractionation of Xylose Oligomers from Switchgrass Hemicelluloses Using Centrifugal Partition Chromatography, Journal of Liquid Chromatography & Related Technologies 38 (2014) 801–809.

[103] C.-S. Lau, K.A. Bunnell, E.C. Clausen, G.J. Thoma, J.O. Lay, J. Gidden, D.J. Carrier, Separation and purification of xylose oligomers using centrifugal partition chromatography, Journal of industrial microbiology & biotechnology 38 (2011) 363–370.

[104] D. Bathen, M. Breitbach, Adsorptionstechnik, Springer, Berlin, 2001.

[105] R. Kümmel, E. Worch, Adsorption aus wäßrigen Lösungen: Mit 23 Tabellen, 1st ed., Dt. Verl. für Grundstoffindustrie, Leipzig, 1990.

[106] D.O. Cooney, Adsorption design for wastewater treatment, Lewis Publishers, Boca Raton, Fla., 1999.

[107] R. Ortmann, Untersuchungen zur Adsorption und Desorption von Aldehyden und Aminen im Spurenbereich, Dissertation, University Duisburg-Essen, 2016.

[108] S. Brunauer, L.S. Deming, W.E. Deming, E. Teller, On a Theory of the van der Waals Adsorption of Gases, J. Am. Chem. Soc. 62 (1940) 1723–1732.

[109] H. Sontheimer, B. Frick, J. Fettig, G. Hörner, C. Hubele, G. Zimmer, Adsorptionsverfahren zur Wasserreinhaltung, DVGW Forschungsstelle am Engler-Bunte-Institut der Universität Karlsruhe (TH), Karlsruhe, 1985.

[110] E. Worch, Adsorption Technology in Water Treatment: Fundamentals, Processes, and Modeling, 1st ed., Walter de Gruyter GmbH Co.KG, s.l., 2012.

[111] R. Ranjan, S. Thust, C.E. Gounaris, M. Woo, C.A. Floudas, M.v. Keitz, K.J. Valentas, J. Wei, M. Tsapatsis, Adsorption of fermentation inhibitors from lignocellulosic biomass hydrolyzates for improved ethanol yield and value-added product recovery, Microporous and Mesoporous Materials 122 (2009) 143–148.

[112] D.M. Ruthven, Principles of adsorption and adsorption processes, Wiley, New York, 1984.

[113] W. Otten, E. Gail, T. Frey, Einsatzmöglichkeiten hydrophober Zeolithe in der Adsorptionstechnik, Chemie Ingenieur Technik 64 (1992) 915–925.

[114] A. Dyer, An Introduction to Zeolite Molecular Sieves, John Wiley & Sons, Inc, Chichester, 1988.

[115] R.L. Albright, Porous Polymers as an Anchor for Catalysis, Reactive Polymers (1986) 155–174.

[116] T. Augustin, Neue Entwicklung von Adsorberharzen und deren Einsatzgebiete für die Abreicherung von organischen Stoffen aus gewerblichen und industriellen Abfällen, Gewässerschutz - Wasser - Abwasser 147 (1994) 1–14.

[117] L. Rehmann, B. Sun, A.J. Daugulis, Polymer selection for biphenyl degradation in a solid-liquid two-phase partitioning bioreactor, Biotechnology progress 23 (2007) 814–819.

[118] Gembicki S. A., Oroskar A. R., Johnson J. A., Adsorption, Liquid Separation. In: Kirk-Othmer encyclopedia of chemical technology, Kirk R. E. (Edit.), 4th ed., Wiley, New York, 1991.

[119] M. Al Manasrah, M. Kallioinen, H. Ilvesniemi, M. Mänttäri, Recovery of galactoglucomannan from wood hydrolysate using regenerated cellulose ultrafiltration membranes, Bioresource Technology 114 (2012) 375–381.

[120] S.V. Mohan, J. Karthikeyan, Removal of lignin and tannin colour from aqueous solution by adsorption onto activated charcoal, Environmental Pollution 97 (1997) 183–187.

[121] D. Montané, D. Nabarlatz, A. Martorell, V. Torné-Fernández, V. Fierro, Removal of Lignin and Associated Impurities from Xylo-oligosaccharides by Activated Carbon Adsorption, Ind. Eng. Chem. Res. 45 (2006) 2294–2302.

[122] X. Liu, P. Fatehi, Y. Ni, Removal of inhibitors from pre-hydrolysis liquor of kraft-based dissolving pulp production process using adsorption and flocculation processes, Bioresource Technology 116 (2012) 492–496.

[123] J. Shen, I. Kaur, M.M. Baktash, Z. He, Y. Ni, A combined process of activated carbon adsorption, ion exchange resin treatment and membrane concentration for recovery of dissolved organics in pre-hydrolysis liquor of the kraft-based dissolving pulp production process, Bioresource Technology 127 (2013) 59–65.

[124] J.S. Gütsch, H. Sixta, Regeneration of Spent Activated Charcoals Used for Lignin Removal from Prehydrolysis-Kraft Prehydrolyzates, Industrial & Engineering Chemistry Research 51 (2012) 8624–8630.

[125] K. Chen, H. Lyu, S. Hao, G. Luo, S. Zhang, J. Chen, Separation of phenolic compounds with modified adsorption resin from aqueous phase products of hydrothermal liquefaction of rice straw, Bioresource Technology 182 (2015) 160–168.

[126] T. Schwartz, M. Lawoko, Removal of acid-soluble lignin from biomass extracts using Amberlite XAD-4 resin, Bioresources 5 (2010) 2337–2347.

[127] J.T. Lehto, R.J. Alén, Purification of Hardwood-derived Autohydrolysates, Bioresources 7 (2012).

[128] E. Koivula, M. Kallioinen, T. Sainio, E. Antón, S. Luque, M. Mänttäri, Enhanced membrane filtration of wood hydrolysates for hemicelluloses recovery by pretreatment with polymeric adsorbents, Bioresource Technology 143 (2013) 275–281.

[129] H. Strathmann, Introduction to membrane science and technology, Wiley-VCH, Weinheim, 2011.

[130] M. Kraume, Transportvorgänge in der Verfahrenstechnik: Grundlagen und apparative Umsetzungen, 2nd ed., Springer Vieweg, Berlin, 2012.

[131] G. Bargeman, Transport phenomena during nanofiltration of concentrated solutions, University of Twente, Netherlands, 2016.

[132] K. Ohlrogge, K. Ebert, Membranen - Grundlagen, Verfahren und industrielle Anwendungen, Wiley-VCH Verlag GmbH & Co. KGaA, Weinheim, 2006.

[133] D.Y. Kwon, S. Vigneswaran, A.G. Fane, R.B. Aim, Experimental determination of critical flux in cross-flow microfiltration, Separation and Purification Technology 19 (2000) 169–181.

[134] J.G. Wijmans, R.W. Baker, The solution-diffusion model: A review, Journal of Membrane Science 107 (1995) 1–21.

[135] H. Thiess, Thermische Verfahrens- und Prozesstechnik - Modellierung von Membrantrennverfahren am Beispiel der Ultrafiltration in der biotechnologischen und der Pervaporation in der chemischen Verfahrenstechnit, Shaker Verlag, Düren, 2019.

[136] S. Zeidler, P. Puhlfürß, U. Kätzel, I. Voigt, Preparation and characterization of new low MWCO ceramic nanofiltration membranes for organic solvents, Journal of Membrane Science 470 (2014) 421–430.

[137] M. Dalwani, J. Zheng, M. Hempenius, M.J.T. Raaijmakers, C.M. Doherty, A.J. Hill, M. Wessling, N.E. Benes, Ultra-thin hybrid polyhedral silsesquioxane–polyamide films with potentially unlimited 2D dimensions, J. Mater. Chem. 22 (2012) 14835.

[138] A.F.M. Pinheiro, D. Hoogendoorn, A. Nijmeijer, L. Winnubst, Development of a PDMS-grafted alumina membrane and its evaluation as solvent resistant nanofiltration membrane, Journal of Membrane Science 463 (2014) 24–32.

[139] A.I. Schäfer, A.G. Fane, Nanofiltration: Principles, applications, and new materials, 2021.

[140] T.K. Sherwood, P.L.T. Brian, R.E. Fisher, L. Dresner, Salt Concentration at Phase Boundaries in Desalination by Reverse Osmosis, Ind. Eng. Chem. Fund. 4 (1965) 113–118.

[141] M. Cheryan, S. Strauss, Ultrafiltration and Microfiltration Handbook, 2nd ed., Chapman and Hall/CRC, Boca Raton, 1998.

[142] M.F.A. Goosen, S.S. Sablani, H. Al-Hinai, S. Al-Obeidani, R. Al-Belushi, D. Jackson, Fouling of Reverse Osmosis and Ultrafiltration Membranes: A Critical Review, Separation Science and Technology 39 (2005) 2261–2297.

[143] G. BOLTON, D. LACASSE, R. KURIYEL, Combined models of membrane fouling: Development and application to microfiltration and ultrafiltration of biological fluids, Journal of Membrane Science 277 (2006) 75–84.

[144] M. Cai, S. Wang, H. Liang, Modeling and fouling mechanisms for ultrafiltration of Huanggi (Radix astragalus) extracts, Food Sci Biotechnol 22 (2013) 407–412.

[145] M.J. González-Muñoz, J.C. Parajó, Diafiltration of Eucalyptus wood autohydrolysis liquors: Mathematical modeling, Journal of Membrane Science 346 (2010) 98–104.

[146] C. Duclos-Orsello, W. Li, C.-C. Ho, A three mechanism model to describe fouling of microfiltration membranes, Journal of Membrane Science 280 (2006) 856–866.

[147] E.-E. Chang, S.-Y. Yang, C.-P. Huang, C.-H. Liang, P.-C. Chiang, Assessing the fouling mechanisms of high-pressure nanofiltration membrane using the modified Hermia model and the resistance-in-series model, Separation and Purification Technology 79 (2011) 329–336.

[148] S. Mondal, S. De, A fouling model for steady state crossflow membrane filtration considering sequential intermediate pore blocking and cake formation, Separation and Purification Technology 75 (2010) 222–228.

[149] T. Persson, A.-S. Jönsson, Fouling of Ultrafiltration Membranes during Isolation of Hemicelluloses in the Forest Industry, Scholarly Research Exchange 2009 (2009) 1–7.

[150] L. Puro, M. Kallioinen, M. Mänttäri, M. Nyström, Evaluation of behavior and fouling potential of wood extractives in ultrafiltration of pulp and paper mill process water, Journal of Membrane Science 368 (2011) 150–158.

[151] H. Susanto, I.N. Widiasa, Ultrafiltration fouling of amylose solution: Behavior, characterization and mechanism, Journal of Food Engineering 95 (2009) 423–431.

[152] X. Du, Y. Shi, V. Jegatheesan, I.U. Haq, A Review on the Mechanism, Impacts and Control Methods of Membrane Fouling in MBR System, Membranes 10 (2020).

[153] G. Blandin, A.R.D. Verliefde, J. Comas, I. Rodriguez-Roda, P. Le-Clech, Efficiently Combining Water Reuse and Desalination through Forward Osmosis-Reverse Osmosis (FO-RO) Hybrids: A Critical Review, Membranes 6 (2016).

[154] J.H. Hanemaaijer, T. Robbertsen, T. van den Boomgaard, J.W. Gunnink, Fouling of ultrafiltration membranes. The role of protein adsorption and salt precipitation, Journal of Membrane Science 40 (1989) 199–217.

[155] H. Krawczyk, A. Arkell, A.-S. Jönsson, Membrane performance during ultrafiltration of a high-viscosity solution containing hemicelluloses from wheat bran, Separation and Purification Technology 83 (2011) 144–150.

[156] M.G. Alriols, A. García, R. Llano-ponte, J. Labidi, Combined organosolv and ultrafiltration lignocellulosic biorefinery process, Chemical Engineering Journal 157 (2010) 113–120.

[157] E. Sjöman, M. Mänttäri, M. Nyström, H. Koivikko, H. Heikkilä, Xylose recovery by nanofiltration from different hemicellulose hydrolyzate feeds, Journal of Membrane Science 310 (2008) 268–277.

[158] B. Qi, J. Luo, X. Chen, X. Hang, Y. Wan, Separation of furfural from monosaccharides by nanofiltration, Bioresource Technology 102 (2011) 7111–7118.

[159] F. Zhou, C. Wang, J. Wei, Separation of acetic acid from monosaccharides by NF and RO membranes: Performance comparison, Journal of Membrane Science 429 (2013) 243–251.

[160] H.-J. Huang, S. Ramaswamy, W.W. Al-Dajani, U. Tschirner, Process modeling and analysis of pulp mill-based integrated biorefinery with hemicellulose pre-extraction for ethanol production: A comparative study, Bioresource Technology 101 (2010) 624–631.

[161] P. Schulze, A. Seidel-Morgenstern, H. Lorenz, M. Leschinsky, G. Unkelbach, Advanced process for precipitation of lignin from ethanol organosolv spent liquors, Bioresource Technology 199 (2016) 128–134.

[162] K. Abburi, Adsorption of phenol and p-chlorophenol from their single and bisolute aqueous solutions on Amberlite XAD-16 resin, Journal of hazardous materials 105 (2003) 143–156.

[163] Y. Ku, K.-C. Lee, Removal of phenols from aqueous solution by XAD-4 resin, Journal of hazardous materials 80 (2000) 59–68.

[164] A. Gupta, C. Balomajumder, Simultaneous adsorption of Cr(VI) and phenol onto tea waste biomass from binary mixture: Multicomponent adsorption, thermodynamic and kinetic study, Journal of Environmental Chemical Engineering 3 (2015) 785–796.

[165] A.W. Adamson, A.P. Gast, Physical chemistry of surfaces, 6th ed., Wiley, New York, 1997.

[166] K. Vijayaraghavan, T.V.N. Padmesh, K. Palanivelu, M. Velan, Biosorption of nickel(II) ions onto Sargassum wightii: Application of two-parameter and three-parameter isotherm models, Journal of hazardous materials 133 (2006) 304–308.

[167] O. Redlich, D.L. Peterson, A Useful Adsorption Isotherm, J. Phys. Chem. 63 (1959) 1024.

[168] Z. Aksu, Ü. Açıkel, T. Kutsal, Application of multicomponent adsorption isotherms to simultaneous biosorption of iron(iii) and chromium(vi) onC.vulgaris, J. Chem. Technol. Biotechnol. 70 (1997) 368–378.

[169] A. Dean, D. Voss, D. Draguljić, Design and Analysis of Experiments, Springer, Cham, 2017.

[170] T. Lundstedt, E. Seifert, L. Abramo, B. Thelin, Å. Nyström, J. Pettersen, R. Bergman, Experimental design and optimization, Chemometrics and Intelligent Laboratory Systems (1998) 3–40.

[171] L. Lu, C.M. Anderson-Cook, T.J. Robinson, Optimization of Designed Experiments Based on Multiple Criteria Utilizing a Pareto Frontier, Technometrics 53 (2011) 353–365.

[172] K. Deb, Multi-objective optimization using evolutionary algorithms, Wiley, Chichester, 2004.

[173] K. Chircop, D. Zammit-Mangion, On e-Constraint Based Methods for the Generation of Pareto Frontiers, Journal of Mechanics Engineering and Automation 3 (2013) 279–289.

[174] E. Ballestero, C. Romero, A theorem connecting utility function optimization and compromise programming, Operations Research Letters 10 (1991) 421–427.

[175] S. Shirazi, C.-J. Lin, D. Chen, Inorganic fouling of pressure-driven membrane processes — A critical review, Desalination 250 (2010) 236–248.

[176] M. Mulder, Basic Principles of Membrane Technology, Springer Netherlands, Dordrecht, 1996.

[177] J. Park, S. Lee, J. You, S. Park, Y. Ahn, W. Jung, K.H. Cho, Evaluation of fouling in nanofiltration for desalination using a resistance-in-series model and optical coherence tomography, The Science of the total environment 642 (2018) 349–355.

[178] R. Nitzsche, A. Gröngröft, I. Goj, M. Kraume, Ultrafiltration of Beechwood Hydrolysate for Concentrating Hemicellulose Sugars and Removal of Lignin—Parameter Estimation Using Statistical Methods and Multiobjective Optimization, Ind. Eng. Chem. Res. 59 (2020) 7875–7887.

[179] J. Cho, G. Amy, J. Pellegrino, Membrane filtration of natural organic matter: Initial comparison of rejection and flux decline characteristics with ultrafiltration and nanofiltration membranes, Water Research 33 (1999) 2517–2526.

[180] P. Rai, C. Rai, G.C. Majumdar, S. DasGupta, S. De, Resistance in series model for ultrafiltration of mosambi (Citrus sinensis (L.) Osbeck) juice in a stirred continuous mode, Journal of Membrane Science 283 (2006) 116–122.

[181] A. Sluiter, B. Hames, R. Ruiz, C. Scarlata, J. Sluiter, D. Templeton, D. Crocker, Determination of Structural Carbohydrates and Lignin in Biomass – Laboratory Analytical Procedure. Technical Report, NREL/TP-510-42618, 2012.

[182] TAPPI standard UM 250, Acid-soluble lignin in wood and pulp: TAPPI Useful Methods (2000) 47–48.

[183] Gwyddion, http://gwyddion.net/ (accessed on 10th February 2023).

[184] S. Brunauer, P.H. Emmett, E. Teller, Adsorption of gases in multimolecular layers, J. Am. Chem. Soc. 60 (1938) 309–319.

[185] J. Lindorfer, M. Lettner, K. Fazeni, D. Rosenfeld, B. Annevelink, M. Mandl, Technical, Economic and Environmental Assessment of Biorefinery Concepts: Developing a practical approach for characterisation, IEA Bioenergy, Task 42:2019:01, 2019.

[186] S. Takkellapati, T. Li, M.A. Gonzalez, An Overview of Biorefinery Derived Platform Chemicals from a Cellulose and Hemicellulose Biorefinery, Clean technologies and environmental policy 20 (2018) 1615–1630.

[187] R. Kajaste, Chemicals from biomass – managing greenhouse gas emissions in biorefinery production chains – a review, Journal of Cleaner Production 75 (2014) 1–10.

[188] R.H. Natelson, W.-C. Wang, W.L. Roberts, K.D. Zering, Technoeconomic analysis of jet fuel production from hydrolysis, decarboxylation, and reforming of camelina oil, Biomass Bioenergy 75 (2015) 23–34.

[189] A. Aden, M. Ruth, K. Ibsen, J. Jechura, K. Neeves, J. Sheehan, B. Wallace, Lignocellulosic Biomass to Ethanol Process Design and Economics Utilizing Co-Current Dilute, Boston, 2002.

[190] P. Sassner, M. Galbe, G. Zacchi, Techno-economic evaluation of bioethanol production from three different lignocellulosic materials, Biomass and Bioenergy 32 (2008) 422–430.

[191] L. Luo, E. van der Voet, G. Huppes, Biorefining of lignocellulosic feedstock—Technical, economic and environmental considerations, Bioresource Technology 101 (2010) 5023–5032.

[192] R. Wooley, V. Putsche, Development of an ASPEN PLUS Physical Property Database for Biofuels Components, National Renewable Energy Laboratory, Technical Report, 1996.

[193] A. Aden, M. Ruth, K. Ibsen, J. Jechura, K. Neeves, J. Sheehan, B. Wallace, Lignocellulosic Biomass to Ethanol Process Design and Economics Utilizing CoCurrent Dilute Acid Pre hydrolysis and Enzymatic Hydrolysis for Corn Stover, National Renewable Energy Laboratory, Technical Report NREL/TP-510-32438, 2002.

[194] United States. Environmental Protection Agency (Ed.), Treatability Manual Volume IV - Cost Estimating, Office of Research and Development, U.S. Environmental Protection Agency, Washington D.C., 1980.

[195] G. Murthy, S. Sridhar, M. Shyamsunder, B. Shankaraiah, M. Ramakrishn, Concentration of xylose reaction liquor by nanofiltration for the production of xylitol sugar alcohol, Separation and Purification Technology 44 (2005) 221–228.

[196] E. Larsson, Preconcentration of dilute acid hydrolyzate by membrane filtration, Department of chemical engineering, Lund University (2009) 1–6.

[197] A. Arkell, H. Krawczyk, J. Thuvander, A.-S. Jönsson, Evaluation of membrane performance and cost estimates during recovery of sodium hydroxide in a hemicellulose extraction process by nanofiltration, Separation and Purification Technology 118 (2013) 387–393.

[198] Mitsubishi Chemical Corporation, Product Data Sheet - SEPABEADSTM SP700, Available online: https://www.diaion.com/en/products/synthetic_adsorbents/data_sheet_sp/pdf/SP700_Product_data_sheet.pdf (accessed on 10th February 2023).

[199] O. Wallberg, A.-S. Jönsson, Influence of the Membrane Cut-off During Ultrafiltration of Kraft Black Liquor with Ceramic Membranes, Chemical Engineering Research and Design 81 (2003) 1379–1384.

[200] I. Dimitriou, P. García-Gutiérrez, R.H. Elder, R.M. Cuéllar-Franca, A. Azapagic, R.W.K. Allen, Carbon dioxide utilisation for production of transport fuels: Process and economic analysis, Energy Environ. Sci. 8 (2015) 1775–1789.

[201] M. Haase, Entwicklung eines Energie- und Stoffstrommodells zur ökonomischen und ökologischen Bewertung der Herstellung chemischer Grundstoffe aus Lignocellulose. Zugl.: Karlsruhe, KIT, Diss., 2011, KIT Scientific Publ, Karlsruhe, 2012.

[202] M.S. Peters, K.D. Timmerhaus, R.E. West, Plant design and economics for chemical engineers, 5th ed., McGraw-Hil, Boston, 2004.

[203] A. Chauvel, G. Fournier, C. Raimbault, Manual of Process Economic Evaluation, ED TECHNIP, Paris, 2003.

[204] Verband der Chemischen Industrie e. V., Chemiewirtschaft in Zahlen 2020, 2020.

[205] R. Turton (Ed.), Analysis, synthesis, and design of chemical processes, 4th ed., Prentice Hall, Upper Saddle River, NJ, 2012.

[206] L. Bertin, F. Ferri, A. Scoma, L. Marchetti, F. Fava, Recovery of high added value natural polyphenols from actual olive mill wastewater through solid phase extraction, Chemical Engineering Journal 171 (2011) 1287–1293.

[207] K.R. Hall, L.C. Eagleton, A. Acrivos, T. Vermeulen, Pore- and Solid-Diffusion Kinetics in Fixed-Bed Adsorption under Constant-Pattern Conditions, Ind. Eng. Chem. Fund. 5 (1966) 212–223.

[208] C. Sheindorf, M. Rebhun, M. Sheintuch, A Freundlich-type multicomponent isotherm, Journal of colloid and interface science 79 (1981) 136–142.

[209] Z. Aksu, H. Gülen, Binary biosorption of iron(III) and iron(III)-cyanide complex ions on Rhizopus arrhizus: Modelling of synergistic interaction, Process Biochemistry 38 (2002) 161–173.

[210] D. Mohan, K.P. Singh, Single- and multi-component adsorption of cadmium and zinc using activated carbon derived from bagasse—an agricultural waste, Water Research 36 (2002) 2304–2318.

[211] T. Sainio, M. Kallioinen, O. Nakari, M. Mänttäri, Production and recovery of monosaccharides from lignocellulose hot water extracts in a pulp mill biorefinery, Bioresource Technology 135 (2013) 730–737.

[212] K. Boussu, B. van der Bruggen, A. Volodin, J. Snauwaert, C. van Haesendonck, C. Vandecasteele, Roughness and hydrophobicity studies of nanofiltration membranes using different modes of AFM, Journal of colloid and interface science 286 (2005) 632–638.

[213] J. Brant, K. Johnson, A. Childress, Examining the electrochemical properties of a nanofiltration membrane with atomic force microscopy, Journal of Membrane Science 276 (2006) 286–294.

[214] E.M. Vrijenhoek, S. Hong, M. Elimelech, Influence of membrane surface properties on initial rate of colloidal fouling of reverse osmosis and nanofiltration membranes, Journal of Membrane Science 188 (2001) 115–128.

[215] M. Elimelech, X. Zhu, A.E. Childress, S. Hong, Role of membrane surface morphology in colloidal fouling of cellulose acetate and composite aromatic polyamide reverse osmosis membranes, Journal of Membrane Science 127 (1997) 101–109.

[216] M. Esmaeili, T. Virtanen, J. Lahti, M. Mänttäri, M. Kallioinen, Vanillin as an Antifouling and Hydrophilicity Promoter Agent in Surface Modification of Polyethersulfone Membrane, Membranes 9 (2019).

[217] M.A. Bezerra, R.E. Santelli, E.P. Oliveira, L.S. Villar, L.A. Escaleira, Response surface methodology (RSM) as a tool for optimization in analytical chemistry, Talanta 76 (2008) 965–977.

[218] A. Koocheki, A.R. Taherian, S.M.A. Razavi, A. Bostan, Response surface methodology for optimization of extraction yield, viscosity, hue and emulsion stability of mucilage extracted from Lepidium perfoliatum seeds, Food Hydrocolloids 23 (2009) 2369–2379.

[219] A. Rai, B. Mohanty, R. Bhargava, Supercritical extraction of sunflower oil: A central composite design for extraction variables, Food Chemistry 192 (2016) 647–659.

[220] L. Puro, M. Kallioinen, M. Mänttäri, G. Natarajan, D. C. Cameron, M. Nyström, Performance of RC and PES ultrafiltration membranes in filtration of pulp mill process waters, Desalination 264 (2010) 249–255.

[221] R.R. Sharma, R. Agrawal, S. Chellam, Temperature effects on sieving characteristics of thin-film composite nanofiltration membranes: Pore size distributions and transport parameters, Journal of Membrane Science 223 (2003) 69–87.

[222] C. Bellona, J.E. Drewes, The role of membrane surface charge and solute physico-chemical properties in the rejection of organic acids by NF membranes, Journal of Membrane Science 249 (2005) 227–234.

[223] J. Branke, K. Deb, H. Dierolf, M. Osswald, Finding Knees in Multi-objective Optimization, KanGAL Report Number 2004010 Indian Institut of Technology (2004).

[224] L. Rachmawati, D. Srinivasan, Multiobjective Evolutionary Algorithm With Controllable Focus on the Knees of the Pareto Front, IEEE Trans. Evol. Computat. 13 (2009) 810–824.

[225] O. Schütze, M. Laumanns, Coello C.A.C., Approximating the Knee of an MOP with Stochastic Search Algorithms, udolph G., Jansen T., Beume N., Lucas S., Poloni C. (eds) Parallel Problem Solving from Nature – PPSN X. PPSN 2008. Lecture Notes in Computer Science (2008).

[226] M. Kallioinen, E. Koivula, L. Puro, M. Mänttäri, Influence of operating temperature on fractionation in ultrafiltration of wood-based hydrolysate, Proceedings of the Nordic Wood Biorefinery Conference Stockholm, Sweden (2011).

[227] O. Bobleter, Hydrothermal degradation of polymers derived from plants, Progress in Polymer Science 19 (1994) 797–841.

[228] G. Derringer, R. Suich, Simultaneous Optimization of Several Response Variables, Journal of Quality Technology 12 (2018) 214–219.

[229] S. Yammine, R. Rabagliato, X. Vitrac, M. Mietton Peuchot, R. Ghidossi, The use of nanofiltration membranes for the fractionation of polyphenols from grape pomace extracts, OENO One 53 (2019) 11–26.

[230] G.S. Vieira, F.K.V. Moreira, R.L.S. Matsumoto, M. Michelon, F.M. Filho, M.D. Hubinger, Influence of nanofiltration membrane features on enrichment of jussara ethanolic extract (Euterpe edulis) in anthocyanins, Journal of Food Engineering 226 (2018) 31–41.

[231] S.K. Maiti, Y. Lukka Thuyavan, S. Singh, H.S. Oberoi, G.P. Agarwal, Modeling of the separation of inhibitory components from pretreated rice straw hydrolysate by nanofiltration membranes, Bioresource Technology 114 (2012) 419–427.

[232] Y.-H. Weng, H.-J. Wei, T.-Y. Tsai, W.-H. Chen, T.-Y. Wei, W.-S. Hwang, C.-P. Wang, C.-P. Huang, Separation of acetic acid from xylose by nanofiltration, Separation and Purification Technology 67 (2009) 95–102.

[233] G. Laufenberg, S. Hausmanns, B. Kunz, The influence of intermolecular interactions on the selectivity of several organic acids in aqueous multicomponent systems during reverse osmosis, Journal of Membrane Science 110 (1996) 59–68.

[234] M.K. Ko, J.J. Pellegrino, Determination of osmotic pressure and fouling resistance and their effects of performance of ultrafiltration membranes, Journal of Membrane Science 74 (1992) 141–157.

[235] A. Arora, B.S. Dien, R.L. Belyea, P. Wang, V. Singh, M.E. Tumbleson, K.D. Rausch, Thin stillage fractionation using ultrafiltration: Resistance in series model, Bioprocess and biosystems engineering 32 (2009) 225–233.

[236] A.K. Gautam, T.J. Menkhaus, Surface Modified Reverse Osmosis and Nano-Filtration Membranes for the Production of Biorenewable Fuels and Chemicals, MRS Proc. 1502 (2013).

[237] J. Leberknight, T.J. Menkhaus, Membrane separations for solid-liquid clarification within lignocellulosic biorefining processes, Biotechnology progress 29 (2013) 1246–1254.

[238] P. BACCHIN, P. AIMAR, R. FIELD, Critical and sustainable fluxes: Theory, experiments and applications, Journal of Membrane Science 281 (2006) 42–69.

[239] M. Nilsson, G. Trägårdh, K. Östergren, The influence of pH, salt and temperature on nanofiltration performance, Journal of Membrane Science 312 (2008) 97–106.

[240] J.G. Stichlmair, J.R. Fair, Distillation: Principles and practices, Wiley-VCH, New York, 1998.

[241] F.O. Licht (Ed.), World Ethanol & Biofuels Report, 2018.

[242] European Commission (Ed.), Energy statistics - prices of natural gas and electricity, 2018.

[243] W. Geng, R.A. Venditti, J.J. Pawlak, T. de Assis, R.W. Gonzalez, R.B. Phillips, H.-m. Chang, Techno-economic analysis of hemicellulose extraction from different types of lignocellulosic feedstocks and strategies for cost optimization, Biofuels, Bioprod. Bioref. 14 (2019) 225–241.

[244] M. O'Donohue, Technical note on pentose sugars and their applications, HAL open science 2013, pp.4, hal-01268773 (2020).

PUBLICATIONS

Previously published reports:

DBFZ Report Nr. 47 WasteGui: Guideline for organic waste treatment in East Africa
DBFZ Report Nr. 46 Wasserstoff aus Biomasse
DBFZ Report Nr. 45 Status-Quo of organic waste collection, transport and treatment in East Africa and Ethiopia
DBFZ Report Nr. 44 Monitoring erneuerbarer Energien im Verkehr
DBFZ Report Nr. 43 Beitrag zur Optimierung des Pelletierverhaltens von Gärresten und Landschaftspflegeheu sowie deren Mischungen
DBFZ Report Nr. 42 Rahmenbedingungen für einen optimierten Betrieb von kleinen biomassebasierten BHKW
DBFZ Report Nr. 41 National Resource Monitoring for Biogenic Residues, By-products and Wastes – Development of a Systematic Data Collection, Management and Assessment for Germany
DBFZ Report Nr. 40 Basics of Anaerobic Digestion - Biochemical Conversion and Process Modelling
DBFZ Report Nr. 39 Optimierte Regelungsstrategien für Pellet-Solar-Kombiheizanlagen zur Steigerung der Systemeffizienz bei gleichzeitiger Minimierung der Energiekosten
DBFZ Report Nr. 38 Hydrothermal processing of biogenic residues in Germany - A technology assessment considering development paths by 2030
DBFZ Report Nr. 37 Economic assessment of biogas plants as a flexibility option in future electricity systems
DBFZ Report Nr. 36 BioplanW: Systemlösungen Bioenergie im Wärmesektor im Kontext zukünftiger Entwicklungen
DBFZ Report Nr. 35 Leitfaden zur Substrat- und Effzienzbewertung an Biogasanlagen
DBFZ Report Nr. 34 Entwicklung einer Methode zur Verwendung der Daten des Schornsteinfegerhandwerks für die energiewirtschaftliche Berichterstattung - Dissertationsschrift
DBFZ Report No. 33 Recommendations for reliable methane emission rate quantification at biogas plants
DBFZ Report Nr. 32 Wärmenutzung von Biogasanlagen
DBFZ Report Nr. 31 Die Niedertemperatursynthese von Methan in Thermoöl-temperierten Plattenreaktoren – Dissertationsschrift –
DBFZ Report Nr. 30 Anlagenbestand Biogas und Biomethan – Biogaserzeugung und -nutzung in Deutschland
DBFZ Report Nr. 29 Effiziente Bioenergie für Regionen - Ergebnisse der technisch-ökonomischen Begleitforschung zur Fördermaßname Bioenergie-Regionen 2012-2015
DBFZ Report Nr. 28 Potenziale zur Steigerung der Leistungsfähigkeit von Biogasanlagen - Energetische Effizienz von Repoweringmaßnahmen
DBFZ Report Nr. 27 Neuartiger emissionsarmer Kaminofen (DBU-NEKO)
DBFZ Report Nr. 26 Bewertung technischer und wirtschaftlicher Entwickoungspotenziale künftiger und bestehender Biomasse-zu-Methan-Konversionsprozesse - Dissertationsschrift
DBFZ Report Nr. 25 Nachrüstlösung zum katalytischen Abbau von gasförmigen organischen Emissionen aus Kaminöfen
DBFZ Report Nr. 24 Biomasse zur Wärmeerzeugung– Methoden zur Quantifizierung des Brennstoffeinsatzes
DBFZ Report Nr. 23 Technisch-ökonomische Begleitforschung des Bundeswettbewerbes „Bioenergie-Regionen“
DBFZ Report Nr. 22 Die Biokraftstoffproduktion in Deutschland – Stand der Technik und Optimierungsansätze
DBFZ Report Nr. 21 Entwicklung der Förderung der Stromerzeugung aus Biomasse im Rahmen des EEG
DBFZ Report Nr. 20 KlimaCH4 – Klimaeffekte von Biomethan
DBFZ Report Nr. 19 Hy-NOW – Evaluierung der Verfahren und Technologien für die Bereitstellung von Wasserstoff auf Basis von Biomasse
DBFZ Report Nr. 18 Kleintechnische Biomassevergasung – Option für eine nachhaltige und dezentrale Energieversorgung
DBFZ Report Nr. 17 Grünlandenergie Havelland – Entwicklung von übertragbaren Konzepten zur naturverträglichen energetischen Nutzung von Gras und Schilf am Beispiel der Region Havelland
DBFZ Report Nr. 16 Algae biorefinery – material and energy use of algae
DBFZ Report Nr. 15 Politics and Economics of Ethanol and Biodiesel Production and Consumption in Brazil
DBFZ Report Nr. 14 Holzpelletbereitstellung für Kleinfeuerungsanlagen
DBFZ Report Nr. 13 Basisinformationen für eine nachhaltige Nutzung von landwirtschaftlichen Reststoffen zur Bioenergiebereitstellung
DBFZ Report Nr. 12 Monitoring zur Wirkung des Eneuerbare-Energien-Gesetz (EEG) auf die Entwicklung der Stromerzeugung aus Biomasse
DBFZ Report Nr. 11 Monitoring Biokraftstoffsektor
DBFZ Report Nr. 10 Ermittlung des Verbrauchs biogener Festbrennstoffe im Sektor Gewerbe, Handel, Dienstleistungen (GHD-Sektor) – Endbericht
DBFZ Report Nr. 9 Analyse und Bewertung ausgewählter zukünftiger Biokraftstoffoptionen auf der Basis fester Biomasse
DBFZ Report Nr. 8 – Kompakt – Sammelband
DBFZ Report Nr. 7 Final Report – Global and Regional Spatial Distribution of Biomass Potentials – Status quo and options for specication –
DBFZ Report Nr. 6 Katalytisch unterstützte Minderung von Emissionen aus Biomasse-Kleinfeuerungsanlagen
DBFZ Report Nr. 5 Optimierung und Bewertung von Anlagen zur Erzeugung von Methan, Strom und Wärme aus biogenen Festbrennstoffen
DBFZ Report Nr. 4 Identifzierung strategischer Hemmnisse und Entwicklung von Lösungsansätzen zur Reduzierung der Nutzungskonkurrenzen beim weiteren Ausbau der Biomassenutzung
DBFZ Report Nr. 3 Feinstaubminderung im Betrieb von Scheitholzkaminöfen unter Berücksichtigung der toxikologischen Relevanz
DBFZ Report Nr. 2 Methodische Vorgehensweise zur Standortidentifikation und Planung der Biomassebereitstellung für Konversionsanlagen am Beispiel von Bio-SNG-Produktionsanlagen
DBFZ Report Nr. 1 Bewertung und Minderung von Feinstaubemissionen aus häuslichen Holzfeuerungsanlagen

Further information and free downloads:
www.dbfz.de/en/press-media-library/publication-series/dbfz-reports

DBFZ Deutsches Biomasseforschungszentrum
gemeinnützige GmbH
Torgauer Straße 116
D - 04347 Leipzig
Phone: +49 (0)341 2434-112
E-Mail: info@dbfz.de

www.dbfz.de/en